JSCSEN 87(11)1237–1348(2022)

ISSN 1820-7421(Online)

Journal of the Serbian Chemical Society

Electronic version

Serbian Chemical Society 125 ANNIVERSARY

Available on line at

CXII 1897

www.shd.org.rs/JSCS/

VOLUME 87

No 11

BELGRADE 2022

The full search of JSCS is available through

DOAJ DIRECTORY OF OPEN ACCESS JOURNALS

www.doaj.org

The **Journal of the Serbian Chemical Society** (formerly Glasnik Hemijskog društva Beograd), one volume (12 issues) per year, publishes articles from the fields of chemistry. The **Journal** is financially supported by the **Ministry of Education, Science and Technological Development of the Republic of Serbia.**

Articles published in the **Journal** are indexed in **Clarivate Analytics products: Science Citation Index-Expanded™** – accessed *via* **Web of Science®** and **Journal Citation Reports®**.

Impact Factor announced 2022: **1.100; 5-year Impact Factor**: **1.175**.

Articles appearing in the **Journal** are also abstracted by: **Scopus, Chemical Abstracts Plus (CAplus℠), Directory of Open Access Journals, Referativnii Zhurnal (VINITI), RSC Analytical Abstracts, EuroPub, Pro Quest** and **Asian Digital Library.**

Publisher:	**Serbian Chemical Society**, Karnegijeva 4/III, P. O. Box 36, 1120 Belgrade 35, Serbia tel./fax: +381–11–3370–467, E-mails: **Society** – shd@shd.org.rs; **Journal** – jscs@shd.org.rs Home Pages: **Society** – http://www.shd.org.rs/, **Journal** – http://www.shd.org.rs/JSCS/
Internet Service:	Contents, Abstracts and full papers (from Vol 64, No. 1, 1999) are available in the electronic form at the Web Site of the **Journal** (http://www.shd.org.rs/JSCS/).
Former Editors:	**Nikola A. Pušin** (1930–1947), **Aleksandar M. Leko** (1948–1954), **Panta S. Tutundžić** (1955–1961), **Miloš K. Mladenović** (1962–1964), **Đorđe M. Dimitrijević** (1965–1969), **Aleksandar R. Despić** (1969–1975), **Slobodan V. Ribnikar** (1975–1985), **Dragutin M. Dražić** (1986–2006).
Editor-in-Chief:	BRANISLAV Ž. **NIKOLIĆ**, Serbian Chemical Society (E-mail: jscs-ed@shd.org.rs)
Deputy Editor:	DUŠAN **SLADIĆ**, Faculty of Chemistry, University of Belgrade
Sub editors:	
Organic Chemistry	DEJAN **OPSENICA**, Institute of Chemistry, Technology and Metallurgy, University of Belgrade JÁNOS **CSANÁDI**, Faculty of Science, University of Novi Sad
Biochemistry and Biotechnology	OLGICA **NEDIĆ**, INEP – Institute for the Application of Nuclear Energy, University of Belgrade
Inorganic Chemistry	MILOŠ **ĐURAN**, Serbian Chemical Society
Theoretical Chemistry	IVAN **JURANIĆ**, Serbian Chemical Society
Physical Chemistry	LJILJANA **DAMJANOVIĆ-VASILIĆ**, Faculty of Physical Chemistry, University of Belgrade
Electrochemistry	SNEŽANA **GOJKOVIĆ**, Faculty of Technology and Metallurgy, University of Belgrade
Analytical Chemistry	SLAVICA **RAŽIĆ**, Faculty of Pharmacy, University of Belgrade
Polymers	BRANKO **DUNJIĆ**, Faculty of Technology and Metallurgy, University of Belgrade
Thermodynamics	MIRJANA **KIJEVČANIN**, Faculty of Technology and Metallurgy, University of Belgrade
Chemical Engineering	TATJANA **KALUĐEROVIĆ RADOIČIĆ**, Faculty of Technology and Metallurgy, University of Belgrade
Materials	RADA **PETROVIĆ**, Faculty of Technology and Metallurgy, University of Belgrade
Metallic Materials and Metallurgy	ANA **KOSTOV**, Mining and Metallurgy Institute Bor, University of Belgrade
Environmental and Geochemistry	VESNA **ANTIĆ**, Faculty of Agriculture, University of Belgrade
History of and Education in Chemistry	DRAGICA **TRIVIĆ**, Faculty of Chemistry, University of Belgrade
English Language Editors:	LYNNE **KATSIKAS**, Serbian Chemical Society VLATKA **VAJS**, Serbian Chemical Society JASMINA **NIKOLIĆ**, Faculty of Technology and Metallurgy, University of Belgrade
Technical Editors:	VLADIMIR **PANIĆ**, ALEKSANDAR **DEKANSKI**, VUK **FILIPOVIĆ**, Institute of Chemistry, Technology and Metallurgy, University of Belgrade
Journal Manager & Web Master:	ALEKSANDAR **DEKANSKI,** Institute of Chemistry, Technology and Metallurgy, University of Belgrade
Office:	VERA **ĆUŠIĆ**, Serbian Chemical Society

Editorial Board

From abroad: **R. Adžić**, Brookhaven National Laboratory (USA); **A. Casini**, University of Groningen (The Netherlands); **G. Cobb**, Baylor University (USA); **D. Douglas**, University of British Columbia (Canada); **G. Inzelt**, Etvos Lorand University (Hungary); **J. Kenny**, University of Perugia (Italy); **Ya. I. Korenman**, Voronezh Academy of Technology (Russian Federation); **M. D. Lechner**, University of Osnabrueck (Germany); **S. Macura**, Mayo Clinic (USA); **M. Spiteller**, INFU, Technical University Dortmund (Germany); **M. Stratakis**, University of Crete (Grecce); **M. Swart**, University de Girona (Cataluna, Spain); **G. Vunjak-Novaković**, Columbia University (USA); **P. Worsfold**, University of Plymouth (UK); **J. Zagal**, Universidad de Santiago de Chile (Chile).

From Serbia: **B. Abramović**, **V. Antić**, **V. Beškoski**, **J. Csanadi**, **Lj. Damjanović-Vasilić**, **A. Dekanski**, **V. Dondur**, **B. Dunjić**, **M. Đuran, S. Gojković**, **I. Gutman**, **B. Jovančićević**, **I. Juranić**, **T. Kaluđerović Radioičić**, **L. Katsikas**, **M. Kijevčanin**, **A. Kostov**, **V. Leovac**, **S. Milonjić**, **V.B. Mišković-Stanković**, **O. Nedić**, **B. Nikolić**, **J. Nikolić**, **D. Opsenica**, **V. Panić**, **M. Petkovska**, **R. Petrović**, **I. Popović**, **B. Radak**, **S. Ražić**, **D. Sladić**, **S. Sovilj**, **S. Šerbanović**, **B. Šolaja**, **Ž. Tešić**, **D. Trivić**, **V. Vajs**.

Subscription: The annual subscription rate is **150.00 €** including postage (surface mail) and handling. For Society members from abroad rate is **50.00 €**. For the proforma invoice with the instruction for bank payment contact the Society Office (E-mail: shd@shd.org.rs) or see JSCS Web Site: http://www.shd.org.rs/JSCS/, option Subscription.

Godišnja pretplata: Za članove SHD: **2.500,00 RSD**, za penzionere i studente: **1000,00 RSD**, a za ostale: **3.500,00 RSD**:za organizacije i ustanove: **16.000,00 RSD**. Uplate se vrše na tekući račun Društva: **205-13815-62**, poziv na broj **320**, sa naznakom "pretplata za JSCS".

Nota: Radovi čiji su svi autori članovi SHD prioritetno se publikuju.

Odlukom Odbora za hemiju Republičkog fonda za nauku Srbije, br. 66788/1 od 22.11.1990. godine, koja je kasnije potvrđena odlukom Saveta Fonda, časopis je uvršten u kategoriju međunarodnih časopisa (**M-23**). Takođe, aktom Ministarstva za nauku i tehnologiju Republike Srbije, 413-00-247/2000-01 od 15.06.2000. godine, ovaj časopis je proglašen za publikaciju od posebnog interesa za nauku. **Impact Factor** časopisa objavljen 2022. godini iznosi **1,100**, a petogodišnji **Impact Factor 1,175**.

INSTRUCTIONS FOR AUTHORS (2021)

GENERAL

The *Journal of the Serbian Chemical Society* (the *Journal* in further text) is an international journal publishing papers from all fields of chemistry and related disciplines. Twelve issues are published annually. The Editorial Board expects the editors, reviewers, and authors to respect the well-known standard of professional ethics.

Types of Contributions

Original scientific papers	(up to 15 typewritten pages, including Figures, Tables and References) report original research which must not have been previously published.
Short communications	(up to 8 pages) report unpublished preliminary results of sufficient importance to merit rapid publication.
Notes	(up to 5 pages) report unpublished results of short, but complete, original research
Authors' reviews	(up to 40 pages) present an overview of the author's current research with comparison to data of other scientists working in the field
Reviews[a]	(up to 40 pages) present a concise and critical survey of a specific research area. Generally, these are prepared at the invitation of the Editor
Surveys	(about 25 pages) communicate a short review of a specific research area.
Book and Web site reviews	(1 - 2 pages)
Extended abstracts	(about 4 pages) of Lectures given at meetings of the Serbian Chemical Society Divisions
Letters to the Editor	report miscellaneous topics directed directly to the Editor

[a]Generally, Authors' reviews, Reviews and Surveys are prepared at the invitation of the Editor.

Submission of manuscripts

Manuscripts should be submitted using the **OnLine Submission Form**, available on the JSCS Web Site (**http://www.shd-pub.org.rs/index.php/JSCS**). The manuscript must be uploaded as a Word.doc or .rtf file, with tables and figures (including the corresponding captions – above Tables and below Figures), placed within the text to follow the paragraph in which they were mentioned for the first time.

Please note that **Full Names (**First Name, Last Name), **Full Affiliation** and **Country** (from drop down menu) of **ALL OF AUTHORS** (written in accordance with English spelling rules - the first letter capitalized) must be entered in the manuscript Submission Form (Step 3). Manuscript Title, authors' names and affiliations, as well as the Abstract, **WILL APPEAR** in the article listing, as well as in **BIBLIOGRAPHIC DATABASES (WoS, SCOPUS...)**, in the form and in the order entered in the author details

Graphical abstract

Graphical abstract is a one-image file containing the main depiction of the authors work and/or conclusion and must be supplied along with the manuscript. It must enable readers to quickly gain the main message of the paper and to encourage browsing, help readers identify which papers are most relevant to their research interests. Authors must provide an image that clearly represents the research described in the paper. The most relevant figure from the work, which summarizes the content, can also be submitted. The image should be submitted as a separate file in **Online Submission Form - Step 2**.

Specifications: The graphical abstract should have a clear start and end, reading from top to bottom or left to right. Please omit unnecessary distractions as much as possible.

- **Image size:** minimum of 500×800 pixels (W×H) and a minimum resolution of 300 dpi. If a larger image is sent, then please use the same ratio: 16 wide × 9 high. Please note that your image will be scaled proportionally to fit in the available window in TOC; a 150x240 pixel rectangle. Please be sure that the quality of an image cannot be increased by changing the resolution from lower to higher, but only by rescanning or exporting the image with a higher resolution, which can be set in usual "settings" option.
- **Font:** Please use Calibri and Symbol font with a large enough font size, so it is readable even from the image of a smaller size (150 × 240 px) in TOC.
- **File type:** JPG and PNG only.

No additional text, outline or synopsis should be included. Please do not use white space or any heading within the image.

Cover Letter

Manuscripts must be accompanied by a cover letter (strictly uploaded in **Online Submission Step 2**) in which the type of the submitted manuscript and a warranty as given below are given. The Author(s) has(have) to warranty that the manuscript submitted to the *Journal* for review is original, has been written by the stated author(s) and has not been published elsewhere; is currently not being considered for publication by any other journal and will not be submitted for such a review while under review by the *Journal*; the manuscript contains no libellous or other unlawful statements and does not contain any materials that violate any personal or proprietary rights of any other person or entity. All manuscripts will be acknowledged on receipt (by e-mail).

Illustrations

Illustrations (Figs, schemes, photos…) in TIF or EPS format (JPG format is acceptable for colour and greyscale photos, only), must be additionally uploaded (Online Submission Step 2) as a separate file or one archived (.zip, .rar or .arj) file. Figures and/or Schemes should be prepared according to the **Artwork Instructions -** http://www.shd.org.rs/JSCS/jscs-pdf/Artwork_Instructions.pdf!

For any difficulties and questions related to **OnLine Submission Form -** https://www.shd-pub.org.rs/index.php/JSCS/submission/wizard, please refer to **User Guide -** https://openjournal-systems.com/ojs-3-user-guide/ , Chapter **Submitting an Article -** https://openjournalsystems.com/ojs-3-user-guide/submitting-an-article/. If difficulties still persist, please contact JSCS Editorial Office at **JSCS@shd.org.rs**

A manuscript not prepared according to these instructions will be returned for resubmission without being assigned a reference number.

Conflict-of-Interest Statement*: Public trust in the peer review process and the credibility of published articles depend in part on how well a conflict of interest is handled during writing, peer review, and editorial decision making. A conflict of interest exists when an author (or the author's institution), reviewer, or editor has financial or personal relationships that inappropriately influence (bias) his or her actions (such relationships are also known as dual commitments, competing interests, or competing loyalties). These relationships vary from those with negligible potential to those with great potential to influence judgment, and not all relationships represent true conflict of interest. The potential for a conflict of interest can exist whether or not an individual believes that the relationship affects his or her scientific judgment. Financial relationships (such as employment, consultancies, stock ownership, honoraria, paid expert testimony) are the most easily identifiable conflicts of interest and the most likely to undermine the credibility of the journal, the authors, and of science itself. However, conflicts can occur for other reasons, such as personal relationships, academic competition, and intellectual passion.

Informed Consent Statement*: Patients have a right to privacy that should not be infringed without informed consent. Identifying information, including patients' names, initials, or hospital numbers, should not be published in written descriptions, photographs, and pedigrees unless the information is essential for scientific purposes and the patient (or parent or guardian) gives written informed consent for publication. Informed consent for this purpose requires that a patient who is identifiable be shown the manuscript to be published. Authors should identify Individuals who provide writing assistance and disclose the funding source for this assistance. Identifying details should be omitted if they are not essential. Complete anonymity is difficult to achieve, however, and informed consent should be obtained if there is any doubt. For example, masking the eye region in photographs of patients is inadequate protection of anonymity. If identifying characteristics are altered to protect anonymity, such as in genetic pedigrees, authors should provide assurance that alterations do not distort scientific meaning and editors should so note. The requirement for informed consent should be included in the journal's instructions for authors. When informed consent has been obtained it should be indicated in the published article.

Human and Animal Rights Statement* When reporting experiments on human subjects, authors should indicate whether the procedures followed were in accordance with the ethical standards of the responsible committee on human experimentation (institutional and national) and with the Helsinki Declaration of 1975, as revised in 2000 (5). If doubt exists whether the research was conducted in accordance with the Helsinki Declaration, the authors must explain the rationale for their approach, and demonstrate that the institutional review body explicitly approved the doubtful aspects of the study. When reporting experiments on animals, authors should be asked to indicate whether the institutional and national guide for the care and use of laboratory animals was followed.

---

*International Committee of Medical Journal Editors ("Uniform Requirements for Manuscripts Submitted to Biomedical Journals"), February 2006

PROCEDURE

All contributions will be peer reviewed and only those deemed worthy and suitable will be accepted for publication. The Editor has the final decision. To facilitate the reviewing process, authors are encouraged to suggest up to three persons competent to review their manuscript. Such suggestions will be taken into consideration but not always accepted. If authors would prefer a specific person not be a reviewer, this should be announced. The Cover Letter must be accompanied by these suggestions. Manuscripts requiring revision should be returned according to the requirement of the Editor, within 60 days upon reception of the reviewing comments by e-mail.

The *Journal* maintains its policy and takes the liberty of correcting the English as well as false content of manuscripts **provisionally accepted** for publication in the first stage of reviewing process. In this second stage of manuscript preparation by JSCS Editorial Office, the author(s) may be required to supply some **additional clarifications and corrections**. This procedure will be executed during copyediting actions, with a demand to author(s) to perform corrections of unclear parts before the manuscript would be published OnLine as **finally accepted manuscript (OLF Section of the JSCS website)**. Please note that the manuscript can receive the status of **final rejection** if the author's corrections would not be satisfactory.

When finally accepted manuscript is ready for printing, the corresponding author will receive a request for proof reading, which should be performed within 2 days. Failure to do so will be taken as the authors agree with any alteration which may have occurred during the preparation of the manuscript for printing.

Accepted manuscripts of active members of the Serbian Chemical Society (all authors) have publishing priority.

MANUSCRIPT PRESENTATION

Manuscripts should be typed in English (either standard British or American English, but consistent throughout) with 1.5 spacing (12 points Times New Roman; Greek letters in the character font Symbol) in A4 format leaving 2.5 cm for margins. For Regional specific, non-standard characters that may appear in the text, save documents with Embed fonts Word option: *Save as -> (Tools) -> Save Options… -> Embed fonts in the text.*

The authors are requested to seek the assistance of competent English language expert, if necessary, to ensure their English is of a reasonable standard. The Serbian Chemical Society can provide this service in advance of submission of the manuscript. If this service is required, please contact the office of the Society by e-mail (jscs-info@shd.org.rs).

Tables, figures and/or schemes must be embedded in the main text of the manuscript and should follow the paragraph in which they are mentioned for the first time. **Tables** must be prepared with the aid of the **WORD table function**, without vertical lines. The minimum size of the font in the tables should be **10 pt**. Table columns must not be formatted using multiple spaces. Table rows must not be formatted using any returns (enter key; ↵ key) and are **limited to 12 cm width**. Tables should not be incorporated as graphical objects. **Footnotes to Tables** should follow them and are to be indicated consequently (in a single line) in superscript letters and separated by semi-column.

Table caption must be placed above corresponding Table, while **Captions of the Illustrations** (Figs. Schemes...) must follow the corresponding item. **The captions, either for Tables or Illustrations**, should make the items comprehensible without reading of the main text (but clearly referenced in), must follow numerical order (Roman for Tables, Arabic for Illustrations), and should not be provided on separate sheets or as separate files.

High resolution Illustrations (named as Fig. 1, Fig. 2… and/or Scheme 1, Scheme 2…) in **TIF or EPS format** (JPG format is acceptable for photos, only) **must be additionally uploaded as a separate files or one archived (.zip, .rar) file.**

Illustrations should be prepared according to the ARTWORK INSTRUCTIONS - http://www.shd.org.rs/JSCS/jscs-pdf/Artwork_Instructions.pdf. **!**

All pages of the manuscript must be numbered continuously.

DESIGNATION OF PHYSICAL QUANTITIES AND UNITS

IUPAC recommendations for the naming of compounds should be followed. SI units, or other permissible units, should be employed. The designation of physical quantities must be in italic throughout the text (including figures, tables and equations), whereas the units and indexes (except for indexes having the meaning of physical quantities) are in upright letters. They should be in Times New Roman font. In graphs and tables, a slash should be used to separate the designation of a physical quantity from the unit

(example: p / kPa, j / mA cm^{-2}, t / °C, T_0 / K, τ / h, ln (j / mA cm^{-2})…). Designations such as: p (kPa), t [min]…, are not acceptable. However, if the full name of a physical quantity is unavoidable, it should be given in upright letters and separated from the unit by a comma (example: Pressure, kPa; Temperature, K; Current density, mA cm^{-2}…). Please do not use the axes of graphs for additional explanations; these should be mentioned in the figure captions and/or the manuscript (example: "pressure at the inlet of the system, kPa" should be avoided). The axis name should follow the direction of the axis (the name of y-axis should be rotated by 90°). Top and right axes should be avoided in diagrams, unless they are absolutely necessary.

Latin words, as well as the names of species, should be in *italic*, as for example: *i.e.*, *e.g.*, *in vivo*, *ibid*, *Calendula officinalis* L., *etc*. The branching of organic compound should also be indicated in *italic*, for example, *n*-butanol, *tert*-butanol, *etc*.

Decimal numbers must have decimal points and not commas in the text (except in the Serbian abstract), tables and axis labels in graphical presentations of results. Thousands are separated, if at all, by a comma and not a point.

Mathematical and chemical equations should be given in separate lines and must be numbered, Arabic numbers, consecutively in parenthesis at the end of the line. All equations should be embedded in the text Complex equations (fractions, integrals, matrix…) should be prepared with the aid of the **Microsoft Equation 3.0** (or higher) or **MathType** (Do not use them to create simple equations and labels). **Using the Insert -> Equation option, integrated in MS Office 2010 and MS Office 2013, as well as insertion of equation objects within paragraph text IS NOT ALLOWED.**

ARTICLE STRUCTURE

- TITLE PAGE;
- MAIN TEXT – including Tables and Illustrations with corresponding captions;
- SUPPLEMENTARY MATERIAL (optional**)**

Title page

- **Title** in bold letters, should be clear and concise, preferably 12 words or less. The use of non-standard abbreviations, symbols and formulae is discouraged.
- AUTHORS' NAMES in capital letters with the full first name, initials of further names separated by a space and surname. Commas should separate the author's names except for the last two names when 'and' is to be used. In multi-affiliation manuscripts, the author's affiliation should be indicated by an Arabic number placed in superscript after the name and before the affiliation. Use * to denote the corresponding author(s).
- *Affiliations* should be written in italic. The e-mail address of the corresponding author should be given after the affiliation(s).
- *Abstract:* A one-paragraph abstract written of 150 – 200 words in an impersonal form indicating the aims of the work, the main results and conclusions should be given and clearly set off from the text. Domestic authors should also submit, on a separate page, an Abstract - Izvod, the author's name(s) and affiliation(s) in Serbian (Cyrillic letters). (Домаћи аутори морају доставити Извод (укључујући имена аутора и афилијацију) на српском језику, исписане ћирилицом, иза Захвалнице, а пре списка референци.) For authors outside Serbia, the Editorial Board will provide a Serbian translation of their English abstract.
- *Keywords:* Up to 6 keywords should be given. Do not use words appearing in the manuscript title
- RUNNING TITLE: A one line (maximum five words) short title in capital letters should be provided.

Main text – should have the form:

- **INTRODUCTION,**
- **EXPERIMENTAL (RESULTS AND DISCUSSION),**
- **RESULTS AND DISCUSSION (EXPERIMENTAL),**
- **CONCLUSIONS,**
- **NOMENCLATURE (optional) and**
- ***Acknowledgements*: If any.**
- REFERENCES (Citation of recent papers published in chemistry journals that highlight the significance of work to the general readership is encouraged.)

The sections should be arranged in a sequence generally accepted for publication in the respective fields. They subtitles should be in capital letters, centred and NOT numbered.

- The INTRODUCTION should include the aim of the research and a concise description of background information and related studies directly connected to the paper.
- The EXPERIMENTAL section should give the purity and source of all employed materials, as well as details of the instruments used. The employed methods should be described in sufficient detail to enable experienced persons to repeat them. Standard procedures should be referenced and only modifications described in detail. On no account should results be included in the experimental section.

Chemistry

Detailed information about instruments and general experimental techniques should be given in all necessary details. If special treatment for solvents or chemical purification were applied that must be emphasized.

Example: Melting points were determined on a Boetius PMHK or a Mel-Temp apparatus and were not corrected. Optical rotations were measured on a Rudolph Research Analytical automatic polarimeter, Autopol IV in dichloromethane (DCM) or methanol (MeOH) as solvent. IR spectra were recorded on a Perkin-Elmer spectrophotometer FT-IR 1725X. ^{1}H and ^{13}C NMR spectra were recorded on a Varian Gemini-200 spectrometer (at 200 and 50 MHz, respectively), and on a Bruker Ultrashield Advance III spectrometer (at 500 and 125 MHz, respectively) employing indicated solvents (*vide infra*) using TMS as the internal standard. Chemical shifts are expressed in ppm (δ / ppm) values and coupling constants in Hz (J / Hz). ESI-MS spectra were recorded on Agilent Technologies 6210 Time-Of-Flight LC-MS instrument in positive ion mode with CH_3CN/H_2O 1/1 with 0.2 % HCOOH as the carrying solvent solution. Samples were dissolved in CH_3CN or MeOH (HPLC grade purity). The selected values were as follows: capillary voltage = 4 kV, gas temperature = 350 °C, drying gas flow 12 L min^{-1}, nebulizer pressure = 310 kPa, fragmentator voltage = 70 V.The elemental analysis was performed on the Vario EL III- C,H,N,S/O Elemental Analyzer (Elementar Analysensysteme GmbH, Hanau-Germany). Thin-layer chromatography (TLC) was performed on precoated Merck silica gel 60 F254 and RP-18 F254 plates. Column chromatography was performed on Lobar LichroPrep Si 60 (40-63 μm), RP-18 (40-63 μm) columns coupled to a Waters RI 401 detector, and on Biotage SP1 system with UV detector and FLASH 12+, FLASH 25+ or FLASH 40+ columns pre packed with KP-SIL [40-63 μm, pore diameter 6 nm (60 Å)], KP-C18-HS (40-63 μm, pore diameter 9 nm (90 Å) or KP-NH [40-63 μm, pore diameter 10 nm (100 Å)] as adsorbent. Compounds were analyzed for purity (HPLC) using a Waters 1525 HPLC dual pump system equipped with an Alltech, Select degasser system, and dual λ 2487 UV-VIS detector. For data processing, Empower software was used (methods A and B). Methods C and D: Agylent Technologies 1260 Liquid Chromatograph equipped with Quat Pump (G1311B), Injector (G1329B) 1260 ALS, TCC 1260 (G1316A) and Detector 1260 DAD VL+ (G1315C). For data processing, LC OpenLab CDS ChemStation software was used. For details, see Supporting Information.

1. Synthesis experiments

Each paragraph describing a synthesis experiment should begin with the name of the product and any structure number assigned to the compound in the Results and Discussions section. Thereafter, the compound should be identified by its structure number. Use of standard abbreviations or unambiguous molecular formulas for reagents and solvents, and of structure numbers rather than chemical names to identify starting materials and intermediates, is encouraged.

When a new or improved synthetic method is described, the yields reported in key experimental examples, and yields used for comparison with existing methods, should represent amounts of isolated and purified products, rather than chromategraphically or spectroscopically determined yields. Reactant quantities should be reported in weight and molar units and for product yields should be reported in weight units; percentage yields should only be reported for materials of demonstrated purity. When chromatography is used for product purification, both the support and solvent should be identified.

2. Microwave experiments

Reports of syntheses conducted in microwave reactors must clearly indicate whether sealed or open reaction vessels were used and must document the manufacturer and model of the reactor, the method of monitoring the reaction mixture temperature, and the temperature-time profile. Reporting a wattage rating or power setting is not an acceptable alternative to providing temperature data. Manuscripts describing work done with domestic (kitchen) microwave ovens will not be accepted except for studies where the unit is used for heating reaction mixtures at atmospheric pressure.

3. Compound characterization

The Journal upholds a high standard for compound characterization to ensure that substances being added to the chemical literature have been correctly identified and can be synthesized in known yield and purity by the reported preparation and isolation methods. For **all new** compounds, evidence adequate to establish both **identity** and **degree of purity** (homogeneity) must be provided.

Identity *- Melting point.* All homogeneous solid products (*e.g.* not mixtures of isomers) should be characterized by melting or decomposition points. The colors and morphologies of the products should also be noted.

Specific rotations. Specific rotations based on the equation $[\alpha]^t; D = (100\ \alpha) / (l\ c)$ should be reported as unitless numbers as in the following example: $[\alpha]^{20}$; D = -25.4 (c 1.93, $CHCl_3$), where c / g mL^{-1} is concentration and l / dm is path length. The units of the specific rotation, (deg mL) / (g dm), are implicit and are not included with the reported value.

Spectra/*Spectral Data.* Important IR adsorptions should be given.

For all new diamagnetic substances, NMR data should be reported (^1H, ^{13}C, and relevant heteronuclei). ^1H NMR chemical shifts should be given with two digits after the decimal point. Include the number of protons represented by the signal, signal multiplicity, and coupling constants as needed (*J* italicized, reported with up to one digit after the decimal). The number of bonds through which the coupling is operative, ^xJ, may be specified by the author if known with a high degree of certainty. ^{13}C NMR signal shifts should be rounded to the nearest 0.01 ppm unless greater precision is needed to distinguish closely spaced signals. Field strength should be noted for each spectrum, not as a comment in the general experimental section. Hydrogen multiplicity (C, CH, CH_2, CH_3) information obtained from routine DEPT spectra should be included. If detailed signal assignments are made, the type of NOESY or COSY methods used to establish atom connectivity and spatial relationships should be identified in the Supporting Information. Copies of spectra should also be included where structure assignments of complex molecules depend heavily on NMR interpretation. Numbering system used for assignments of signals should be given in the Supporting Information with corresponding general structural formula of named derivative.

HPLC/LCMS can be substituted for biochemistry papers where the main focus is not on compound synthesis.

HRMS/*elemental analysis.* To support the molecular formula assignment, HRMS data accurate within 5 ppm, or combustion elemental analysis [carbon and hydrogen (and nitrogen, if present)] data accurate within 0.5 %, should be reported for new compounds. HRMS data should be given in format as is usually given for combustion analysis: calculated mass for given formula following with observed mass: (+)ESI-HRMS *m*/*z*: [molecular formula + H]$^+$ calculated mass, observed mass. Example: (+)ESI-HRMS *m*/*z*: calculated for [$C_{13}H_8BrCl_2N + H^+$] 327.92899, observed 327.92792.

NOTE: in certain cases, a crystal structure may be an acceptable substitute for HRMS/elemental analysis.

Biomacromolecules. The structures of biomacromolecules may be established by providing evidence about sequence and mass. Sequences may be inferred from the experimental order of amino acid, saccharide, or nucleotide coupling, from known sequences of templates in enzyme-mediated syntheses, or through standard sequencing techniques. Typically, a sequence will be accompanied by MS data that establish the molecular weight.

Example: Product was isolated upon column chromatography [dry flash (SiO_2, eluent EA, EA/MeOH gradient 95/5 → 9/1, EA/MeOH/NH_3 gradient 18/0.5/0.5 → 9/1/1, and flash chromatography (Biotage SP1, RP column, eluent MeOH/H_2O gradient 75/25 → 95/5, N-H column, eluent EA/Hex gradient 6/3 → EA). was obtained after flash column chromatography (Biotage SP NH column, eluent hexane/EA 4:6 → 2:6). Yield 968.4 mg (95 %). Colorless foam softens at 96-101 °C. $[\alpha]^{20}$; D = +0,163 (c =2.0×10^{-3} g/mL, CH_2Cl_2). IR (ATR): 3376w, 2949m, 2868w, 2802w, 1731s, 1611w, 1581s, 1528m, 1452m, 1374s, 1331w, 1246s, 1171m, 1063w, 1023m, 965w, 940w, 881w, 850w, 807w, cm^{-1}. ^1H NMR (500 MHz, $CDCl_3$, δ): 8.46 (*d*, 1H, J = 5.4, H-2'), 7.89 (*s*, 1H, J = 2.0, H-8'), 7.71 (*d*, 1H, J = 8.9, H-5'), 7.30 (*dd*, 1H, J_1 = 8.8, J_2 = 2.1, H-6'), 6.33 (*d*, 1H, J = 5.4, H-3'), 6.07 (*s*, HN-Boc, exchangeable with D_2O), 5.06 (*s*, 1H, H-12), 4.92-4.88 (*m*, 1H, H-7), 4.42 (*bs*, H-3), 3.45 (*s*,CH_3-N), 3.33 (*bs*, H-9'), 3.05-2.95 (*m*, 2H, H-11'), 2.70-2.43 (*m*, 2H, H-24) and HN, exchangeable with D_2O), 2.07 (*s*, CH_3COO), 2.04 (*s*, CH_3COO), 1.42 (*s*, 9H, $(CH_3)_3$C-N(Boc)), 0.88 (*s*, 3H, CH_3-10), 0.79 (*d*, 3H,J = 6.6, CH_3-20), 0.68 (*s*, 3H, CH_3-13). ^{13}C NMR (125 MHz, $CDCl_3$, δ): 170.34, 170.27, 151.80, 149.92, 148.87, 134.77, 128.36, 125.11, 121.43, 117.29, 99.98, 75.41, 70.82, 50.43, 49.66, 47.60, 47.33, 44.97, 43.30, 41.83, 41.48, 37.65, 36.35, 35.44, 34.89,

34.19, 33.23, 31.24, 28.79, 28.35, 27.25, 26.45, 25.45, 22.74, 22.63, 21.57, 21.31, 17.85, 12.15. (+)ESI-HRMS (*m/z*): calculated for $[C_{45}H_{67}ClN_4O_6 + H]^+$ 795.48219, observed 795.48185. Combustion analysis for $C_{45}H_{67}ClN_4O_6$: Calculated. C 67.94, H 8.49, N 7.04; found C 67.72, H 8.63, N 6.75. HPLC purity: method A: RT 1.994, area 99.12 %; method C: RT 9.936, area 98.20 %.

Purity **-** Evidence for documenting compound purity should include one or more of the following:

a) Well-resolved high field 1D ^{1}H NMR spectrum showing at most only trace peaks not attributable to the assigned structure and a standard 1D proton-decoupled ^{13}C NMR spectrum. Copies of the spectra should be included as figures in the Supporting Information.
b) Quantitative gas chromatographic analytical data for distilled or vacuum-transferred samples, or quantitative HPLC analytical data for materials isolated by column chromatography or separation from a solid support. HPLC analyses should be performed in two diverse systems. The stationary phase, solvents (HPLC), detector type, and percentage of total chromatogram integration should be reported; a copy of the chromatograms may be included as a figure in the Supporting Information.
c) Electrophoretic analytical data obtained under conditions that permit observing impurities present at the 5 % level.

HRMS data may be used to support a molecular formula assignment **but cannot be used as a criterion of purity**.

4. Biological Data

Quantitative biological data are required for all tested compounds. Biological test methods must be referenced or described in sufficient detail to permit the experiments to be repeated by others. Detailed descriptions of biological methods should be placed in the experimental section. Standard compounds or established drugs should be tested in the same system for comparison. Data may be presented as numerical expressions or in graphical form; biological data for extensive series of compounds should be presented in tabular form. Tables consisting primarily of negative data will not usually be accepted; however, for purposes of documentation they may be submitted as supporting information. Active compounds obtained from combinatorial syntheses should be resynthesized and retested to verify that the biology conforms to the initial observation.

Statistical limits (statistical significance) for the biological data are usually required. If statistical limits cannot be provided, the number of determinations and some indication of the variability and reliability of the results should be given. References to statistical methods of calculation should be included. Doses and concentrations should be expressed as molar quantities (*e.g.*, mol/kg, μmol/kg, M, mM). The routes of administration of test compounds and vehicles used should be indicated, and any salt forms used (hydrochlorides, sulfates, *etc.*) should be noted. The physical state of the compound dosed (crystalline, amorphous; solution, suspension) and the formulation for dosing (micronized, jet-milled, nanoparticles) should be indicated. For those compounds found to be inactive, the highest concentration (*in vitro*) or dose level (*in vivo*) tested should be indicated.

- The RESULTS AND DISCUSSION should include concisely presented results and there significance discussed and compared to relevant literature data. The results and discussion may be combined or kept separate.
- The inclusion of a CONCLUSION section, which briefly summarizes the principal conclusions, is recommended.
- NOMENCLATURE is optional but, if the authors wish, a list of employed symbols may be included.
- REFERENCES should be numbered sequentially as they appear in the text. Please note that any reference numbers appearing in the Illustrations and/or Tables and corresponding captions must follow the numbering sequence of the paragraph in which they appear for the first time. When cited, the reference number should be superscripted in Font 12, following any punctuation mark. In the reference list, they should be in normal position followed by a full stop. Reference entry must not be formatted using Carriage returns (enter key; ↵ key) or multiple space key. The formatting of references to published work should follow the *Journal'*s style as follows:

Journals[a]:	A. B. Surname1, C. D. Surname2, *J. Serb. Chem. Soc.* **Vol** (Year) first page Number (https://doi.org/doi)[b]
Books:	A. B. Surname1, C. D. Surname2, *Name of Book*, Publisher, City, Year, pp. 100-101 (https://doi.org/doi)[b]
Compilations:	A. B. Surname1, C. D. Surname2, in *Name of Compilation*, A. Editor1, C. Editor2, Ed(s)., Publisher, City, Year, p. 100 (https://doi.org/doi)[b]
Proceedings:	A. B. Surname1, C. D. Surname2, in *Proceedings of Name of the Conference or Symposium*, (Year), Place of the Conference, Country, *Title of the Proceeding*, Publisher, City, Year, p. or Abstract No. 100
Patents:	A. B. Inventor1, C. D. Inventor2, (Holder), Country Code and patent number (registration year)
Chemical Abstracts:	A. B. Surname1, C. D. Surname2, *Chem. Abstr*. CA 234 567a; For non-readily available literature, the Chemical Abstracts reference should be given in square brackets: [C.A. 139/2003 357348t] after the reference
Standards:	EN ISO 250: *Name of the Standard* (Year)
Websites:	Title of the website, URL in full (date accessed)

[a] When citing Journals, the International Library Journal abbreviation is required. Please consult, *e.g.*, https://images.webofknowledge.com/WOK46/help/WOS/A_abrvjt.html

[b] doi should be replaced by doi number of the Article, for example: http://dx.doi.org/10.2298/JSC161212085B (as active link). If doi do not exist, provide the link to the online version of the publication.

Only the last entry in the reference list should end with a full stop.

The names of all authors should be given in the list of references; the abbreviation *et al.* may only be used in the text. The original journal title is to be retained in the case of publications published in any language other than English (please denote the language in parenthesis after the reference). Titles of publications in non-Latin alphabets should be transliterated. Russian references are to be transliterated using the following transcriptions:

ж→zh, х→kh, ц→ts, ч→ch, ш→sh, щ→shch, ы→y, ю→yu, я→ya, э→e, й→i, ь→’.

Supplementary material

Authors are encouraged to presentthe information and results non-essential to the understanding of their paper as SUPPLEMENTARY MATERIAL (can be uploaded inStep 4 of Online Submission). This material may include as a rule, but is not limited to, the presentation of analytical and spectral data demonstrating the identity and purity of synthesized compounds, tables containing raw data on which calculations were based, series of figures where one example would remain in the main text, etc. The Editorial Board retain the right to assign such information and results to the Supplementary material when deemed fit. Supplementary material does not appear in printed form but can be downloaded from the web site of the JSCS.

Mathematical and chemical equations should be given in separate lines and must be numbered, Arabic numbers, consecutively in parenthesis at the end of the line. All equations should be embedded in the text Complex equations (fractions, integrals, matrix…) should be prepared with the aid of the Microsoft Equation 3.0 (or higher) or MathType (Do not use them to create simple equations and labels). Using the Insert -> Equation option, integrated in MS Office 2010 and MS Office 2013, as well as insertion of equation objects within paragraph text IS NOT ALLOWED.

Deposition of crystallographic data

Prior to submission, the crystallographic data included in a manuscript presenting such data should be deposited at the appropriate database. Crystallographic data associated with organic and metal-organic structures should be deposited at the Cambridge Crystallographic Data Centre (CCDC) by e-mail to **deposit@ccdc.cam.ac.uk**

Crystallographic data associated with inorganic structures should be deposited with the Fachinformationszentrum Karlsruhe (FIZ) by e-mail to **crysdata@fiz-karlsruhe.de**. A deposition number will then be provided, which should be added to the reference section of the manuscript.

For detailed instructions please visit the JSCS website:
https://www.shd-pub.org.rs/index.php/JSCS/Instructions

ARTWORK INSTRUCTIONS

JSCS accepts only **TIFF** or **EPS** formats, as well as **JPEG** format (only for colour and greyscale photographs) for electronic artwork and graphic files. **MS files** (Word, PowerPoint, Excel, Visio) **NOT acceptable**. Generally, scanned instrument data sheets should be avoided. Authors are responsible for the quality of their submitted artwork. Every single Figure or Scheme, as well as any part of the Figure (A, B, C…) should be prepared according to following instructions (every part of the figure, A, B, C…, must be submitted as an independent single graphic file):

TIFF

Virtually all common artwork and graphic creation software is capable of saving files in TIFF format. This 'option' can normally be found under 'the 'Save As...' or 'Export...' commands in the 'File' menu.

TIFF (Tagged Image File Format) is the recommended file format for bitmap, greyscale and colour images.

- Colour images should be in the RGB mode
- When supplying TIFF files, please ensure that the files are supplied at the correct resolution:
    1. Line artwork: minimum of 1000 dpi
    2. RGB image: minimum of 300 dpi
    3. Greyscale image: minimum of 300 dpi
    4. Combination artwork (line/greyscale/RGB): minimum of 500 dpi
- Images should be tightly cropped, without frame and any caption.
- If applicable please re-label artwork with a font supported by JSCS (Arial, Helvetica, Times, Symbol) and ensure it is of an appropriate font size.
- Save an image in TIFF format with LZW compression applied.
- It is recommended to remove Alpha channels before submitting TIFF files.
- It is recommended to flatten layers before submitting TIFF files.

Please be sure that quality of an image cannot be increased by changing the resolution from lower to higher, but only by rescanning or exporting the image with higher resolution, which can be set in usual "settings" facilities.

EPS

Virtually all common artwork creation software, such as Canvas, ChemDraw, CorelDraw, SigmaPlot, Origin Lab…, are capable of saving files in EPS format. This 'option' can normally be found under the 'Save As...' or 'Export...' commands in the 'File' menu.

For vector graphics, EPS (Encapsulated PostScript) files are the preferred format as long as they are provided in accordance with the following conditions:

- when they contain bitmap images, the bitmaps should be of good resolution (see instructions for TIFF files)
- when colour is involved, it should be encoded as RGB
- an 8-bit preview/header at a resolution of 72 dpi should always be included
- embed fonts should always included and only the following fonts should be used in artwork: Arial, Helvetica, Times, Symbol
- the vertical space between the parts of an illustration should be limited to the bare necessity for visual clarity
- no data should be present outside the actual illustration area
- line weights should range from 0.35 pt to 1.5 pt
- when using layers, they should be reduced to one layer before saving the image (Flatten Artwork)

JPEG

Virtually all common artwork and graphic creation software is capable of saving files in JPEG format. This 'option' can normally be found under 'the 'Save As...' or 'Export...' commands in the 'File' menu.

JPEG (Joint Photographic Experts Group) is the acceptable file format **only for colour and greyscale photographs**. JPEG can be created with respect to photo quality (low, medium, high; from 1 to 10), ensuring file sizes are kept to a minimum to aid easy file transfer. Images should have a minimum resolution of 300 dpi. Image width: minimum 3.0 cm; maximum 12.0 cm.

Please be sure that quality of an image cannot be increased by changing the resolution from lower to higher, but only by rescanning or exporting the image with higher resolution, which can be set in usual "settings" facilities.

SIZING OF ARTWORK

- JSCS aspires to have a uniform look for all artwork contained in a single article. Hence, it is important to be aware of the style of the journal.
- Figures should be submitted in black and white or, if required, colour (charged). If coloured figures or photographs are required, this must be stated in the cover letter and arrangements made for payment through the office of the Serbian Chemical Society.
- As a general rule, the lettering on an artwork should have a finished, printed size of 11 pt for normal text and no smaller than 7 pt for subscript and superscript characters. Smaller lettering will yield a text that is barely legible. This is a rule-of-thumb rather than a strict rule. There are instances where other factors in the artwork, (for example, tints and shadings) dictate a finished size of perhaps 10 pt. Lines should be of at least 1 pt thickness.
- When deciding on the size of a line art graphic, in addition to the lettering, there are several other factors to address. These all have a bearing on the reproducibility/readability of the final artwork. Tints and shadings have to be printable at the finished size. All relevant detail in the illustration, the graph symbols (squares, triangles, circles, *etc*.) and a key to the diagram (to explain the explanation of the graph symbols used) must be discernible.
- The sizing of halftones (photographs, micrographs,...) normally causes more problems than line art. It is sometimes difficult to know what an author is trying to emphasize on a photograph, so you can help us by identifying the important parts of the image, perhaps by highlighting the relevant areas on a photocopy. The best advice that can be given to graphics suppliers is not to over-reduce halftones. Attention should also be paid to magnification factors or scale bars on the artwork and they should be compared with the details inside. If a set of artwork contains more than one halftone, again please ensure that there is consistency in size between similar diagrams.

General sizing of illustrations which can be used for the Journal of the Serbian Chemical Society:

- Minimum fig. size: 30 mm width
- Small fig. size - 60 mm width
- Large fig. size - 90 mm width
- Maximum fig. size - 120 mm width

Pixel requirements (width) per print size and resolution for bitmap images:

	Image width	A	B	C
Minimal size	30 mm	**354**	**591**	**1181**
Small size	60 mm	**709**	**1181**	**2362**
Large size	90 mm	**1063**	**1772**	**3543**
Maximal size	120 mm	**1417**	**2362**	**4724**

A: 300 dpi > RGB or Greyscale image
B: 500 dpi > Combination artwork (line/greyscale/RGB)
C: 1000 dpi> Line artwork

The designation of physical quantities and graphs formatting

The designation of physical quantities on figures must be in italic, whereas the units are in upright letters. They should be in Times New Roman font. In graphs a slash should be used to separate the designation of a physical quantity from the unit (example: p / kPa, t °C, T_0 / K, τ / h, ln (j / mA cm^{-2})…). Designations such as: p (kPa), t [min]…, are not acceptable. However, if the full name of a physical quantity is unavoiable, it should be given in upright letters and separated from the unit by a comma (example: Pressure, kPa, Temperature, K…). Please do not use the axes of graphs for additional explanations; these should be mentioned in the figure captions and/or the manuscript (example: "pressure at the inlet of the system, kPa" should be avoided). The axis name should follow the direction of the axis (the name of y-axis should be rotated by 90°). Top and right axes should be avoided in diagrams, unless they are absolutely necessary. Decimal numbers must have decimal points and not commas in the axis labels in graphical presentations of results. Thousands are separated, if at all, by a comma and not a point.

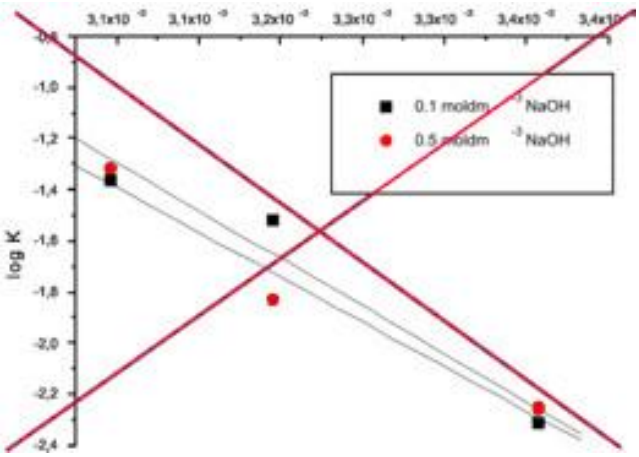

INCORRECT

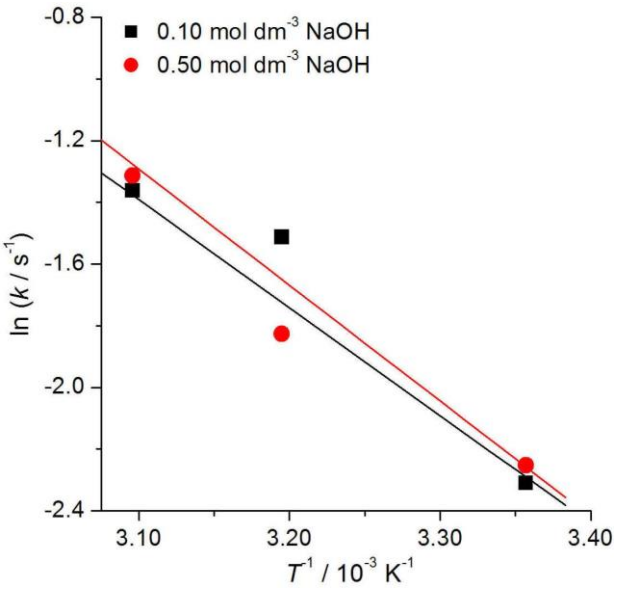

CORRECT

Journal of the Serbian Chemical Society
JSCS-info@shd.org.rs • www.shd.org.rs/JSCS

J. Serb. Chem. Soc. Vol. 87, No. 11 (2022)

CONTENTS*

Published by the Serbian Chemical Society
Karnegijeva 4/III, P.O. Box 36, 11120 Belgrade, Serbia
Printed by the Faculty of Technology and Metallurgy
Karnegijeva 4, P.O. Box 35-03, 11120 Belgrade, Serbia

* For colored figures in this issue please see electronic version at the Journal Home Page: http://www.shd.org.rs/JSCS/

Journal of the Serbian Chemical Society
JSCS@tmf.bg.ac.rs • www.shd.org.rs/JSCS
J. Serb. Chem. Soc. *87* (11) 1237–1244 (2022)
JSCS–5590
Original scientific paper
Published 10 October 2022

HPTLC-based metabolomics for the investigation of metabolic changes during plant development: The case study of *Artemisia annua*

JOVANA STANKOVIĆ JEREMIĆ[1]*, DEJAN GOĐEVAC[1], STEFAN IVANOVIĆ[1], KATARINA SIMIĆ[1], ANTOANETA TRENDAFILOVA[2], MILICA AĆIMOVIĆ[3] and SLOBODAN MILOSAVLJEVIĆ[4,5#]

[1]*University of Belgrade – Institute of Chemistry, Technology and Metallurgy – National Institute of the Republic of Serbia, 11000 Belgrade, Serbia,* [2]*Institute of Organic Chemistry with Centre of Phytochemistry, Bulgarian Academy of Sciences, 1113 Sofia, Bulgaria,* [3]*Institute of Field and Vegetable crops, 21000 Novi Sad, Serbia and* [4]*University of Belgrade – Faculty of Chemistry, Studentski trg 12–16, 11000 Belgrade, Serbia and* [5]*Serbian Academy of Sciences and Arts, Knez Mihailova 35,11000 Belgrade, Serbia*

(Received 7 May, revised 12 November 2021, accepted 14 February 2022)

Abstract: The application of high performance thin layer chromatography (HPTLC)-based non-targeted metabolomics as a holistic approach to compare fingerprints of metabolite changes during *Artemisia annua* development is described. Images of HPTLC chromatograms obtained after derivatization with anisaldehyde-sulphuric acid reagent were used as a dataset for multivariate analysis. Principal component analysis and orthogonal partial least squares discriminant analysis confirmed the differentiation of samples belonging to vegetative phase, flowering stage, and seed formation stage of the plant development. The obtained results showed that the HPTLC-based metabolomics approach can be a very reliable technique for the investigation of metabolic changes during plant development, complementary to gas chromatography–mass spectrometry and nuclear magnetic resonance-based metabolomics.

Keywords: plant metabolomics; PCA; OPLS-DA.

INTRODUCTION

In this study, the cultivated *Artemisia annua* was used as a model system for the assessment the application of high performance thin layer chromatography (HPTLC) based untargeted metabolomics to probe unique metabolites during the life cycle of the plant. Since the discovery of its constituent antimalarial artemisinin, *A. annua*, which is the only viable resource of this drug, has been the

* Corresponding author. E-mail: jovanas@chem.bg.ac.rs
# Serbian Chemical Society member.
https://doi.org/10.2298/JSC210507007S

subjects of extensive research on its chemical composition. More than 600 secondary metabolites have been identified throughout the plant including several sesquiterpenoids, triterpenoids, monoterpenoids, steroids, flavonoids, coumarins, alkaloids and benzenoids.[1,2] The method of untargeted metabolomics considers simultaneous measurement of as many metabolites as possible from each sample, thus providing a holistic, general overview of a sample composition.[3] HPTLC is an emerging analytical tool in metabolomics research in the last decade.[4,5] Even conventional thin layer chromatography (TLC) offers the advantages over other analytical methods, such as short measuring time and capability of parallel analysis, and the availability of chemical reagents. Many improvements in HPTLC over conventional TLC such as high resolution and data robustness, also improved some metabolomics and profiling studies. Furthermore, metabolites which are difficult to be identified by nuclear magnetic resonance (NMR) or mass spectrometry (MS)-based methods could be visualized on HPTLC plates and isolated from the plate for further chemical elucidation.[6] The main idea of this study is the application of an HPTLC-based non-targeted metabolomics as a holistic approach to compare fingerprints of metabolites changing during the plant development.

EXPERIMENTAL

General methods

All used solvents were of analytical grade. Glass HPTLC silica gel 60 CN F254s plates 10 cm×20 cm were purchased from Merck (Darmstadt, Germany); anisaldehyde-sulphuric acid used as a spray reagent was freshly made according to Wagner *et al.*[7] Artemisinin standard was isolated previously in the laboratory of Bulgarian Academy of Sciences. All NMR spectra (^{1}H, ^{13}C, correlated spectroscopy (COSY), heteronuclear single quantum coherence (HSQC) and heteronuclear multiple bond coherence (HMBC)) were recorded in $CDCl_3$ (with tetramethylsilane (TMS) for referencing) on a Bruker Avance III 500 NMR spectrometer operating at a proton NMR frequency of 500.26 MHz, equipped with a 5 mm broadband probe (BBI) probehead. Gas chromatography (GC)/MS analyses were performed according to Stankovic *et al*. (2019)[8] with some modifications of the temperature program and split ratio. The oven temperature was programmed from 60 to 240 °C at 3 °C/min, then from 240 to 310 °C at 35 °C/min, and then held isothermally for 8 min.

Injection volume was 1 μL, split ratio, 20:1. For lipid fraction the oven temperature was kept constant at 40 °C for 1 min, then was linearly programmed from 40 to 315 °C at 10 °C/min and then held isothermally for 6.5 min. Injection volume was 1 μL, split ratio 50:1.

Plant material

Artemisia annua L. is grown at Institute of Field and Vegetable Crops, Novi Sad. The plants samples were collected 14 times at intervals of 7 or 14 days, successively in different phenophases – from May 27 to November 3, 2018. Thus, vegetative phase (collections 1–6), flowering stage (collections 7–11), and seed formation stage (collections 12–14) were collected. The Voucher specimens (determined by Milica Rat, M.Sc., as No. 2-1514) were confirmed and deposited at the Herbarium of the Department of Biology and Ecology (BUNS Herbarium), Faculty of Natural Sciences, University of Novi Sad.

Extraction of plant material

Dry and ground plant materials of each collection (150 mg) were extracted with a mixture of hexane:ethyl acetate, 95:5 volume ratio (1 mL) for 15 min in an ultrasound water bath. The extracts were centrifuged for 15 min at 13,600 rpm. The extraction procedure was independently repeated with four biological replicates of each collection. The obtained extracts were used for HPTLC analysis.

HPTLC analysis

The 3 μL of the extracts were sprayed with a 25-μL syringe as an 7-mm band on the HPTLC plate using the Linomat 5 (CAMAG, Switzerland). The application position *Y* was 8.0 mm, the first application position *X* was 10.0 mm, and the distance between tracks was 10.0 mm. The plates were developed in a previously saturated CAMAG automatic developing chamber 2 with a mobile phase consisting of hexane:ethyl acetate:formic acid (19:11:0.5 volume ratio). After a drying time of 4 min developed HPTLC plates were derivatized by dipping in the anisaldehyde reagent (CAMAG chromatogram immersion device 3), followed by heating at 100 °C for 5 min.

Fractionation by dry-column flash chromatography

Dry and ground average samples of all collections (167.0 g) were extracted with hexane:ethyl acetate, 95:5 volume ratio(2×600 mL) for 15 min in an ultrasound water bath. The extracts were combined, filtered, and concentrated under reduced pressure to give 1.1 g of residue. Dry-column flash chromatography fractionation was performed in a glass column (300 mm×22 mm) packed with silica gel (100 g Merck, <0.08 mm) using a water vacuum pump. The column was equilibrated with the mobile phase *n*-hexane:ethyl acetate (95:5 volume ratio) mixture. The extract (m = 1.1 g) was diluted with the mobile phase (1:1) before applying to the column. The elution was performed with hexane:ethyl acetate mixture with increasing polarity (Table S-I, Supplementary material to this paper) and 34 fractions were collected.

Methylation of non-polar lipid fraction with MeOH/H_2SO_4

A mixture of the lipid fraction (30 mg) and MeOH (6 mL+ two drops of conc. H_2SO_4) was refluxed in a test tube fitted with condenser for 2 h. After neutralization with saturated sodium bicarbonate solution, the methyl esters were extracted with *n*-hexane. The organic layer was dried over anhydrous Na_2SO_4 and evaporated under reduced pressure in a rotavapor.

Image and multivariate data analysis

The HPTLC chromatograms were processed with the Image J processing program (version 1.47q). The chromatograms were denoised using the median filter function with two pixels width filter, and the tracks were outlined with rectangular selection tool. The line profile plots (gray scale) were generated using Plot Profile option for each sample. On this way, two-dimensional graphs containing the pixel intensities toward distance along the line were obtained. The HPTLC image data were then normalized to the total area, mean centred and pareto scaled. Principal component analysis (PCA) and orthogonal partial least squares to latent structures – discriminant analysis (OPLS-DA) method was performed with SIMCA software (version 15, Sartorius, Göttingen, Germany).

RESULTS AND DISCUSSION

The HPTLC conditions regarding amount of sample applied and mobile phase composition were optimised to detect the maximum number of resolved

bands per sample. Four biological replicates for each of the 14 collections of *A. annua* were then fingerprinted using the HPTLC method. Thus, vegetative phase (collections 1-6), flowering stage (collections 7–11), and seed formation stage (collections 12–14), were covered. The fingerprint patterns visualized after derivatization with anisaldehyde-sulphuric acid reagent are depicted in Fig. 1.

Fig. 1. HPTLC metabolic fingerprint of 14 samples (red) *A. annua* collected in different developmental stages.

For the identification of the components found in the studied extracts, dry-column flash chromatography of the plant extract was used, followed by NMR and/or GC/MS analyses. As a result of the purification, the isolated fractions appeared as a single band on HPTLC plate. Each band of the purified fraction was then connected to those of *A. annua* extracts by co-chromatography comprising their R_F values and colours after derivatization (Table I). The identity of the purified metabolites was then performed by NMR and/or GC/MS analyses (Supplementary material). Only artemisinin was not isolated as a pure compound, and its HPTLC band was compared to that of the standard compound.

TABLE I. Identified metabolites in *A. annua* extracts

No.	R_F value	Identified metabolites	Colour after derivatization	Identification
1	0.94	Triacylglycerol	Dark green	NMR; GC/MS after transesterification
2	0.86	α-Pinene, α-copaene, caryophyllene E and β-selinene	Purple	GC/MS
3	0.78	Artemisia ketone	Orange	NMR; GC/MS
4	0.68	1,8-Cineole	Purple	GC/MS
5	0.66	Caryophyllene oxide	Purple	GC/MS
6	0.58	Artemisia alcohol	Dark green	GC/MS
7	0.46	Artemisinin	Pink	Comparison to standard
8	0.20	Arteannuin B	Pink	GC/MS

The line profile plots generated from the images obtained using visible light were used as a dataset for multivariate analysis. Firstly, the principal component analysis (PCA), as a variable reduction technique to develop a smaller number of novel variables that will account for most of the variation in the observed variables, was performed. It has resulted in five principal components (PCs) model explaining 84.3 % of the total data of variances.

Based on PCA score plot (Fig. 2A), three groups of samples were separated to some extent, according to the plant development stages.

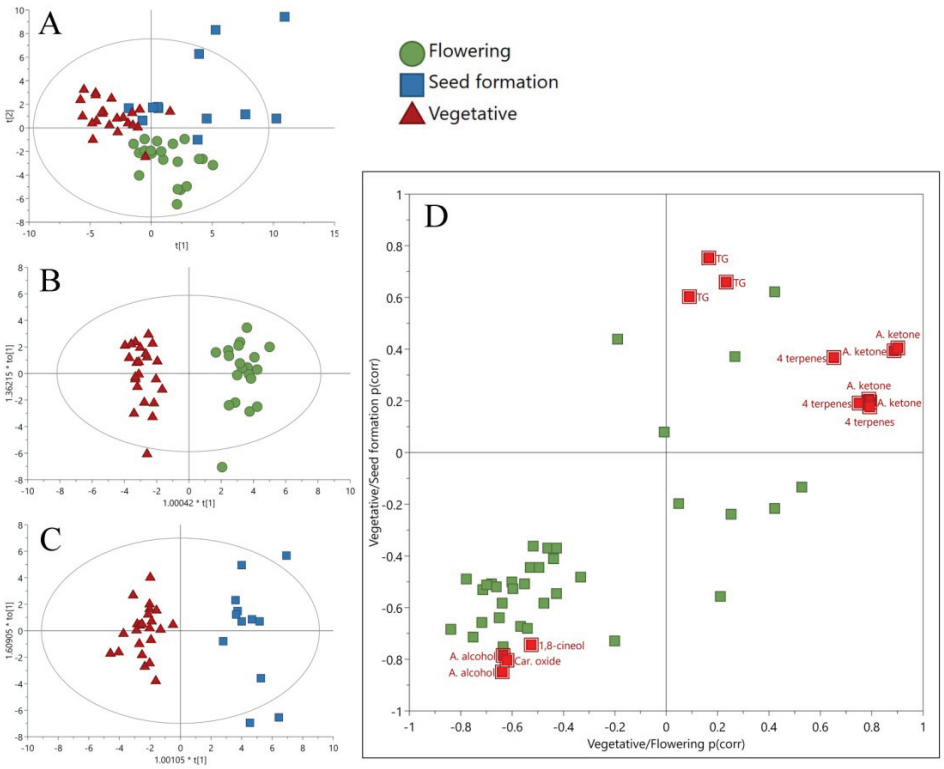

Fig. 2. A) PCA score plot; B) OPLS-DA score plot containing vegetative and flowering phase of *A. annua*; C) OPLS-DA score plot containing vegetative and seed formation phase of *A. annua*; D) OPLS-DA SUS-plot, all obtained from HPTLC fingerprints; four (4) terpenes: α-pinene, α-copaene, caryophyllene E and β-selinene.

Next, the orthogonal partial least squares to latent structures–discriminant analysis (OPLS-DA) was applied, where novel variables will account for the maximum separation between predefined classes. An additional advantage of the orthogonal model is the facilitated interpretation due to separation of the systematic variation of the variables into two parts: one linearly related to class information and one orthogonal to the class information.[9] Two OPLS-DA models were

created containing HPTLC data of: a) vegetative phase versus flowering stage and b) vegetative phase versus seed formation stage of *A. annua* development. The quality of the obtained models was assessed by goodness of fit (R^2) indicating how well the variation of variables is explained using the predictive components and predictive ability of the model (Q^2), indicating how well the model predicts new data, estimated by cross validation. In both created OPLS-DA models, large R^2 and Q^2 values over 0.5 and close to 1 indicated high goodness of fit and good predictivity (Table II).

TABLE II. Parameters of the OPLS-DA models

Model	Number of components (predictive + orthogonal)	R^2	Q^2	p (CV-NOVA)	F (CV-ANOVA)
Vegetative/ Flowering	1 + 4	0.951	0.897	4.88×10^{-13}	28
Vegetative/ Seed formation	1 + 3	0.918	0.784	6.45×10^{-7}	12

The models were validated by permutation tests and CV-ANOVA, the significance of the models was clearly shown with p values far less than 0.05 (Table II). In the score plots (Fig. 2B and C) a clear separation between the samples was obtained along to the predictive components. The most influential variables were selected based on the variable influence on projection (*VIP*) scores of the predictive components, and the loadings scaled as a correlation coefficient (p(corr)). $VIP > 1$ and $|p(\text{corr})| > 0.5$ were considered as important for the separation. Shared and unique structure plot (SUS-plot) containing p(corr) from both OPLS-DA models was used to reveal the changes in the metabolomes in each of the three predefined group of samples (Fig. 2D). The unique metabolites were found close to either the X or Y axis, and the shared were located on the diagonals. Also, the metabolites which are on the extreme ends of the axes contribute more significantly than those close to the centre. Thus, the accumulation of triacylglycerol (**1**) is characteristic for the seed formation phase since it is an unique metabolite in Vegetative/Seed formation model. Similarly, four terpenes (α-pinene (**2**), α-copaene (**2**), caryophyllene E (**2**) and β-selinene (**2**)) and artemisia ketone (**3**) were accumulated in the flowering stage since they are unique metabolites in the vegetative/flowering model. Artemisia alcohol (**6**), caryophyllene oxide (**5**), and 1,8-cineole (**4**) were the main metabolites in the vegetative stage, since they are shared in both models. For artemisinin (**7**) and arteannuin B (**8**) there was no significant change in their amount during plant development.

Metabolomics fingerprinting of *A. annua* in different stages of development has also been performed previously by GC/MS.[10] Our objective was to highlight the advantages of HPTLC: no need for derivatization prior to chromatography,

and thus detection of thermolabile and non-volatile metabolites, which is not possible using GC/MS. HPTLC is also complementary technique to NMR-based metabolomics, offering solutions where crowded regions in the NMR spectra are difficult to resolve.[4]

CONCLUSION

This work presents an efficient way for analysing metabolic fingerprinting data of *A. annua* L. generated by HPTLC. As a result, we demonstrated that HPTLC may be applied as a simple and reliable untargeted approach to rapidly differentiate the extracts originating from various developmental stages of the plant. HPTLC also demonstrated to be the method of choice for the routine study of complex matrices and could be used as an alternative and/or complementary method to techniques, such as GC/MS or NMR.

SUPPLEMENTARY MATERIAL

Additional data and information are available electronically at the pages of journal website: https://www.shd-pub.org.rs/index.php/JSCS/article/view/10744, or from the corresponding author on request.

Acknowledgments. The authors are grateful for the support from Joint Research Project between Serbian Academy of Science and Arts and Bulgarian Academy of Sciences, "Phytochemical investigation of secondary metabolites from plants and fungi and their biotransformed products".

ИЗВОД

МЕТАБОЛОМИКА БАЗИРАНА НА HPTLC ЗА ИСПИТИВАЊЕ МЕТАБОЛИЧКИХ ПРОМЕНА ТОКОМ РАЗВОЈА БИЉКЕ: СТУДИЈА СЛУЧАЈА *Artemisia annua*

ЈОВАНА СТАНКОВИЋ ЈЕРЕМИЋ[1], ДЕЈАН ГОЂЕВАЦ[1], СТЕФАН ИВАНОВИЋ[1], КАТАРИНА СИМИЋ[1], ANTOANETA TRENDAFILOVA[2], МИЛИЦА АЋИМОВИЋ[3] и СЛОБОДАН МИЛОСАВЉЕВИЋ[4,5]

[1]Универзитет у Београду, Институт за хемију технологију и металургију, Институт од националног значаја за Републику Србију, Студентски трг 12–16, 11000, Београд, [2]Institute of Organic Chemistry with Centre of Phytochemistry, Bulgarian Academy of Sciences, 1113 Sofia, Bulgaria, [3]Институт за ратарство и повртарство, 21000 Нови Сад, [4]Универзитет у Београду – Хемијски факултет, Студентски трг 16, 11000 Београд и [5]Српска академија наука и уметности, Кнез Михајлова 35, 11000, Београд

Описана је холистичка примена нетаргетне метаболомике базиране на високоефикасној танкослојној хроматографији (HPTLC) која омогућава поређење метаболичких профила *Artemisia annua* и праћење њихових промена током развоја биљке. HPTLC хроматограми након развијања анизалдехидом и сумпорном киселином су коришћени за генерисање података за мултиваријантну анализу. Анализа главних компоненти и ортогонална дискриминанта анализа најмањих квадрата су потврдиле разлике између узорака који припадају различитим фенофазама – вегетативној фази, фази цветања и фази формирања семена. Добијени резултати указују да метаболомички приступ заснован на HPTLC методи која је комплементарна са GC/MS и NMR анализом, може бити веома поуздана техника за анализу промене током развоја биљке.

(Примљено 7. маја, ревидирано 12. новембра 2021, прихваћено 14. фебруара 2022)

REFERENCES

1. V. Vajs, A. Jokić, S. Milosavljević, *Nat. Prod. Commun*. **12** (2017) 1157 (https://doi.org/10.1177/1934578X1701200802)
2. G. D. Brown, *Molecules* **15** (2010) 7603 (https://doi.org/10.3390/molecules15117603)
3. J. L. Wolfender, S. Rudaz, Y. H. Choi, H. K. Kim, *Curr. Med. Chem.* **20** (2013) 1056 (https://doi.org/10.2174/0929867311320080009)
4. L. F. Salomé-Abarca, M. Mandrone, C. Sanna, F. Poli, C. A. M. J. J. van der Hondel, P. G. L. Klinkhamer, Y. H. Choi, *Phytochemistry* **176** (2020) 112402 (https://doi.org/10.1016/j.phytochem.2020.112402)
5. M. Maldini, G. D'Urso, G. Pagliuca, G. L. Petretto, M. Foddai, F. R. Gallo, G. Multari, D. Caruso, P. Montoro, G. Pintore, *Foods* **8** (2019) 294 (https://doi.org/10.3390/foods8080294)
6. Y. Ge, X. Chen, D. Gođevac, P. C. P. Bueno, L. F. Salomé Abarca, Y. P.Jang, M. Wang, Y. H. Choi, *Planta Med*. **85** (2019) 917 (https://doi.org/10.1055/a-0947-5797)
7. H. Wagner, S. Bladt, E. M. Zgainski, *Plant Drug Analysis*, Springer-Verlag, Heidelberg, 1984 (https://doi.org/10.1007/978-3-662-02398-3)
8. J. Stanković, M. Novaković, V. Tešević, A. Ćirić, M. Soković, G. Zdunić, Z. Dajić-Stevanović, D. Gođevac, *J. Serb. Chem. Soc.* **84**, (2019) 1355 (https://doi.org/10.2298/JSC190513106S)
9. S. Wiklund, E. Johansson, L. Sjöström, E. J. Mellerowicz, U. Edlund, J. P. Shockcor, J. Gottfries, T. Moritz, J. Trygg, *Anal. Chem*. **80** (2008) 115 (https://doi.org/10.1021/ac0713510)
10. M. Chenfei, W. Huahong, L. Xin, X. Guowang, L. Benye, *J. Chromatogr., A* **1186** (2008) 412 (https://doi.org/10.1016/j.chroma.2007.09.023).

Journal of the Serbian Chemical Society
JSCS@tmf.bg.ac.rs • www.shd.org.rs/JSCS
J. Serb. Chem. Soc. 87 (11) S405–S421 (2022) *Supplementary material*

SUPPLEMENTARY MATERIAL TO

HPTLC-based metabolomics for the investigation of metabolic changes during plant development: The case study of *Artemisia annua*

JOVANA STANKOVIĆ JEREMIĆ[1]*, DEJAN GOĐEVAC[1], STEFAN IVANOVIĆ[1], KATARINA SIMIĆ[1], ANTOANETA TRENDAFILOVA[2], MILICA AĆIMOVIĆ[3] and SLOBODAN MILOSAVLJEVIĆ[4,5]

[1]*University of Belgrade – Institute of Chemistry, Technology and Metallurgy – National Institute of the Republic of Serbia, 11000 Belgrade, Serbia,* [2]*Institute of Organic Chemistry with Centre of Phytochemistry, Bulgarian Academy of Sciences, 1113 Sofia, Bulgaria,* [3]*Institute of Field and Vegetable crops, 21000 Novi Sad, Serbia and* [4]*University of Belgrade – Faculty of Chemistry, Studentski trg 12–16, 11000 Belgrade, Serbia and* [5]*Serbian Academy of Sciences and Arts, Knez Mihailova 35,11000 Belgrade, Serbia*

J. Serb. Chem. Soc. 87 (11) (2022) 1237–1244

Table S-I. Fractionation by dry-column flash (DF) chromatography

Number of fraction	Hexane:ethyl acetate volume ratio	Volume, mL
DF1-DF9	95:5	400
DF10-DF18	90:10	400
DF19-DF22	85:15	200
DF23-DF26	80:20	200
DF27-DF30	75:25	200
DF31-DF34	70:30	200

IDENTIFICATION OF THE COMPOUNDS – SPECTRAL DATA

Compounds on HPTLC plate (Fig. 1) Triacylglycerol retention factors, R_f = 0.92 – 0.96.

* Corresponding author. E-mail: jovanas@chem.bg.ac.rs

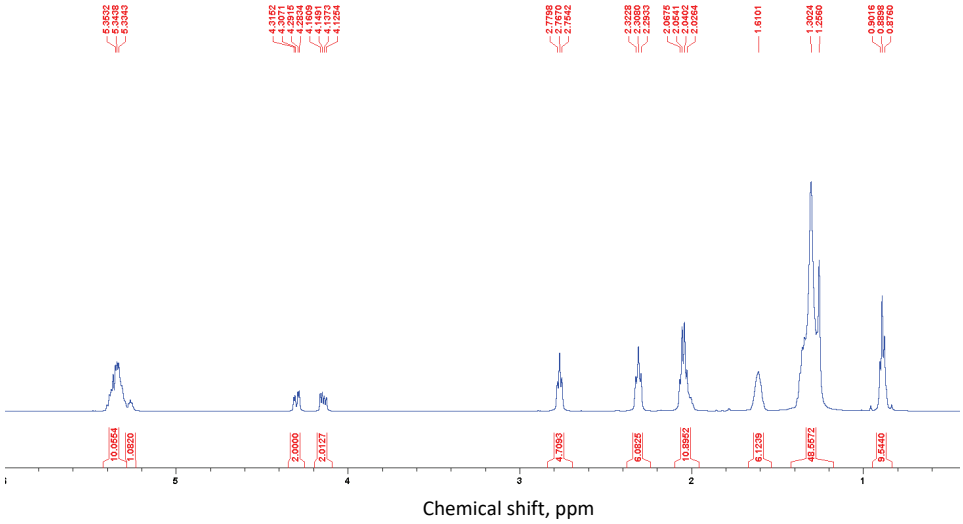

Fig. S-1. ^{1}H NMR spectrum of triacylglycerol.

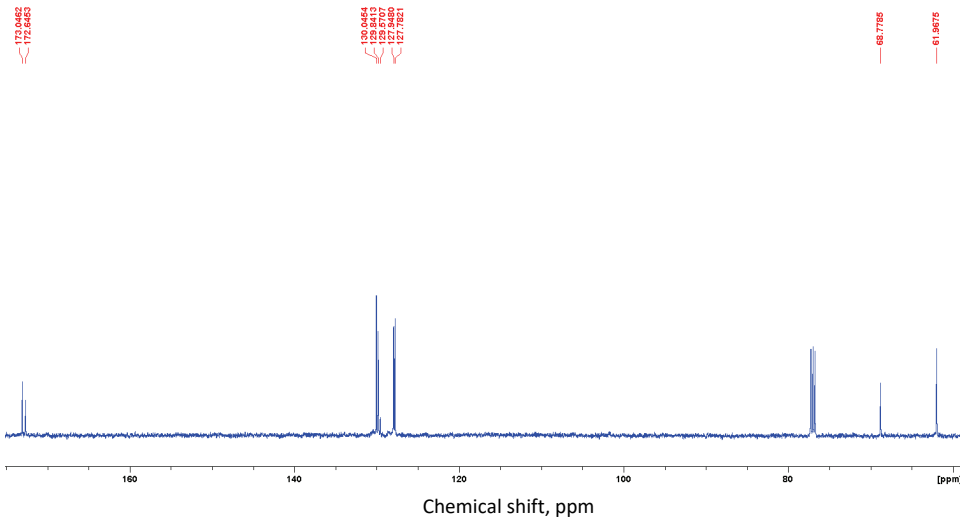

Fig. S-2. ^{13}C NMR spectrum of triacylglycerol.

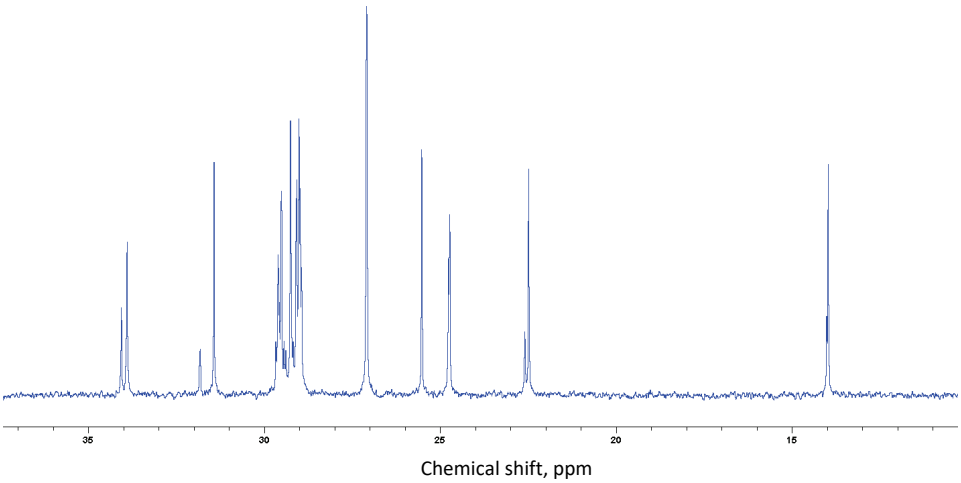

Fig. S-3. ^{13}C NMR spectrum of triacylglycerol.

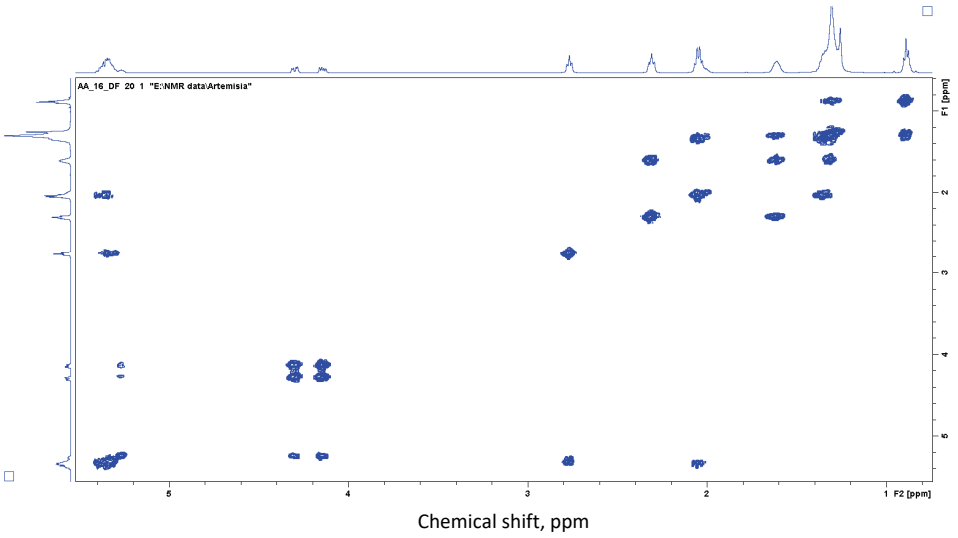

Fig. S-4. COSY spectrum of triacylglycerol.

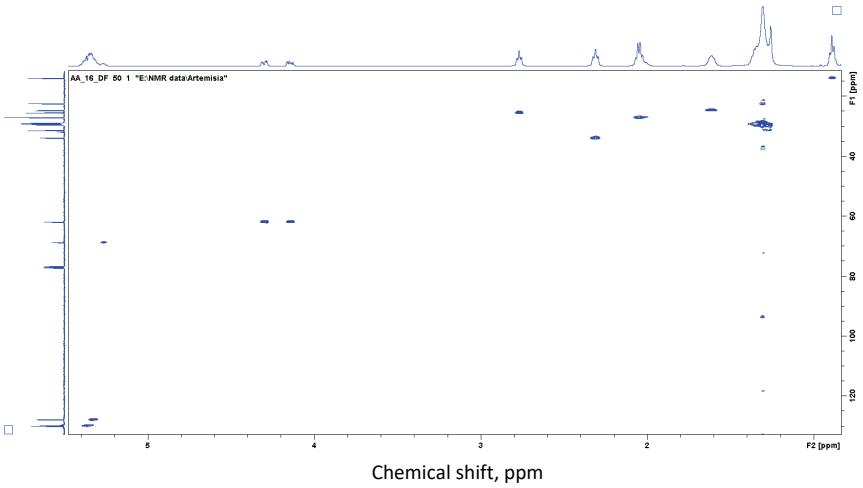

Fig. S-5. HSQC spectrum of triacylglycerol.

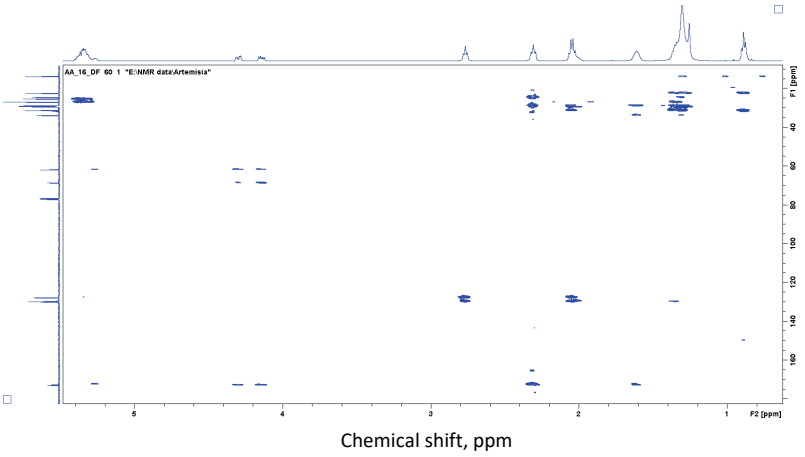

Fig. S-6. HMBC spectrum of triacylglycerol.

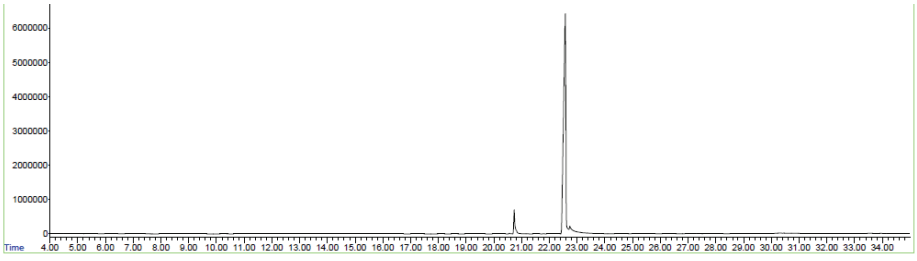

Fig S-7. GC-FID chromatogram of fraction DF16 containing Methyl palmitoleate (Retention time - *RT* = 20.560 min, Retenrion index - *RI* 1935), Methyl Palmitate (*RT* = 20.73 min, *RI* = 1950) and 9,12-Octadecadienoic acid (Z,Z)-, methyl ester (*RT* = 22.53 min, *RI* = 2116).

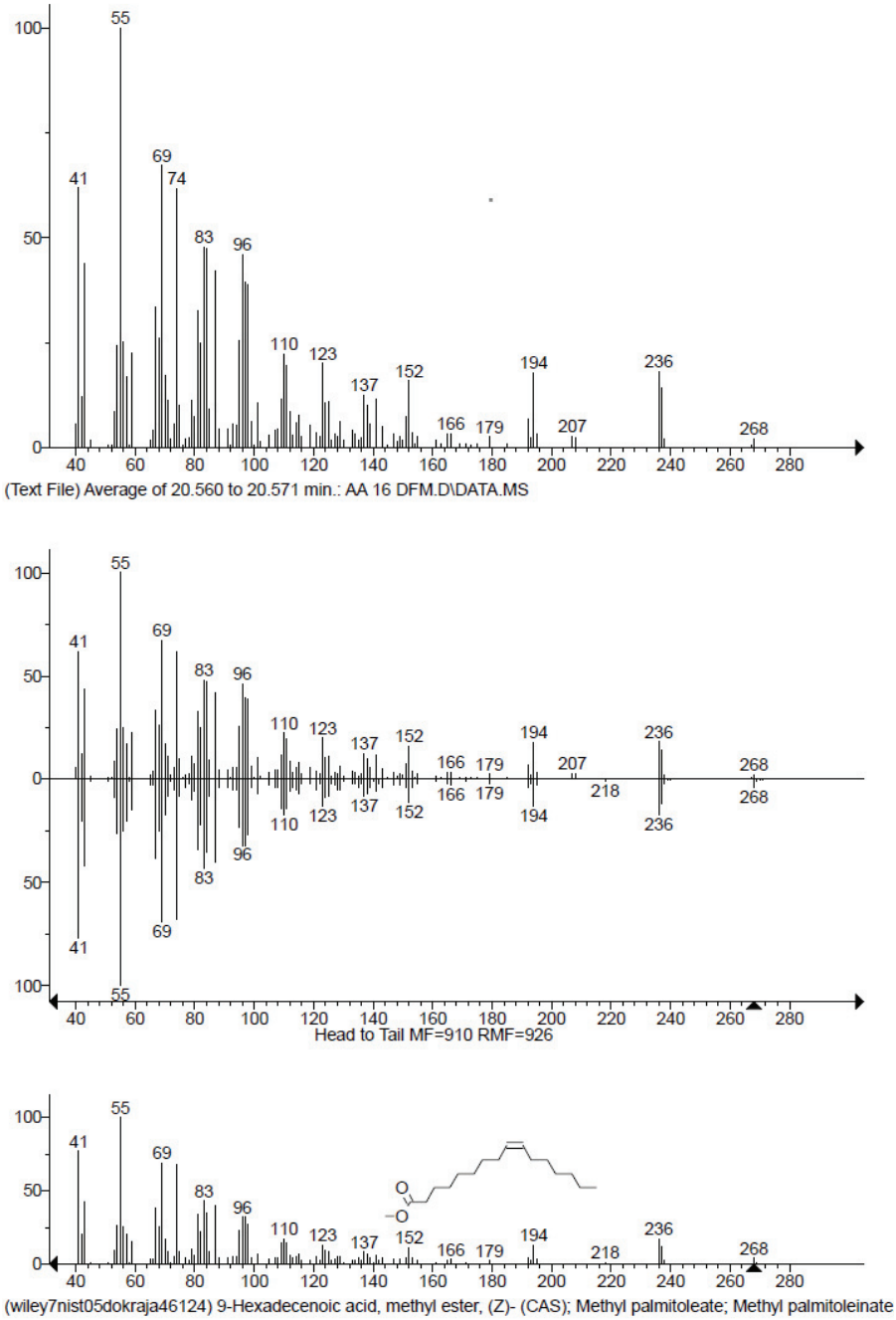

Fig. S-8. MS spectrum of methyl palmitoleate (top) and its comparison with the spectrum from the database (middle and bottom).

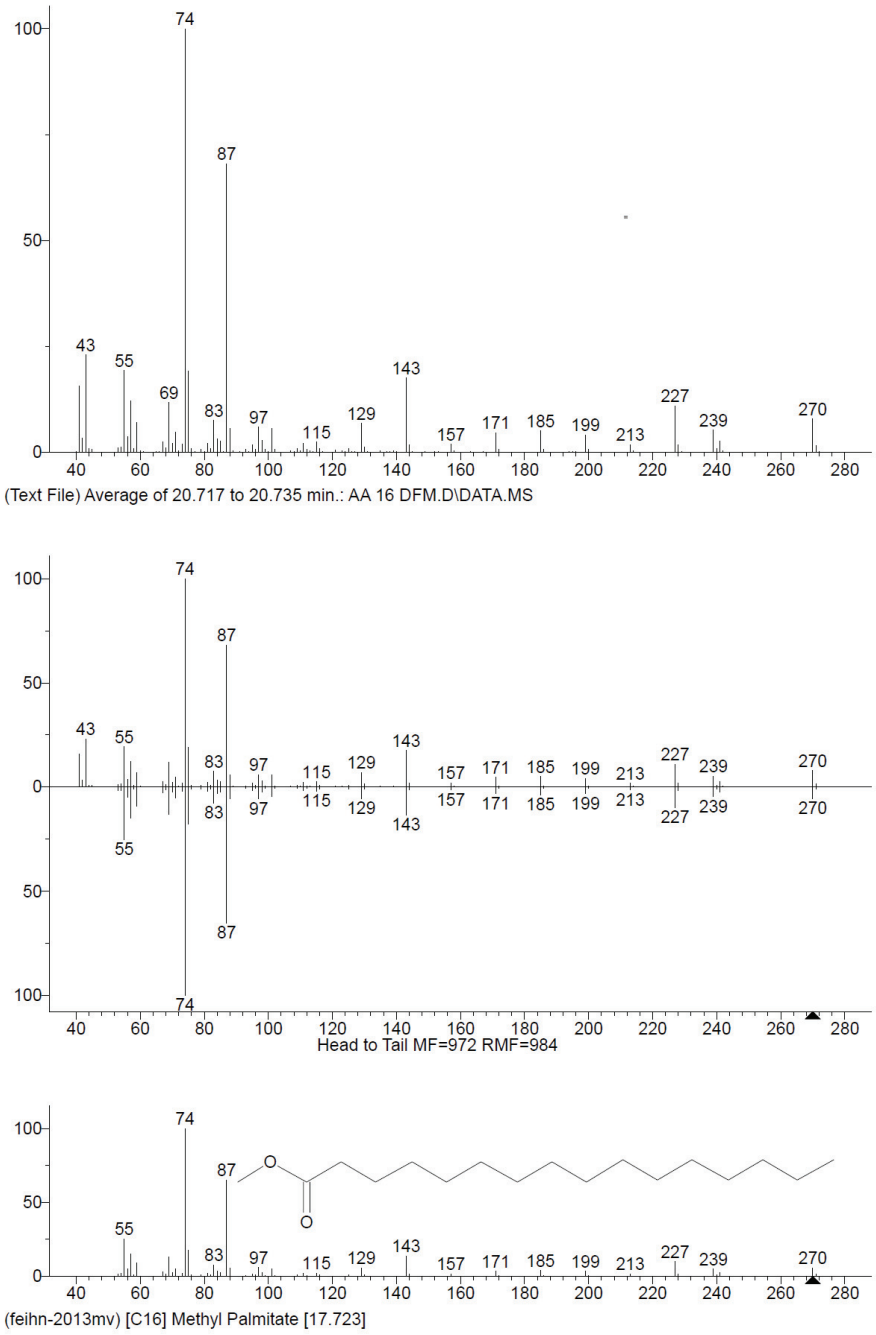

Fig. S-9. MS spectrum of methyl palmitate (top) and its comparison with the spectrum from the database (middle and bottom).

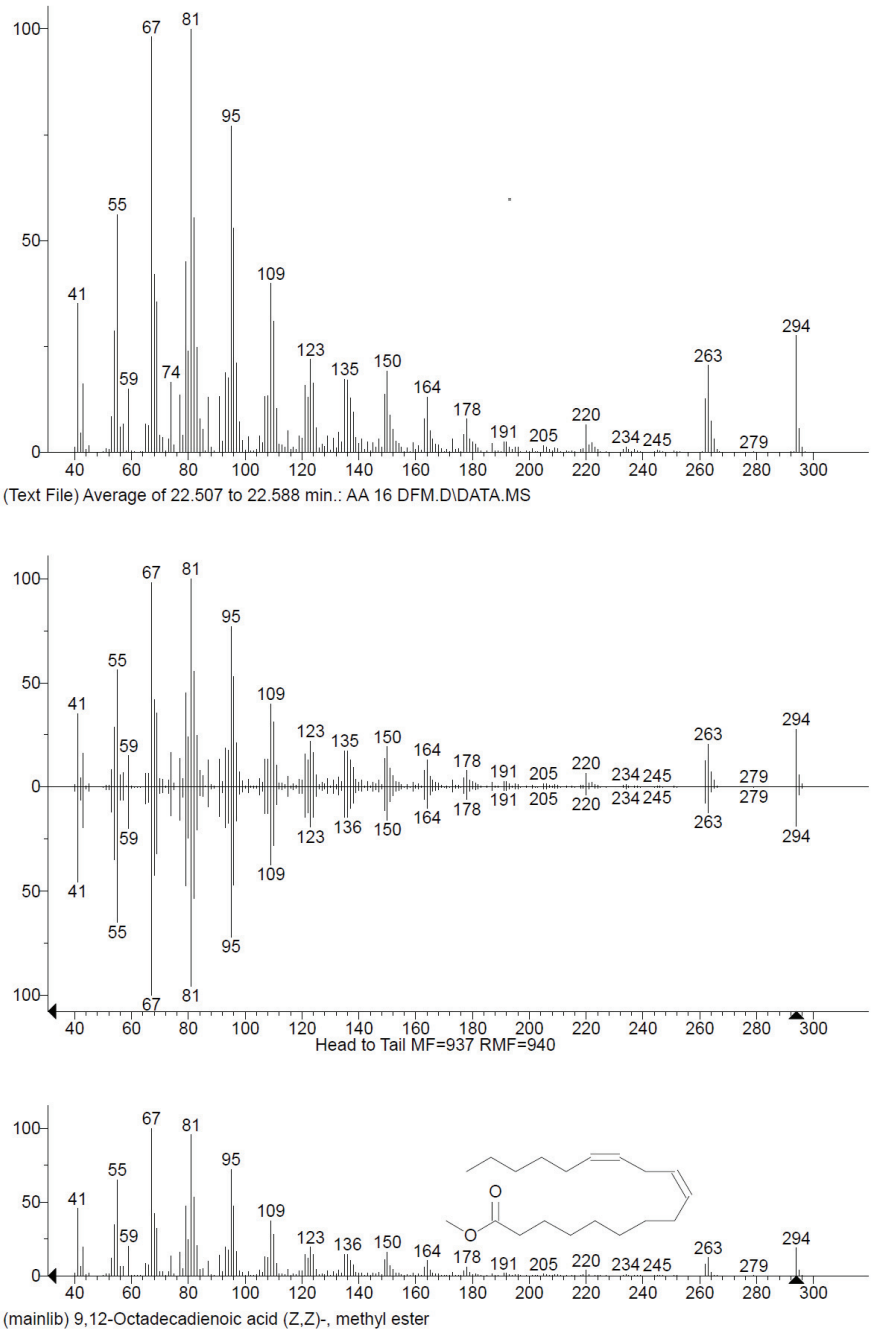

Fig. S-10. MS spectrum 9,12-Octadecadienoic acid (Z,Z)-, methyl ester (top) and its comparison with the spectrum from the database (middle and bottom).

Compounds on HPTLC plate (Fig. 1): *α*-pinene (*RI* = 932), *α*-copaene (*RI* = 1373), E-cariophylene (*RI* = 1416); *β*-selinene (*RI* = 1484), R_f = 0.84 - 0.88

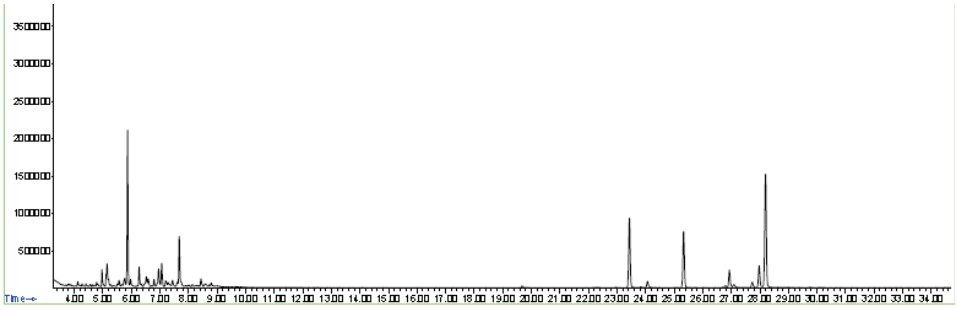

Fig S-11. GC-MS chromatogram of fraction DF1 containing *α*-pinene, *α*-copaene, E-caryophyllene, and *β*-selinene.

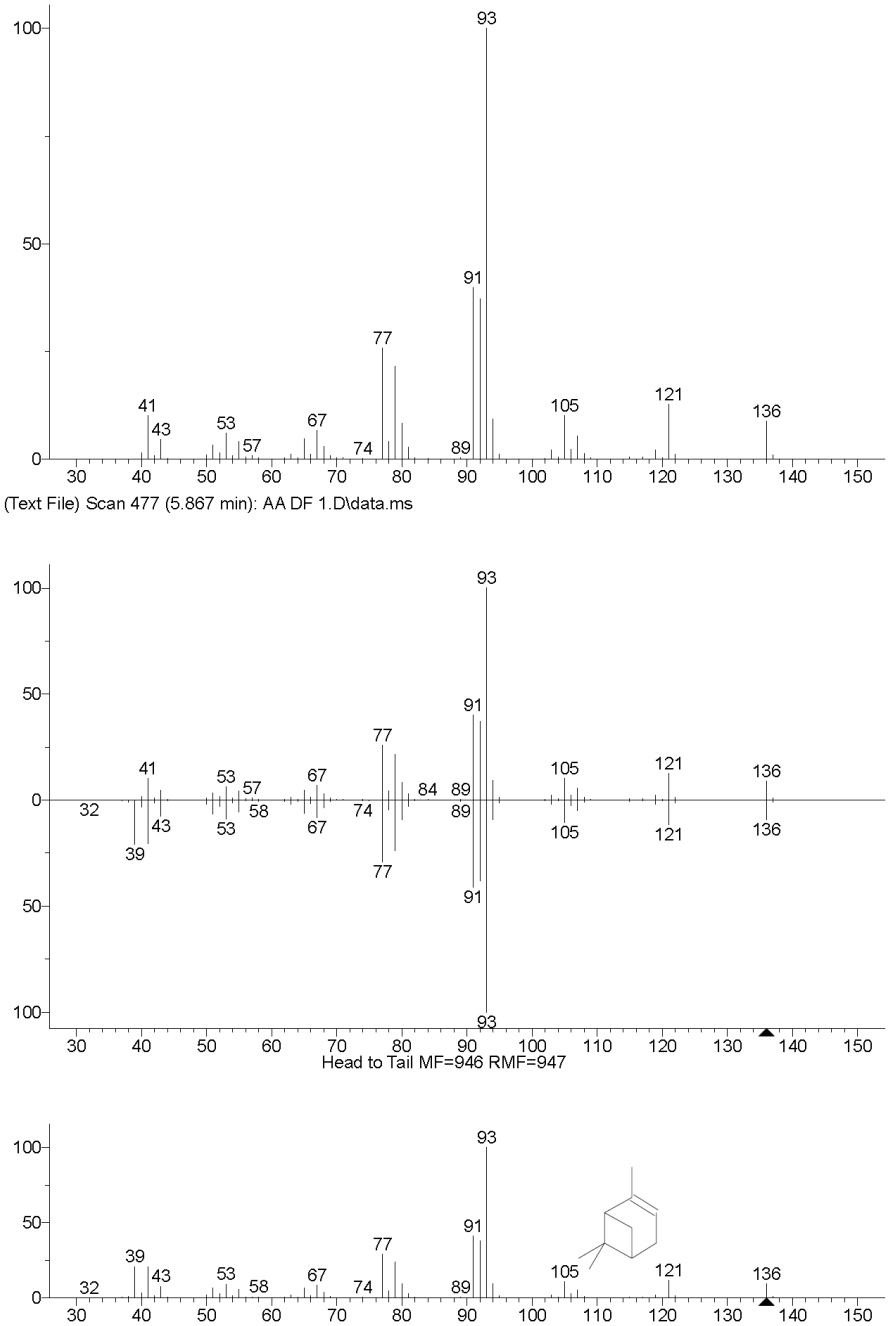

Fig. S-12. MS spectrum of α-pinene (top) and its comparison with the spectrum from the database (middle and bottom).

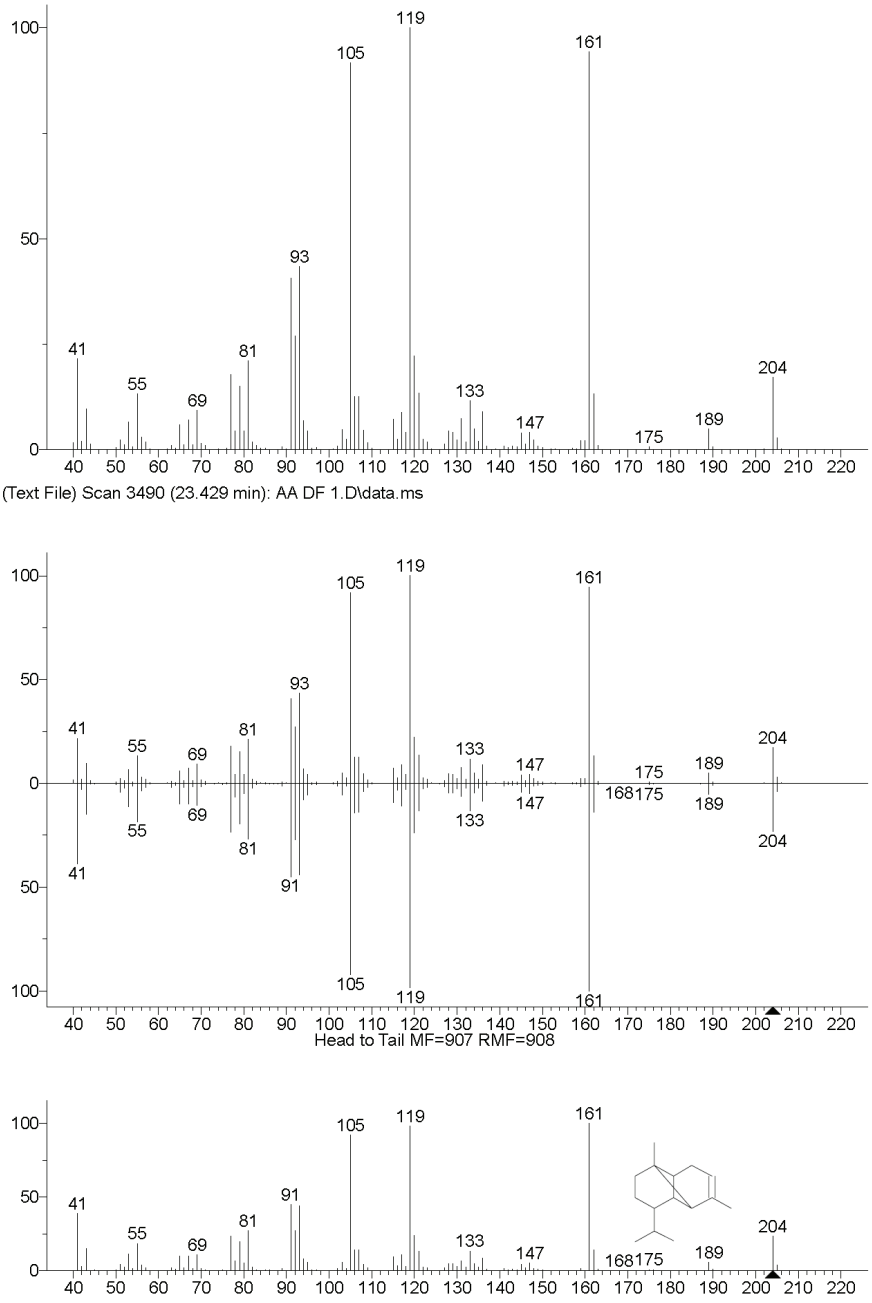

Fig. S-13. MS spectrum of α-copaene (top) and its comparison with the spectrum from the database (middle and bottom).

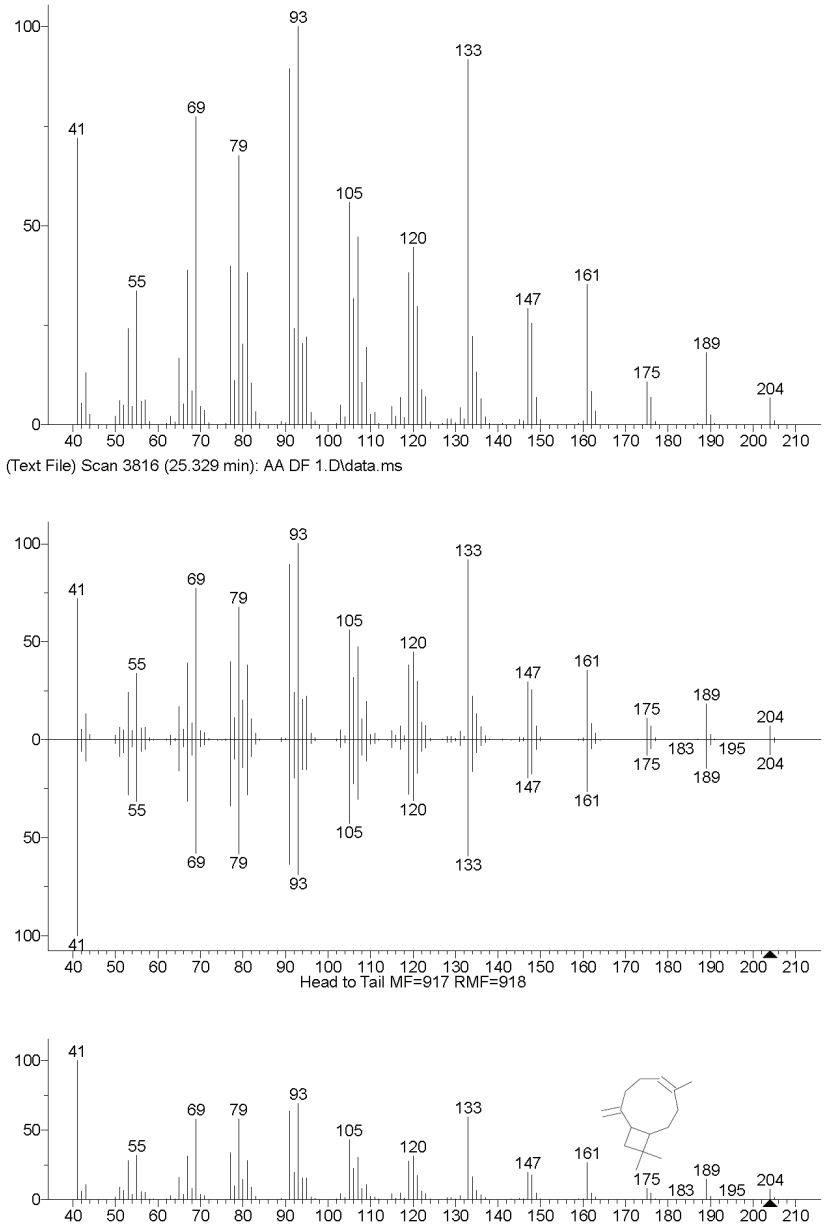

Fig. S-14. MS spectrum of E- β-caryophyllene (top) and its comparison with the spectrum from the database (middle and bottom).

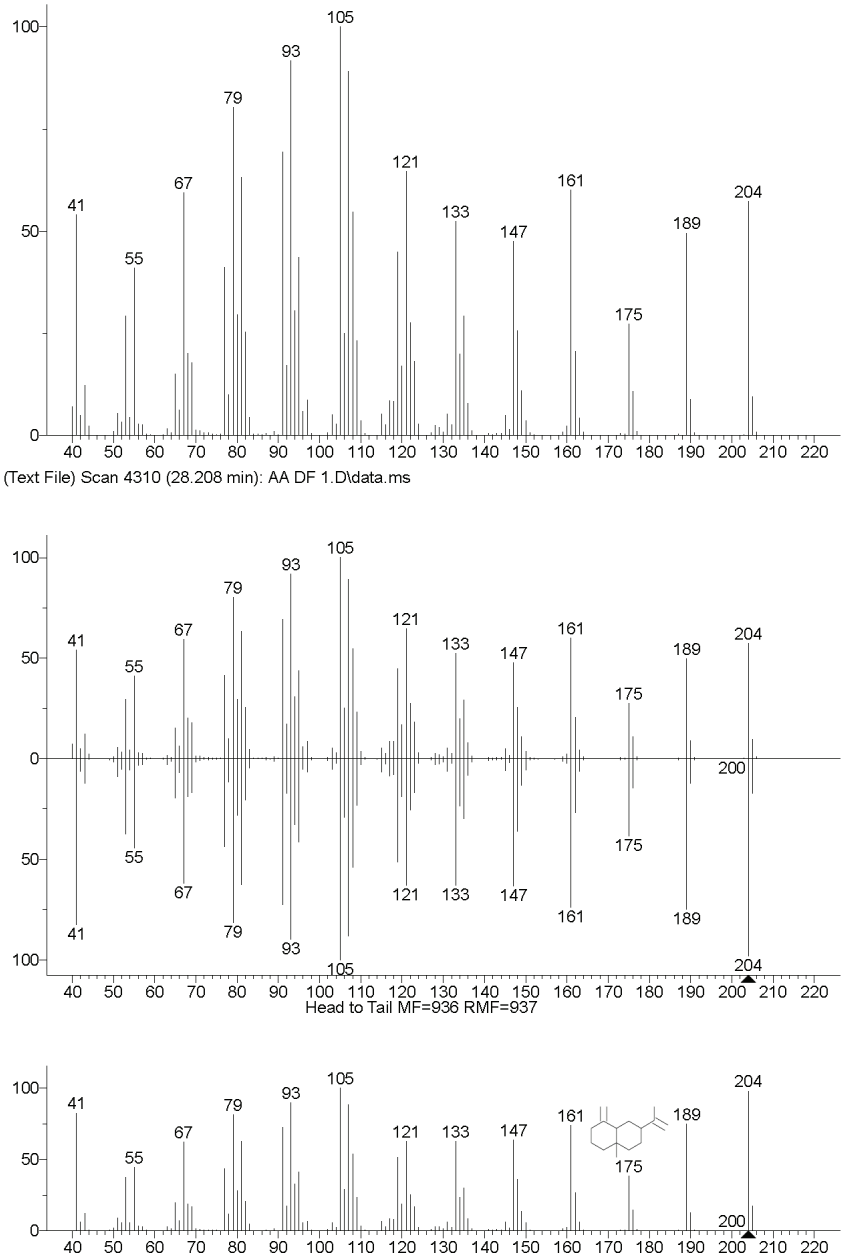

Fig. S-15. MS spectrum of *β*-selinene (top) and its comparison with the spectrum from the database (middle and bottom).

Compound on HPTLC plate (Fig 1.) Artemisia ketone R_f = 0.74 - 0.82.

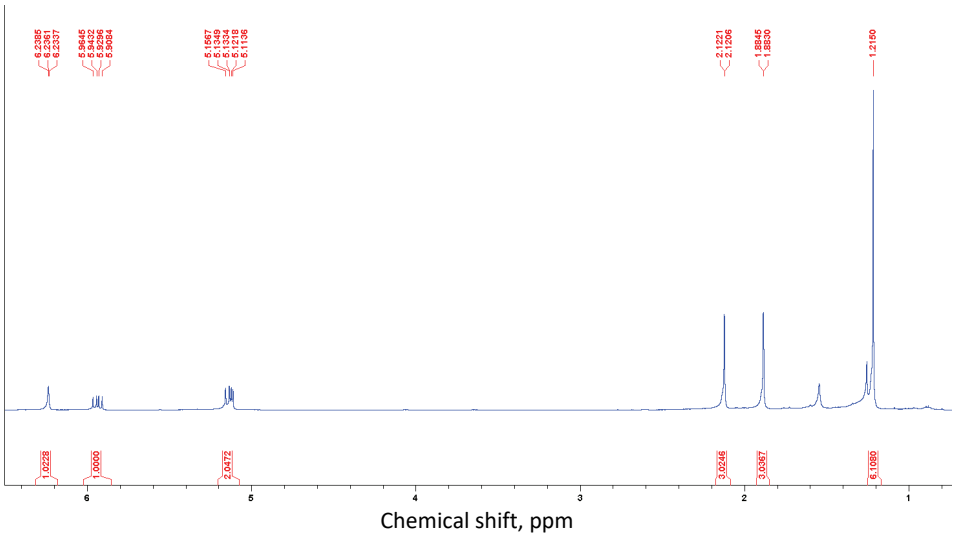

Fig. S-16. ^{1}H NMR spectrum of artemisia ketone.

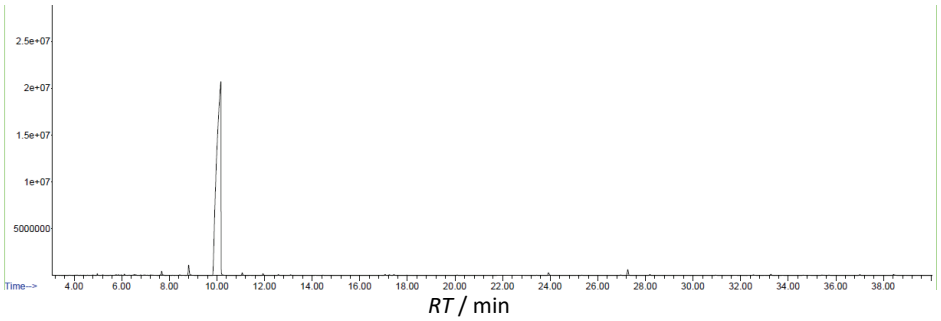

Fig. S-17. GC-MS chromatogram of fraction DF3 containing artemisia ketone (*RI* = 1057.5).

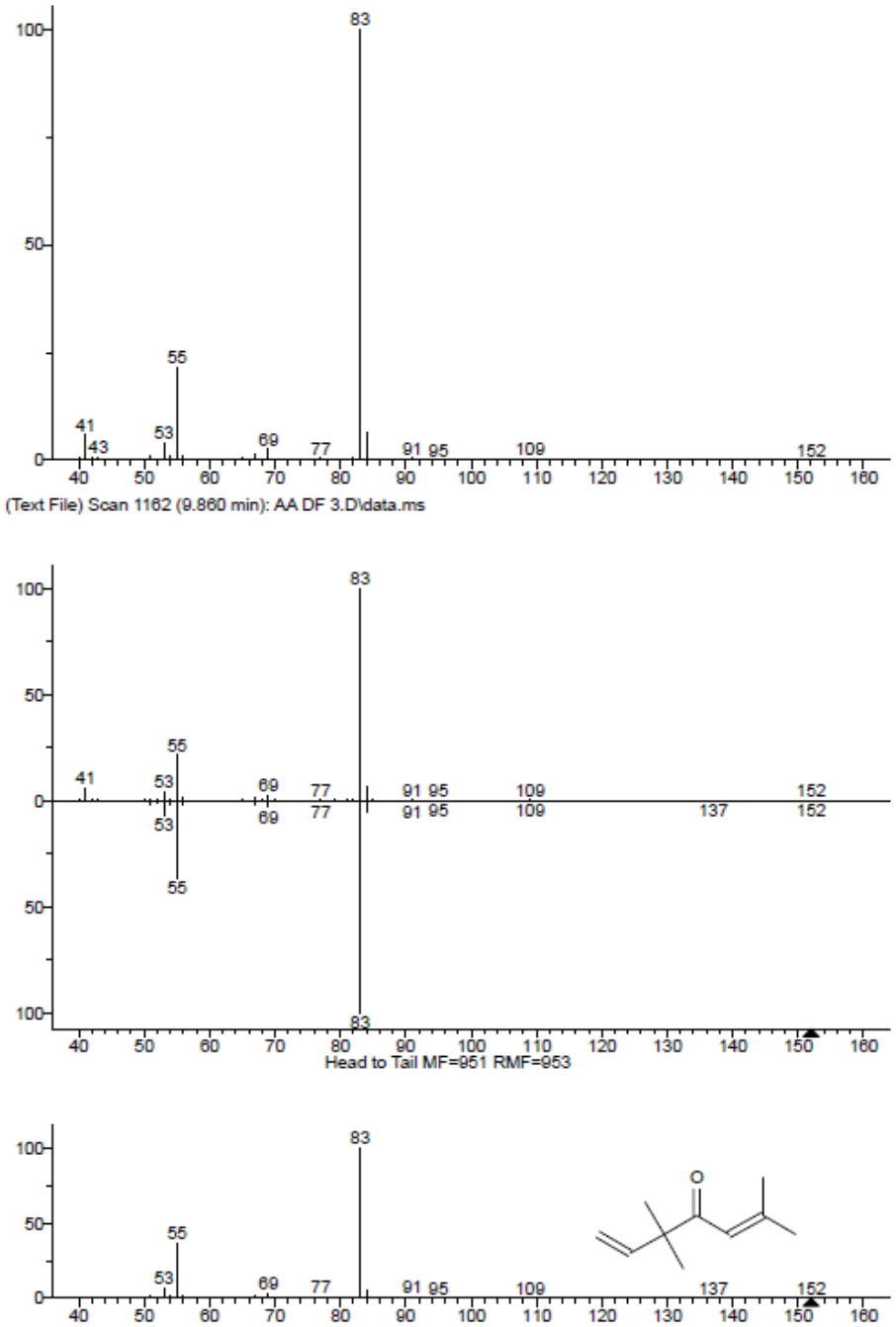

Fig. S-18. MS spectrum of artemisia ketone (top) and its comparison with the spectrum from the database (middle and bottom).

Compound on HPTLC plate (Fig 1.) 1,8-cineole $R_f = 0.68$

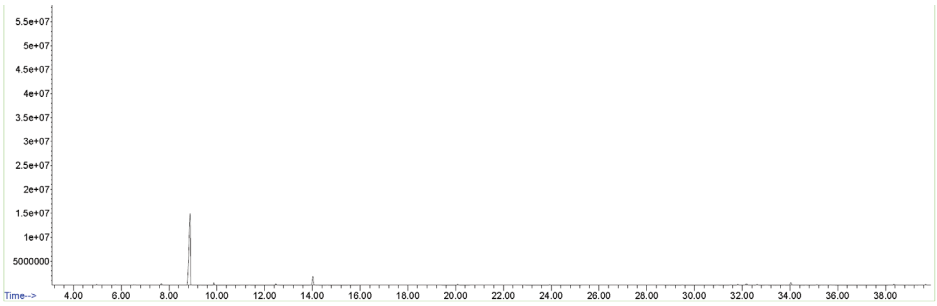

Fig. S-19. GC-MS chromatogram of fraction AA DF5 containing 1,8-cineole (*RI* = 1028).

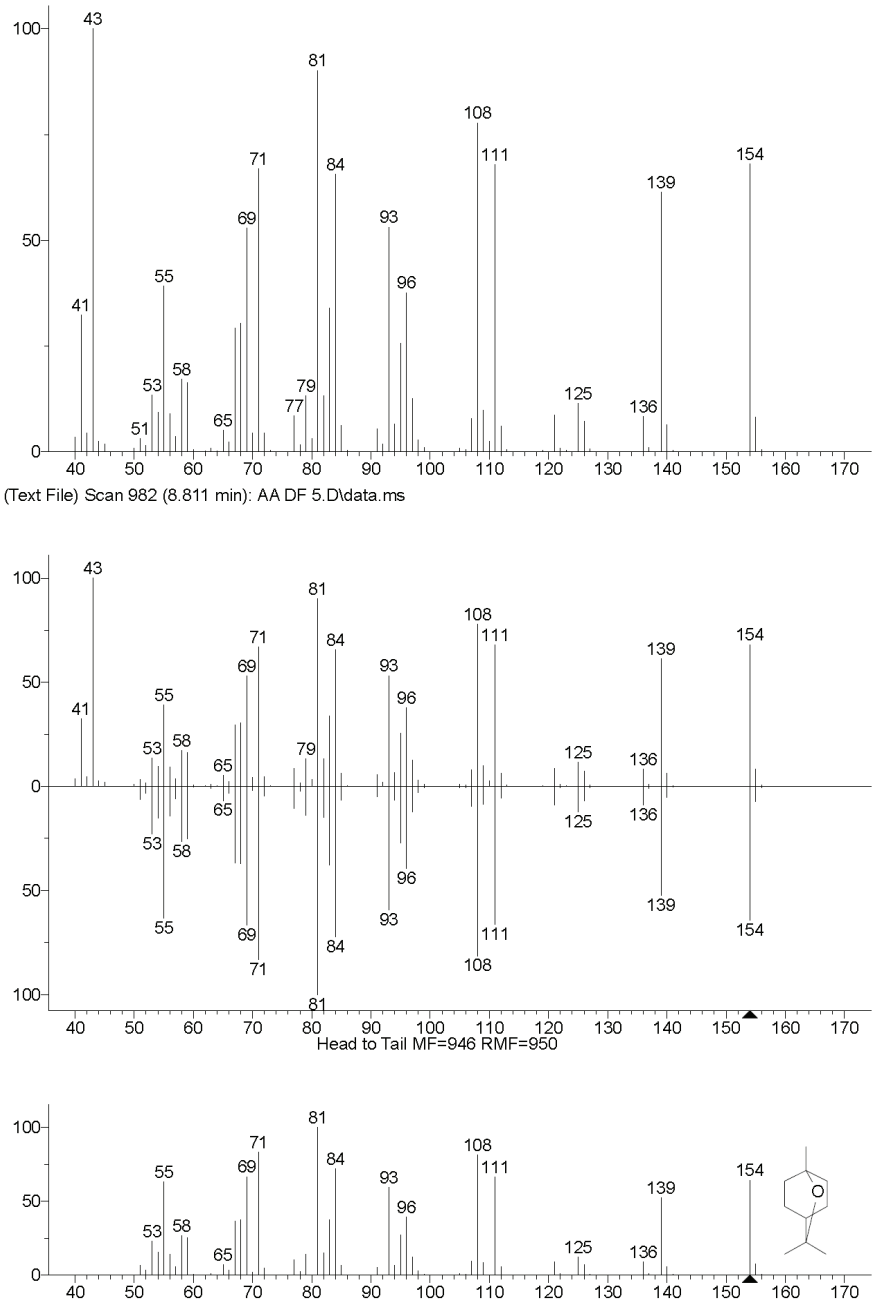

Fig. S-20. MS spectrum of 1,8-cineole (top) and its comparison with the spectrum from the database (middle and bottom).

Compound on HPTLC plate (Fig 1.) Caryophyllene oxide *Rf* = 0.66.

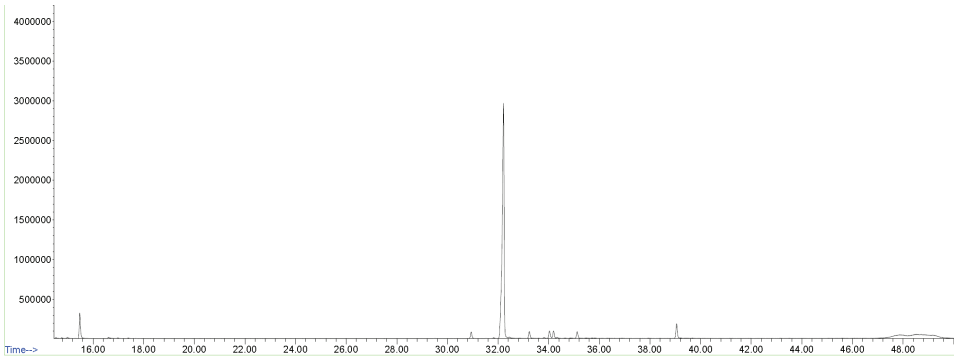

Fig. S-21. GC-MS chromatogram of fraction DF7 containing caryophyllene oxide (*RI* 1581).

Journal of the Serbian Chemical Society
JSCS@tmf.bg.ac.rs • www.shd.org.rs/JSCS
J. Serb. Chem. Soc. *87* (11) 1245–1258 (2022)
JSCS–5591
Original scientific paper
Published 30 September 2022

Synthesis and biological activity of alkylthio and arylthio derivatives of *tert*-butylquinone

JELENA ĐORĐEVIĆ[1,2], STOIMIR KOLAREVIĆ[3], JOVANA JOVANOVIĆ MARIĆ[3], MARIANA OALĐE PAVLOVIĆ[4], DUŠAN SLADIĆ[5], IRENA NOVAKOVIĆ[6]*# and BRANKA VUKOVIĆ-GAČIĆ[2]

[1]University of Belgrade, Institute for Multidisciplinary Research, Belgrade, Serbia, [2]University of Belgrade, Centre for Genotoxicology and Ecogenotoxicology, Faculty of Biology, Belgrade, Serbia, [3]University of Belgrade, Institute for Biological Research "Siniša Stanković", National Institute of the Republic of Serbia, Belgrade, Serbia, [4]University of Belgrade, Chair of Plant Morphology and Systematics, Faculty of Biology, Belgrade, Serbia, [5]University of Belgrade, Faculty of Chemistry, Belgrade, Serbia and [6]University of Belgrade, Institute for Chemistry, Technology and Metallurgy, Department for Chemistry, Belgrade, Serbia

(Received 4 March, revised 13 May, accepted 16 May 2022)

Abstract: Biological activity of 2-*tert*-butyl-1,4-benzoquinone (TBQ) and its derivatives, 2-*tert*-butyl-5-(2-propylthio)-1,4-benzoquinone, 2-*tert*-butyl-5--(propylthio)-1,4-benzoquinone, 2-*tert*-butyl-5,6-(ethylenedithio)-1,4-benzoquinone, 2-*tert*-butyl-5-(phenylthio)-1,4-benzoquinone and 2-*tert*-butyl-6-(phenylthio)-1,4-benzoquinone, were tested for their antioxidant, antibacterial, toxic, cytotoxic and genotoxic potential. Using the DPPH test, all derivatives showed good antioxidant activity, better than ascorbic acid, and the 2-tert--butyl-5-(propylthio)-1,4-benzoquinone derivative showed the strongest effect. Better antibacterial potential was observed against Gram-positive bacteria in the broth microdilution method in which the 2-*tert*-butyl-5-(phenylthio)-1,4--benzoquinone derivative showed the strongest activity (*MIC* = 15.6 μM). The results of toxicity tests, using the Brine shrimp test, indicated that the derivatives lose their toxic potential compared to TBQ, except for 2-*tert*-butyl-6--(phenylthio)-1,4-benzoquinone, which showed a 3 times stronger effect. Cytotoxicity was assessed by the MTT assay in 24 and 72 h treatments in MRC-5, HS 294T and A549 cell lines in threefold decreasing gradient (11, 33 and 100 μM). Modifications potentiate the cytotoxic effect, and the strongest effect was observed with the 2-*tert*-butyl-5,6-(ethylendithio)-1,4-benzoquinone derivative. In addition, the genotoxic potential was examined in the MRC-5 cell line using the comet assay. All tested derivatives of TBQ showed a genotoxic effect at all

* Corresponding author. E-mail: irenan@chem.bg.ac.rs
# Serbian Chemical Society member.
https://doi.org/10.2298/JSC220304044D

applied subtoxic concentrations. In general, the chemical modifications of TBQ enhanced its biological activity.

Keywords: TBQ; toxicity; MTT assay; antibacterial activity; antioxidant activity; comet test.

INTRODUCTION

Cancer is a disease of altered signaling and metabolism, which causes uncontrolled division and survival of the transformed cells.[1] According to the World Health Organization, in 2018 alone, there were 18.1 million new cancer patients and 9.6 million cancer deaths.[2] The process of developing this disease is not sufficiently elucidated and modern treatments, although much more effective, are not effective enough to reduce the mortality rate to an acceptable level. Biologically active compounds originating from a variety of natural sources, plants, animals, and microorganisms, have great potential for use in the treatment of malignancies.[3] According to the work of Amaral *et al.*,[4] from 1980 to 2019, a total of 174 new compounds with indications for cancer treatment were commercialized, with 53 % of these drugs being natural products, compounds based on them, or compounds that mimic their action. Since the biodiversity of marine organisms is approximately half of the total biodiversity on Earth, marine organisms are a good basis for the creation of modern chemotherapeutics and have been involved in various clinical trials.[5] However, although they show good biological activities, natural products originating from marine organisms have certain limiting factors in the form of availability and an adequate amount of the active compound obtained because of their low yield. This problem could be solved by creating synthetic compounds modeled from natural products. Many biologically active compounds isolated from marine organisms are hydroquinones and quinones, such as avarol/avarone redox pair isolated from the Mediterranean sponge *Dysidea avara*. Avarol and avaron have shown great and diverse biological activity, such as antimicrobial, antiviral, antioxidant and antitumor.[6–10] In previous studies, the biological activity of avarol/avaron and their methoxy and methylamino derivatives,[11] alkylamino and aralkylamino derivatives,[12] amino acid derivatives[13] and alkyl(aryl)thio derivatives[10] were examined. The yield of biologically active compounds originating from marine organisms is generally good, as is the case with avarol/avaron, but the problem is in the availability of marine organisms and, hence, the solution could be to design specific synthetic compounds that are similar in structure and their derivatives in order to enhance activity and reduce potential side effects. Bearing this in mind, in previous research a relatively crude model was used, based on *tert*-butylquinone – TBQ.[14,15] The results of previous studies showed that modifications increase the cytotoxic and antibacterial activity of TBQ and the alkylamino and aralkylamino derivatives of TBQ show a more selective effect over avarone derivatives.[14,15] In

this work, TBQ and its alkylthio derivatives 2-*tert*-butyl-5-(isopropylthio)-1.4--benzoquinone, 2-*tert*-butyl-5-(propylthio)-1.4-benzoquinone, 2-*tert*-butyl-5,6--(ethylenedithio)-1.4-benzoquinone) and arylthio derivatives (2-*tert*-butyl-5--(phenylthio)-1.4-benzoquinone and 2-*tert*-butyl-6-(phenylthio)-1.4-benzoquinone) were examined for their antioxidant, antibacterial, toxic, cytotoxic and genotoxic potentials. According to the work of Božić *et al.*,[10] alkylthio and arylthio derivatives were selected to cover the range of redox potentials between those of alkoxy and alkylamino derivatives on the one end, and the chloro derivatives on the other. The alkylthio group is also found in many compounds and mixtures of natural origin, such as allicin (a thiosulfinate compound originating from *Allium sativum* L.) that induces apoptosis in tumor cells.[16,17] Allicin reduces cell viability and cell proliferation in healthy and cancers cells.[18] By selecting this group, the aim was to combine the action of two strong functional groups of natural origin - quinones and alkylthio sulfides.

EXPERIMENTAL

Synthesis of derivatives

Alkylthio-derivatives of 2-*tert*-butyl-1,4-benzoquinone were synthesized by nucleophilic addition of thiols to quinones.[19] Synthesis of TBQ and derivatives commenced with commercially available *tert*-butylhydroquinone which were oxidized using silver oxide to the corresponding quinone. Conditions described in the paper by Božić *et al.*,[10] for the synthesis of alkylthio and aralkylthio derivatives of avarone were the same for the synthesis of TBQ and its derivatives. Briefly, the optimum reaction conditions for the synthesis of alkylthio derivatives were: equimolar amount of reactants, slightly alkaline medium, nitrogen atmosphere, temperatures of 60 °C, and a 30-min reaction time. Phenylthio derivatives were synthesized under neutral conditions in the air atmosphere while the other conditions were the same. The names and chemical structures of the derivatives are shown in Fig. 1.

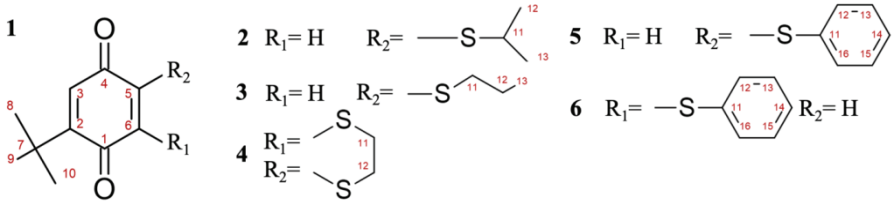

Fig. 1. Chemical structure of *tert*-butylquinone-TBQ and its derivatives: TBQ (**1**) 2-*tert*-butyl--1.4-benzoquinone, **2**) 2-*tert*-butyl-5-(isopropylthio)-1.4-benzoquinone, **3**) 2-*tert*-butyl-5-(propylthio)-1,4-benzoquinone, **4**) 2-*tert*-butyl-5,6-(ethylenedithio)-1.4-benzoquinone, **5**) 2-*tert*--butyl-5-(phenylthio)-1.4-benzoquinone and **6**) 2-*tert*-butyl-6-(phenylthio)-1.4-benzoquinone.

Details on synthesis and spectral data are given in Supplementary material to this paper.

Biological activities testing

Assessment of antioxidant potential by the 1,1-diphenyl-2-picrylhydrazyl (DPPH) test. The antioxidant effects of TBQ and its derivatives were determined using the DPPH assay, which measures the radical scavenging potential of selected compounds. The test was per-

formed according to the protocol developed by Blois (1958).[20] A total of 180 μL of freshly prepared methanolic DPPH solution (concentration of 40 μg mL^{-1}) was added to each well of the microtiter plate, followed by 20 μL of TBQ and its derivatives in DMSO at the appropriate concentration. Seven concentrations were tested for each test compound in a threefold gradient with the highest concentration of 1 mM. The test was performed in triplicate. Samples were incubated for 30 min in the dark at room temperature, after which the absorbance was measured at 517 nm using a microplate reader (Multiskan Sky Thermo Scientific, Finland).

Evaluation of antibacterial activity by the broth microdilution method. The antibacterial activity of TBQ and its derivatives against four strains of Gram-positive (*Enterococcus faecalis* ATCC 29212, *Listeria innocua* ATCC 33090, *Staphylococcus aureus* ATCC 25923 and *Bacillus subtilis* ATCC 6633) and three strains of Gram-negative (*Escherichia coli* ATCC 25922, *Salmonella typhimurium* ATCC 14028 and *Pseudomonas aeruginosa* ATCC 15442) bacteria was tested using the double microdilution method according to Sarker *et al*.[21] The highest concentration tested for TBQ and its derivatives were 1 mM. *E. faecalis* and *L. innocua* were grown in brain heart infusion broth (BHI), while the other bacteria were grown in Mueller Hinton broth (MHB). After double dilution of the derivatives in the appropriate broth, 10 μL of bacterial suspension (10^4 cells per well), and resazurin at a final concentration of 67.5 μg mL^{-1} were added per well. After thermostating for 24 h at 37 °C, the *MIC* value was determined as the lowest concentration that led to a change in the color of resazurin from blue to pink. Rifampicin and streptomycin with the highest concentrations of 30 and 43 μM, respectively, were used as positive controls. As the solvent control 5 % DMSO was tested. The antibacterial effect was categorized as strong (0–100 μM), moderate (100–500 μM) and weak (500–1000 μM).[22]

Assessment of toxic potential by the Brine shrimp test with Artemia salina (ARC test). A commercially available mixture (Artemia eggs, Dajana, Czech Republic) of lyophilized *A. salina* eggs were put in saltwater solution (3.3 % of sea salt). The test was performed according to Vanhaecke and Persoone[23] in triplicate over a 24-hour incubation period. TBQ and its derivatives were tested in six concentrations in a triple or double gradient (depending on the test compound) with a maximum tested concentration of 500 μM. The experiment had a negative control (saltwater only), positive control ($K_2Cr_2O_7$, concentration range 50–10 μg mL^{-1}), and solvent control (5 % DMSO).

Assessment of the cytotoxic potential using the MTT assay on different cell lines. The cytotoxic effect was assessed by the MTT assay on three cell lines: MRC-5 (healthy human fetal lung cell line; ECACC No. 84101801), HS 294T (cancer cell line – human melanocytes; ATCC HTB-140) and A549 (human lung cancer cell line; ATCC CCL-185) according to the protocol described by Kolarević *et al*.[11] Cells in monolayer were treated with TBQ and its derivatives at concentrations of 11, 33 and 100 μM while 5 % DMSO was used as the solvent control. The following passages were used for cell lines MRC-5, A549, HS 294 T: passage 25 and 26; passage 7, 10, 12 and 19; passage 14, respectively. The MTT assay was performed in 3 individual experiments during 24- and 72-hour incubation.

Assessment of the genotoxic potential in MRC-5 cell line by the Comet assay. As described in Kolarević *et al*.,[11] cells were grown 24 h until monolayer formation, washed with 1 x PBS and treated with non-toxic concentrations of the test compound (TBQ: 1.3, 3.7 and 11 μM; derivative **4**: 0.41, 1.23 and 3.7 μM, derivatives **2**, **3**, **5**, **6**: 3.7, 11 and 33 μM). Etoposide (33 μM) and 5 % DMSO were used as the positive and solvent control, respectively. The experiments were performed in triplicate in mini gel format as described in Azqueta *et al*.[24] with some modifications. Aliquots of cell suspensions obtained after treatment (30 μL) were mixed

with 70 μL of 1 % low melting point agarose. For each sample, 15 μL of the mixture was placed in duplicate on slides pre-coated with 1 % normal melting point agarose. Each microscope slide (prepared individually for each substance) contained duplicates of negative and positive controls and three concentrations of tested substances. Lysis, denaturation, electrophoresis, and neutralization were performed as described in Gačić *et al.*[25] A total of 150 nuclei were analyzed for each compound tested, controls were made separately for each microscopic plate examined. Acridine Orange (2 μg mL^{-1}) was used for staining and the analysis was performed with a fluorescence microscope (Leica, DMLS, Austria, under magnification 400×, excitation filter 450–490 nm, barrier filter 510 nm) by Comet IV computer software (Perceptive Instruments, UK). DNA damage was monitored *via* the tail intensity parameter (*T.I.*). Statistical analysis was performed by IBM SPSS Software. The results did not show a normal statistical distribution using the Kolmogorov–Smirnov test. Non-parametric tests were further performed: Kruskal–Wallis one-way ANOVA followed by Wilcoxon signed ranks test for pairwise comparison of treated groups with negative and positive controls with the significance level at $p < 0.05$.

RESULTS AND DISCUSSION

Assessment of the antioxidant potential of TBQ and its derivatives by the DPPH test

Based on the results obtained by DPPH (Table I), it could be concluded that the strongest antioxidant effect was observed for derivative **3,** which was also stronger than TBQ. On the other hand, **6** exhibits the lowest antioxidant activity. Additionally, derivatives **2**, **4** and **5** show activity similar to the parent compound TBQ. It should be noted that derivative **3** with a propyl group on the quinone moiety has a higher activity compared to derivative **2** with a voluminous isopropyl substituent. In addition to the size of the substituents, it is obvious that the activity is also influenced by their position on the quinone nucleus, since a striking difference in activity occurs with two regioisomers **5** and **6**, the 5-phenylthio isomer **5** being more active than 6-phenylthio regioisomer **6**. It should be noted that all tested compounds have higher activity than ascorbic acid, which is a control compound.

TABLE I. DPPH test results (IC_{50} / μM) of *tert*-butylquinone and its derivatives, AsAc – ascorbic acid as control

Compound						
TBQ	**2**	**3**	**4**	**5**	**6**	AsAc
77.27±5.07	80.75±4.10	70.48±3.04	81.98±1.96	80.61±2.14	108.03±1.08	177.81±2.68

The scavenging activity of TBQ and its alkylthio and arylthio derivatives was evaluated using the DPPH assay. DPPH is a relatively stable free radical. This assay is based on the color change of the DPPH solution (from purple to yellow) as the radical receives an electron or a hydrogen atom from the antioxidant. It is a simple and widely used method to evaluate the ability of compounds to act as free radical scavengers or hydrogen donors.[26] The obtained

results show that all the tested compounds have good antioxidant activity, better than that of ascorbic acid. The antioxidant activity of thio derivatives is not surprising. Namely, by the introduction of alkylthio and arylthio groups, the molecules get a sulfur atom that can lose an electron and thus increase the antioxidant activity of the compounds. Furthermore, alkylthio derivatives have a slightly stronger activity than that of the arylthio derivatives. This may be due to electron delocalization in the phenylthio group, which reduces the electron availability for sulfur atoms.

Evaluation of antibacterial activity

The microdilution method on different bacterial strains showed antibacterial effects of different strengths depending on the tested compound. Ethylenedithio **4** and phenylthio derivatives **5** and **6** show a strong antibacterial effect against *S. aureus*, and TBQ and the **2**, **4** and **5** derivatives against *B. subtilis* (Table II). Other derivatives showed a moderate to weak effect on the tested Gram-positive bacterial strains, while no antibacterial effect was observed against Gram-negative bacteria. It could be concluded that both TBQ and all the tested compounds show selectivity towards Gram-positive bacterial strains. Against *E. faecalis* and *S. aureus*, derivatives **4**, **5** and **6** show a stronger antibacterial activity than the parent compound (TBQ) which justifies the synthesis and introduction of S-substituents to the quinone moiety.

TABLE II. Antibacterial activity (*MIC* / μM) of *tert*-butylquinone and its derivatives, AB – antibiotics rifampicin ([a]) or streptomycin ([b]) as positive controls

Compound	Bacterium						
	E. faecalis	*L. innocua*	*S. aureus*	*B. subtilis*	*S. typhimurium*	*P. aeruginosa*	*E. coli*
TBQ	1000	250	125	62.5	>1000	>1000	>1000
2	>1000	250	125	62.5	>1000	>1000	>1000
3	>1000	1000	500	250	>1000	>1000	>1000
4	125	250	62.5	62.5	>1000	>1000	>1000
5	500	250	15.6	62.5	>1000	>1000	>1000
6	250	125	31.2	125	>1000	>1000	>1000
AB	3.79[a]	1.90[a]	10.75[b]	10.75[b]	21.50[b]	42.99[b]	42.99[b]

TBQ and its derivatives were assigned values (1, 2, 4, 8, 16, 32, 64, 128) depending on the obtained minimum inhibitory concentration (*MIC*: 1000, 500, 250, 125, 62.5, 31.25, 15.62, 7.81 μM). The assigned values obtained for the derivatives are compared with the assigned values for TBQ and shown on the radial diagram in Fig. 2, to show how many times stronger the derivatives are relative to the starting compound TBQ. The derivatives **4**, **5** and **6** showed better antibacterial activity against bacterial strains: *E. faecalis* and *S. aureus*, while towards *L. innocua*, derivative **6** showed better activity than TBQ. The highest

activity, 8 times stronger than TBQ, was shown by derivatives **4** (against *E. faecalis*) and **5** (against *S. aureus*).

The introduction of a substituent on the quinone moiety of TBQ, generally leads to an improvement of the antibacterial activity for most synthesized derivatives. Selectivity of both TBQ and all its derivatives to Gram-positive bacteria was observed.

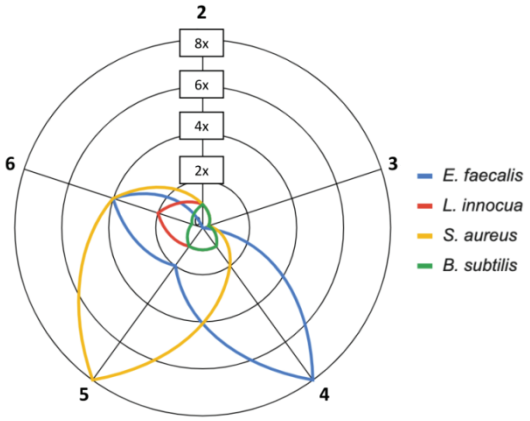

Fig. 2. Antimicrobial activity of derivatives relative to TBQ against bacterial strains: *E. faecalis*, *L. innocua*, *S. aureus* and *B. subtilis*.

From a structure–activity relationship (SAR) analysis, it could be noticed that the derivatives with a more voluminous substituent show stronger antibacterial activity. In accordance with this data, the isopropylthio derivative showed better activity than the propylthio derivative, while bulky groups ethylenedithio and phenylthio also exhibited an increased activity. On the other hand, two phenylthio regioisomers (**5** and **6**) showed different activities, but with no clear preference. Derivative **5** showed promising antibacterial properties because of an activity against *S. aureus* similar to that of streptomycin. Alkylthio and arylthio derivatives of avaron were less or equally active than avarone on *S. aureus* and *E. coli* bacterial strains.[10] On the same bacterial strains, alkylamino, aralkylamino and amino acid derivatives of TBQ mostly showed stronger activity compared to TBQ.[12–14]

Assessment of toxic potential by the Brine shrimp test

Based on the obtained results (Table III), it could be concluded that all the tested derivatives, except **6,** showed lower toxicity than TBQ. Toxicity of TBQ and derivatives **3**, **4** and **6** were higher than the toxicity of potassium dichromate ($K_2Cr_2O_7$), which was used as a positive control (**6** > TBQ > **3** > **4**).

The lowest activity was observed for derivative **5** which is interesting since it contains the same substituent as derivative **6** but at a different position.

Since *A. salina* shrimps live in symbiosis with some types of bacteria and that the toxicity of the compounds may be related to the lysis of the cell wall of bacteria present in the digestive tract of *A. salina* adults,[27] false-positive toxicity results are avoided by using nauplii in which the digestive tract is not yet developed. The fact that the most toxic TBQ derivatives are not those which are the most active against bacterial cells corroborates with this conclusion. The most toxic compound is derivative **6** that is almost 10 times more toxic than its regioisomer **5**. Since quinone toxicity is associated with either ROS formation or alkylation of cellular nucleophiles, a possible explanation for this activity difference is the fact that in derivative **6,** the most active position for nucleophilic attack is available. The toxicity of other derivatives could be explained by ROS formation since nucleophilic addition is either unlikely (derivatives **2**, **3**, **5**) or impossible (derivative **4**).

TABLE III. Brine shrimp test results (LC_{50} / μM) of *tert*-butylquinone and its derivatives. Control – potassium dichromate ($K_2Cr_2O_7$)

Compound						
TBQ	**2**	**3**	**4**	**5**	**6**	$K_2Cr_2O_7$
58.68± 4.72	159.20± 46.36	69.85± 17.67	85.55± 11.34	183.83± 11.88	19.21± 0.88	92.29± 0.34

Assessment of cytotoxic potential using the MTT assay on different cell lines

The results presented in Table IV confirm that the derivatives show a stronger cytotoxic effect than TBQ and the effect is more pronounced after a longer incubation period (72 h). Exceptions were only observed for derivatives **3**, **4** and **6** on the A549 cell line where the derivatives had a lower cytotoxic effect than TBQ after 72 h. The strongest cytotoxic effect on the MRC-5 cell was exhibited by derivative **4** (20.61 and 11.12 μM for 24 and 72 h incubation periods, respectively), while on HS 294T, the compounds were active only at 72 h treatment, whith derivative **3** showing the strongest effect (53.12 μM). On the A549 cell line, derivative **5** (57.04 and 52.80 μM for 24 and 72 h treatments, respectively) was the most active, while derivative **2** showed a similar effect but only at

TABLE IV. Cytotoxic activity (IC_{50} / μM) of *tert*-butylquinone and its derivatives on different cell lines after 24 and 72 h treatment; nt – not tested

Compound	MRC-5		HS 294T		A549	
	Time, h					
	24	72	24	72	24	72
TBQ	82.93±4.79	54.22±8.02	>100	>100	>100	67.58±0.87
2	64.14±3.66	51.51±5.38	>100	83.77±7.88	>100	52.99±4.01
3	61.15±4.89	35.516±9.79	>100	53.12±9.80	>100	75.72±1.18
4	20.61±12.87	11.12±15.65	>100	94.74±18.07	>100	>100
5	64.32±2.36	55.16±3,68	>100	nt	57.04±6.63	52.80±6.98
6	82.51±2.94	37.11±3.47	>100	68.09±3.66	>100	75.73±1.18

72 h treatment (52.99 μM). In general, the MRC-5 cell line was more sensitive in regard to DNA damage by TBQ and its derivatives when compared to tested cancer lines. All tested compounds showed a low selectivity index (SI < 2), hence, according to Koch *et al.*,[28] they may be considered generally toxic.

In this work, modifications increase the cytotoxic effect of TBQ with a more pronounced effect after a 72-hour incubation period. The tested compounds showed as active (IC_{50} less than 20 μg mL^{-1}) or moderately active (IC_{50} between 20 and 100 μg mL^{-1}) in the inhibition of cell growth.[29] According to Sladic and Gasic,[30] the main mechanism of quinone cytotoxicity may be nucleophilic addition and ROS production, resulting in oxidative stress and cell death. Tumor cells are more susceptible to oxidative stress. This combined mechanism is not possible with derivative **4**, which explains why this derivative is less active on the tumor cell lines than the other derivatives. The stronger cytotoxic effects on the normal MRC-5 cell line compared to tumor cell lines cannot be explained by generation of radicals, and is possibly a consequence of enhanced transport through cell the membrane and/or difference in metabolic transformations in normal and tumor cells. The conflicting results with the previously described antioxidant effect of the derivatives could be explained by the fact that antioxidant supplements, such as vitamins and/or flavonoids, under conditions of increased oxidative stress also exacerbate the pro-oxidant effect.[31] Candidate anticancer drugs should ideally be selective, potent, and relatively non-toxic.[32] However, based on the selectivity index, these compounds show a low selectivity index and are considered generally toxic. The low selectivity index could be a problem when using these derivatives as anticancer drugs. Additional modifications could improve the selectivity and reduce the genotoxicity of the derivatives. All tested compounds, except derivative **4**, showed a lower cytotoxic effect on the MRC-5 cell line at the highest tested concentration (100 μM) compared to avarol and avarone examined in the work of Kolarević *et al*.[11] On the A549 cell line, the cytotoxic effect of the derivatives was lower relative to avarol and lower or similar to avarone. In the work of Božić *et al.*,[10] alkyl(aryl)thio derivatives of avarone were less (or equally) active than avarone, whereas in the present work, the opposite results were obtained. This indicates that alkyl(aryl)thio groups enhance the activity of TBQ but not of avarone. Amino acid derivatives of TBQ showed a lower cytotoxic activity compared to TBQ,[13] while the same avarone derivatives generally proved to be more active. On the other hand, alkylamino and aralkylamino derivatives of TBQ generally had a higher activity than the parent compounds.[12,14]

Assessment of genotoxic potential in MRC-5 cell line by Comet assay

All tested derivatives of TBQ induced DNA damage in a dose-dependent way and show statistically significant differences in comparison with the negat-

ive control (Fig. 3). The highest genotoxic potential was observed for derivative **4**. In the previous work, no statistically significant difference was observed for TBQ compared to the control.[15] The tested TBQ derivatives showed a lower genotoxic potential than the positive control (etoposide).

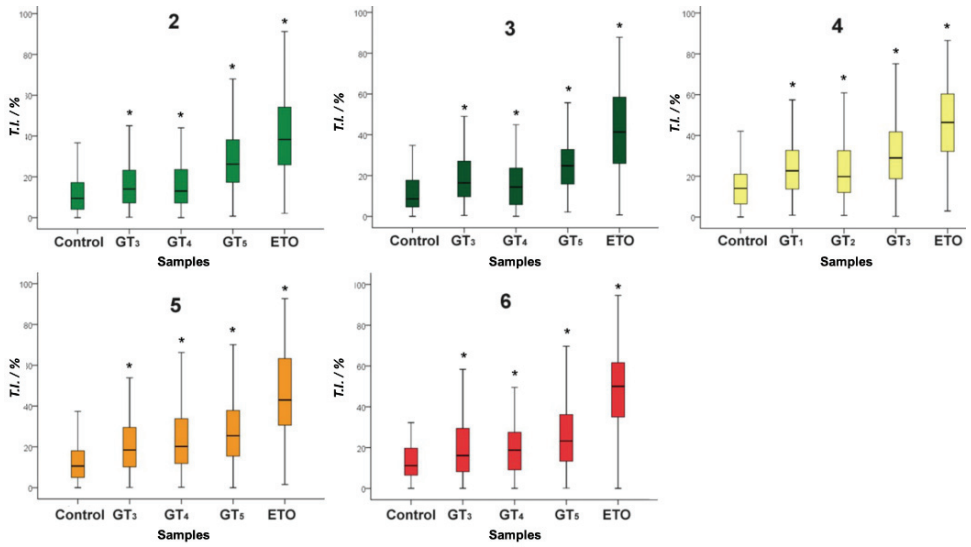

Fig 3. Comet assay results of *tert*-butylquinone derivatives represented by the tail intensity parameter (*T.I.*). Concentrations of test compounds: GT_1–0.41, GT_2–1.3, GT_3–3.7, GT_4–11 and GT_5–33; control-cells without treatment; ETO-etoposide (33 μM); *significant increase of DNA damage in comparison with the negative control (Control).

Various chemical, biological or physical agents damage DNA molecules and thus cause a genotoxic effect. The resulting damage to DNA molecules, if not repaired, can cause mutations and consequent pathological consequences, such as cancer, which is why it is important to examine the possible genotoxic effect of selected TBQ derivatives before their possible use as drugs.

All the tested derivatives at all the tested subtoxic concentrations showed a genotoxic effect, while the opposite effect was observed for TBQ in the work of Đorđević *et al.*[15] Alkylthio and arylthio derivatives showed stronger genotoxic potential than alkylamino and aralkylamino derivatives, where the effect was observed only at the highest tested concentration of 11 μM, except for 2-(benzylamino)-6-(*tert*-butyl)-1,4-benzoquinone, which showed a genotoxic effect at a concentration of 4 μM.[15] The alkylthio and arylthio derivatives of TBQ showed genotoxic potential at three times lower concentrations than 2-(benzylamino)-6--(*tert*-butyl)-1,4-benzoquinone, while derivative **4** was genotoxic even at a concentration that was nine times lower. These results confirm that the selected modifications of the starting compound enhance their genotoxic potential. How-

ever, the genotoxicity of alkylthio and arylthio derivatives was not higher than the genotoxicity of etoposide at the same concentration tested. The stronger genotoxic potential of alkylthio and arylthio derivatives of TBQ compared to TBQ may be related to cytotoxicity and should be further investigated. Avarol and avarone did not exert genotoxic potential in the same concentration range according to the work of Kolarević *et al.*,[11] while 3'-methoxyavarone and 3'--(methylamino) avarone have genotoxic potential. According to Okubo *et al.*,[33] TBQ induced a decrease in the potential of the mitochondrial membrane, disruption of the mitochondrial structure with the formation of cytosolic vacuoles, release of cytochrome *c* from mitochondria, caspase activation, poly(ADP-ribose)polymerase (PARP) cleavage, and a decrease of intracellular GSH and ATP. However, in the same work, neither oligonucleosomal degradation of nuclear DNA nor nuclear fragmentation in DAPI stained cells were detected, which excludes apoptosis as a cell death pathway. The authors suggest, based on research by Fiers *et al.*,[34] that it is possible that there are multiple pathways leading to cell death and different pathways (apoptosis, necrosis, and reactive oxygen damage) could co-exist in the same cell.

CONCLUSIONS

In general, the results indicated that modification of TBQ enhanced its activity, but increased genotoxicity was also observed. The synthesized compounds have good antioxidant activity, better than ascorbic acid, and exhibited antibacterial potential against tested Gram-positive bacteria with the strongest effect on *S. aureus* and *B. subtilis*. The results of the ARC test indicated that the toxicity of the derivatives is diminished compared to TBQ except for 2-*tert*--butyl-6-(phenylthio)-1,4-benzoquinone. The derivatives show a stronger cytotoxic effect than TBQ whereby the effect is more pronounced after a longer incubation period (72 h), with the 2-*tert*-butyl-5,6-(ethylendithio)-1,4-benzoquinone derivative showing the strongest cytotoxic activity. The tested compounds behaved as active or moderately active in the inhibition of cell growth. However, they show a low selectivity index and are considered generally toxic. In the studied concentration range, all tested derivatives possess genotoxic potential while TBQ does not exert genotoxic potential. In further studies, it is necessary to examine the mechanism of action of TBQ derivatives on DNA molecules and to determine whether genotoxicity is a consequence of cytotoxicity or vice versa.

SUPPLEMENTARY MATERIAL

Additional data and information are available electronically at the pages of journal website: https://www.shd-pub.org.rs/index.php/JSCS/article/view/11670, or from the corresponding author on request.

Acknowledgements. The authors are grateful to Luka Gačić who provided improvements to our English. This study was financially supported by the Ministry of Education, Science

and Technological Development of the Republic of Serbia (Grant No. 451-03-9/2021-14/ /200053, 451-03-9/2021-14/200007, 451-03-68/2022-14/200178, 451-03-9/2021-14/200168 and 451-03-68/2022-14/200026).

ИЗВОД

СИНТЕЗА И БИОЛОШКА АКТИВНОСТ АЛКИЛТИО И АРИЛТИО ДЕРИВАТА *терц*-БУТИЛХИНОНА

ЈЕЛЕНА ЂОРЂЕВИЋ[1, 2], СТОИМИР КОЛАРЕВИЋ[3], ЈОВАНА ЈОВАНОВИЋ МАРИЋ[3], МАРИАНА ОАЉЂЕ ПАВЛОВИЋ[4], ДУШАН СЛАДИЋ[5], ИРЕНА НОВАКОВИЋ[6] и БРАНКА ВУКОВИЋ-ГАЧИЋ[2]

[1]Универзитет у Београду, Институт за мултидисциплинарна истраживања, Београд, [2]Универзитет у Београду, Центар за генотоксикологију и екогенотоксикологију, Биолошки факултет, Београд, [3]Универзитет у Београду, Институт за биолошка истраживања „Синиша Станковић", Институт од националног значаја за Републику Србију, Београд, [4]Универзитет у Београду, Катедра за морфологију и систематику биљака, Биолошки факултет, Београд, [5]Универзитет у Београду, Хемијски факултет, Београд и [6]Универзитет у Београду, Институт за хемију, технологију и металургију, Центар за хемију, Београд

Испитана је биолошка активност 2-*терц*-бутил-1,4-бензохинона (TBQ) и његових деривата: 2-*терц*-бутил-5-(изопропилтио)-1,4-бензохинона, 2-*терц*-бутил-5-(пропилтио)-1,4-бензохинона, 2-*терц*-бутил-5,6-(етиленедитио)-1,4-бензохинона, 2-*терц*-бутил-5-(фенилтио)-1,4-бензохинона и 2-*терц*-бутил-6-(фенилтио)-1,4-бензохинона укључујући њихов антиоксидативни, антибактеријски, токсични, цитотоксични и генотоксични потенцијал. Применом DPPH теста, сви деривати су показали добру антиоксидативну активност, бољу од аскорбинске киселине, а најјаче дејство показао је дериват 2-*терц*-бутил-5-(пропилтио)-1,4-бензохинон. Бољи антимикробни потенцијал је примећен против Грам-позитивних бактерија методом микродилуције у бујону, где је дериват 2-*терц*-бутил-5-(фенилтио)-1,4-бензохинон показао најјачу активност (*MIC* = 15,6 μM). Резултати испитивања токсичности, применом теста на *Artemia salina*, показују да деривати губе токсични потенцијал у односу на TBQ, осим 2-*терц*-бутил-6-(фенилтио)-1,4-бензохинона, који је показао 3 пута јачи ефекат. Цитотоксичност је испитана MTT тестом у третманима од 24 и 72 h на ћелијским линијама MRC-5, HS 294T и A549 у троструко опадајућем градијенту (11, 33 и 100 μM). Модификације појачавају цитотоксични ефекат, а најјачи ефекат је примећен код деривата 2-*терц*-бутил-5,6-(етилендитио)-1,4-бензохинона. Поред тога, генотоксични потенцијал је испитан на ћелијској линији MRC-5 комет тестом. Сви испитивани деривати су показали генотоксични ефекат при свим примењеним субтоксичним концентрацијама. Генерално, хемијске модификације побољшавају биолошку активност 2-*терц*-бутил-1,4-бензохинона.

(Примљено 4. марта, ревидирано 13. маја, прихваћено 16. маја 2022)

REFERENCES

1. A. Upadhyay, *Genes Dis.* **8** (2021) 655 (https://doi.org/10.1016/j.gendis.2020.09.002)
2. IARC, *Press Release* **263** (2018) (https://www.iarc.who.int/wp-content/uploads/2018/09/pr263_E.pdf) (accessed on March 4, 2022)
3. J. Khazir, B. A. Mir, S. A. Mir, D. Cowan, *J. Asian Nat. Prod. Res.* **15** (2013) 764 (https://doi.org/10.1080/10286020.2013.798314)
4. R. G. Amaral, S. A. dos Santos, L. N. Andrade, P. Severino, A. A. Carvalho, *Clin. Oncol* **4** (2019) 1562 (https://www.clinicsinoncology.com/open-access/natural-products-as-treatment-against-cancer-a-historical-and-current-vision-1716.pdf)

5. J. T. Jimenez, M. Sturdíkova, E. Sturdík, *Acta Chim. Slov.* **2** (2009) 63 (http://acs.chtf.stuba.sk/papers/acs_0047.pdf)
6. E. Batke, R. Ogura, P. Vaupel, K. Hummel, F. Kallinowski, M. J. Gasić, H. C. Schröder, W. E. G. Müllerm, *Cell Biochem. Funct.* **6** (1988) 123 (https://doi.org/10.1002/cbf.290060207)
7. M. L. Ferrándiz, M. J. Sanz, G. Bustos, M. Payá, M. J. Alcaraz, S. de Rosa, *Eur. J. Pharmacol.* **253** (1994) 75 (https://doi.org/10.1016/0014-2999(94)90759-5)
8. M. Tsoukatou, J. P. Maréchal, C. Hellio, I. Novaković, S. Tufegdzic, D. Sladić, M. J. Gašić, A. S. Clare, C. Vagias, V. Roussis, *Molecules* **12** (2007) 1022 (https://doi.org/10.3390/12051022)
9. N. Aktaş, B. Gözcelioğlu, Y. Zang, W.-H. Lin, B. Konuklugil, *FABAD J. Pharm. Sci.* **35** (2010) 119 (http://dergi.fabad.org.tr/pdf/volum35/issue3/119-123.pdf)
10. T. Božić, I. Novaković, M. J. Gašić, Z. Juranić, T. Stanojković, S. Tufegdžić, Z. Kljajić, D. Sladić, *Eur. J. Med. Chem.* **45** (2010) 923 (https://doi.org/10.1016/j.ejmech.2009.11.033)
11. S. Kolarević, D. Milovanović, M. Kračun-Kolarević, J. Kostić, K. Sunjog, R. Martinović, J. Đorđević, I. Novaković, D. Sladić, B. Vuković-Gačić, *Drug Chem. Toxicol.* **42** (2019) 130 (https://doi.org/10.1080/01480545.2017.1413108)
12. M. Jeremić, J. Dinić, M. Pešić, M. Stepanovic, I. Novaković, D. Šegan, D. Sladić, *J. Serb. Chem. Soc.* **83** (2018) 1193 (https://doi.org/10.2298/JSC180627062J)
13. J. Vilipić, I. Novaković, T. Stanojković, I. Matić, D. Šegan, Z. Kljajić, D. Sladić, *Bioorg. Med. Chem.* **23** (2015) 6930 (https://doi.org/10.1016/j.bmc.2015.09.044)
14. M. Jeremić, M. Pešić, J. Dinić, J. Banković, I. Novaković, D. Šegan, D. Sladić, *Eur. J. Med. Chem.* **118** (2016) 107 (https://doi.org/10.1016/j.ejmech.2016.04.011)
15. J. Đorđević, S. Kolarević, J. Jovanović, J. Kostić-Vuković, I. Novaković, M. Jeremić, D. Sladić, B. Vuković-Gačić, *Drug Chem. Toxicol.* **43** (2020) 522 (https://doi.org/10.1080/01480545.2018.1514043)
16. X. Li, J. Ni, Y. Tang, X. Wang, H. Tang, H. Li, S. Zhang, X. Shen, *Nat. Prod. Res.* **33** (2019) 2722 (https://doi.org/10.1080/14786419.2018.1465425)
17. M. Sarvizadeh, O. Hasanpour, Z. Naderi Ghale-Noie, S. Mollazadeh, M. Rezaei, H. Pourghadamyari, M. Masoud Khooy, M. Aschner, H. Khan, N. Rezaei, L. Shojaie, H. Mirzaei, *Front. Oncol.* **11** (2021) 650256 (https://doi.org/10.3389/fonc.2021.650256)
18. M. C. H. Gruhlke, C. Nicco, F. Batteux, A. J. Slusarenko, *Antioxidants* **6** (2017) 1 (https://doi.org/10.3390/antiox6010001)
19. I. Novaković, Z. Vujčić, T. T. Božić, N. Božić, N. B. Milosavić, D. Sladić, *J. Serb. Chem. Soc.* **68** (2003) 243 (https://doi.org/10.2298/JSC0305243N)
20. M. S. Blois, *Nature* **181** (1958) 1199 (http://dx.doi.org/10.1038/1811199a0)
21. S. D. Sarker, L. Nahar, Y. Kumarasamy, *Methods* **42** (2007) 321 (https://doi.org/10.1016/j.ymeth.2007.01.006)
22. E. J. Crevelin, S. C. Caixeta, H. J. Dias, M. Groppo, W. R. Cunha, C. H. G. Martins, A. E. M. Crotti, *Evid. Based Complementary Altern. Med. (*2015) 102317 (https://doi.org/10.1155/2015/102317)
23. P. Vanhaecke, G. Persoone, *Ecotoxicol. Test. Mar. Environ.* **2** (1984) 588 (https://www.researchgate.net/publication/36455047)
24. A. Azqueta, K. B. Gutzkow, C. C. Priestley, S. Meier, J. S. Walker, G. Brunborg, A. R. Collins, *Toxicol. in Vitro* **27** (2013) 768 (https://doi.org/10.1016/j.tiv.2012.12.006)

25. Z. Gačić, S. Kolarević, K. Sunjog, M. Kračun-Kolarević, M. Paunović, J. Knežević--Vukčević, B. Vuković-Gačić, *Environ. Pollut.* **191** (2014) 145 (https://doi.org/10.1016/j.envpol.2014.04.024)
26. H. Lai, Y. Lim, *Int. J. Environ. Sci.* **2** (2011) 442 (https://doi.org/10.7763/IJESD.2011.V2.166)
27. S. A. Soto-Rodriguez, A. Roque, M. L. Lizarraga-Partida, A. L. Guerra-Flores, B. Gomez-Gil, *Dis. Aquat. Org.* **53** (2003) 231 (https://doi.org/10.3354/dao053231)
28. A. Koch, P. Tamez, J. Pezzuto, D. Soejarto, *J. Ethnopharmacol.* **101** (2005) 95 (https://doi.org/10.1016/j.jep.2005.03.011)
29. P. Tanamatayarat, P. Limtrakul, S. Chunsakaow, C. Duangrat, *Thai J. Pharm. Sci.* **27** (2003) 167 (https://www.thaiscience.info/Article%20for%20ThaiScience/Article/5/10016408.pdf)
30. D. Sladic, M. J. Gasic, *Molecules* **11** (2006) 1 (https://doi.org/10.3390/11010001)
31. I. Pérez-Torres, V. Guarner-Lans, M. E. Rubio-Ruiz, *Int. J. Mol. Sci.* **18** (2017) 2098 (https://doi.org/10.3390/ijms18102098)
32. C. P. Wu, S. Ohnuma, S. V. Ambudkar, *Curr. Pharm. Biotechnol.* **12** (2011) 609 (https://doi.org/10.2174/138920111795163887)
33. T. Okubo, Y. Yokoyama, K. Kano, I. Kano, *Food Chem. Toxicol.* **41** (2003) 679 (https://doi.org/10.1016/S0278-6915(03)00002-4)
34. W. Fiers, R. Beyaert, W. Declercq, P. Vandenabeele, *Oncogene* **18** (1999) 7719 (https://doi.org/10.1038/sj.onc.1203249).

Journal of the Serbian Chemical Society
JSCS@tmf.bg.ac.rs • www.shd.org.rs/JSCS
J. Serb. Chem. Soc. *87* (11) S422–S435 (2022) *Supplementary material*

SUPPLEMENTARY MATERIAL TO

Synthesis and biological activity of alkylthio and arylthio derivatives of *tert*-butylquinone

JELENA ĐORĐEVIĆ[1,2], STOIMIR KOLAREVIĆ[3], JOVANA JOVANOVIĆ MARIĆ[3], MARIANA OALĐE PAVLOVIĆ[4], DUŠAN SLADIĆ[5], IRENA NOVAKOVIĆ[6]*# and BRANKA VUKOVIĆ-GAČIĆ[2]

[1]University of Belgrade, Institute for Multidisciplinary Research, Belgrade, Serbia, [2]University of Belgrade, Centre for Genotoxicology and Ecogenotoxicology, Faculty of Biology, Belgrade, Serbia, [3]University of Belgrade, Institute for Biological Research "Siniša Stanković", National Institute of the Republic of Serbia, Belgrade, Serbia, [4]University of Belgrade, Chair of Plant Morphology and Systematics, Faculty of Biology, Belgrade, Serbia, [5]University of Belgrade, Faculty of Chemistry, Belgrade, Serbia and [6]University of Belgrade, Institute for Chemistry, Technology and Metallurgy, Department for Chemistry, Belgrade, Serbia

J. Serb. Chem. Soc. *87* (11) (2022) 1245–1258

General information

All reagents used were commercial products purchased from Sigma-Aldrich or Merck, except for silver(I)-oxide which was synthesized. Column chromatography was performed on silica gel (0.063−0.200 mm, Merck). Analytical thin-layer chromatography (TLC) was performed on precoated aluminum-backed plates (silica gel 60 GF_{254}, Merck). ^{1}H- and ^{13}C-NMR spectra were recorded at 500 MHz (Bruker Avance III) in deuterated chloroform (CD_3Cl). Chemical shifts are reported in parts per milion (ppm), relative to tetramethylsilane. Coupling constants are reported in hertz (Hz). EI MS spectra were recorded on Agilent 7890A – 5975 inert XL EI CI. UV/Vis spectra were recoreded on a LLG-uniSPEC 2 Spectrophotometer in methanol.

*Synthesis of 2-*tert*-butyl-1,4-benzoquinone (TBQ)*

2-*tert*-Butyl-1,4-benzohydroquinone (2.13 g) was dissolved in 150 mL of diethyl ether in a 250 ml flask. After dissolution, 3.70 g of silver(I)-oxide was gradually added to the reaction mixture with constant stirring over 3.5 h at room temperature, after which the stirring was stopped, anhydrous sodium sulfate was added to the reaction mixture and the mixture were dried overnight. Oxidation was monitored by thin-layer chromatography in a toluene:ethyl acetate system (9:1). After 12 h, the mixture was filtered through a layer of celite and the solvent

* Corresponding author. E-mail: irenan@chem.bg.ac.rs

was evaporated under reduced pressure. Yellow crystals (m.p. 56-58 °C) of 2-*tert*-butyl-1,4-benzoquinonewere obtained. The yield was 2.05 g (98 %).

Synthesis of 2-tert-*butyl-5-(isopropylthio)-1,4-benzoquinone (**2**)*

2-*tert*-Butyl-1,4-benzoquinone (312 mg) was dissolved in 40 mL of EtOH/saturated $NaHCO_3$ solution (1:1). Then 498 mg (600 μL) of 2-propanethiol was added in one portion. The reaction was performed under an argon atmosphere, with constant stirring at 60 °C and lasted about 30 min. The aqueous-ethanolic solution was neutralized with 5 % HCl and then extracted with toluene. The organic solution was dried over anhydrous Na_2SO_4. Toluene was evaporated and a crude red product (444 mg) was applied to a column formed of 22 g of silica gel (0.063–0.200 mm). After elution with toluene, several fractions were obtained, the major fraction (136 mg) being rechromatographed on a 7 g silica gel column. An 87 mg mass fraction was obtained which was purified by preparative thin layer chromatography (silica gel 60 GF_{254}) with toluene as the eluent. An oily yellow colored product was obtained in an amount of 43 mg (19 %).

^{1}H-NMR (500 MHz, $CDCl_3$, δ / ppm): 6.62 (1H, *s*), 6.32 (1H, *s*), 3.26 (1H, septet, J = 6.5 Hz,), 1.37 (6H, *d*, J = 6.5 Hz), 1.26 (9H, s).

^{13}C-NMR (125 MHz, CDCl3, δ / ppm): 186.67 (C1), 185.92 (C4), 158.34 (C2), 151.73 (C5), 132.79 (C6), 129.01 (C3), 36.93 (C7), 35.78 (C11), 30.76 (C8, C9, C10), 23.70 (C12, C13).

UV/Vis, λ_{max} / nm (ε / dm^2 mol^{-1}): 252 (1.5×10^4), 290 (1.9×10^4), 420 (1.5×10^3).

EI MS, *m/z* (relative abundance, %): 238.2 (M^+, 100), 223.1 (100), 196.1 (80), 181.1 (50), 154.1 (55), 85.0 (70), 41.1 (55)

Synthesis of 2-tert-*butyl-5-(propylthio)-1,4-benzoquinone (**3**)*

2-*tert*-Butyl-1,4-benzoquinone (271 mg) was dissolved in 40 mL of EtOH/saturated $NaHCO_3$ solution (1:1) after which 368 mg (584 μL) of 1-propanethiol was added. The reaction was performed as with 2-propanethiol (with constant stirring at 60 °C under an argon atmosphere). The crude red product (432 mg) was applied to a column prepared from 22 g of silica gel (0.063–0.200 mm) and eluted with toluene. Multiple fractions were obtained and the selected fraction (133 mg) was purified by preparative thin layer chromatography (silica gel 60 GF_{254}) with toluene as the eluent. An oily orange compound was obtained in an amount of 63 mg (32 %).

^{1}H-NMR (500 MHz, $CDCl_3$, δ / ppm): 6.61 (1H, *s*), 6.27 (1H, *s*), 2.73 (2H, *t*, J = 4 Hz), 1.76 (2H, *sextet*, J = 6.5 Hz), 1.28 (9H, *s*), 1.07 (3H, *t*, J = 4 Hz).

^{13}C-NMR (125 MHz, $CDCl_3$, δ / ppm): 186.51 (C1), 185.71 (C4), 158.49 (C2), 152.47 (C5), 132.59 (C6), 128.28 (C3), 36.87 (C7), 33.64 (C11), 30.61 (C8, C9, C10), 22.18 (C12), 15.09 (C13).

UV/Vis, λ_{max} / nm (ε / dm^2mol^{-1}): 250 (1.8×10^4), 292 (1.4×10^4), 440 (1.4×10^3).

EI MS, *m/z* (relative abundance, %): 238.2 (M^+, 100), 223.1 (100), 196.1 (80), 181.1 (50), 154.1 (55), 85.0 (70), 41.1 (55).

*Synthesis of 2-*tert*-butyl-5,6-(ethylenedithio)-1,4-benzoquinone (**4**)*

2-*tert*-Butyl-1,4-benzoquinone (303 mg) was dissolved in 40 mL of EtOH/saturated $NaHCO_3$ aqueous solution (1: 1) after which 92 mg (82 μL) of ethylenedithiol was added to the resulting solution. The reaction was performed under an argon atmosphere, with constant stirring at 60 °C and lasted about 50 min. 412 mg of crude product was obtained and applied to a column of 20 g of silica gel (0.063–0.200 mm). The solvent was eluted with a mixture of petroleum ether (30-50 °C)−benzene (3:1), and the chromatography was followed by thin layer chromatography. An oily purple substance, 39 mg (17 %), was obtained.

^{1}H-NMR (500 MHz, $CDCl_3$, δ / ppm): 6.57 (1H, *s*), 3.23 (4H, *dd*, J_1 = 5 Hz, J_2 = 10 Hz,), 1.28 (9H, *s*).

^{13}C-NMR (125 MHz, $CDCl_3$ δ / ppm): 181.44 (C1), 180.57 (C4), 156.17 (C2), 139.61 (C6), 136.54 (C5), 131.41 (C3), 35.45 (C7), 29.11 (C8, C9, C10), 27.06 (C12), 26.34 (C11).

UV/Vis, λ_{max} / nm (ε / dm^2 mol^{-1}): 230 (8.9×10^4), 275 (4.1×10^4), 535 ($1.3x10^3$).

EI MS, *m/z* (relative abundance, %): 254.1 (M^+, 100), 239.1 (30), 210.9 (40), 193.0 (25), 183.0 (20), 88.0 (15), 67.1 (15), 41.1 (20).

*Synthesis of 2-*tert*-butyl-5-(phenylthio)-1,4-benzoquinone (**5**) and 2-*tert*-butyl-6-(phenylthio)-1,4-benzoquinone (**6**)*

2-*tert*-Butyl-1,4-benzoquinone (313 mg) and 55 mg (51 μL) of thiophenol were mixed. The reaction was performed under an air atmosphere in 96 % ethanol at 60 °C for 30 min. The dark red crude product (466 mg) was applied to a column of 24 g silica gel (0.063–0.200 mm). It was eluted with toluene and the chromatography was evaluated by TLC. Two products were obtained: 2-*tert*-butyl-5-(phenylthio)-1,4-benzoquinone **(5)** in an amount of 29 mg (11 %) and 2-*tert*-butyl-6-(phenylthio)-1,4-benzoquinone **(6)** in amount of 51 mg (19 %).

(5) ^{1}H-NMR (500 MHz, $CDCl_3$, δ / ppm): 7.48 (5H, *m*), 6.49 (1H, *s*), 5.82 (1H, *s*), 1.31 (9H, *s*).

^{13}C-NMR (125 MHz, $CDCl_3$, δ / ppm): 186.96 (C1), 185.71 (C4), 157.80 (C6), 156.99 (C2), 137.23 (C5), 134.00 (C3), 132.01 (C11), 131.86 (C12, C16), 129.27 (C13, C15), 126.62 (C14), 36.88 (C7), 30.58 (C8, C9, C10).

UV/Vis, λ_{max} / nm (ε / dm^2 mol^{-1}): 253 (2.1×10^4), 290 (1.4×10^4), 443 (5.8×10^3).

EI MS, *m/z* (relative abundance, %): 272.1 (M^+, 100), 257.1 (20), 229.1 (30), 188.1 (20), 134.1 (20), 109.1 (20), 95.1 (20), 67.1 (20).

(6) ^{1}H-NMR (500 MHz, $CDCl_3$) δ / ppm: 7.47 (5H, *m*), 6.48 (1H, *d*, J = 5 Hz,), 5.80 (1H, *d*, J = 5 Hz), 1.30 (9H, *s*)

^{13}C-NMR (125 MHz, $CDCl_3$, δ / ppm): 186.74 (C1), 185.45 (C4), 157.69 (C6), 156.99 (C2), 137.16 (C5), 133.85 (C3), 132.38 (C11), 131.79 (C12, C16), 129.18 (C13, C15), 126.57 (C14), 36.87 (C7), 30.36 (C8, C9, C10)

UV/Vis, λ_{max} / nm (ε / dm^2 mol^{-1}): 250 (6.1×10^3), 298 (4.9×10^3), 440 (1.5×10^3);

EI MS, *m/z* (relative abundance, %): 272.1 (M^+, 100), 257.1 (20), 229.1 (30), 188.1 (20), 134.1 (20), 109.1 (20), 95.1 (20), 67.1 (20)

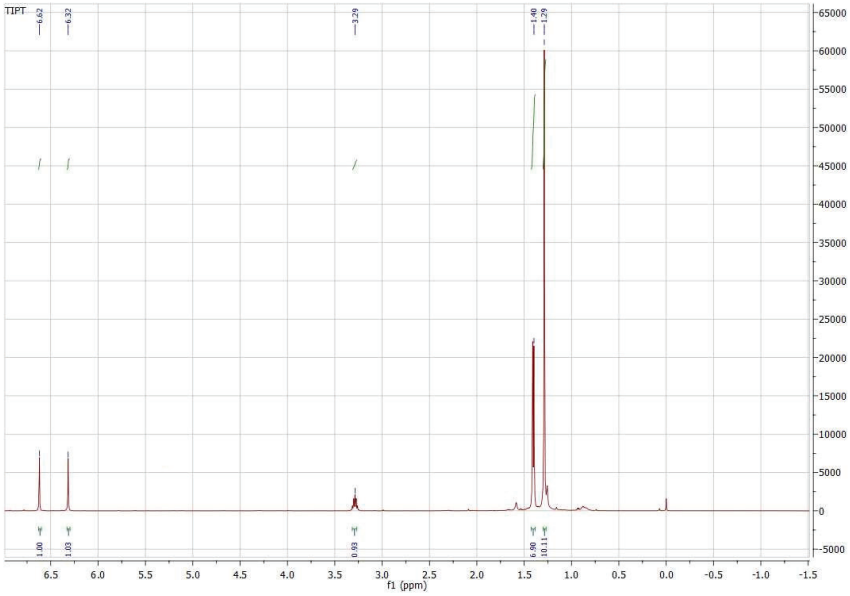

Fig. S-1. ^{1}H-NMR spectrum of 2-*tert*-butyl-5-(isopropylthio)-1,4-benzoquionone.

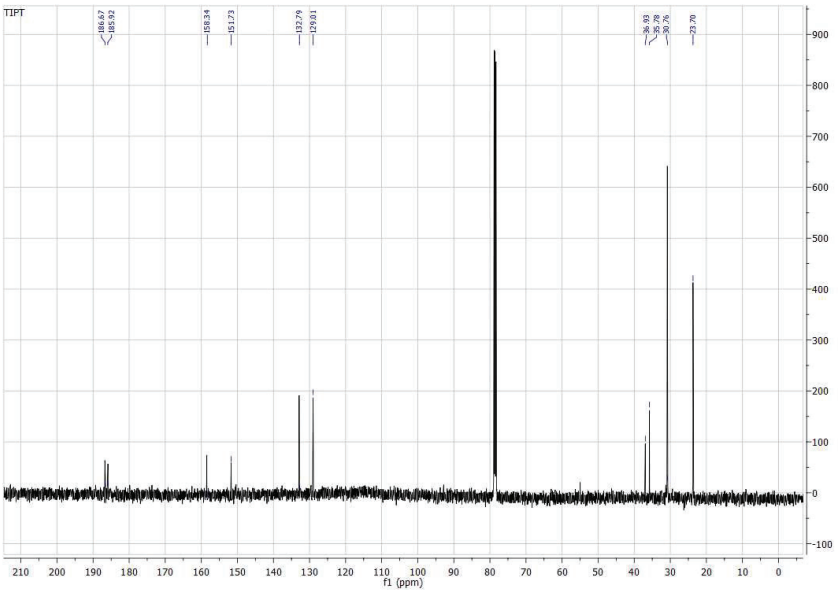

Fig. S-2. ^{13}C-NMR spectrum of 2-*tert*-butyl-5-(isopropylthio)-1,4-benzoquionone.

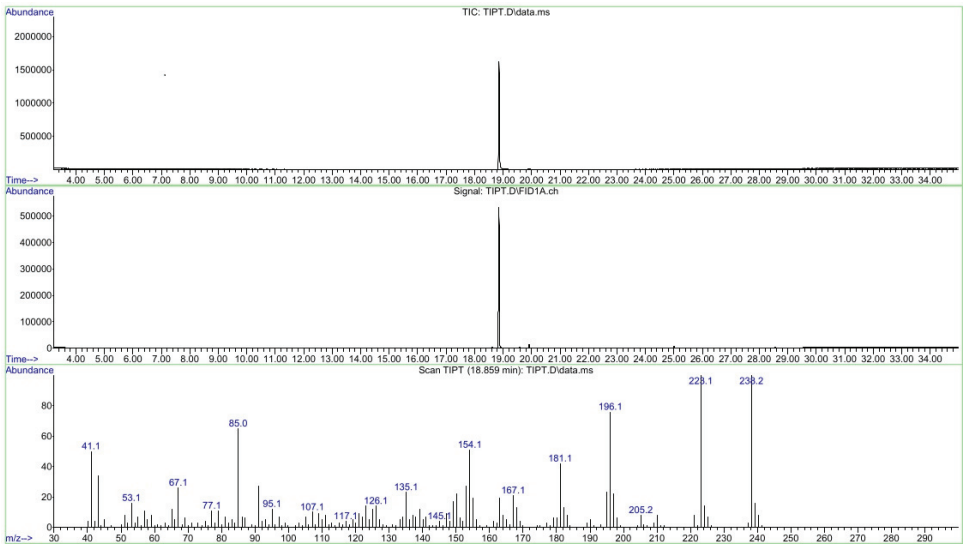

Fig. S-3. EI MS spectrum of 2-*tert*-butyl-5-(isopropylthio)-1,4-benzoquionone.

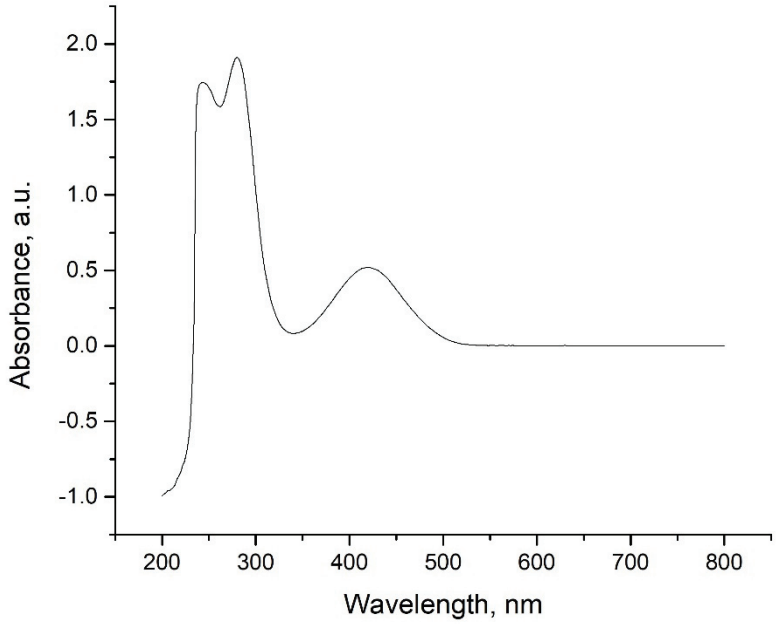

Fig. S-4. UV/Vis spectrum of 2-*tert*-butyl-5-(isopropylthio)-1,4-benzoquionone.

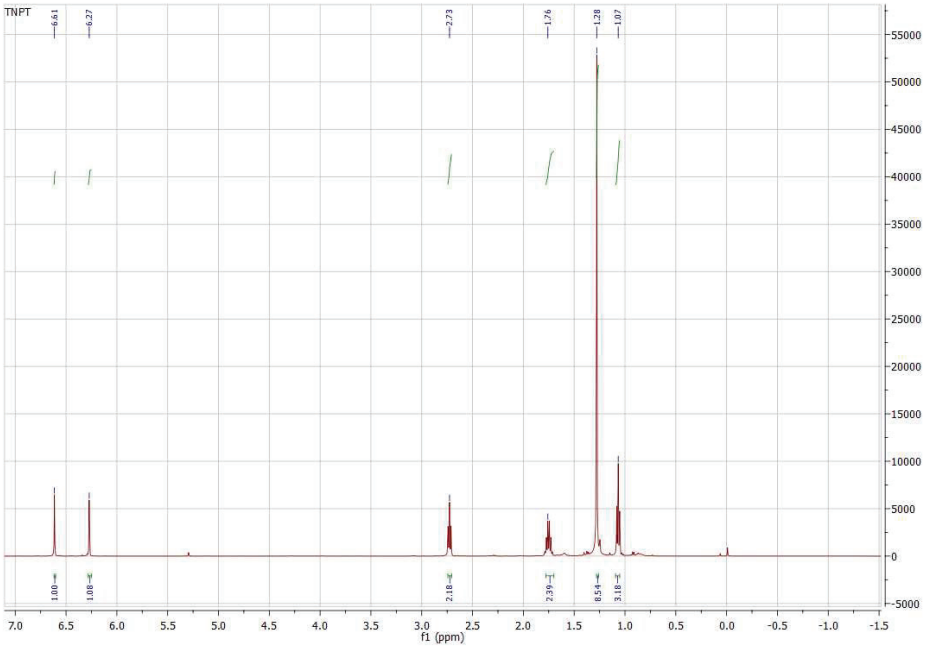

Fig. S-5. ^{1}H-NMR spectrum of 2-*tert*-butyl-5-(propylthio)-1,4-benzoquionone.

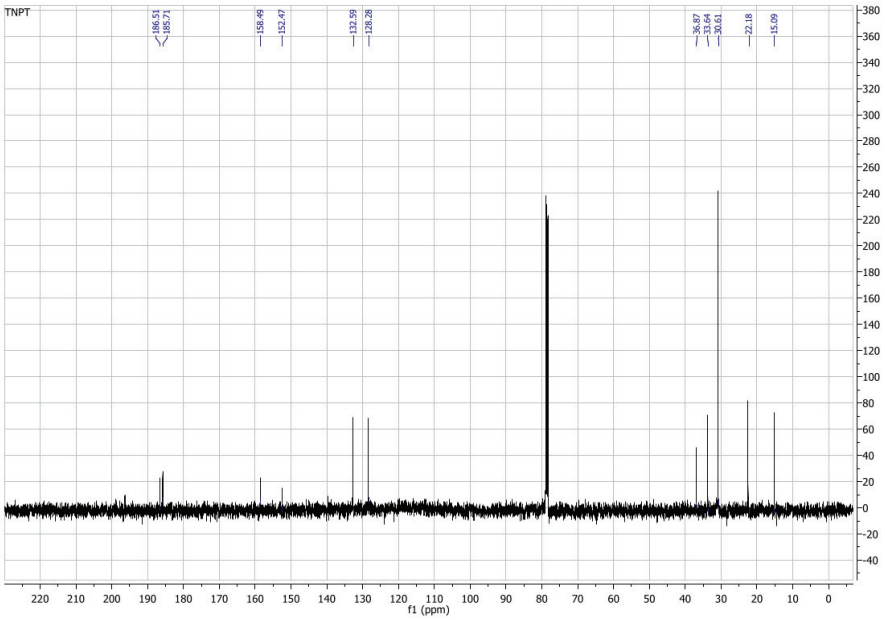

Fig. S-6. ^{13}C-NMR spectrum of 2-*tert*-butyl-5-(propylthio)-1,4-benzoquionone.

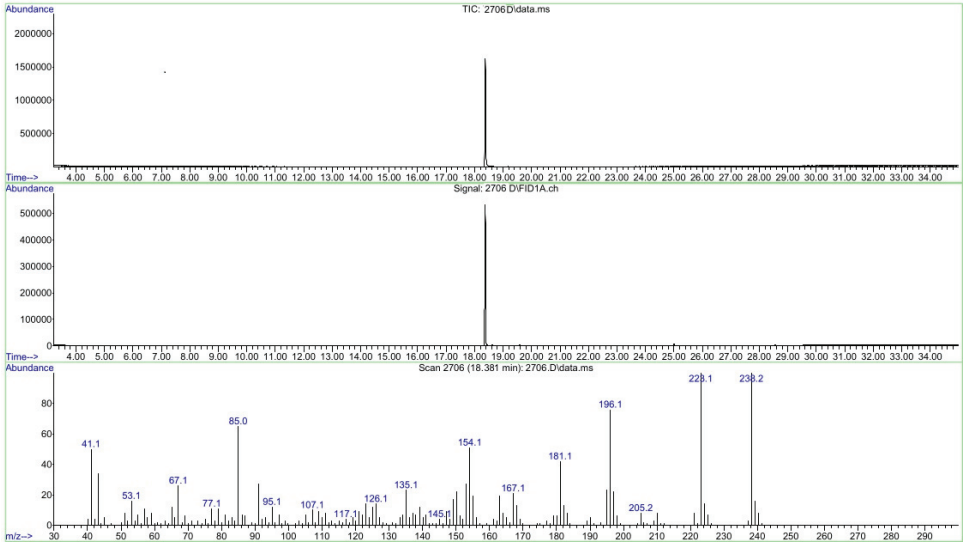

Fig. S-7. EI MS spectrum of 2-*tert*-butyl-5-(propylthio)-1,4-benzoquionone.

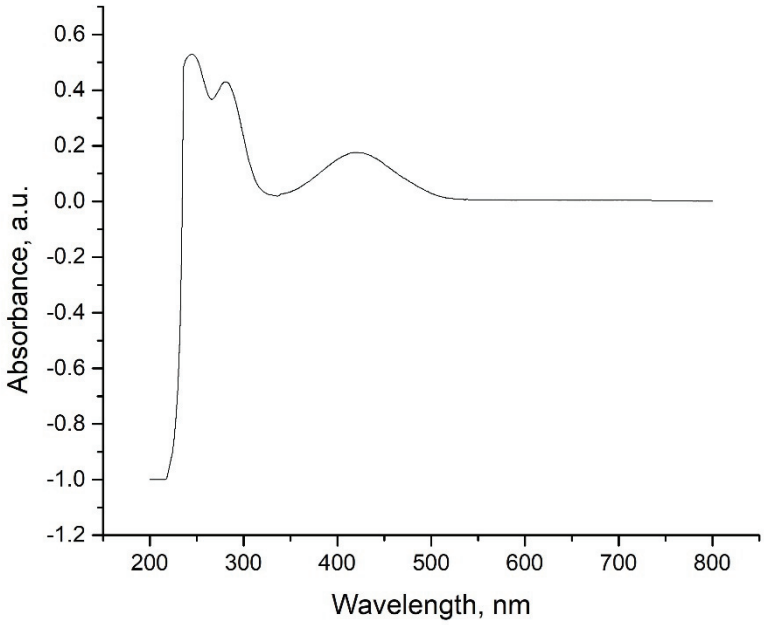

Fig. S-8. UV/Vis spectrum of 2-*tert*-butyl-5-(propylthio)-1,4-benzoquionone.

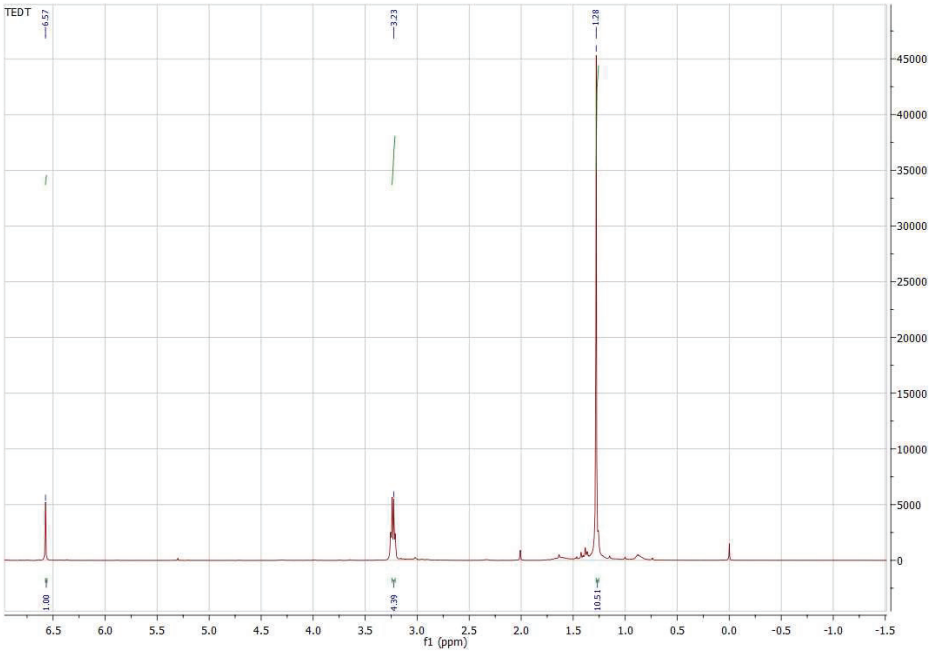

Fig. S-9. ^{1}H-NMR spectrum of 2-*tert*-butyl-5,6-(ethylenedithio)-1,4-benzoquionone.

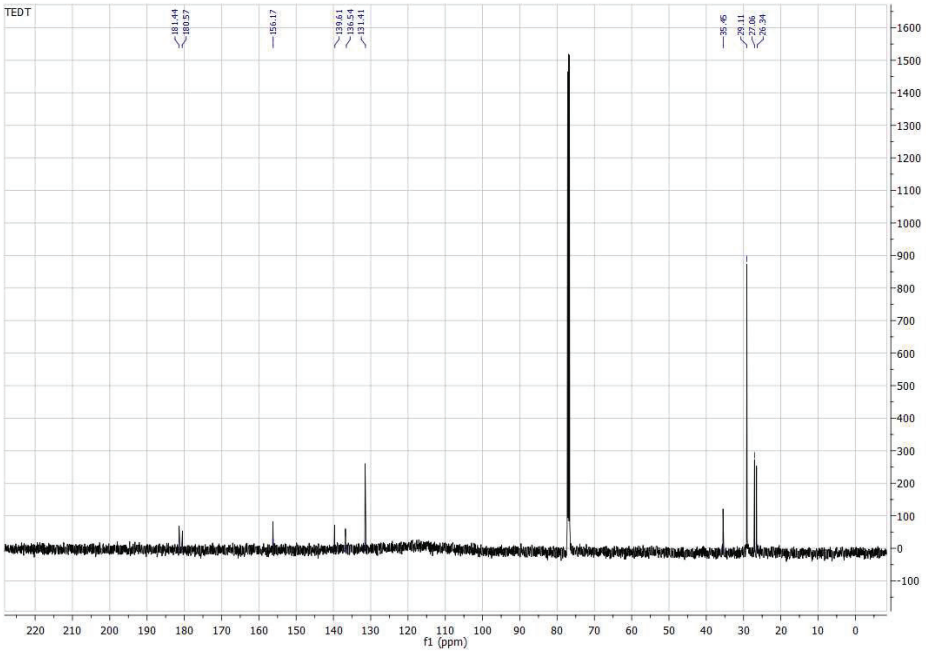

Fig. S-10. ^{13}C-NMR spectrum of 2-*tert*-butyl-5,6-(ethylenedithio)-1,4-benzoquionone.

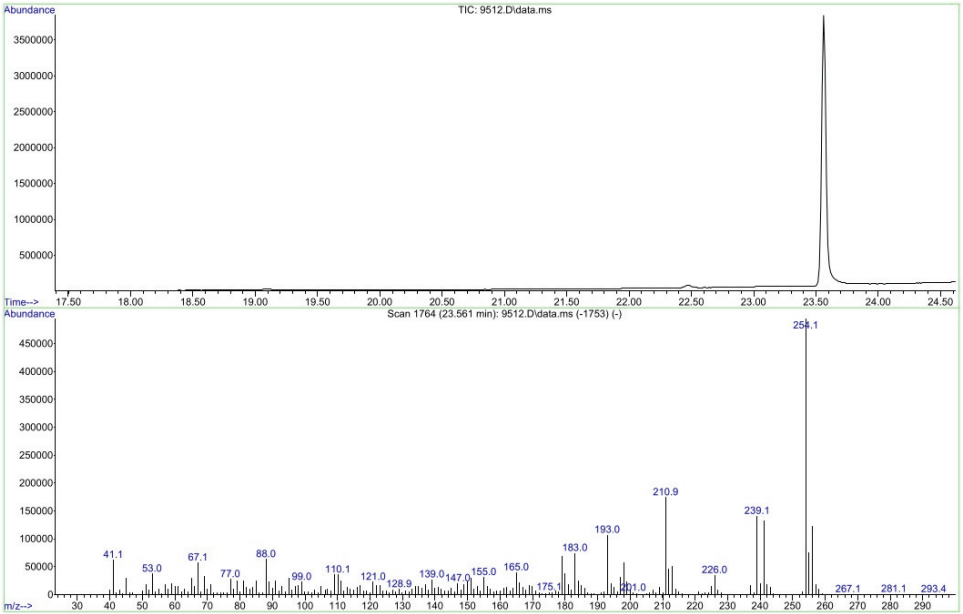

Fig. S-11. EI MS spectrum of 2-*tert*-butyl-5,6-(ethylenedithio)-1,4-benzoquionone.

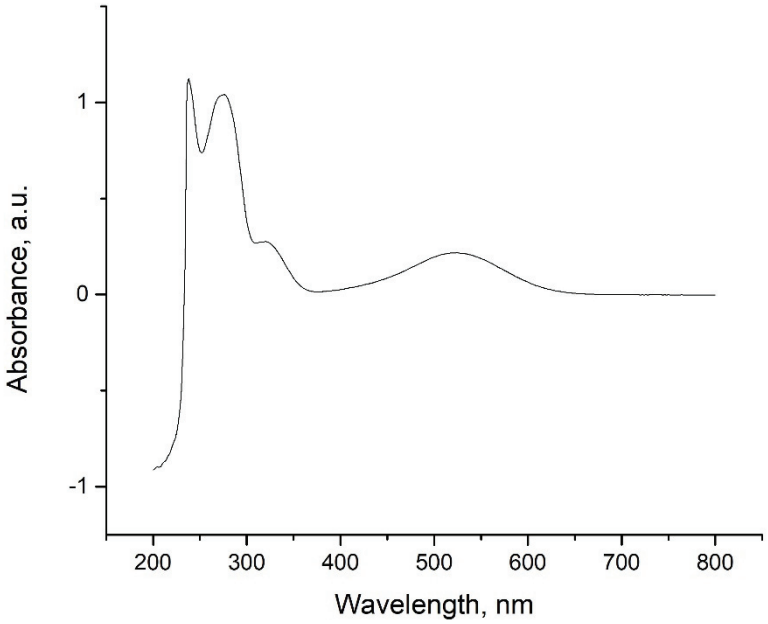

Fig. S-12. UV/Vis spectrum of 2-*tert*-butyl-5,6-(ethylenedithio)-1,4-benzoquionone.

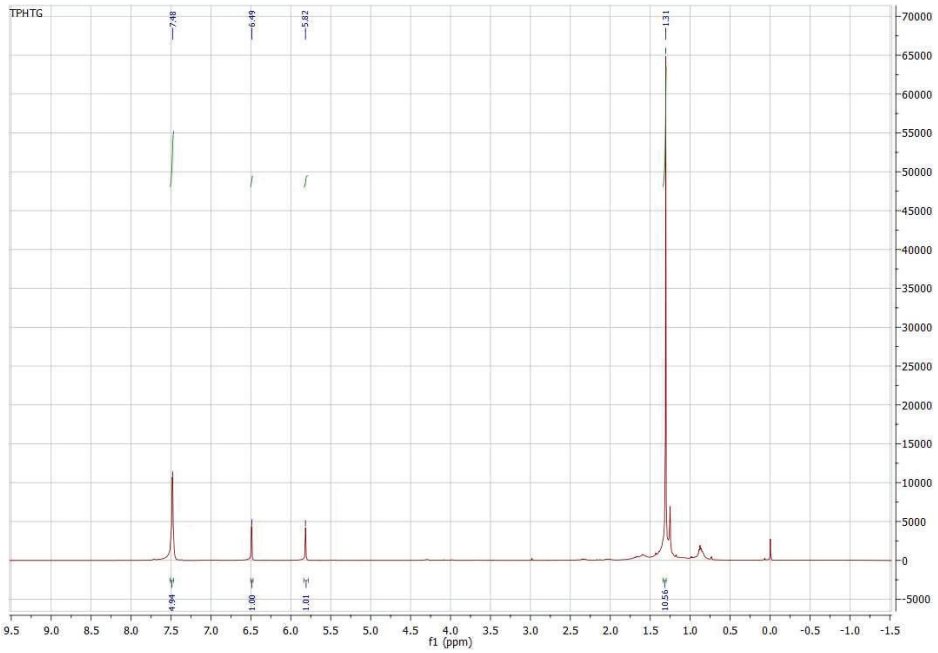

Fig. S-13. ^{1}H-NMR spectrum of 2-*tert*-butyl-5-(phenylthio)-1,4-benzoquionone.

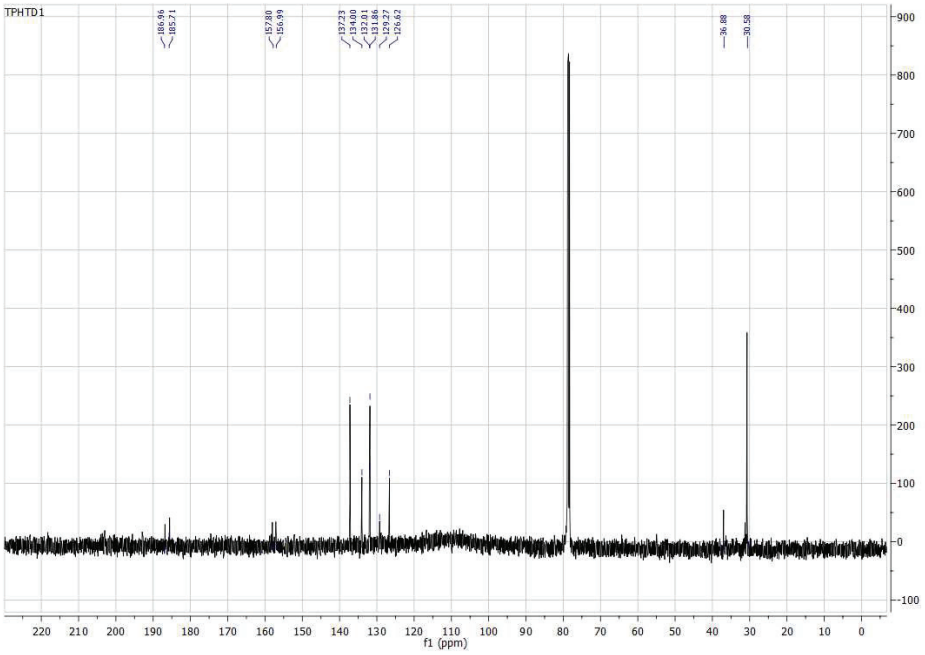

Fig. S-14. ^{13}C-NMR spectrum of 2-*tert*-butyl-5-(phenylthio)-1,4-benzoquionone.

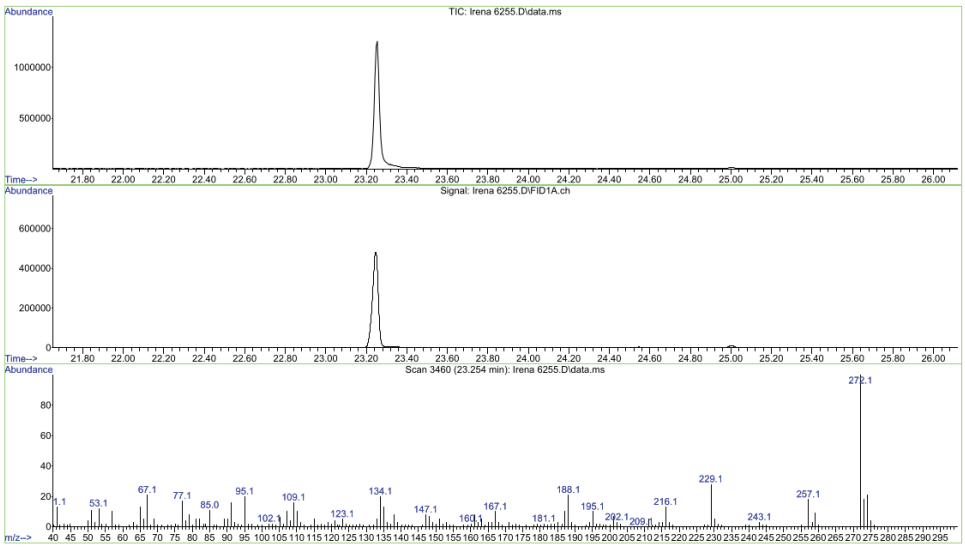

Fig. S-15. EI MS spectrum of 2-*tert*-butyl-5-(phenylthio)-1,4-benzoquionone.

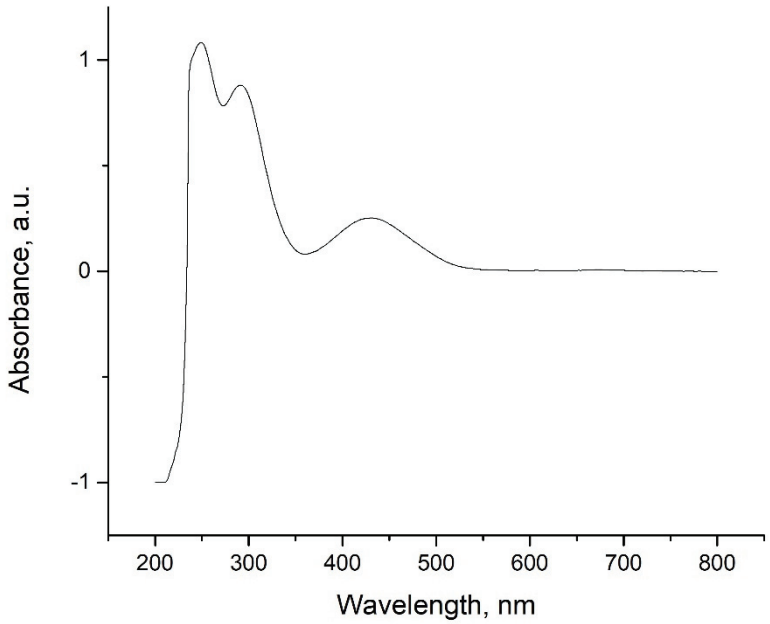

Fig. S-16. UV/Vis spectrum of 2-*tert*-butyl-5-(phenylthio)-1,4-benzoquionone.

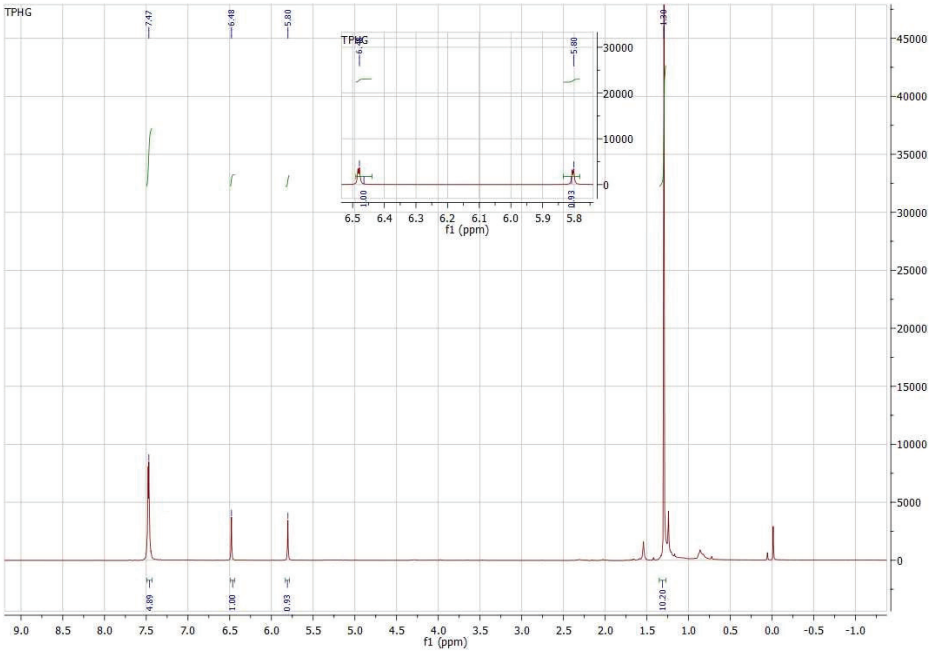

Fig. S-17. ^{1}H-NMR spectrum of 2-*tert*-butyl-6-(phenylthio)-1,4-benzoquionone.

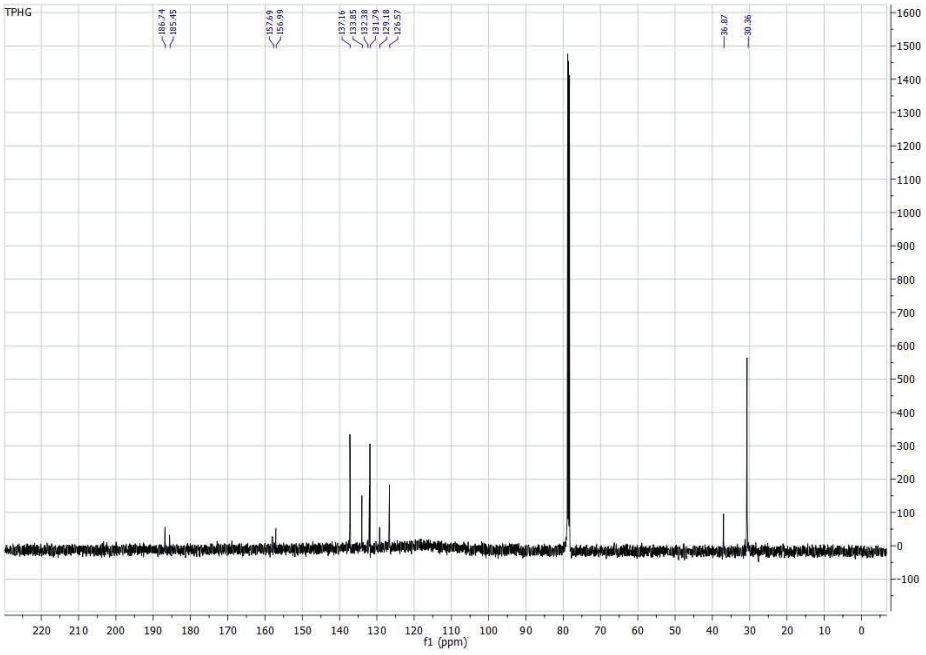

Fig. S-18. ^{13}C-NMR spectrum of 2-*tert*-butyl-6-(phenylthio)-1,4-benzoquionone.

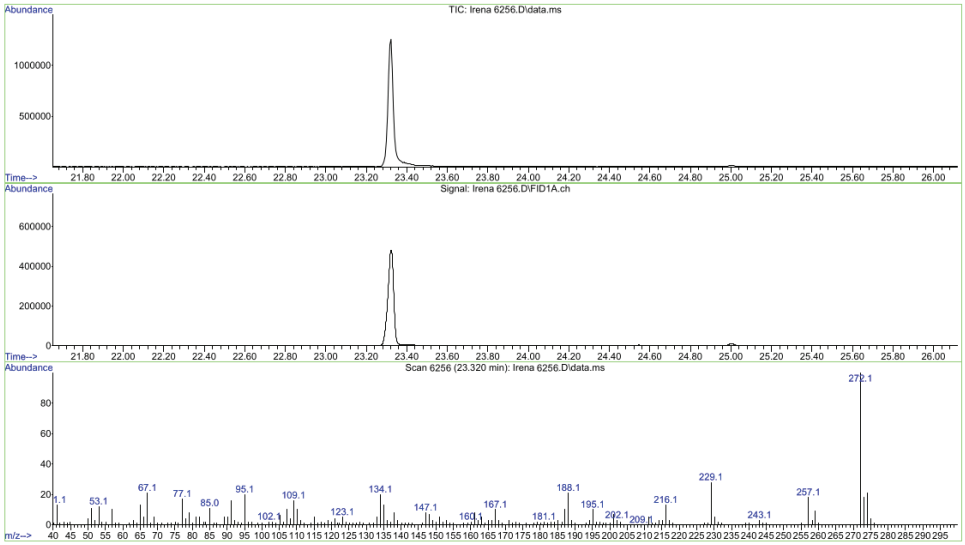

Fig. S-19. EI MS spectrum of 2-*tert*-butyl-6-(phenylthio)-1,4-benzoquionone.

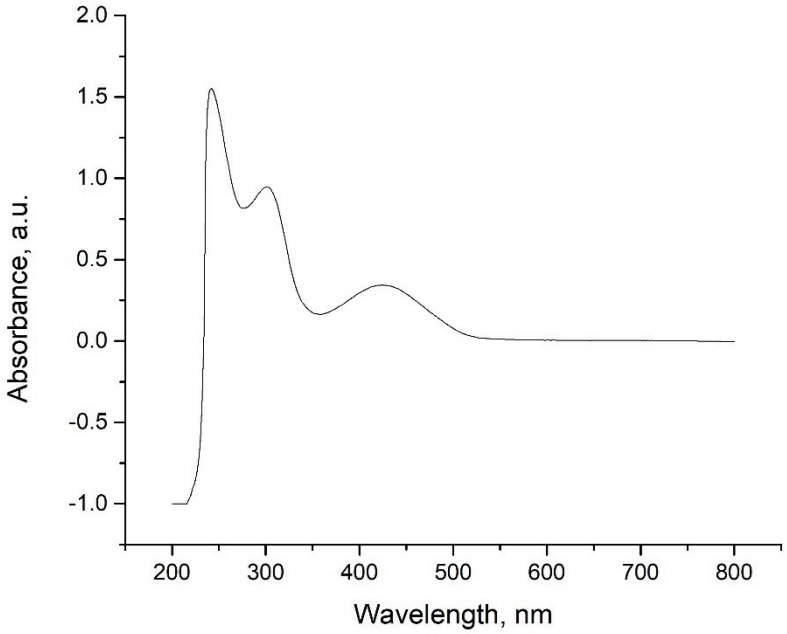

Fig. S-20. UV/Vis spectrum of 2-*tert*-butyl-6-(phenylthio)-1,4-benzoquionone.

Journal of the Serbian Chemical Society
JSCS@tmf.bg.ac.rs • www.shd.org.rs/JSCS
J. Serb. Chem. Soc. *87* (11) 1259–1272 (2022)
JSCS–5592
Original scientific paper
Published 4 November 2022

Synthesis and structural characterization of Cd(II) complexes with 2-acetylpyridine-aminoguanidine – A novel coordination mode

MIRJANA M. RADANOVIĆ[1]*#, SLAĐANA B. NOVAKOVIĆ[2#], MARKO V. RODIĆ[1#], LJILJANA S. VOJINOVIĆ-JEŠIĆ[1#], CHRISTOPH JANIAK[3] and VUKADIN M. LEOVAC[1#]

[1]*University of Novi Sad Faculty of Sciences, Trg D. Obradovića 3, 21000 Novi Sad, Serbia,* [2]*"Vinča" Institute of Nuclear Sciences, National Institute of the Republic of Serbia, University of Belgrade, P.O. Box 522, 11001 Belgrade, Serbia and* [3]*Heinrich-Heine-Universität Düsseldorf, Institute for Inorganic Chemistry and Structural Chemistry, Universitätsstraße 1, Düsseldorf, D-40225, Germany*

(Received 13 June, revised 30 July, accepted 8 September 2022)

Abstract: The structures of the first two complexes with bidentate coordination of aminoguanidine Schiff base, *i.e.*, 2-acetylpyridine-aminoguanidine (**L**), are reported. The complex of the formula $[Cd_2Cl_6(HL)_2]$ (**1**) was obtained in the reaction of warm aqueous solutions of chloride salts of Cd(II), Zn(II) and the ligand, while the reaction of cadmium bromide and the ligand in the presence of deprotonating agent as well as ammonium thiocyanate resulted in the formation of the complex in which Schiff base has both the role of the ligand and the counterion, *viz.*, $[HL][Cd(HL)(NCS)_2XY]\cdot H_2O$ (**2**), where X is Cl^- or Br^-, and Y Br^- or SCN^-. The complexes were characterized by IR spectroscopy, elemental analysis, conductometric measurements and single crystal X-ray diffraction. The unusual bidentate coordination of the Schiff base lead to significant changes in the geometry of this molecule (from almost planar in free form and as a tridentate ligand to twisted as a bidentate ligand). Besides, in complex **1** relatively rare bridging coordination of Cl^- in octahedral Cd(II) is found, while the crystal structure of complex **2** exhibits substitutional disorder, and contains four different anions: $[Cd(HL)(NCS)_2Br(SCN)]^-$ (*ca.* 61 %), $[Cd(HL)(NCS)_2Cl(SCN)]^-$ (*ca.* 35 %), $[Cd(HL)(NCS)_2Br_2]^-$ (*ca.* 3 %) and $[Cd(HL)(NCS)_2ClBr]^-$ (*ca.* 1 %).

Keywords: guanylhydrazone; Schiff base; crystal structure; physicochemical properties; metal complexes.

* Corresponding author. E-mail: mirjana.lalovic@dh.uns.ac.rs
# Serbian Chemical Society member.
https://doi.org/10.2298/JSC220613072R

INTRODUCTION

This study emerged from our ongoing research on metal complexes with Schiff base ligands, as this class of compounds has shown wide spectra of biological activities,[1] catalytic behavior,[2] magnetism[3] and optoelectronic properties,[4] depending on the choice of the particular metal, and Schiff base ligand. Besides the simple synthetic routes, the importance of these compounds lies in their ability to act as ligands of various denticities, thus the structural versatility and different potential application.[5,6] Thiocyanate is an interesting ambidentate co-ligand due to its ability to coordinate to the metal ion not only in the monodentate manners at one of its terminal atoms but also as a $\mu_{1,1}$ bridge (through sulfur or nitrogen) and $\mu_{1,3}$ bridge (*via* both).[7]

Researches have shown that Group 12 complexes are important in the field of supramolecular chemistry, crystal growth[8] and materials science.[9] However, cadmium is known to be a human carcinogen[10] and environmental pollutant, and some studies show[11,12] cadmium exposure can lead to genomic instability and inhibition of DNA damage repair. On the other hand, there is also evidence of anticancer activity of cadmium and its complexes with bioactive heterocyclic Schiff bases.[13–16] Since the mechanisms of these processes remain unknown it is of high importance to broaden the knowledge on structural properties of cadmium(II) complexes with potentially bioactive Schiff bases. Here, the syntheses and structure of two new Cd(II) complexes with 2-acetylpyridine-aminoguanidine (**L**), of the formulas $[Cd_2Cl_6(HL)_2]$ (**1**) and $[HL][Cd(HL)(NCS)_2XY]\cdot H_2O$ (**2**) (where X is Cl^- or Br^- and Y Br^- or SCN^-) is described. The free Schiff base is isolated as chloride (Fig. 1) and thiocyanate salt, while the coordinated form is usually neutral.[17] These are the first two complexes in which this Schiff base coordinates in a monoprotonated form and acts as a bidentate ligand.

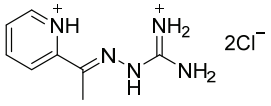

Fig. 1. Structural formula of 2-acetylpyridine-aminoguanidine dihydrogendichloride, $[H_2L]Cl_2$.

EXPERIMENTAL

Reagents

All commercially obtained reagent-grade chemicals were used without further purification except for the ligand 2-acetylpyridine-aminoguanidine dihydrogendichloride, $[H_2L]Cl_2$, which was synthesized according to the previously described procedure.[17]

Preparation of the complex $[Cd_2Cl_6(HL)_2]$ (1)

The mixture of 0.5 mmol (0.09 g) $CdCl_2$, 0.5 mmol (0.07 g) $ZnCl_2$, and 0.5 mmol (0.125 g) $[H_2L]Cl_2$ was mildly heated in 6 mL H_2O until dissolution. The resulting yellow solution was left at the room temperature and after 3 weeks orange prismatic single crystals were filtered and washed with EtOH. Yield: 0.14 g (70 %). Anal. Calcd. for $C_{16}H_{24}N_{10}Cl_6Cd_2$: C, 24.20; H, 3.05; N, 17.65. Found: C, 24.62; H, 3.18; N, 18.02 %. Conductivity, Λ = 130 S cm^2

mol^{-1} (in DMF). M.p. > 250 °C. Selected IR bands (wavenumber, cm^{-1}): 3337 (*s*), 3206 (*s*), 3084 (*s*), 1688 (*vs*), 1610 (*s*), 1580 (*s*), 1529 (*s*), 1450 (*m*), 1298 (*m*), 1225 (*m*), 1163 (*m*), 1093 (*m*), 935 (*w*), 782 (*m*), 622 (*m*), 591 (*m*), 558 (*m*), 519 (*m*).

*Preparation of the complex [HL][Cd(HL)(NCS)$_2$XY]·H$_2$O (**2**)*

The mixture of the ligand (0.5 mmol; 0.125 g) and LiOAc (1 mmol; 0.1 g) was dissolved in 5 mL of warm H_2O. To this solution the $CdBr_2$ (0.5 mmol; 0.09 g) and NH_4NCS (1 mmol; 0.08 g) were added and slightly heated for about 5 min. The yellow solution was left at the room temperature and after 8 days the orange precipitate was filtered, washed with H_2O and EtOH. Upon recrystallization form MeOH rod-like single crystals of the complex were obtained. Yield: 0.14 g (42 %). Anal. Calcd. for $C_{19}H_{26}N_{13}OS_3BrClCd$: C, 29.39; H, 3.37; N, 23.46; S, 12.39. Found: C, 29.87; H, 3.50; N, 22.95; S, 12.78 %. Conductivity, Λ = 142 S cm^2 mol^{-1} (in DMF). M.p. = 175 °C. Selected IR bands (wavenumber, cm^{-1}): 3420 (*s*), 3345 (*s*), 3157 (*s*), 2112 (*vs*), 2077 (*vs*), 2058 (*vs*), 1676 (*vs*), 1629 (*vs*), 1586 v(*s*), 1477 (*m*), 1434 (*m*), 1162 (*m*), 1149 (*m*), 1100 (*w*), 1003 (*w*), 786 (*m*), 561 (*w*).

Analytical methods

Elemental analyses (C, H, N and S) of air-dried compounds were carried out by standard micro-methods. Molar conductivity measurements of freshly prepared solutions (c = 1 mmol L^{-1}) were performed on a Jenway 4010 conductivity meter. IR spectra were recorded on a Nicolet Nexus 670 FTIR (Thermo Scientific) spectrophotometer, in the range of 400–4000 cm^{-1} by the KBr pellet technique. Melting points were measured on a Nagema melting point microscope Rapido.

Single crystal X-ray diffraction

Diffraction experiments for **1** and **2** were performed on Bruker APEX-II CCD and Oxford Diffraction Gemini S diffractometers at 140 and 295 K, respectively. Reflection integration and data reduction were performed with the corresponding software Bruker SAINT[18] and CrysAlisPro.[19] Crystal structures were solved with the SHELXT[20] and refined with the SHELXL.[21] In the case of [HL][Cd(HL)(NCS)$_2$XY]·H$_2$O (**2**) the coordination site X was refined as being substitutionally disordered between bromine and chlorine ligands, with the corresponding occupancies of 0.640(2) and 0.360(2), respectively; the coordination site Y was refined as being substitutionally disordered between SCN^- and Br^- ligands with the corresponding occupancies of 0.943(2) and 0.057(2), respectively. Hydrogen atoms bonded to carbon atoms were introduced in idealized positions and treated with a riding model. Hydrogen atoms bonded to nitrogen were found in residual electron density maps and refined with distance restraints (d(N–H) = 0.88(2) Å for **1** and 0.86(2) Å for **2**) or introduced in idealized positions and treated with a riding model. Their displacement parameters are derived from their parent atoms (U_{iso}(H) = 1.2U_{eq}(N)). Hydrogen atoms of water molecule were refined freely. Crystallographic and refinement details are listed in Table I.

RESULTS AND DISCUSSION

Syntheses and characterization

The previous research concerning coordination behavior of Zn(II) and Cd(II) and the titled Schiff base, showed that there are a lot of similarities, but also there are some fine differences, *i.e.*, Cd(II) being prone to form dimeric complexes with bridging coordination of ions.[22] Hence, in the attempt to examine the competitive coordination of these two cations to the ligand, in the reaction of metal

chlorides and the chloride ligand salt in the aqueous solution, complex **1** was obtained in the form of yellow prismatic single crystals.

TABLE I. Crystal data, data collection and refinement details

Chemical formula	$C_{16}H_{24}N_{10}Cl_6Cd_2$ (**1**)	$C_{19}H_{26}N_{13}OS_3BrClCd$ (**2**)
Temperature, K	140(2)	295(2)
Formula weight, g mol^{-1}	793.95	776.47
Crystal system	triclinic	triclinic
Space group	$P\bar{1}$	$P\bar{1}$
a / Å	8.4921(6)	7.9033(3)
b / Å	8.7865(7)	11.4014(4)
c / Å	10.6536(8)	16.5784(7)
α / °	76.4318(13)	97.450(3)
β / °	70.7718(12)	90.557(3)
γ / °	64.4782(12)	99.580(3)
V / Å^3	673.32(9)	1459.84(10)
Crystal size, mm^3	0.50×0.25×0.20	0.56×0.37×0.29
Reflections collected / unique	27790 / 6537	19089 / 6799
Observed reflections [$I > 2\sigma(I)$]	6367	5829
R_{int}	0.021	0.022
R [$I > 2\sigma(I)$]	0.015	0.030
R (all data)	0.016	0.039
Goodness-of-fit	1.179	1.010
$\Delta\rho_{max}$, $\Delta\rho_{min}$, e Å^{-3}	0.562, −0.656	0.561, −0.541

Complex **2** was formed in the reaction of warm aqueous solutions of $CdBr_2$ and $[H_2L]Cl_2$, in mole ratio 1:1, in the presence of double excess of LiOAc and NH_4NCS. The white rod-like single crystals suitable for single crystal X-ray diffraction (SC-XRD) were obtained upon the recrystallization from MeOH.

It is interesting to mention that a similar reaction with $CdCl_2$, and in the absence of deprotonating agent, yielded in the hydrolysis of the imine group of the Schiff base thus the formation of Cd(II) complex with 2-acetylpyridine with thiocyanates as bridging ligands. This complex was previously synthesized in the reaction of $Cd(NO_3)_2$, 2-acetylpyridine and ammonium thiocyanate in methanolic solution thus structurally characterized.[23]

Having in mind the pronounced alkaline nature of the aminoguanidine residue it is not surprising that its Schiff bases in the complexes can have a role of both the ligand and the counter-ion.[22] The survey of Cambridge Structural Database (CSD)[24] revealed 49 complex compounds containing Schiff bases of aminoguanidine. Namely, the majority of these contain the Schiff base coordinated in the tridentate manner (33 structures), while there are only 4 structures with the Schiff base of AG having the role of a tetradentate[25–28] and only 1 structure in which monodentate[29] coordination was found. In 11 structures the guanylhydrazone has the role of counter-ion. However, these are the first two examples in

which the bidentate mode of coordination of Schiff base of aminoguanidine is found. Details of CSD search are given in Supplementary material to this paper (Tables S-I–S-IV).

Both complexes are well soluble in DMF, while poorly soluble in H_2O and alcohols. Molar conductivity of DMF solution complex **1** has value characteristic for the 2:1 type of electrolytes, which suggests the substitution of anionic ligands by solvent molecules. Complex **1** is stable at higher temperatures (m.p. >250 °C), while complex **2** appears to decompose at higher temperatures (135 °C) and the residue finally melts at 175 °C.

Comparative analysis of the IR spectrum of the free ligand and the spectra of the complexes showed a lot more similarities than differences, thus very few things about the coordination of the Schiff base could be concluded with certainty. The reasons for this were revealed by X-ray analysis (*vide infra*). Namely, the ligand coordinates as NN bidentate, *via* pyridine and azomethine nitrogen atoms, while the aminoguanidine residue stays protonated thus non-coordinated. So, in the spectra of both the complexes ν(CN) bands originating from the imino group of aminoguanidine residue appear at nearly the same wavenumbers (1622 cm^{-1} for complex **1** and 1629 cm^{-1} for complex **2**) as in the spectrum of the ligand (1624 cm^{-1}).[17] Also, in the structure of complex **2** one cation of the Schiff base is coordinated, while the other has a role of a counterion. This makes the identification of the corresponding bands' shifts, upon coordination, difficult. Additionally, in the spectrum of complex **2** three very strong bands, present in the range 2060 to 2110 cm^{-1}, are attributed to coordinated NCS^- – two coordinated through N atom (2060 and 2077 cm^{-1}) and the third coordinated through S atom (2110 cm^{-1}).

Crystal structure analysis

Molecular structures of complexes **1** and **2** are presented in Fig. 2, while selected structural data are summarized in Table II. Both complexes are characterized by unusual, bidentate coordination mode of 2-acetylpyridine-aminoguanidine ligand and, to our knowledge, represent the first cases of metal complexes where this Schiff base coordinates as a bidentate ligand. Up to now several complexes of Cu(II), Zn(II), as well as Cd(II) with the same organic ligand, have been reported.[17,22,30] In these compounds the ligand is present in its neutral form and exhibits tridentate coordination by pyridine N5, azomethine N3 and imino N1 nitrogen of aminoguanidine. The specific feature of **1** and **2** is that the organic ligand is protonated at aminoguanidine nitrogen N1. The resulting monocation coordinates to the Cd(II) in a bidentate fashion by pyridine N5 and azomethine N3 donors, forming a single chelate ring (Fig. 2).

Complex **1** consists of the neutral binuclear units, where two Cd(II) centers are bridged by a pair of chloride ions to form a Cd_2Cl_2 square-like metallocycle (Fig.

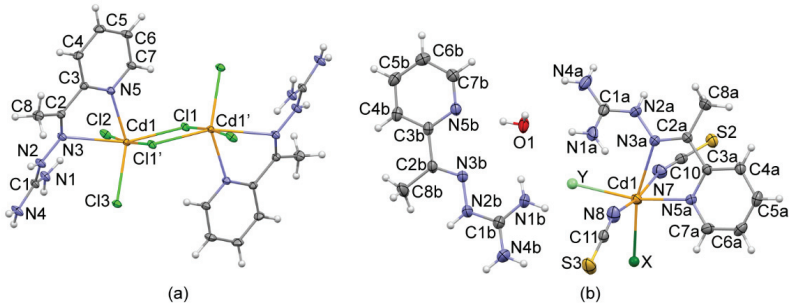

Fig. 2. Molecular structure of: a) $[Cd_2Cl_6(HL)_2]$ (**1**) and b) $[HL][Cd(HL)(NCS)_2XY]\cdot H_2O$, X = Cl^- or Br^- and Y = Br^- or SCN^- (**2**) with the atom labelling scheme. Displacement ellipsoids are drawn at the 30 % probability level.

TABLE II. Selected bond lengths and bond angles (comprehensive list is given in Tables S-V and S-VI of the Supplementary material)

Bond	**1**	**2**	
		A	B
Bond length, Å			
Cd1−N3	2.7483(8)	2.605(2)	–
Cd1−N5	2.2992(8)	2.348(2)	–
C1−N1	1.3212(13)	1.297(4)	1.303(3)
C1−N2	1.3512(12)	1.337(3)	1.335(3)
C1−N4	1.3253(12)	1.325(3)	1.326(3)
C2−N3	1.2939(12)	1.282(3)	1.277(3)
N2−N3	1.3796(11)	1.377(3)	1.378(3)
Bond angle, °			
N3−Cd1−N5	64.33(3)	65.86(6)	–
N2−N3−C2	115.94(8)	116.8(2)	116.8(2)
N3−N2−C1	118.98(8)	118.4(2)	117.9(2)
N1−C1−N2	121.19(8)	121.0(2)	120.3(2)
N1−C1−N4	121.41 (9)	121.7(3)	121.6(3)
N3−C2−C3	115.76(8)	115.5(2)	115.0(2)
C2−C3−N5	117.62(7)	117.3(2)	117.1(2)

2a). Each Cd(II) is placed in a distorted octahedral environment which, apart from two bridging Cl, also includes two terminal Cl ligands as well as the pyridine and azomethine N donors of the cationic Schiff base. The binuclear complex has a crystallographic inversion center in the middle of the Cd_2Cl_2 bridge. The Cd···Cd atom separation is 3.901(3) Å. Though the CSD[24] search reveals the relatively frequent occurrence of the Cd_2Cl_2 square-like fragment (223 CSD hits), it mainly belongs to the polymeric structures, while only in 34 cases it belongs to the discrete binuclear complexes. A similar bridge between the octahedrally coordinated Cd(II) centers is rare. It is found in two neutral Cd(II) complexes where the monodentate organic ligands bind next to the Cl (CSD Refcodes:

LOYZAC,[31] FOKMEZ[32]) and also in two anionic species where the water molecules bind next to the Cl ligands (QELLAX[22] and WIPTAQ[33]). The structures show wide variation in bridging Cd–Cl bond lengths, with values ranging from 2.36 to 2.76 Å, and bridging Cd–Cl–Cd' angles, with values ranging from 91.8 to 105.6 Å.

As mentioned above, unlike the previously reported complexes where 2-acetylpyridine-aminoguanidine ligand exhibits tridentate coordination,[17,22,30] the protonated ligand in complex **1** binds to the metal ion by two donor atoms. The different coordination mode significantly changes the geometry of the ligand, from almost flat in the previous complexes with tridentate ligand such as $[CdCl_2L]$,[22] to markedly twisted geometry in the novel complexes. Thus in complex **1**, the five-membered chelate ring exhibits considerable twisting on Cd1–N3 bond resulting in maximal torsion angle Cd–N3–C2–C3 of 35.5(1)°. In complex $[CdCl_2L]$,[22] the maximal torsion angle within the same chelate is Cd–N5–C3–N2 with −10.6°. The most pronounced difference in geometry of the two ligand forms is related to the orientation of their guanidine moiety. Since not coordinated, the guanidine residue in **1** points away from the metal ion (Fig. 2a). The dihedral angle between the mean planes of guanidine moiety and the chelate ring is 48.85(5) in **1**, while only 5.32° in $[CdCl_2L]$. The dihedral angle between the chelate and pyridine rings is more comparable, with the values of 10.52(6) and 7.05° in **1** and $[CdCl_2L]$,[22] respectively. The position of the guanidine moiety in **1** is stabilized by the intramolecular N1–H1b···Cl2 hydrogen bond, and also by the intermolecular hydrogen bonds which engage all N–H donors and terminal Cl ligands as acceptors (Table III). The N–H···Cl interactions arrange the complex molecules into 2D structures parallel to the crystallographic *ac* plane (Fig. 3).

In the complex compound of the formula $[HL][Cd(HL)(NCS)_2XY]\cdot H_2O$ (**2**) the protonated 2-acetylpyridine-aminoguanidine is present as a free cation as well as a coordinated ligand. The coordination environment of Cd(II) in the complex anion is distorted octahedral, with two axial sites occupied by NCS^-, two equatorial sites occupied by bidentate coordinated organic ligand, and the remaining two equatorial sites (X and Y) occupied by Cl^-/Br^- and Br^-/SCN^-, respectively. This means that the crystal structure contains four different anions: $[Cd(HL)(NCS)_2Br(SCN)]^-$ (*ca*. 61 %), $[Cd(HL)(NCS)_2Cl(SCN)]^-$ (*ca*. 35 %), $[Cd(HL)(NCS)_2Br_2]^-$ (*ca*. 3 %) and $[Cd(HL)(NCS)_2ClBr]^-$ (*ca*. 1 %).

Comparison between organic cations in free and coordinated form reveals little changes in bond lengths and valence angles (Table II). The coordination in **2**, leads to twisting of organic ligand, similar to that found in complex **1**. Thus, the dihedral angle between the pyridine and guanidine moiety is 7.5(2)° in uncoordinated HL^+, while 51.6(1) and 42.18(5)° in complexes **2** and **1**, respectively. Also similar to **1**, the maximal torsion angle within the five-membered chelate ring is Cd–N3–C2–C3 with −38.4(2)°. In comparison to previously rep-

orted complex $[CdCl_2L]$[22] with the neutral tridentate ligand, the complexes **1** and **2** show longer Cd–N coordination bonds, which is expected considering their different coordination geometry (square pyramidal vs. octahedral). The changes can be also observed for C1–N2 and N2–N3 bonds which in the cationic form of ligand get shorter and longer for 0.03 Å on average. The main difference is related to the angle C2–N3–Cd which in novel compounds reduces by almost 15° in comparison to the corresponding angle in $[CdCl_2L]$.[22]

TABLE III. Geometrical parameters for intermolecular interactions

D–H···A	*d*(D–H) / Å	*d*(H···A) / Å	∠(D–H···A) / °	Symmetry codes
		1		
N1–H1a···Cl2	0.87(1)	2.56(1)	150(1)	−*x*+2, −*y*+1, −*z*+1
N1–H1b···Cl2	0.88(1)	2.36(1)	155(1)	
N2–H2···Cl3	0.88	2.56	151	−*x*+1, −*y*+1, −*z*+1
N4–H4a···Cl3	0.85(1)	2.51(1)	157(1)	−*x*+1, −*y*+1, −*z*+1
N4–H4b···Cl2	0.88(1)	2.54(1)	144(1)	−*x*+2, −*y*+1, −*z*+1
C5–H5···Cl1	0.95	2.68	161	1+*x*, −1+*y*, *z*
C6–H6···Cl2	0.95	2.79	156	1−*x*, −*y*, −*z*
		2[a]		
N1a–H11a···O1	0.86	1.97	170	
N1a–H12a···N8	0.86	2.51	146	
N1b–H11b···S3	0.86	2.90	148	
N1b–H12b···O1	0.86	2.13	164	
N4a–H41a···S2	0.86	2.84	123	−*x*+1, −*y*+1, −*z*+2
N4b–H21···S3	0.86	2.59	161	
O1–H1a···N5b	0.83	1.96	175	
C4a–H4a···S2	0.93	2.88	162	−*x*+1, −*y*, −*z*+2
C6a–H6a···S3	0.93	2.93	145	−*x*+1, −*y*, −*z*+1
C7b–H7b···S2	0.93	2.97	120	−*x*+1, −*y*+1, −*z*+2

[a]Only parameters involving the ordered part of the complex are listed (see also Table S-VII of the Supplementary material)

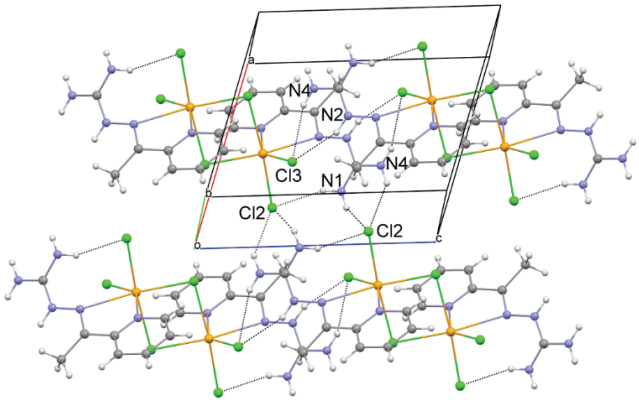

Fig. 3. Hydrogen bonding in **1**.

The crystal structure of **2** is stabilized by a complex hydrogen-bonding network involving N–H donors from both charged species, the acceptors form monodentate ligands as well as the molecule of crystal water (Fig. 4). Table III lists the hydrogen bonding contacts involving only ordered part of the structure.

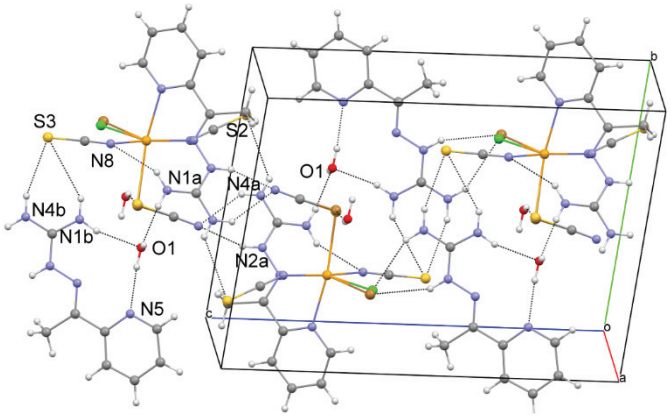

Fig. 4. Hydrogen bonding in **2**. Only two major anion components are shown: $[Cd(HL)(NCS)_2Br(SCN)]^-$ (*ca*. 61 %) and $[Cd(HL)(NCS)_2Cl(SCN)]^-$ (*ca*. 35 %).

To gain more insight in crystal packing features of both complexes, Hirshfeld surface analysis was performed. Hirshfeld surface of complex **1** decorated with d_{norm} has several prominent red patches (Fig. 5b), which correspond to short Cl···H contacts, details of which are listed in Table III. In the fingerprint plot (Fig. 5c), these are displayed as two symmetric prongs with peaks at d_e = 1.5 Å and d_i = 0.8 Å, and at d_e = 0.8 Å and d_i = 1.5 Å.

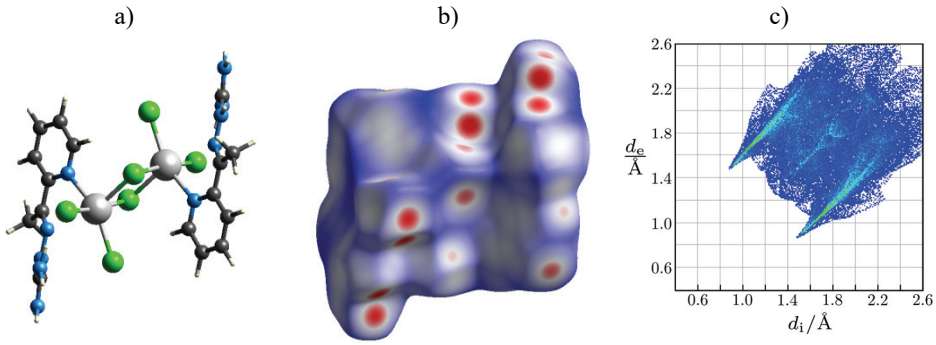

Fig. 5. Molecular structure (a), Hirshfeld surface (b) and corresponding fingerprint plot (c) of $[Cd_2Cl_6(HL)_2]$ (**1**).

The investigation of complex **2** by means of Hirshfeld surface analysis is complicated because of the ionic nature of the compound and presence of four

different anions in the crystal structure. It is worth emphasizing peculiarities of anionic Hirshfeld surfaces to gain insights why this four-component mixture is stable. These are calculated for idealized structures containing only one type of anion (Fig. 6). Two main anions that comprise 61 and 35 % of the mixture ($[Cd(HL)(NCS)_2Br(SCN)]^-$ and $[Cd(HL)(NCS)_2Cl(SCN)]^-$, respectively) show negligible overall difference in the molecular shape defined by their Hirshfeld surfaces. Both structures involve N···H hydrogen bond involving S-coordinated SCN^-, which is represented in their fingerprint plots by two symmetric prongs with peaks at d_e = 1.1 and d_i = 0.8 Å (N6···H2A(i)–N2A(i) hydrogen bond), and at d_e = 0.8 and d_i = 1.1 A (N2A–H2A···N6(i) hydrogen bond); symmetry code (i) –x+1, –*y*+1, –*z*+2.

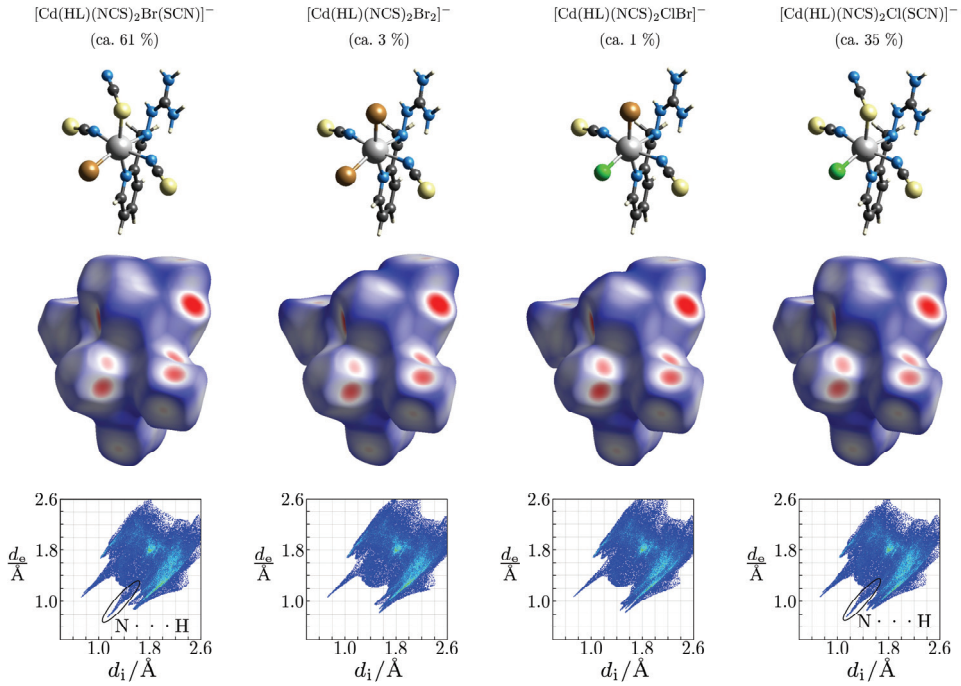

Fig. 6. Molecular structures (top), Hirshfeld surfaces (middle), and corresponding fingerprint plots (bottom) of the four structural components present in substitutionally disordered $[HL][Cd(HL)(NCS)_2XY]\cdot H_2O$.

In two minor components, in which coordinated SCN^- is substituted by Br^-, these hydrogen bonds are absent. Therefore, in the corresponding fingerprint plots, only a single spike is present, with peak at d_e = 1.1 Å and d_i =0.8 Å, that correspond to N1–H11a···O1 hydrogen bond, and the prongs corresponding to H···N hydrogen bonds are missing.

Crystal packing coefficient for idealized structures containing only one type of anion are within expected range, as CSD average packing coefficient for crystal structures of metal-organic molecules is 0.67(5). This explains that all four anions satisfy very well the principle of closest packing and maximal interaction, thus ensuring stability of the crystal structure (weighted average of the packing coefficient is 0.672). However, there is a noticeable trend between anions' amount ratio in the mixture and packing coefficients for its idealized structures, as well as to some extent, also of the volumes of the anions based on their Hirshfeld surfaces calculated for idealized structures (see Supplementary material, Table S-VIII).

CONCLUSION

In the reaction of warm aqueous solutions of the chloride salts of Cd(II), Zn(II), and the ligand, orange prismatic single-crystals of the complex $[Cd_2Cl_6(HL)_2]$ (**1**) were formed, while the reaction of cadmium bromide, chloride ligand salt, lithium acetate and ammonium thiocyanate yielded in the formation of an unusual complex of the formula $[HL][Cd(HL)(NCS)_2XY]\cdot H_2O$ (**2**) where L = 2-acetylpyridine-aminoguanidine, X = Cl^- or Br^-, Y = Br^- or SCN^-. These are the first two complexes in which the bidentate mode of aminoguanidine Schiff base is proven. The coordination is realized through pyridine and azomethine nitrogen, while the protonated aminoguanidine residue does not take part in coordination. The complexes are physicochemically and structurally characterized and compared to the previously synthesized ones. This gave great insight into the structural differences that are caused by the protonation of the aminoguanidine residue and could lead to different properties of these compounds in further research which will include the investigation of photoluminescence and antioxidant properties.

SUPPLEMENTARY MATERIAL

CCDC 2129140 and 2129141 contain the supplementary crystallographic data for this paper. These data can be obtained free of charge from The Cambridge Crystallographic Data Centre (https://www.ccdc.cam.ac.uk/structures/). The characterization data and pertinent crystallographic and refinement details are available electronically at the pages of journal website: https://www.shd-pub.org.rs/index.php/JSCS/article/view/11928, or from the corresponding author on request.

Acknowledgements. The authors acknowledge the financial support of the Ministry of Education, Science and Technological Development of the Republic of Serbia (Grant No. 451-03-9/2021-14/200125). MVR is grateful to the Deutscher Akademischer Austauschdienst (DAAD) for the awarded scholarship in the Research Stays for University Academics and Scientists programme in 2018. We are grateful to Simon-Patrick Höfert for help with diffraction data collection.

ИЗВОД

СИНТЕЗА И КАРАКТЕРИЗАЦИЈА КОМПЛЕКСА Cd(II) СА 2-АЦЕТИЛПИРИДИН--АМИНОГВАНИДИНОМ – НОВИ НАЧИН КООРДИНАЦИЈЕ

МИРЈАНА М. РАДАНОВИЋ[1], СЛАЂАНА НОВАКОВИЋ[2], МАРКО В. РОДИЋ[1], ЉИЉАНА С. ВОЈИНОВИЋ-ЈЕШИЋ[1], CHRISTOPH JANIAK[3] и ВУКАДИН М. ЛЕОВАЦ[1]

[1]*Универзитет у Новом Саду Природно-математички факултет, Трг Д. Обрадовића 3, 21000 Нови Сад,* [2]*Институт за нуклеарне науке „Винча", Лабораторија за теоријску физику и физику кондензоване материје, 11001 Београд и* [3]*Heinrich-Heine-Universität Düsseldorf, Institute for Inorganic Chemistry and Structural Chemistry, Universitätsstraße 1, Düsseldorf, D-40225, Germany*

У овом раду описане су структуре прва два комплекса са бидентатном координацијом Шифове базе аминогванидина и 2-ацетилпиридина. Комплекс формуле $[Cd_2Cl_6(HL)_2]$ добијен је у реакцији топлих водених раствора хлоридних соли Cd(II), Zn(II) и лиганда, док је реакцијом кадмијум-бромида и лиганда у присуству агенса за депротонацију, као и амонијум-тиоцијаната добијен комплекс у којем поменута Шифова база има улогу бидентатног лиганда, али и улогу контра-јона. Координациона формула комплекса је $[HL][Cd(HL)(NCS)_2XY]\cdot H_2O$, где је L = 2-ацетилпиридин-аминогванидин, а X Cl^- или Br^- и Y Br^- или SCN^-. Оба комплекса су окарактерисана ИЦ спектрима, елементалном анализом и кондуктометријским мерењима, а структура им је одређена дифракцијом рендгенских зрака на монокристалу. Необичан бидентатни начин координације Шифове базе доводи до значајних одступања у геометрији овог молекула (од готово планарне геометрије у слободној и тридентатно координованој форми до увијене у бидентатно координовном облику). Осим тога, у комплексу **1** нађен је релативно редак мостовни начин координације Cl^-, док је у кристалној структури комплекса **2** присутна супституциона неуређеност, те ова структура садржи четири различита јона, и то: $[Cd(HL)(NCS)_2Br(SCN)]^-$ (око 61 %), $[Cd(HL)(NCS)_2Cl(SCN)]^-$ (око 35 %), $[Cd(HL)(NCS)_2Br_2]^-$ (око 3 %) и $[Cd(HL)(NCS)_2ClBr]^-$ (око 1 %).

(Примљено 13. јуна, ревидирано 30. јула, прихваћено 8. септембра 2022)

REFERENCES

1. R. Hernández-Molina, A. Mederos, in *Comprehensive Coordination Chemistry II*, J. A. McCleverty, T. J. Meyerpp, Eds., Elsevier, Amsterdam, 2003, pp. 411–446 (https://doi.org/10.1016/B0-08-043748-6/01070-7)
2. K. C. Gupta, A. K. Sutar, *Coord. Chem. Rev.* **252** (2008) 1420 (https://doi.org/10.1016/j.ccr.2007.09.005)
3. J. Zhang, L. Xu, W.-Y. Wong, *Coord. Chem. Rev.* (2017) (https://doi.org/10.1016/j.ccr.2017.08.007)
4. S. Saeednia, P. Iranmanesh, M. H. Ardakani, M. Mohammadi, Gh. Norouzi, *Mat. Res. Bull.* **78** (2016) 1 (https://doi.org/10.1016/j.materresbull.2016.02.010)
5. H.-B. Yang, K. Ghosh, Y. Zhao, B. H. Northrop, M. M. Lyndon, D. C. Muddiman, H. S. White, P. J. Stang, *J. Am. Chem. Soc.* **130** (2008) 839 (https://doi.org/10.1021/JA710349J)
6. P. A. Vigato, S. Tamburini, L. Bertolo, *Coord. Chem. Rev.* **251** (2007) 1311 (https://doi.org/10.1016/J.CCR.2006.11.016)
7. S. Satapathi, S. Das, K. Bhar, R. K. Kumar, T. K. Maji, B. K. Ghosh, *Polyhedron* **30** (2011) 387 (https://doi.org/10.1016/j.poly.2010.11.006)
8. S. Das, K. Bhar, S. Chattopadhyay, P. Mitra, V. J. Smith, L. J. Barbour, B. K. Ghosh, *Polyhedron* **38** (2012) 26 (https://doi.org/10.1016/J.POLY.2012.02.013)

9. S. Manna, E. Zangrando, S. C. Manna, *Polyhedron* **177** (2020) 114296 (https://doi.org/10.1016/J.POLY.2019.114296)
10. C. L. Siewit, B. Gengler, E. Vegas, R. Puckett, M. C. Louie, *Mol. Endocrinol.* **24** (2010) 981 (https://doi.org/10.1210/ME.2009-0410)
11. P. Joseph, *Toxicol. Appl. Pharm.* **238** (2009) 272 (https://doi.org/10.1016/J.TAAP.2009.01.011)
12. M. Filipič, *Mut. Res.* **733** (2012) 69 (https://doi.org/10.1016/J.MRFMMM.2011.09.002)
13. K. Golovine, P. Makhov, R. G. Uzzo, A. Kutikov, D. J Kaplan, E. Fox, V. M. Kolenko, *Mol. Cancer* **9** (2010) (https://doi.org/10.1186/1476-4598-9-183)
14. C. Casano, M. Agnello, R. Sirchia, C. Luparello, *Biometals* **23** (2010) 83 (https://doi.org/10.1007/S10534-009-9268-6)
15. N. Zhang, Y. Fan, Z. Zhang, J. Zuo, P. Zhang, Q. Wang, S. Liu, C. Bi, *Inorg. Chem. Commun.* (2012) 68 (https://doi.org/10.1016/J.INOCHE.2012.05.022)
16. N. Zhang, Y. Fan, G. Huang, D. Buac, C. Bi, Y. Ma, X. Wang, Z. Zhang, X. Zhang, Q. P. Dou, *Inorg. Chim. Acta* **466** (2017) 478 (https://doi.org/10.1016/J.ICA.2017.07.006)
17. Lj. S. Vojinović-Ješić, M. M. Radanović, M. V. Rodić, V. Živković-Radovanović, L. S. Jovanović, V. M. Leovac, *Polyhedron* **117** (2016) 526 (https://doi.org/10.1016/j.poly.2016.06.032)
18. *Bruker APEX2, SAINT, and SADABS.Bruker AXS Inc.,* Madison, WI, 2009 (n.d.)
19. Rigaku Oxford Diffraction, *CrysAlisPro Software system*, Rigaku Corporation, Oxford, 2018
20. G. M. Sheldrick, *Acta Crystallogr., A* **71** (2015) 3 (https://doi.org/10.1107/S2053273314026370)
21. G. M. Sheldrick, *Acta Crystallogr., C* **71** (2015) 3 (https://doi.org/10.1107/S2053229614024218)
22. M. M. Radanović, M. V. Rodić, Lj. S. Vojinović-Ješić, S. Armaković, S. J. Armaković, V. M. Leovac, *Inorg. Chim. Acta* **473** (2018) 160 (https://doi.org/10.1016/J.ICA.2017.12.038)
23. J.-Y. Miao, *Acta Crystallogr., E* **66** (2010) m868 (https://doi.org/10.1107/S1600536810025225)
24. C. R. Groom, I. J. Bruno, M. P. Lightfoot, S. C. Ward, *Acta Crystallogr., B* **72** (2016) 171 (https://doi.org/10.1107/S2052520616003954)
25. O. Yu. Vassilyeva, E. A. Buvaylo, V. N. Kokozay, S. L. Studzinsky, B. W. Skelton, G. S. Vasyliev, *Acta Crystallogr., E* **78** (2022) 173 (https://doi.org/10.1107/S2056989022000317)
26. G. R. Andrade, J. Kunsminskas, L. Pizzuti, A. dos Anjos, S. D. Inglez, B. Tirloni, P. H. Suegama, *Inorg. Chem. Commun.* **61** (2015) 210 (https://doi.org/10.1016/j.inoche.2015.09.022)
27. Z. A. Starikova, A. I. Yanovsky, Yu. T. Struchkov, S. V. Zubkov, I. I. Seifullina, *Russ. Chem. Bull.* (1996) 2157 (https://doi.org/10.1007/BF01430730)
28. B. W. Skelton, V. N. Kokozay, O. Yu. Vassilyeva, E. A. Buvaylo, *CSD Commun.*, *Database Identifier GOTFIH,* Deposition Number 1959073 (2019) (https://doi.org/10.5517/ccdc.csd.cc23rkxc)
29. O. T. Ujam, S. M. Devoy, W. Henderson, B. K. Nicholson, T. S. A. Hor, *Inorg. Chim. Acta* **363** (2010) 3558 (https://doi.org/10.1016/j.ica.2010.07.011)
30. M. M. Radanović, S. B. Novaković, Lj. S. Vojinović-Ješić, M. V. Rodić, V. M. Leovac, *J. Serb. Chem. Soc.* **83** (2018) 157 (https://doi.org/10.2298/JSC170922116R)

31. Q. Li, H.-T. Wang, L. Zhou, *Acta Crystallogr., C* **71** (2015) 93 (https://doi.org/10.1107/S2053229614028009)
32. S. Khanna, S. Verma, *CrystEngComm* **16** (2014) 6680 (https://doi.org/10.1039/C4CE00611A)
33. Á. García-Raso, J. J. Fiol, F. Bádenas, X. Solans, M. Font-Bardia, *Polyhedron* **18** (1999) 765 (https://doi.org/10.1016/S0277-5387(98)90351-5)
34. P. R. Spackman, M. J. Turner, J. J. McKinnon, S. K. Wolff, D. J. Grimwood, D. Jayatilaka, M. A. Spackman, *J. Appl. Crystallogr.* **54** (2021) 1006 (https://dx.doi.org/10.1107/S1600576721002910).

Journal of the Serbian Chemical Society
JSCS@tmf.bg.ac.rs • www.shd.org.rs/JSCS
J. Serb. Chem. Soc. *87* (11) S436–S439 (2022) *Supplementary material*

SUPPLEMENTARY MATERIAL TO

Synthesis and structural characterization of Cd(II) complexes with 2-acetylpyridine-aminoguanidine – A novel coordination mode

MIRJANA M. RADANOVIĆ[1]*, SLAĐANA B. NOVAKOVIĆ[2], MARKO V. RODIĆ[1], LJILJANA S. VOJINOVIĆ-JEŠIĆ[1], CHRISTOPH JANIAK[3] and VUKADIN M. LEOVAC[1]

[1]*University of Novi Sad Faculty of Sciences, Trg D. Obradovića 3, 21000 Novi Sad, Serbia,* [2]*"Vinča" Institute of Nuclear Sciences, National Institute of the Republic of Serbia, University of Belgrade, P.O. Box 522, 11001 Belgrade, Serbia and* [3]*Heinrich-Heine-Universität Düsseldorf, Institute for Inorganic Chemistry and Structural Chemistry, Universitätsstraße 1, Düsseldorf, D-40225, Germany*

J. Serb. Chem. Soc. *87* (11) (2022) 1259–1272

TABLE S-I. Complexes with a monodentate aminoguanidine-derived Schiff base ligand

REFCODE	Reference
GAKSIW	O. T. Ujam, S. M. Devoy, W. Henderson, B. K. Nicholson, T. S. A. Hor, *Inorg. Chim. Acta* 363 (2010) 3558 (https://doi.org/10.1016/j.ica.2010.07.011)

TABLE S-II. Complexes with a tridentate aminoguanidine-derived Schiff base ligand

REFCODES	References
GOTGEE	B. W. Skelton, V. N. Kokozay, O. Yu.Vassilyeva, E. A. Buvaylo (2019) *CSD Communication (Private Communication)* (https://doi.org/10.5517/ccdc.csd.cc23rl6p)
BUWNUE BUWQOB	M. G. Jelic, N. Boukos, M. M. Lalovic, N. Z. Romcevic,V. M. Leovac, B. B. Hadzic, S. S. Balos, L. S. Jovanovic, M. P. Slankamenac, M. B. Zivanov, L. S. Vojinovic-Jesic, *Opt. Mater.* 35 (2013) 2728 (https://doi.org/10.1016/j.optmat.2013.08.023)
CEKNIS	M. M. Radanovic, M. V. Rodic, S. A. Armakovic, S. J. Armakovic, L. S. Vojinovic-Jesic, V. M. Leovac, *J. Coord. Chem.* 70 (2017) 2870 (https://doi.org/10.1080/00958972.2017.1367388)
CELHIM CELHOS	M. M. Lalovic, L. S. Jovanovic, L. S. Vojinovic-Jesic, V. M. Leovac, V. I. Cesljevic, M. V. Rodic, V. Divjakovic, *J. Coord. Chem.* 65 (2012) 4217 (https://doi.org/10.1080/00958972.2012.737916)
GANQEU	E. A. Buvaylo, V. N. Kokozay, O. Yu. Vassilyeva, B. W. Skelton, O. V. Nesterova, A. J. L. Pombeiro, *Inorg. Chem. Commun.* 78 (2017) 5 (https://doi.org/10.1016/j.inoche.2017.03.008)
GEMJOY	Yu. M. Chumakov, V. I. Tsapkov, G. Bocelli, B. Ya. Antosyak, S. G. Shova, A. P. Gulya, *Crystallogr. Rep.* 51 (2006) 66 (https://doi.org/10.5517/cc8w217)

* Corresponding author. E-mail: mirjana.lalovic@dh.uns.ac.rs

REFCODES	References
IPOFAN	E. A. Buvaylo, K. A. Kasyanova, O. Y. Vassilyeva, B. W. Skelton, *Acta Crystallogr., Sect. E: Cryst. Commun.* **72** (2016) 907 (https://doi.org/10.1107/S2056989016008690)
IQEDOZ IQEDOZ01 IQEFAN IQEFER IQEFIV	L. S. Vojinovic-Jesic, M. M. Radanovic, M. V. Rodic, V. Zivkovic-Radovanovic, L. S. Jovanovic, V. M. Leovac, *Polyhedron* **117** (2016) 526 (https://doi.org/10.1016/j.poly.2016.06.032)
MECJOV	M. M. Lalovic, L. S. Vojinovic-Jesic, L. S. Jovanovic, V. M. Leovac, V. I. Cesljevic, V. Divjakovic, *Inorg. Chim. Acta* **388** (2012) 157 (https://doi.org/10.1016/j.ica.2012.03.026)
MEXGED	E. A. Buvaylo, V. N. Kokozay, O. Yu. Vassilyeva, B. W. Skelton, *Acta Crystallogr., Sect. E: Struct. Rep. Online* **69** (2013) m165 (https://doi.org/10.1107/S1600536813004534)
MOHHIC MOHHOI MOHHUO	L. S. Vojinovic-Jesic, M. M. Radanovic, M. V. Rodic, L. S. Jovanovic, V. I. Cesljevic, M. D. Joksovic, *Polyhedron* **80** (2014) 90 (https://doi.org/10.1016/j.poly.2014.02.003)
QEHSUT	V. Jevtovic, D. Vidovic, S. Ivkovic, *Cont. Mat.* 2 (2011) 55 (https://doi.org/10.5767/anurs.cmat.110201.en.055J)
QEHSUT01	M. M. Radanovic, M. V. Rodic, S. A. Armakovic, S. J. Armakovic, L. S. Vojinovic-Jesic, V. M. Leovac, *J. Coord. Chem.* 70 (2017) 2870 (https://doi.org/10.1080/00958972.2017.1367388)
QELKIE QELKUQ	M. M. Radanovic, M. V. Rodic, L. S. Vojinovic-Jesic, S. Armakovic, S. J. Armakovic, V. M. Leovac, *Inorg. Chim. Acta* 473 (2018) 160 (https://doi.org/10.1016/j.ica.2017.12.038)
QOHDEY QOHDUO	M.M.Lalovic, V.M.Leovac, L.S.Vojinovic-Jesic, M.V.Rodic, L.S.Jovanovic, V.I.Cesljevic, *J. Serb. Chem. Soc.* 78 (2013) 1161 (https://doi.org/10.2298/JSC130326038L)
RIYMIV RIYMIV01	K. D. Onuska, N. J. Taylor, J. Carsky, *J. Chem. Cryst.* 26 (1996) 841 (https://doi.org/10.1007/BF01670317)
WIDTIN	V. M. Leovac, M. D. Joksovic, V. Divjakovic, L. S. Jovanovic, Z. Saranovic, A. Pevec, *J. Inorg. Biochem.* 101 (2007) 1094 (https://doi.org/10.1016/j.jinorgbio.2007.04.004)
XEDDEE	M. M. Radanovic, S. B. Novakovic, L. S. Vojinovic-Jesic, M. V. Rodic, V. M. Leovac, *J. Serb. Chem. Soc.* 83 (2018) 157 (https://doi.org/10.2298/JSC170922116R)
XIXTOO XIXVAC	C. I. Turta, L. F. Chapurina, I. G. Donica, V. Voronkova, E. R. Healey, V. Ch. Kravtsov, *Inorg. Chim. Acta* 361 (2008) 309 (https://doi.org/10.1016/j.ica.2007.07.017)
YEDJOM	E. B. Shamuratov, Kh. T. Sharipov, A. S. Batsanov, Yu. T. Struchkov, A. B. Khudoyarov, F. F. Mirdzhalalov, *Koord. Khim. (Russ.)(Coord. Chem.)* 19 (1993) 155
YUCMOZ	V. M. Leovac, L. S. Vojinovic-Jesic, V. I. Cesljevic, S.B.Novakovic, G.A.Bogdanovic, *Acta Crystallogr. Sect. C: Cryst. Struct. Commun.* 65 (2009) m337 (https://doi.org/10.1107/S0108270109029023)
YUJGIV YUJGIV01 YUJGIV02	G. R. Andrade, J. Kunsminskas, L. Pizzuti, A. dos Anjos, S. D. Inglez, B. Tirloni, P. H. Suegama, *Inorg. Chem. Commun.* 61 (2015) 210 (https://doi.org/10.1016/j.inoche.2015.09.022)
HUDHAE	A. Mondal, C. Das, M. Corbella, A. Bauza, A. Frontera, M. Saha, S. Mondal, K. D. Saha, S. K. Chattopadhyay, *New J. Chem.* 44 (2020) 7319 (https://doi.org/10.1039/C9NJ05712A)

TABLE S-III. Complexes with a tetradentate aminoguanidine-derived Schiff base ligands

REFCODES	References
GOQMAD	O. Yu. Vassilyeva, E. A. Buvaylo, V. N. Kokozay, S. L. Studzinsky, B. W. Skelton, G. S. Vasyliev, *Acta Crystallogr., Sect. E: Cryst. Commun.* 78 (2022) 173 (https://doi.org/10.1107/S2056989022000317)
GOTFIH	B. W. Skelton, V. N. Kokozay, O. Yu. Vassilyeva, *CSD Communication* (*Private Communication*) (2019) (https://doi.org/10.5517/ccdc.csd.cc23rkxc)
TUFDAZ	Z. A. Starikova, A. I. Yanovsky, Yu. T. Struchkov, S. V. Zubkov, I. I. Seifullina, *Izv. Akad. Nauk SSSR, Ser. Khim.* (*Russ*.) (*Russ. Chem. Bull*.) (1996) 2157
YUJGIV	G. R. Andrade, B. Tirloni, (2015) *CSD Communication* (*Private Communication*) (https://doi.org/10.5517/cc1j9wxm)
YUJGIV01	G. R. Andrade, J. Kunsminskas, L. Pizzuti, A. dos Anjos, S. D. Inglez, B. Tirloni, P. H. Suegama, *Inorg. Chem. Commun*. 61 (2015) 210. (https://doi.org/10.1016/j.inoche.2015.09.022)
YUJGIV02	G. R. Andrade, B. Tirloni, (2015) *CSD Communication* (*Private Communication*) (https://doi.org/10.5517/cc1j9wvk)

TABLE S-IV. Complexes in which a Schiff base of aminoguanidine has a role of a counter-ion

REFCODE	Reference
QIBPIA	J. Valdes-Martinez, J. H. Alstrum-Acevedo, R. A. Toscano, G. Espinosa-Perez, B. A. Helfrich, D. X. West, *Acta Crystallogr., Sect.E: Struct. Rep. Online* 57 (2001) m137 (https://doi.org/10.1107/S1600536801003725)
QELLAX QELKOK	M. M. Radanovic, M. V. Rodic, L. S. Vojinovic-Jesic, S. Armakovic, S. J. Armakovic, V. M. Leovac, *Inorg. Chim. Acta* 473 (2018) 160 (https://doi.org/10.1016/j.ica.2017.12.038)
MINQIJ MINQOP MINQUV	J. Valdes-Martinez, J. H. Alstrum-Acevedo, R. A. Toscano, S.Hernandez-Ortega, G.Espinosa-Perez, D.X.West, B.Helfrich, *Polyhedron* 21 (2002) 409 (https://doi.org/ 10.1016/S0277-5387(01)01006-3)
FOWLEJ	Rui-jun Xu, *Acta Crystallogr., Sect. E: Struct. Rep. Online,* 65 (2009) m951 (https:/doi.org/10.1107/S1600536809027196)
YUMZUD	M. M. Radanovic, M. G. Jelic, N. Z. Romcevic, N. Boukos, L. S. Vojinovic-Jesic, V. M. Leovac, B. B. Hadzic, B. M. Bajac, L. F. Nad, C. Chandrinou, S. S. Balos, *Mater. Res. Bull.* 70 (2015) 951 (https:/doi.org/10.1016/j.materresbull.2015.06.034)
GEMJIS	Yu. M. Chumakov, V. I. Tsapkov, G. Bocelli, B. Ya. Antosyak, S. G. Shova, A. P. Gulya, *Kristallografiya (Russ.) (Crystallogr. Rep.)* 51 (2006) 66 (https://doi.org/10.5517/cc8w206)
YEDJUM	E. B. Shamuratov, Kh. T. Sharipov, A. S. Batsanov, Yu. T. Struchkov, A. B. Khudoyarov, F. F. Mirdzhalalov, *Koord. Khim. (Russ.) (Coord. Chem.)* 19 (1993) 155
KABLEH	Xiaoni Gao, Ting An, Jizhen Li, Fengqi Zhao, Xuezhong Fan, Xinyan Li, Guofang Zhang, Ziwei Gao, *Z. Anorg. Allg. Chem.* 642 (2016) 155 (https://doi.org/10.1002/zaac.201500690).

TABLE S-V. Coordination bond distances and angles in $[Cd_2Cl_6(HL)_2]$.

Bond	Bond distance, Å	Bonds	Bond angle, °
Cd1−Cl1	2.5632(3)	Cl1−Cd1−Cl3	112.948(9)
Cd1−Cl2	2.5638(3)	Cl2−Cd1−Cl3	96.734(9)
Cd1−Cl3	2.5272(3)	N3− Cd1− Cl3	85.334(18)
Cd1−Cl1^{i}	2.7148(3)	N5− Cd1− Cl2	96.50(2)
Cd1−N3	2.7483(8)	Cl1− Cd1− N3	161.69(3)
Cd1−N5	2.2992(8)	Cl2− Cd1− Cl1^{i}	174.132(7)

Symmetry code: (i) 1–x, 1–y, 2–z.

TABLE S-VI. Coordination bond distances and angles in $[HL][Cd(HL)(NCS)_2XY]\cdot H_2O$

Bond	Bond distance, Å	Bonds	Bond angle, °
Cd1−N7	2.285(2)	N7−Cd1−N5a	88.46(8)
Cd1−N8	2.348(2)	N7−Cd1−N3a	78.18(8)
Cd1−Cl1/Br1	2.580(14)/2.636(3)	N7−Cd1−N8	166.11(9)
Cd1−S1/Br2	2.663(3)/2.72(2)	N8−Cd1−N3a	88.24(8)
Cd1−N3	2.605(2)	N5a−Cd1−N8	88.66(8)
Cd1−N5	2.348(2)	N5a−Cd1−Cl1	99.6(3)
		N5a−Cd1−Br1	97.73(8)
		N3a−Cd1−S1	98.99(8)
		N3a−Cd1−Br2	99.3(6)

TABLE S-VII. Potential interactions in $[HL][Cd(HL)(NCS)_2XY]\cdot H_2O$ involving substitutionally disordered ligands

D–H···A	*d*(D–H) / Å	*d*(H···A) / Å	∠(D–H···A) / °	Symmetry codes:
N2a−H2a···N6_c	0.86	2.057	159.31	–*x*+1, –*y*+1, –*z*+2
N4a−H42a···N6_c	0.86	2.451	143.07	*x*+1, –*y*+1, –*z*+2
C7a−H7a···Br1_a	0.93	3.103	125.78	
N2a−H2a···Br1_a	0.86	2.601	143.44	–*x*+1, -*y*+1, –*z*+1
N2a−H2a···Cl1_b	0.86	2.464	142.65	–*x*+1, –*y*+1, –*z*+1
N4a−H22···Br1_a	0.86	2.854	139.63	–*x*+1, –*y*+1, –*z*+1
N4a−H22···Cl1_b	0.86	2.636	140.57	–*x*+1, –*y*+1, –*z*+1
O1−H1a···S1_c	0.92	2.511	164.41	*x*–1, *y*, *z*

TABLE S-VIII. Global packing features of idealized structures derived from complex **2**.

Idealized structure	Crystal packing coefficient	Anion volume defined by Hirshfeld surface, Å^3	Anion mole ratio in **2**
$[HL][Cd(HL)(NCS)_2Br(SCN)]\cdot H_2O$	0.675	468.9	0.61
$[HL][Cd(HL)(NCS)_2Cl(SCN)]\cdot H_2O$	0.669	466.8	0.35
$[HL][Cd(HL)(NCS)_2Br_2]\cdot H_2O$	0.653	466.8	0.03
$[HL][Cd(HL)(NCS)_2BrCl]\cdot H_2O$	0.647	464.8	0.01

Journal of the Serbian Chemical Society
JSCS@tmf.bg.ac.rs • www.shd.org.rs/JSCS
J. Serb. Chem. Soc. *87* (11) 1273–1284 (2022)
JSCS–5593
Original scientific paper
Published 16 September 2022

Binding of *β*-casein with fluvastatin and pitavastatin

HAMID DEZHAMPANAH* and OMIDEH RAJABI MIANDEHI

Department of Chemistry, Faculty of Science, University of Guilan, P.O.B. 1914, Rasht 0098, Iran

(Received 6 June, revised 30 July, accepted 9 August 2022)

Abstract: In this work, the binding interaction of fluvastatin (FLU) and pit-avastatin (PIT) with bovine *β*-casein (*β*-CN) were performed under physiological conditions (pH 7.2) by fluorescence emission spectroscopy, synchronous fluorescence spectroscopy, Fourier transform infrared spectroscopy (FTIR) and molecular docking methods. Due to the formation of FLU-*β*-CN and PIT-*β*-CN complexes, the intrinsic fluorescence of *β*-CN was quenched. The number of bound FLU and PIT per protein molecule (*n*) were about 1, also the binding constant of FLU-*β*-CN and PIT-*β*-CN complexes were 7.96×10^4 and 3.44×10^4 M^{-1} at 298 K, respectively. This result suggests that the binding affinity of FLU to *β*-CN was higher than that for PIT. Molecular modelling showed different binding sites for FLU and PIT on *β*-CN. All these experimental results suggest that *β*-CN can be used as a carrier protein which delivers FLU and PIT based drugs to target molecules.

Keywords: milk protein; statin; molecular modelling; spectroscopy.

INTRODUCTION

Statins are a group of medicines that can help lower the level of low-density lipoprotein (LDL) cholesterol in blood. They act as potentially competitive inhibitors of 3-hydroxy-3-methylglutaryl-coenzyme A (HMG-CoA) reductase, which catalyzes the rate-limiting phase of the cholesterol biosynthesis cascade.[1,2] Statins can be classified as natural statins and synthetic statins. Lovastatin is a fermentation-derived statin whereas simvastatin is a semi-synthetic statin synthesized from lovastatin either by synthetic or enzymatic biotransformation routes. There are several synthetic statins are available at the market, such as cerivastatin, atorvastatin, fluvastatin, pitavastatin and rosuvastatin, which are more effective than fermentation-derived statins. FLU (Fig. S-1 of the Supplementary material to this paper) is an HMG-CoA reductase inhibitor that is used to lower lipid levels.[4] It effectively lowers the serum LDL-cholesterol level and reduces

* Corresponding author. E-mail: h.dpanah@guilan.ac.ir
https://doi.org/10.2298/JSC220606067D

the risk of the development of atherosclerosis. Recent studies have reported that FLU is a new therapeutic agent for the prevention and the treatment of breast cancer,[5] and it has also been shown that some statins, including FLU, may have a potential effect in the treatment of COVID-19.[6] PIT (Fig. S-1) is also a unique lipophilic statin with a strong effect in lowering total plasma cholesterol and triglycerides. The unique lipid and non-lipid effects of PIT make this molecule a particularly interesting option for the management of different human diseases.[7]

Milk is a unique source of nutrients and is widely recognized by consumers as a source of compounds beneficial to growth and health in children and adults.[8] Milk proteins are classified into two distinct groups, casein, and whey or serum protein. Caseins as a functional food have a great variety and play an essential role in the development of new food products. Casein is one of the two main components of milk protein, making up about 40 % of the protein in human milk and approximately between 78 and 86 % of the protein in house mice, cow, sheep, goat and buffalo milk.[9] Casein is found in local milk as supramolecular aggregates called casein micelles, which are between 50 to 600 nm in diameter.[10] They occur as micelles made up of four main components: α_{s1}-, α_{s2}-, β- and κ-casein at a mole ratio of about 4:1:4:1. About 38 % of this structure is formed by β-CN, which contains 209 amino acids, has a monomeric molecular mass of approximately 24 kDa. It is more hydrophobic than that in α- and κ-casein and contains one tryptophan (Trp) residu.[11,12] Bovine β-casein is an extremely amphiphilic protein consisting of a hydrophilic N-terminal segment with a hydrophobic C-terminal segment and a group consisting of five phosphoryl residues.[12]

The aim of this work was to investigate the interaction of bovine β-CN with FLU and PIT. The overall binding constant of FLU and PIT to β-CN were calculated at 298 K and the effect of FLU and PIT on the conformation of β-CN was evaluated. For this purpose, molecular docking experiments and multi-spectroscopic measurements were conducted, which may extend the versatile use of β-CN as a transporter for the delivery of therapeutic, or as solubilizing agents in food applications. We also compared the binding affinity of the β-CN fraction and the probable binding sites of FLU and PIT in the β-CN fraction by both experiments and molecular modelling studies.

EXPERIMENTAL

Fluorescence spectroscopy

The fluorescence measurements were performed using Varian Cary Eclipse spectrofluorometer containing a 1.0 cm quartz cuvette, with an optical pathway of 1 cm, from 290 to 440 nm. The excitation wavelength was set at 280 nm, and the excitation and emission slits were adjusted at 5 nm. For the preparation of FLU and PIT with β-CN complexes, a 1 mM stock solution of FLU and PIT in ethanol and methanol were prepared, respectively. The entrapment of each FLU and PIT in β-CN molar ratios was performed by adding different volumes of FLU and PIT solutions to a β-CN solution with continuous stirring. In this work,

all fluorescence intensities were corrected for inner filter effect, due to the UV absorption of FLU and PIT with β-CN and the mean values were calculated according to:

$$F_c = F_m e^{((A_1 + A_2)/2)} \quad (1)$$

where A_1 and A_2 are the absorbance of FLU and PIT at excitation and emission wavelengths, respectively. F_c and F_m are the corrected and the experimentally measured fluorescence intensities, respectively.

Synchronous fluorescence spectroscopy experiments

Spectra of β-CN solution in the absence and presence of FLU and PIT were measured at 298 K. The values of wavelength intervals which is the difference between the emission wavelength (λ_{em}), and the excitation wavelength (λ_{ex}), was set at 15 and 60 nm, respectively. The scanning wavelength range was set at 200–400 nm. The concentrations of FLU varied from 0 to 18 μM, PIT varied from 0 to 23 μM and the concentration of β-CN was 1 mM.

FT-IR spectroscopic measurements

FT-IR measurements were performed at room temperature by an ALPHA FT-IR spectrometer (Bruker) optics using a KBr pellet in the range of 4000–400 cm^{-1}. FLU and PIT solutions were added dropwise to the β-CN solution with continuous stirring to form a homogeneous solution. The FLU and PIT concentrations were 0, 0.25, and 0.5 mM with a fixed β-CN solution of 0.25 mM.[19] Then the solutions were freeze-dried in Christ Alpha 1-2 LD freeze dryer at –40 °C for 4 h. The pellets were prepared by mixing the freeze-dried sample with KBr and pressed under vacuum at pressure for three minutes.[20]

Molecular modelling and docking

The 3D structure of FLU and PIT were made using Gauss view 5.0. The geometry of FLU and PIT were optimized by the density functional theory (DFT) (B3LYP/6-31G*(d.p)) using Gaussian 03. Milk β-CN structure was made according to Swiss-Model, protein models were first modified by adding all hydrogen atoms and removing water molecules based on the builder module of AutoDock. The macromolecules were rigidly maintained, while all the torsional bonds of the ligands were released for rotation. AutoDock Vina was used to simulate the binding conformation of β-CN with FLU and PIT using the Lamarckian genetic algorithm.[21] AutoDock and Ligplus+ tools were used to get the best molecular docking results. The lowest energy docked structure was obtained using a grid map with 70×70×70 points and a grid point spacing of 0.1 nm and the maps were centered on this new docking location. The Lamarckian genetic algorithm was employed with the following parameters: 10 docking runs with 25,000,000 energy evaluations for each run. The conformer with the lowest binding energy was used for further analyses.[22]

RESULTS AND DISCUSSION

Fluorescence quenching of β-*CN*

When the binding interaction of proteins and drug molecules occurs, fluorescence spectroscopy analysis can be used to obtain the important data of binding constants and the number of binding sites. When excited at 280 nm, amino acids with phenyl rings such as tryptophan (Trp), tyrosine (Tyr) and phenylalanine (Phe) cause the intrinsic fluorescence of the protein.[25] The β-CN contains one tryptophan Trp-143 with an intrinsic fluorescence, when other molecules interact with casein, tryptophan fluorescent can change based on the effect of such inter-

action on protein conformation. The decrease of fluorescence intensity of β-CN has been monitored at 346 nm for β-CN with FLU and PIT in Fig 1a and b. The fluorescence spectra of all β-CN solutions in the absence and presence of FLU and PIT were shown in Fig. 1a and b. The results revealed that the fluorescence intensities of β-CN decreased progressively with the successive increases of FLU and PIT concentrations, suggesting that there were changes in the microenvironment surrounding Trp residue due to the binding interaction of FLU and PIT with β-CN. The decrease in the fluorescence intensity with increasing FLU and PIT concentrations also indicated the energy transfer between the fluorophore in β-CN with FLU and PIT. Also, we observed the blue shift of maximum emission wavelength (λ_{em}) about 1 and 3 nm for β-CN with FLU and PIT, respectively, further indicating that the microenvironment surrounding Trp residue was relatively more hydrophobic upon FLU and PIT binding. The fluorescence quenching of protein can be classified into three. The static quenching is caused by producing a ground-state complex of protein and quenchers. Whereas, dynamic quenching is caused by protein and quencher conflicts, and coupled dynamic and static quenching caused both conflict and complexity.[26] Both static and dynamic processes can be defined the Stern–Volmer Equation as follows:[27]

$$\frac{F_0}{F} = 1 + K_{SV}C_Q = 1 + k_q\tau_0 C_Q \quad (2)$$

where F_0 and F are fluorescence intensities in the absence and presence of quencher, C_Q is quencher concentration and K_{SV} is Stern–Volmer constant, which can be calculated using the linear slope of plot of F_0/F *vs.* C_Q (of FLU or PIT) are shown in Fig 1a and 1b.[29] also (inset), respectively. k_q is the bimolecular quenching rate constant and τ_0 is the lifetime of the fluorophore in

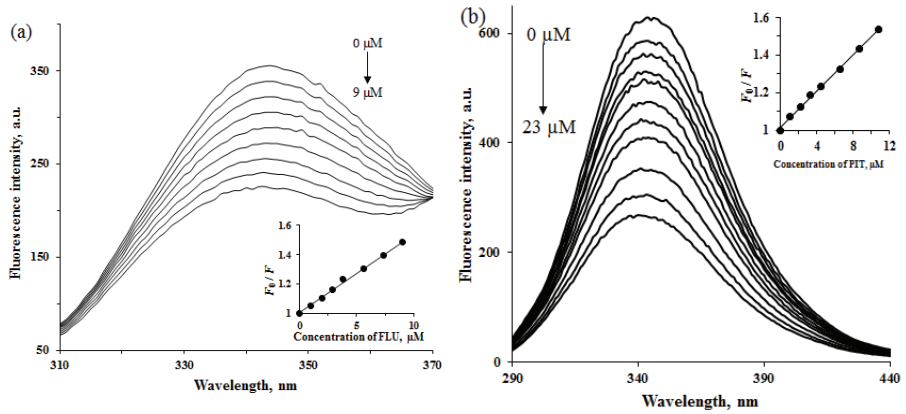

Fig. 1. Fluorescence spectra of β-CN (10 μM) induced by the different concentration of FLU and PIT at 298 K, FLU-β-CN (a) and PIT-β-CN (b). Inset: Stern–Volmer plots for the quenching of β-CN (10 μM) induced by the different concentration of FLU and PIT.

the absence of quencher: 3.30 ns for β-CN.[28] According to the formula, the Stern–Volmer (S–V) curve of β-CN interacting with FLU and PIT were in a linear relationship (Fig. 1).[29] Also, with the use of the equation we observed that k_q for complex FLU–β-CN and PIT–β-CN is 1.6×10^{13} and 1.45×10^{13} M^{-1} s^{-1}, respectively, which is greater than the maximum diffusion collision quenching rate constant (2.0×10^{10} M^{-1} s^{-1}). These results indicate that the static quenching effect exists in the system of FLU and PIT with β-CN.[30,31]

For the quenching process of β-CN, the binding constant (K_b) of a complex of FLU and PIT with β-CN can be determined by (Fig. S-2 of the Supplementary material):[27]

$$\log\frac{F_0 - F}{F} = \log K_b + n\log C_Q \quad (3)$$

which is equal 7.96×10^4 and 3.44×10^4 M^{-1} at 298 K, as shown in Table I, respectively. Also, the number of binding sites (n) obtained for both complexes is about 1. An n value of approximately equal to 1 illustrated that there was only a single binding site in the binding of FLU and PIT with β-CN as shown in Table I.[27]

TABLE I. The quenching constants of β-casein by FLU and PIT

Complex	K_{SV} / mM^{-1}	R^2	n	K_b / mM^{-1}	R^2
FLU–β-casein	0.537±0.001	0.9967	1.02±0.02	0.796	0.9962
PIT–β-casein	0.481±0.012	0.9973	0.96±0.02	0.344	0.9939

Energy transfer from β-*CN to FLU and PIT*

Förster resonance energy transfer (FRET) is a mechanism describing energy transfer between two light-sensitive molecules. A donor chromophore, initially in its electronic excited state, can transfer energy to an acceptor chromophore through nonradiative dipole-dipole coupling.[32] Eq. (4) is used to estimate the spatial distances between the donor (protein) and the receptor (ligand) in which the efficiency of this energy transfer (E) is inversely proportional to the sixth power of the distance between the donor and the acceptor:[33]

$$E = 1 - \frac{F}{F_0} = \frac{R_0^6}{R_0^6 + r^6} \quad (4)$$

where F_0 and F are the fluorescence intensity of donor in the absence and presence of acceptor, respectively. r is the distance between the donor and acceptor, and R_0 is the Förster critical distance when the efficiency (E) is 50 %, which can be computed as:[34]

$$R_0{}^6 = 8.8\times10^{-4}K^2N^{-4}\phi \quad (5)$$

where $K = 2/3$ is a factor describing the relative orientation of the transition dipoles of the donor and acceptor, $N = 1.53$ is the average refractive index of the

environment in the wavelength range where the spectral overlap is significant, φ = 1.49 for casein, which is the fluorescence quantum yield of the donor in the absence of acceptor.[20] Overlap integral J expresses the extent of overlap between the normalized fluorescence emission spectrum of donor and absorption spectrum of the acceptor, which is measured by:[34]

$$J = \frac{\sum F(\lambda)\varepsilon(\lambda)\lambda^4\Delta\lambda}{\sum F(\lambda)\Delta\lambda} \quad (6)$$

Where $F(\lambda)$ is the fluorescence intensity of the fluorescent donor at a wavelength of λ, and $\varepsilon(\lambda)$ is the molar absorption coefficient of the acceptor at a wavelength of λ. (Fig. S-3 of the Supplementary material) show the spectral overlap of fluorescence emission of β-CN and absorption spectrum of FLU and PIT, respectively. According to the above equations, R_0 = 1.52 nm, r = 1.72 nm, and J = = 4.55×10^{-16} cm^3 L mol^{-1} for β-CN-FLU and R_0 = 2.05 nm, r = 2.23 nm, and J = 2.74×10^{-15} cm^3 L mol^{-1} for β-CN-PIT were calculated. As the distance between casein (donor) and FLU or PIT (acceptor) was less than 8 nm with the rule $0.5R_0 < r < 1.5R_0$, suggesting that the energy transfer from β-CN to FLU and PIT occurs with high probability and distance, obtained by Förster resonance energy transfer with higher accuracy.[32] The short distance values also suggested strong interaction between FLU and PIT with residues of β-CN. In addition, the value of r was larger than the respective critical distance (R_0), indicating that the fluorescence quenching mechanism of β-CN is inducted by is static quenching.[32,35]

Synchronous fluorescence spectroscopy

Simultaneous fluorescence spectroscopy is often used to consider changes in the microenvironment of Tyr ($\Delta\lambda$ = 15 nm) and Trp ($\Delta\lambda$ = 60 nm) fluorophores as well as to study changes in protein structure. The shift of maximum emission wavelength (λ_{em}) indicates the change in the polarity of the microenvironment surrounding Tyr or Trp residues. The red shift of λ_{em} indicates the decrease in the hydrophobicity surrounding Tyr or Trp residue and also the increase in the stretching extent of the peptide chain. In contrast, a change in blue λ_{em} indicates an increase in hydrophobicity around the residual Tyr or Trp and a fold state for the macromolecule. The synchronous fluorescence spectra of β-CN with the addition of FLU and PIT were shown in Figs. S-4 and S-5 of the Supplementary material. The results revealed that the fluorescence quenching effect of FLU and PIT on Trp was higher than on Tyr in β-CN. These results indicate that FLU and PIT are located closer to Trp than to Tyr when binding to β-CN. In addition, in Fig.S-4, the weak red shift (1 nm) of the λ_{em} of Tyr residue was observed (1 nm) with $\Delta\lambda_{em}$ setting at 15 nm, while the blue shift of the λ_{em} of Trp residue was observed (3 nm) with $\Delta\lambda_{em}$ setting at 60 nm. The adding of the concentration of

FLU, indicated that the hydrophobic characteristics surrounding Tyr residue and the folding state of β-CN slightly decreased as the hydrophobic characteristics surrounding Trp residues and the folding state of β-CN increased. Also, in Fig. S-5 the red shift (2 and 3 nm) of the λ_{em} of Tyr and Trp residues were observed with $\Delta\lambda_{em}$ setting at 15 and 60 nm respectively, with adding the concentration of PIT, indicating that the hydrophobic characteristics surrounding Tyr and Trp residues and the folding state of β-CN decreased. So, it resulted in the β-CN composition change after binding to FLU and PIT.

FTIR spectroscopy

IR spectroscopy has been used as a powerful method to study the secondary structure of proteins and their dynamics.[36] Because the IR spectra of proteins exhibit several so-called amide bands, which represent different vibrations of the peptide moiety, and there was no major spectral shifting, the protein amide I peak position which occurred in the region between 1600 and 1700 cm^{-1} (principally C=O stretch) and the amide II band 1500–1600 cm^{-1} (C–N stretch coupled with N–H bending mode) have been widely used as typical and both are related to the secondary structure of the protein.[37] The amide I bond is useful in studying the secondary structure because the amide I bond is more sensitive to changes in the secondary structure of the protein than amide II. Here, the amide I absorption peak of β-CN shifted from the wavenumber, and the intensity of β-CN was changed for C=O stretch (amide I band) at 1646 cm^{-1} and C–N stretching participant with N–H bending modes (amide II band) at 1536 cm^{-1}, due to the hydrophilic contacts of FLU and PIT with β-CN. To further investigate the manner of FLU and PIT interaction, the difference spectra for (protein solution + drug solution) – protein solution were obtained. The intensity variations of amide I and amide II bands were monitored upon FLU and PIT complexation, and results are shown in Figs. S-6 and S-7 of the Supplementary material.

In Fig. S-6a, at low FLU concentration (0.25 mM), a decrease in the intensity of β-CN was observed. The spectral shifting was observed for the protein amid II bands at 1534 cm^{-1} for β-CN. As FLU concentration increased to 0.5 mM, a decrease of intensity was observed for amide I and amide II bands at 1644 and 1533 cm^{-1} for FLU β-CN. Also, in Fig. S-6b, at low PIT concentration (0.25 mM), a decrease in the intensity of β-CN was observed. The spectral shifting was observed for the protein amid the I band at 1649 cm^{-1} and amide II at 1514 cm^{-1} for β-CN. While as PIT concentration increased to 0.5 mM, a rise of intensity was observed for amide I and amide II bands at 1649 and 1512 cm^{-1}, respectively, for β-CN-PIT. The hydrophobic contacts in the complex of FLU and PIT with β-CN were analyzed from spectral changes of the β-CN CH_2 antisymmetric and symmetric stretching vibrations, in the region of 2800–3000 cm^{-1}. The CH_2 bands of free β-CN at 2872, 2928 and 2957 cm^{-1} shifted to 2872, 2929 and 2956

cm^{-1} and to 2869, 2928, 2955 cm^{-1} with the addition FLU; it that was shown in Fig. S-7a. With the addition PIT it shifted to 2853, 2928 and 2963 cm^{-1} and to 2855, 2925 and 2952 cm^{-1}, which was observed in Fig. S-7b. These changes in the infrared spectra of *β*-CN confirmed the change in the conformation of *β*-CN by the addition of FLU and PIT.[20] Similar results are obtained from the fluorescence spectroscopy data.

The data in the 1600–1700 cm^{-1} region were further analyzed to quantify the secondary structure content of *β*-CN using the Fourier self-deconvolution and second derivative technique. They were estimated as shown in Fig. S-8a and Table S-I of the Supplementary material; the free *β*-CN has 28.13 % *α*-helix (1646 cm^{-1}), 17.67 % *β*-sheet (1619–1624 cm^{-1}), 22.04 % turn structure (1657 cm^{-1}), 7.13 % *β*-antiparallel (1666 cm^{-1}) and random coil 24.43 % (1635 cm^{-1}). Upon FLU interaction, a decrease of the *β*-turn and *β*-anti-parallel occurred for FLU–*β*-CN complex, while an increase of *α*-helix, *β*-sheet and random coil were observed in Fig. S-8b and Table S-I. Also, a decrease of the *α*-helix, random coil, *β*-turn and *β*-anti parallel and increase of *β*-sheet were observed for PIT–*β*-CN complex, Fig, S-8c and Table S-I. The results revealed that the change in the conformational of *β*-CN was due to the binding *β*-CN with FLU and PIT.

Docking studies

In recent years, molecular docking has been used as an important technique for ligand-protein studies that provides more detailed information about the interaction between ligands and proteins.[38] Based on the experiment data, computational docking studies were made to understand the binding site location and the best conformation for binding of FLU and PIT to *β*-CN using binding free energy evaluation. Using intermolecular energy, internal energy and torsional free energy, the energies estimated by AutoDock can be described. Among these calculated energies by AutoDock, the first two provide the docking energy while the sum of the first and third items account for the binding energy.[18] The dominating conformation of the binding complex of *β*-CN with FLU and PIT, which was the lowest binding free energy, was shown in Fig. 2 and Table S-II. In Fig. 3a (FLU––*β*-CN complex), FLU molecule is surrounded by Ile-41 with forming one hydrogen bond with a length of 3.25 Å (FLU-amino acid) and Leu-6, Leu-9, Val-10, Ala-13, Leu-14, Arg-40, Leu-60, Lys-63, Ile-64 and Phe-67 by hydrophobic interaction and free binding energy of –27.58 kJ mol^{-1} as shown in Table S-II. Fig. 3b (PIT–*β*-CN complex), shows that the PIT molecule is surrounded by His--160, Lys-184, Pro-187 and Pro-196 forming four hydrogen bonds with lengths of 3.06, 2.91, 3.14 and 2.96 Å, and Met-159, His-163, Gln-164, Pro-165, Leu--166, Ser-183 and Pro-189 by hydrophobic interaction and free binding energy of –27.17 kJ mol^{-1}. The binding energy shows the FLU–*β*-CN is more stable than PIT–*β*-CN complex. It can be seen from Fig. 3a and b that the distance between

donor and acceptor atoms is from 2.6 to 3.5, which can play an important role in the binding of FLU and PIT to β-CN. So, it can be concluded that the interaction between β-CN and FLU and PIT is mainly a hydrophobic interaction and a hydrogen bonding interaction in nature. The docking results reveal that the interactions between FLU and PIT and β-CN are in good agreement with experimental results.

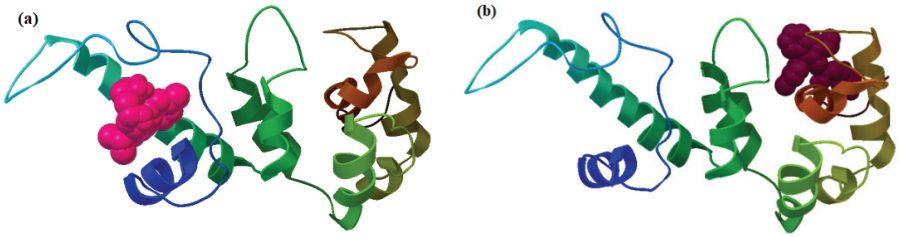

Fig. 2. Structures of complex with lowest binding free energy β-CN+FLU (a) and β-CN+PIT (b).

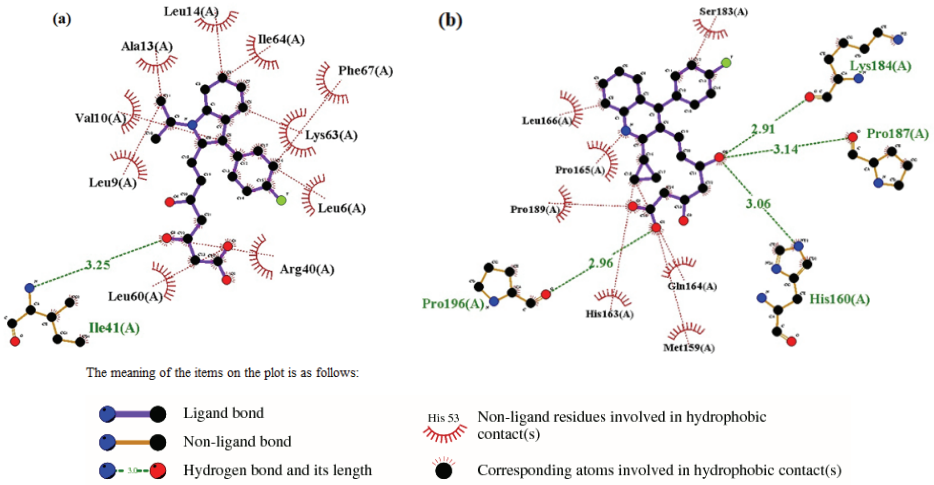

Fig. 3. Best conformations for β-CN docked to: a) FLU and b) PIT.

CONCLUSION

In this work, the binding interactions of FLU–β-CN and PIT–β-CN were studied by multi-spectroscopic and molecular docking methods. The results suggested that the intrinsic fluorescence of β-CN can be quenched by FLU and PIT through the static quenching mechanism. The number of binding sites (n) for FLU and PIT was found to be about 1. The binding constants, at 298 K, were determined according to a modified Stern–Volmer equation as 7.96×10^4 and 3.44×10^4 M^{-1} for FLU–β-CN and PIT–β-CN, respectively. The binding distance

(r_0) between FLU and PIT and Trp-residue of β-CN were calculated as 1.72 and 2.23 nm, respectively, according to Förster's non-radiative energy transfer theory.

SUPPLEMENTARY MATERIAL

Additional data and information are available electronically at the pages of journal website: https://www.shd-pub.org.rs/index.php/JSCS/article/view/11905, or from the corresponding author on request.

ИЗВОД

ВЕЗИВАЊЕ β-КАЗЕИНА ЗА ФЛУВАСТАТИН И ПИТАВАСТАТИН

HAMID DEZHAMPANAH и OMIDEH RAJABI MIANDEHI

Department of Chemistry, Faculty of Science, University of Guilan, P.O.B. 1914, Rasht 0098, Iran

У овом раду су проучене везивне интеракције флувастатина (FLU) и питавастатина (PIT) са говеђим β-казеином (β-CN) у физиолошким условима (pH 7,2) помоћу флуоресцентне емисионе спектроскопије, спектроскопије синхроне флуоресценције, FT инфрацрвене спектроскопије (FTIR) и методама молекулског докинга. Због формирања FLU–β-CN и PIT–β-CN комплекса, својствена флуоресценција β-CN била је пригушена. Број везаних FLU и PIT по молекулу протеина (n) био је око 1, а константе везивања FLU–β-CN и PIT–β-CN комплекса су биле $7{,}96\times10^4$, односно $3{,}44\times10^4$ M^{-1} на 298 K. Ови резултати сугеришу да је везивни афинитет FLU према β-CN већи од везивног афинитета PIT. Молекулско моделовање показује различита везивна места за FLU и PIT на β-CN. Сви ови експериментални резултати сугеришу да β-CN може деловати као носећи протеин за лекове FLU и PIT при њиховом достављању на циљне молекуле.

(Примљено. 6. јуна, ревидирано 30. јула,прихваћено 9. августа 2022)

REFERENCES

1. M. Gupta, R. Sharma, A. Kumar, *Pharm. Exp. Med*. **19** (2019) 259 (https://doi.org/10.1007/s13596-019-00393-x)
2. J. H. Shi, Q. Wang, D. Q. Pan, T. T. Liu, M. Jiang. *J. Biomol. Struct. Dyn*. **35** (2017) 1529 (https://doi.org/10.1080/07391102.2016.1188416)
3. A. L. Toppo, M. Yadav, S. Dhagat, S. Ayothiraman, J. S. Eswari, *Ind. J. Biochem. Biophys*. **58** (2021) 127
4. M. S. Khan, *Ann. Romanian Soc. Cell Biol*. **25** (2021) 6244
5. J. S. Yu, D. H. Shin, J. Kim, *Pharmaceutics* **12** (2020) 1133 (https://doi.org/10.3390/pharmaceutics12121133)
6. Ž. Reiner, M. Hatamipour, M. Banach, M. Pirro, K. Al-Rasadi, *Arch. Med. Sci*. **16** (2020) 490 (https://dx.doi.org/10.5114%2Faoms.2020.94655)
7. A. Sahebkar, N. Kiaie, A. M. Gorabi, M. R. Mannarino, V. Bainaconi, T. Jamialahmadi, M. Pirro, M. Banach, Prog. *Lipid Res*. **84** (2021) 101127 (https://doi.org/10.1016/j.plipres.2021.101127)
8. S. Rahimi Yazdi, M. Corredig, *Food Chem*. **132** (2012) 1143 (https://doi.org/10.1016/j.foodchem.2011.11.019)
9. K. L. Field, B. A. Kimball, J. A. Mennella, G. K. Beauchamp, A. A. Bachmanov, *Physiol. Behav*. **93** (2008) 189 (https://doi.org/10.1016/j.physbeh.2007.08.010)
10. Z. Allahdad, M. Varidi, R. Zadmard, A. Akbar, *Food Chem*. **255** (2018) 187 (https://doi.org/10.1016/j.foodchem.2018.01.143)

11. H. E. Indyk, B. D. Gill, J. E. Wood, S. Chetikam, T. Kobayashi, *J. Food Compos. Anal.* **101** (2021) 103946 (https://doi.org/10.1016/j.jfca.2021.103946)
12. M. Li, R. Kembaren, Y. Ni, J.M. Kleijn, *Food Chem*. **352** (2021) (https://doi.org/10.1016/j.foodchem.2021.129400)
13. N. Sarreshtehdari, F.S. Mohseni-Shahri, F. Moeinpour, *Luminescence* **36** (2021) 360 (https://doi.org/10.1002/bio.3951)
14. I. Portnaya, U. Cogan, Y. D. Livney, O. Ramon, K. Shimoni, M. Rosenberg, D. Danino, *Food Chem*. **54** (2006) 5555 (https://doi.org/10.1021/jf060119c)
15. J. Kaur, L. Katopo, A. Hung, J. Ashton, S. Kasapis, *Food Chem*. **252** (2018) 163 (https://doi.org/10.1016/j.foodchem.2018.01.091)
16. D. C. Thorn, S. Meehan, M. Sunde, A. Rekas, S. L. Gras, C. E. MacPhee, C. M. Dobson, M. R. Wilson, J. A. Carver, *Biochemistry* **44** (2005) 17027 (https://doi.org/10.1021/bi051352r)
17. L. Condict, J. Kaur, A. Hung, J. Ashton, S. Kasapis, *Food Hydrocoll*. **89** (2019) 351 (https://doi.org/10.1016/j.foodhyd.2018.10.055)
18. F. Mehranfar, A. K. Bordbar, H. Parastar, *J. Photochem. Photobiol., B* **127** (2013) 100 (https://doi.org/10.1016/j.jphotobiol.2013.07.019)
19. I. Hasni, P. Bourassa, S. Hamdani, G. Samson, R. Carpentier, H. A. Tajmir-Riahi, *Food Chem*. **126** (2011) 630 (https://doi.org/10.1016/j.foodchem.2010.11.087)
20. H. Dezhampanah, M. Esmaili, A. Khorshidi, *J. Mol. Struct*. **1136** (2017) 50 (https://doi.org/10.1016/j.molstruc.2017.01.065)
21. T. Liao, Y. Zhang, X. Huang, Z. Jiang, X. Tuo, *Spectrochim. Acta, A* **246** (2021) 119000 (https://doi.org/10.1016/j.saa.2020.119000)
22. F. Kong, J. Tian, M. Yang, Y. Zheng, X. Cao, X. Yue, *Spectrochim. Acta A* **243** (2020) (https://doi.org/10.1016/j.saa.2020.118824)
23. B. Li, R. Fu, H. Tan, Y. Zhang, W. Teng, Z. Li, J. Tian, *Spectrochim. Acta, A* **259** (2021) 119910 (https://doi.org/10.1016/j.saa.2021.119910)
24. Q. Wang, C. R. Huang, M. Jiang, Y. Y. Zhu, J. Wang, J. Chen, J. H. Shi, *Spectrochim. Acta, A* **156** (2016) 155 (https://doi.org/10.1016/j.saa.2015.12.003)
25. Z. Yin, X. Qie, M. Zeng, Z. Wang, F. Qin, J. Chen, W. Li, Z. He, *Food Hydrocoll*. **123** (2022) 107177 (https://doi.org/10.1016/j.foodhyd.2021.107177)
26. F. Azarakhsh, A. Divsalar, A. A. Saboury, A. Eidi, *J. Mol. Liq*. **333** (2021) 115999 (https://doi.org/10.1016/j.molliq.2021.115999)
27. G. Ma, C. Tang, X. Sun, J. Zhang, *Food Hydrocoll*. **113** (2021) 106485 (https://doi.org/10.1016/j.foodhyd.2020.106485)
28. 28. A. Chakraborty, S. Basak, *J. Photochem. Photobiol., B* **87** (2007) 191 (https://doi.org/10.1016/j.jphotobiol.2007.04.004)
29. H. Dezhampanah, R. Firouzi, Z. Moradi Shoeili, R. Binazir, *J. Mol. Struct*. **1205** (2020) 127557 (https://doi.org/10.1016/j.molstruc.2019.127557)
30. K. Yang, C. Zhou, C. Liao, J. Sun, Y. Wang, R. Guan, J. Neng, P. Sun, *LWT* **144** (2021) 111225 (https://doi.org/10.1016/j.lwt.2021.111225)
31. M. Ariyaeifar, H. Amiri Rudbari, M. Sahihi, Z. Kazemi, A. A. Kajani, H. Zali-Boeini, N. Kordestani, G. Bruno, S. Gharaghani, *J. Mol. Struct*. **1161** (2018) 497 (https://doi.org/10.1016/j.molstruc.2018.02.042)
32. J. H. Shi, J. Wang, Y. Y. Zhu, J. Chen, *J. Lumin*. **145** (2014) 643 (https://doi.org/10.1016/j.jlumin.2013.08.042)
33. J. Hua Shi, D. Qi Pan, X. Xiou Wang, T. T. Liu, M. Jiang, Q. Wang, *J. Photochem. Photobiol., B* **162** (2016) 14–23 (https://doi.org/10.1016/j.jphotobiol.2016.06.025)

34. B. Hemmateenejad, M. Shamsipur, F. Samari, T. Khayamian, *J. Pharm. Biomed. Anal.* **67**–**68** (2012) 201 (https://doi.org/10.1016/j.jpba.2012.04.012)
35. H. Bi, L. Tang, X. Gao, J. Jia, H. Lv, *J. Lumin*. **178** (2016) 72 (https://doi.org/10.1016/j.jlumin.2016.05.048)
36. S. Gong, C. Yang, J. Zhang, Y. Yu, X. Gu, W. Li, Z. Wang, *Food Hydrocoll.* **111** (2021) 106223 (https://doi.org/10.1016/j.foodhyd.2020.106223)
37. P. Bourassa, L. Bekale, H. A. Tajmir-Riahi, *J. Biol. Macromol*. **70** (2014) 156 (https://doi.org/10.1016/j.ijbiomac.2014.06.038)
38. S. K. Pawar, S. Jaldappagari, *J. Pharm. Anal*. **9** (2019) 274 (https://doi.org/10.1016/j.jpha.2019.03.007).

Journal of the Serbian Chemical Society
JSCS@tmf.bg.ac.rs • www.shd.org.rs/JSCS
J. Serb. Chem. Soc. 87 (11) S440–S444 (2022) *Supplementary material*

SUPPLEMENTARY MATERIAL TO

Binding of *β*-casein with fluvastatin and pitavastatin

HAMID DEZHAMPANAH* and OMIDEH RAJABI MIANDEHI

Department of Chemistry, Faculty of Science, University of Guilan, P.O.B. 1914, Rasht 0098, Iran

J. Serb. Chem. Soc. 87 (11) (2022) 1273–1284

EXPERIMENTAL

Materials

Bovine *β*-CN (with purity 98 %, Sigma- Aldrich, Germany) was dissolved in phosphate buffer solution (PBS) with pH 7.2 and anionic strength of 0.1, which was stored in dark at 4 °C. Ethanol (99.6 %) and methanol (99 %) were obtained from Merck Company. As FLU and PIT were insoluble in water, stock solutions (1 mM) of FLU and PIT in ethanol and methanol were first prepared, respectively, and then diluted to final concentration with phosphate buffer solution (PBS). For the preparation of the *β*-CN solution, the protein solution was filtered through a porous membrane of 0.45 μm.[14] The stock solution of *β*-CN (1 mM) was prepared in PBS (pH 7.2). Above stock solutions were prepared in redistilled water and were used freshly after preparation. The concentration of ethanol and methanol in the final solutions was lower than 2 vol.%.

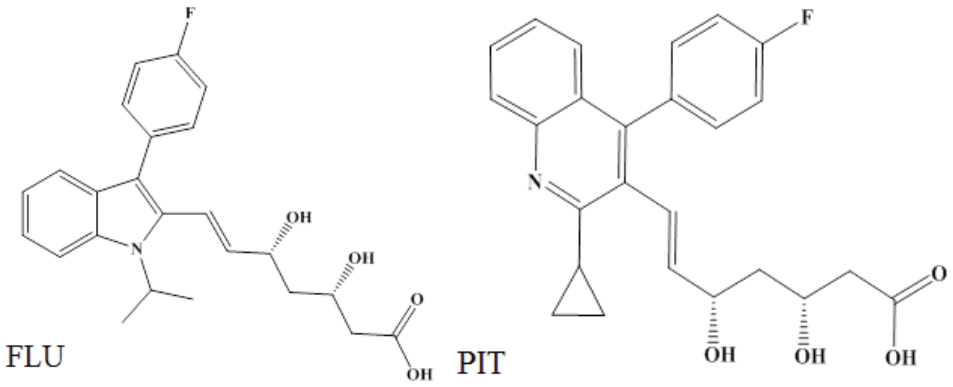

Fig. S-1. Chemical structure of FLU and PIT.

* Corresponding author. E-mail: h.dpanah@guilan.ac.ir

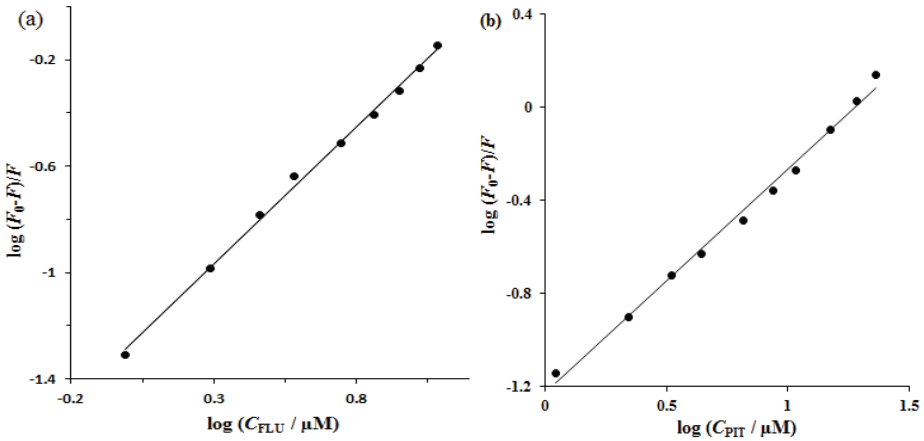

Fig. S-2. Double logarithmic plots of log $(F_0–F)/F$ against log C_Q derived from the fluorescence quenching of *β*-CN (10 μM) induced by the different concentration of FLU and PIT at 298 K, FLU-*β*-CN (a) and PIT-*β*-CN (b).

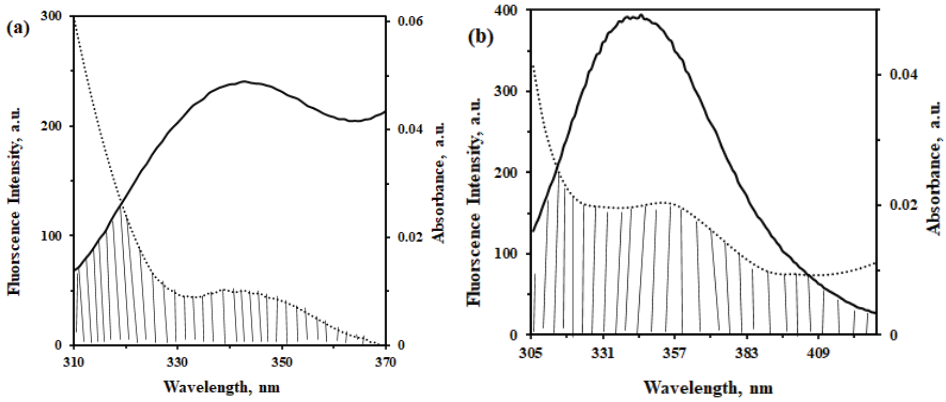

Fig. S-3. (a) *β*-CN fluorescence emission (solid lines) and UV-Vis absorption (dashed lines) of solutions containing FLU and PIT as ligand measured in PBS buffer pH 7.2 and $C_{α\text{-CN}} = C_{FLU} = 10$ μM. $C_{β\text{-CN}} = C_{PIT} = 10$ μM.

TABLE S-I. Secondary structure contents analysis of *β*-CN, FLU-*β*-CN and PIT-*β*-CN system

Structure components	Content, %		
	B-CN	FLU-*β*-CN	PIT-*β*-CN
α-Helix	28.73	31.16	24.97
β-Sheet	17.67	25.19	34.28
Random coil	24.43	27.4	19.39
β-Turn	22.0	14	18.71
β-Anti	7.13	2.24	2.65

TABLE S-II. Amino acid residues involved in interaction of FLU and PIT and *β*-CN with the free binding energy for the best selected docking positions

	Amino acids involved in casein protein bindings	ΔG / kJ mol^{-1}
FLU-*β*-CN	Leu-6, Leu-9, Val-10, Ala-13, Leu-14, Arg-40, Ile-41*, Leu-60, Lys-63, Ile-64, Phe-67	-27.58
PIT-*β*-CN	Met-159, His-160*, His-163, Gln-164, Pro-165, Leu-166, Ser-183, Lys-184*, Pro-187*, Pro-189, Pro-196*	-27.17

*Hydrogen bonding was observed with this amino acid

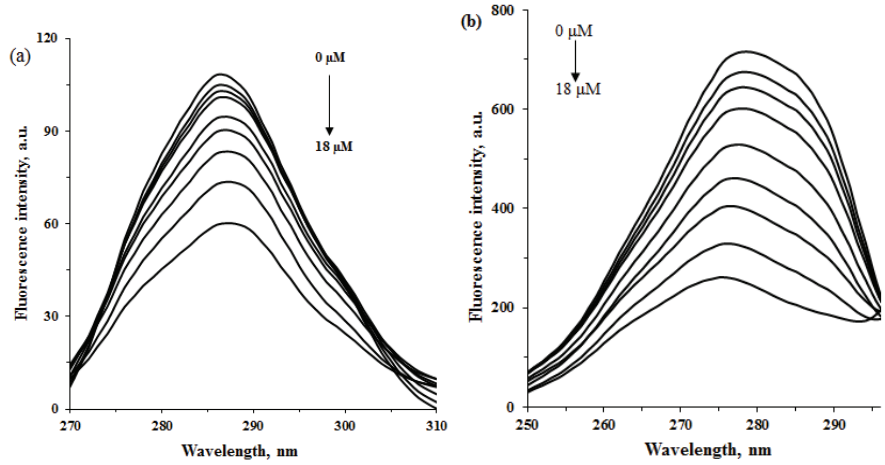

Fig. S-4. Synchronous fluorescence spectra of *β*-CN (10 μM) under physiological conditions (pH 7.2) in the absence and presence of FLU at room temperature when $\Delta\lambda$ values were set at 15 nm (a) and 60 nm (b), respectively. The concentrations of FLU were from 0 to 18 μM.

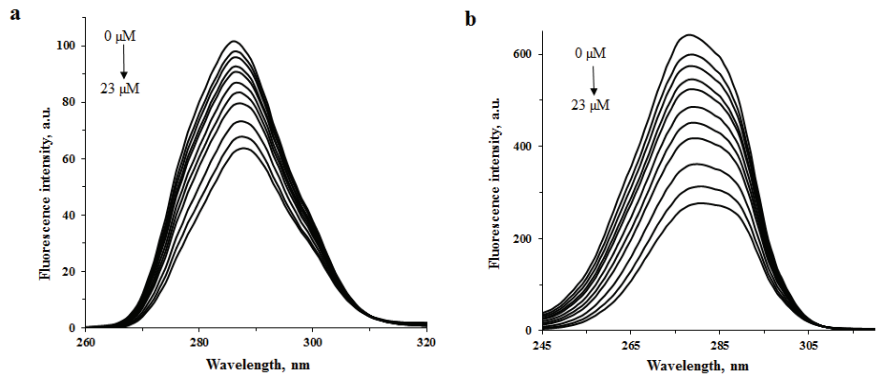

Fig. S-5. Synchronous fluorescence spectra of *β*-CN (10 μM) under physiological conditions (pH 7.2) in the absence and presence of PIT at room temperature when $\Delta\lambda$ values were set at 15 nm (a) and 60 nm (b), respectively. The concentrations of PIT were from 0 to 23 μM,

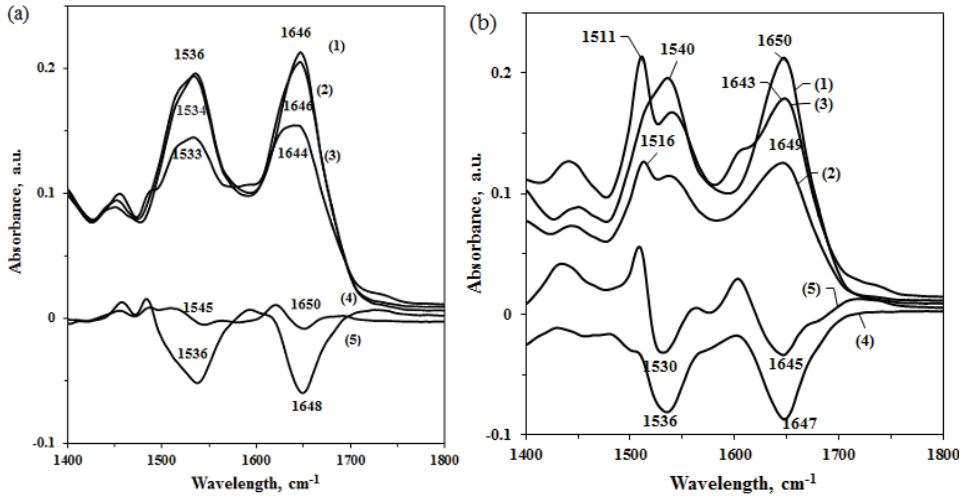

Fig. S-6. FTIR spectra in the region of 1800-1400 cm^{-1} of (a) FLU and (b) PIT for free *β*-CN 0.25 mM (1), *β*-CN -0.25 mM FLU or PIT (2), *β*-CN- 0.5 mM FLU or PIT (3), dif. *β*-CN-0.25 mM FLU or PIT (4) and dif. *β*-CN-0.5 mM FLU or PIT (5).

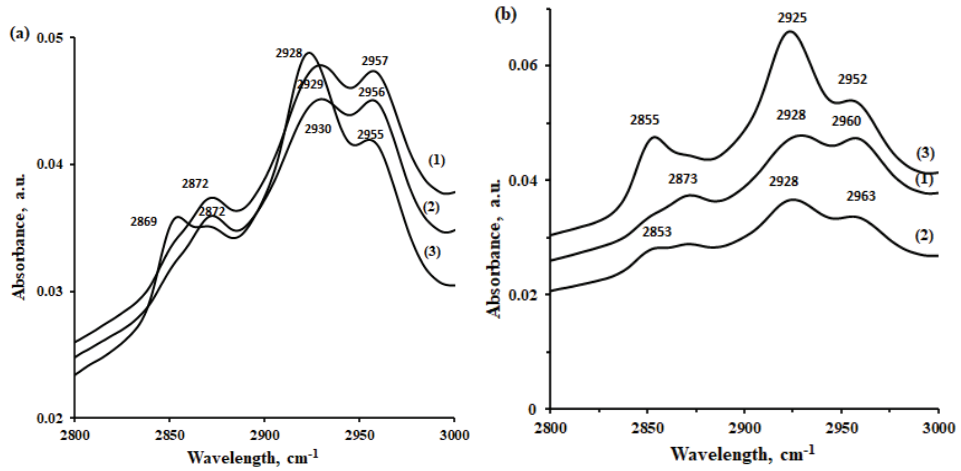

Fig. S-7. Spectral changes of casein CH_2 symmetric and anti-symmetric stretching vibrations *β*-CN complex with (a) FLU and (b) PIT for free *β*-CN 0.25 mM (1), *β*-CN-0.25 mM FLU or PIT (2), *β*-CN-0.5 mM FLU or PIT (3).

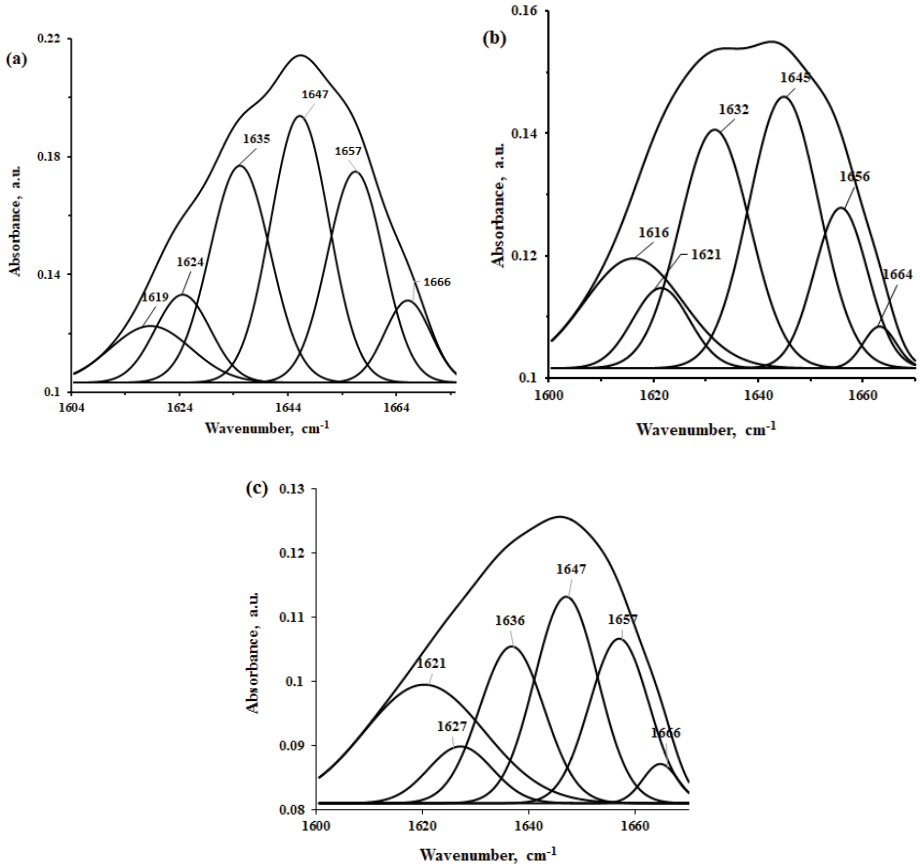

Fig. S-8. The curve-fit for *β*-CN (a), FLU-*β*-CN (b), and PIT-*β*-CN (c) in the amide I region from 1700 to 1600 cm^{-1}.

Journal of the Serbian Chemical Society
JSCS-info@shd.org.rs • www.shd.org.rs/JSCS
J. Serb. Chem. Soc. *87* (11) 1285–1296 (2022)
JSCS–5594
Original scientific paper
Published 20 October 2022

Nanoemulsification synthesis route for obtaining highly efficient Ag_3PO_4 photocatalytic nanomaterial

MARIJA PREKAJSKI ĐORĐEVIĆ[1]*, ALEKSANDRA ZARUBICA[2], ANA KALIJADIS[1], BILJANA BABIĆ[3], SVETLANA BUTULIJA[1], JELENA MALETAŠKIĆ[1] and BRANKO MATOVIĆ[1]

[1]*Department of Materials Science, "Vinča" Institute of Nuclear Science – National Institute of the Republic of Serbia, University of Belgrade, PO Box 522, 11001 Belgrade, Serbia,* [2]*Department of Chemistry, Faculty of Science and Mathematics, University of Niš, Višegradska 33, 18000 Niš, Serbia and* [2]*Institute of Physics Belgrade, University of Belgrade, Pregrevica 118, 11000, Belgrade, Serbia*

(Received 3 November 2021, revised 27 June, accepted 28 June 2022)

Abstract: Nanoemulsion technique based on Ouzo effect was applied for the fast and simple synthesis of Ag_3PO_4 at room temperature. X-ray powder diffraction analysis and Raman spectroscopy reviled that synthesized powder was single-phase. Using scanning electron microscopy analysis, it was found that the synthesized Ag_3PO_4 particles were near-spherical shape with an average diameter of 100 nm. The high value for the specific surface area of obtained powder was measured by Brunauer–Emmet–Teller method. Finally, the Ag_3PO_4 product was used as a photocatalyst for the photodegradation of crystal violet dye in an aqueous solution. Nanoemulsion strategy procedure provides a simple pathway to obtain a highly efficient single-phase Ag_3PO_4 photocatalyst.

Keywords: XRD; Raman; BET; BJH; photodegradation.

INTRODUCTION

The assembly of organic dyes and unsafe wastage from industries produce environmental problems, such as air and water pollution. Many techniques have been developed for the removal of organic dyes from wastewater, including adsorption, photocatalysis, anaerobic treatment, membrane filtration, chemical oxidation, *etc.*[1–3] One of the most promising technologies to address the issues of environmental pollution is the direct use of sun light energy.[4] Among them, semiconductors based photocatalyst used for treating wastewater and organic dye pollutants under ultraviolet (UV) and visible (Vis) light irradiation are especially interesting due to their high efficiency, destruction ability, and availability. How-

* Corresponding author. E-mail: prekajski@vin.bg.ac.rs
https://doi.org/10.2298/JSC211103055P

ever, some photocatalysts can only be excited by UV light. It is well-known that the UV region occupies only approximately 4% of the entire solar spectrum, while 43 % of the energy belongs to Vis light. Therefore, the development of novel photocatalysts, particularly Vis light-responsive catalysts, are necessary for the efficient utilization of solar energy in photocatalysis, and for these reasons, there is an increasing interest in pursuing an ideal photocatalyst to effectively utilize the Vis light of solar radiation.

Among many photocatalyst materials, silver orthophosphate (Ag_3PO_4) has attracted considerable attention since Yi *et al.* discovered it in 2010.[5–7] In the last few years, many efforts have been devoted to further improving and optimizing the photocatalytic activity and stability of Ag_3PO_4. It was found that photodegradation activity and applications of this phosphate are profoundly dependent on its size, morphology, and specific surface area, and thus the photocatalytic efficiency of Ag_3PO_4 can be improved by controlling the morphology and crystal structure of the material. Therefore, great attention has been paid on devising appropriate synthesis processes for obtaining efficient Ag_3PO_4 catalysts. Many methods have been evolved that as result produces various morphologies and sizes of Ag_3PO_4, which include spheres,[8–10] dodecahedrons,[11] tetrahedrons,[11,12] cubes,[13,14] mesocrystals,[11] concave trisoctahedron,[15] gyro shape,[16] *etc*. However, their practical application is restricted because of several limiting factors, for instance, the tedious work involved in the preparation and removal of the surfactants and/or templates. Particularly, the templates or surfactants are not eco-friendly and not suitable for large-scale production.[17] Hence, it is still an important research field to find an economic and green method for controlling the size and morphology of Ag_3PO_4. Although a large number of modifications have been adopted in the synthesis techniques, the optimum synthesis conditions are still required.

In this contribution, the presented work demonstrates the successful synthesis of Ag_3PO_4 *via* an effortless and very efficient nanoemulsion synthesis method, based on the Ouzo effect. Nanoemulsions represent a special class of liquid disperse systems, with droplet diameters smaller than 100 nm.[18] Spontaneous emulsification occurs when a strongly hydrophobic oil is dissolved in a water-miscible solvent. This effect is nanoemulsification and it is usually called the Ouzo effect[19,20] where the Ouzo is a liquor that consists of anise oil dispersed in ethanol. When water is added to the Ouzo, the dissolved anise oil spontaneously nucleates into many small droplets, without the help of a surfactant. These small droplets scatter light causing the sample to appear milky white. The Ouzo effect offers the possibility of obtaining a pure nanopowder, without using any surfactants or templates, because emulsification occurs almost simultaneously in the entire volume.[21]

X-Ray powder diffraction (XRD) accompanied with the Rietveld refinement procedure enabled the crystallite size, structure and phase composition of a synthesized sample to be explored. Raman spectroscopy was used in order to confirms the composition purity of the obtained sample. The morphological properties were studied by field emission scanning electron microscopy (FE-SEM) and Brunauer–Emmett–Teller (BET) measurements. The pore size distribution (PSD) was estimated by applying the Barett–Joyner–Halenda (BJH) method. The photocatalytic activity of as-prepared Ag_3PO_4 product was investigated by photodegradation of crystal violet (CV) dye in an aqueous solution. A simple procedure for the synthesis of the effective photocatalyst was demonstrated. According to the authors' knowledge, this method was used for the very first time for the synthesis of Ag_3PO_4 nanomaterial.

EXPERIMENTAL

Ag_3PO_4 nanoparticles were synthesized using analytical grade $AgNO_3$ (Riedel-de Haën, 99 % purity) and $(NH_4)_2HPO_4$ (Riedel-de Haën, 99 % purity). Analytical grade acetone was the solvent used for making the nanoemulsion. For the synthesis, 3/100 mole of $AgNO_3$ was desolved in 0.05 dm^3 of acetone and then mixed with 1/100 mol of $(NH_4)_2HPO_4$ which was desolved in 0.05 dm^3 of water (the ratio of acetone and aqueous solution phases in nanoemulsion was 1:1). The pH in the aqueous $(NH_4)_2HPO_4$ solution was adjusted to 11 with sodium hydroxide (1 M) prior to mixing. The mixed solutions were stirred for 5 min using a magnetic stirrer. No surfactant was used in any of the synthesis processes. A nanoemulsion (milky white, almost transparent liquid) was obtained that was immediately centrifuged to avoid particle agglomeration and then washed three times using ultra-pure deionized water. Finally, the slurry of nanoprecipitates was dried in an oven at 50 °C, for 12 h, in order to obtain a dry powder.

The phase purity and crystallinity of the produced powder were examined using X-ray diffraction (Raguku Ultima IV, Japan). The X-ray beam was nickel-filtered CuKα_1 radiation (λ = 0.1540 nm, operating at 40 kV and 40 mA). The XRD data were collected at 2θ from 15 to 80 ° at a scanning rate of 2 °min^{-1}. Phase analysis was realized using PDXL2 software (version 2.0.3.0),[22] with referece to the patterns of the American Mineralogist Crystal Structure Database (AMCSD).[23] Calculation of the average crystallite size (D_{hkl}) was performed using the Scherrer formula, Eq. (1):[24]

$$D_{hkl} = \frac{0.9\lambda}{\beta \cos\theta} \quad (1)$$

where λ is the wavelength of the X-rays, θ is the diffraction angle, β is the corrected half-width for instrumental broadening $\beta = (\beta_m - \beta_s)$, β_m is the observed half-width and β_s is the half-width of the standard CeO_2 sample.

The specific surface area and the pore size distribution of Ag_3PO_4 were analyzed using Surfer (Thermo Fisher Scientific, USA). The PSD was estimated using the BJH method[25] to the desorption branch of isotherms and mesopore surface, and the micropore volume were estimated using the α_s-plot method.[26]

The morphology of the dried nanoprecipitates was characterized by a Hitachi S-4800 field emission gun scanning electron microscope, with electron energies of 20 kV in high vacuum. The samples used for FE-SEM characterization were coated with 5 nm thin layer of

Au/Pd using a standard sputtering technique. The results from FE-SEM measurements showed a sample area of 2.5 μm×2.5 μm (275,000× magnification).

The photocatalytic ability of the synthesized Ag_3PO_4 nanomaterial was studied using the degradation of the organic dye crystal violet as a test. The examination the photodegradation of the cationic dye CV was chosen because in all literature data the photodegradation of this dye by Ag_3PO_4. as a photocatalyst is the least researched. Vis irradiation was applied in order to evaluate the photocatalytic activity of the Ag_3PO_4 photocatalyst. The light source was 4 Vis tungsten–halogen lumps, every with a power of 60 W. A quartz cell was used for the photocatalytic degradation test. The reaction was maintained at ambient temperature. The acidity of the solutions was not additionally adjusted, and pH values were in the range from 6.7 to 7.0. In a typical experiment, aqueous suspensions of the dye (initial concentration 500 μmol dm^{-3}) and 50 mg of the synthesized Ag_3PO_4 photocatalyst powder were placed in a beaker. The volume of the test solution (the CV colour solution) was $V = 0.05$ dm^3. Prior to irradiation, the suspension was magnetically stirred in the dark for 1 h to ensure the establishment of the adsorption/desorption equilibrium. The suspension was kept under constant air-equilibrated conditions. In addition, the same experiment was reperformed in a combination of UV + Vis irradiation, using 4 UV low-pressure Hg vapor lamps, each with power 28 W, and 4 Vis tungsten–halogen lumps, each with power 60 W.

RESULTS AND DISCUSSION

Phase structure and morphology of the porous nanospheres

The crystallinity and phase purity of the obtained product was first examined by X-ray diffraction. The XRD pattern of the as-synthesized samples (Fig. 1) revealed that the Ag_3PO_4 phase was already forming at room temperature. The synthesized powder is single-phase and all the diffraction peaks can be well indexed to cubic Ag_3PO_4 (space group *P*-43*n*), which is in accordance with the standard data AMCSD Card No.: 0017250.[23] There were no other characteristic peaks of impurities or secondary phases. The diffraction peaks were broadened that indicates the presence of small crystallite (nanocrystals) in the sample. According to the calculation based on the Scherrer Equation, the crystallite size of as synthesized samples was about 4 nm (Table I). The calculated cell parameters were $a = b = c = 0.6017208(3)$ nm. These results are in good correlation with literature data.[27,28]

The inset in Fig. 1 represents the crystal structure of Ag_3PO_4 modeled using Vesta© software version 3.3.2.[29] It depicts the cubic structure of Ag_3PO_4, in which six Ag atoms occupy only the 6*d* Wyckoff position and have 4-fold coordination by four O atoms resulting in tetrahedral [AgO_4]; the P atoms are each in [PO_4] tetrahedra, while the O atoms possess 4-fold coordination surrounded by three Ag atoms and one P atom. The isolated and regular [PO_4] tetrahedra construct a body-centered cubic lattice structure. In this modeled structure, the Ag and P atoms are coordinated with four O atoms, resulting in tetrahedral [AgO_4] and [PO_4] clusters. Each [PO_4] cluster has in its vicinity three [AgO_4] agglomerates bound by O atoms. The existence of two binding angles (α and β) indicated that

the [AgO_4] agglomerates are highly distorted in the network, because of the inductive effect caused by the high electronegativity of the clusters.[30]

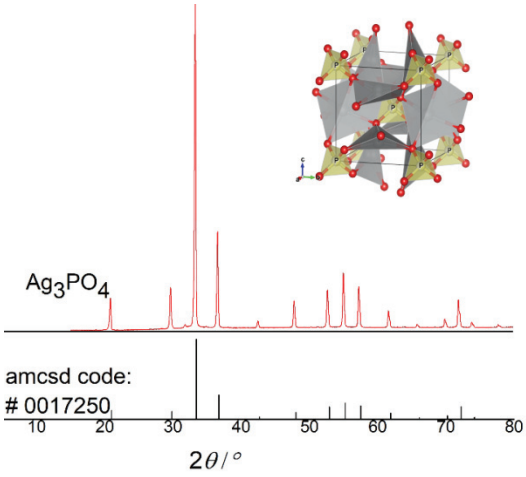

Fig. 1. XRD pattern of the synthesized Ag_3PO_4. Inset: Unit-cell structure showing the polyhedron configuration of the cubic Ag_3PO_4. Red, yellow, and grey spheres represent O, P, and Ag atoms/ /polyhedrons, respectively.

TABLE I. Calculated crystallographic parameters after refinement using PDXL2 software of the synthesized Ag_3PO_4 crystal structure

Atom	Wickoff position	*x*	*y*	*z*	Position occupation
Ag	12*h*	0.22419	0	0.5	1.5
P	2*a*	0	0	0	0.5
O	8*e*	0.1467	0.1467	0.1467	2.5
a / nm	0.6017208(3)				

Raman analysis

Further, Raman spectroscopic analysis was performed to confirm the presence of Ag_3PO_4 single phase. The Raman spectra of an as-synthesized Ag_3PO_4 sample is displayed in Fig. 2. According to literature data,[30] Ag_3PO_4 presents a

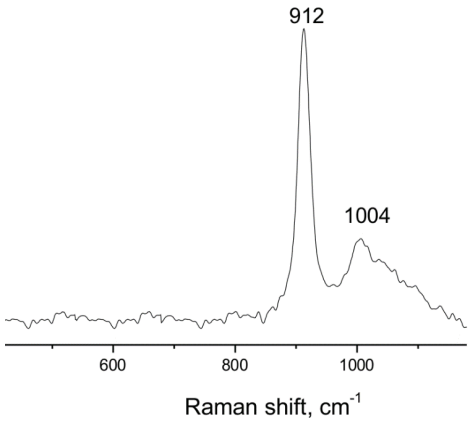

Fig. 2. Raman spectra of an as-synthesized Ag_3PO_4 sample.

total of 18 Raman-active modes. However, in this work, only two Raman-active modes were identified, both related to the PO_4^{3-} clusters. The strong and sharp absorption peak centered at about 912 cm^{-1} is attributed to the PO_4^{3-} symmetric stretching vibration of O–P–O bonds.[31] A small and broad peak at 1004 cm^{-1} is attributed to the PO_4^{3-} asymmetric stretching vibrations of the same bonds.[32] The Raman spectra confirmed the formation of single-phase Ag_3PO_4.

Morphology characterization

Further investigation was performed by FE-SEM technologies to characterize the morphology and crystal structure of the as-obtained Ag_3PO_4 nanomaterial. FE-SEM micrographs of the as-synthesized Ag_3PO_4 powder are shown in Fig. 3, particles with near-spherical shapes with an average diameter of 100–200 nm could be observed. Their morphology also resembles platelets. However, higher magnification (Fig. 3b) revealed that the particles are more likely irregular-shaped spheres. Some particle aggregation also occurs. The formation of spherical Ag_3PO_4 nanoparticles is due to the Ouzo effect, which occurs in the present synthesis method.[33] This characteristic endows the as-prepared Ag_3PO_4 porous nanospheres with a large surface area, which could affect their physicochemical properties.

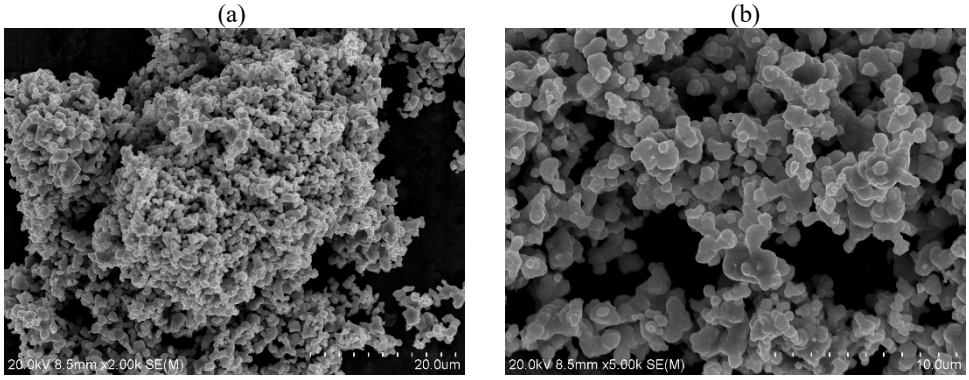

Fig. 3. FE-SEM micrographs of an as-synthesized Ag_3PO_4 sample: a) magnification 2000×; b) magnification 5000×.

Adsorption isotherms – BET experiments

Nitrogen adsorption isotherms for an Ag_3PO_4 sample, as the amount of N_2 adsorbed as a function of relative pressure at –196 °C, are shown in Fig. 4. It could be seen from the analysis that the adsorption–desorption hysteresis loop of the sample can be classified as Type IV,[34] which is associated with mesoporous materials (Fig. 4). The shape of the hysteresis loop is of type H3. Isotherms revealing type H3 hysteresis do not exhibit any limiting adsorption at high P/P_0, which is observed with non-rigid aggregates of plate-like particles giving rise to

slit-shaped pores.[35] Specific surface areas calculated by the BET equation, S_{BET}, are listed in Table II. The S_{BET} value is 42 m^2 g^{-1}. The pore size distribution, as determined with the BJH method, is shown in Fig. 5. The sample is micro- and mesoporous with one peak pore radius at 2.0 nm. The median pore radius (r_{med}) is 2.9 nm (Table II).

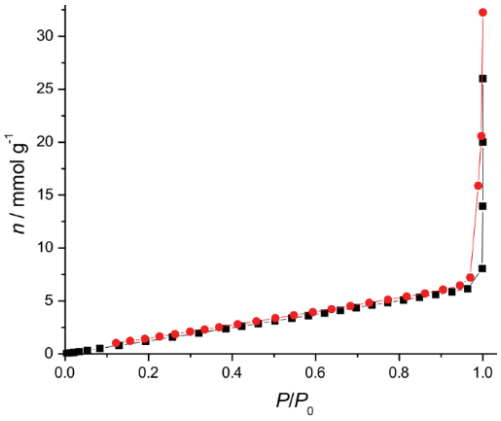

Fig. 4. Nitrogen adsorption isotherms of Ag_3PO_4. Black square symbols – adsorption, red circle symbols – desorption.

TABLE II. Porous properties of the synthesized Ag_3PO_4 nanomaterial

S_{BET} / m^2 g^{-1}	S_{meso} / m^2 g^{-1}	S_{mic} / m^2 g^{-1}	V_{meso} / dm^3 g^{-1}	V_{mic} / dm^3 g^{-1}	r_{med} / nm
42	24	18	3.2×10^{-5}	2.1×10^{-5}	2.9

The α_s-plot, obtained based on the standard nitrogen adsorption isotherm. The straight line in the medium α_s-plot region gives a mesoporous surface area including the contribution of the external surface, S_{meso}, determined by its slope, and the micropore volume, V_{mic}, is given by the intercept. The calculated porosity parameters (S_{meso}, S_{mic}, V_{meso}, V_{mic}) are given in Table II. An α_s-plot analysis confirmed that the sample was micro- and mesoporous.

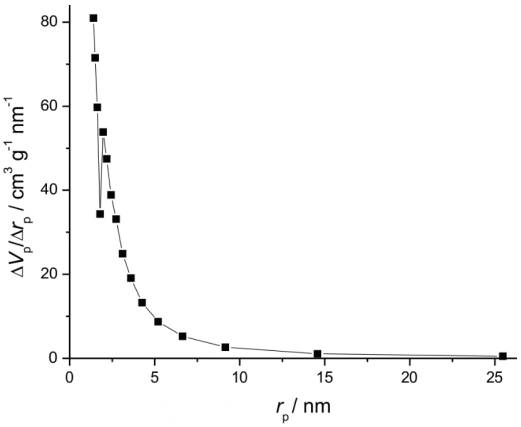

Fig. 5. Pore size distribution of Ag_3PO_4.

The specific surface area of a photocatalyst is a major parameter to measure the characteristics of the material, and its size has a great impact on its photocatalytic properties. It was shown that the specific surface areas of samples produced by the simple nanoemulsion synthesis method have larger specific surface areas than the products of other methods. For example, starting from the same components, but using the precipitation method and the ion-exchange method of synthesis, the authors obtained 8.7 and 1.2 $m^2 g^{-1}$ specific surface areas of the synthesized Ag_3PO_4, for the above-mentioned methods, respectively.[36] On the other hand, the specific surface area that was obtained using the nanoemulsion technique was 42 $m^2 g^{-1}$, which is 5 times higher than in the case of the sample obtained by the precipitation method and even 35 times higher than the specific surface area obtained in samples synthesized by the ion-exchange method. In addition, the particle size for the precipitation method is mainly centered on 0.3––0.4 μm, while the ion-exchange method predominantly ranges from 6 to 10 μm. In the present work, the particle size was the same as the crystallite size (since the crystallite is not glued together into bigger agglomerated particles). This smaller size of crystallites (particles) makes a significant contribution to obtaining higher values of the specific surface area. It could be explained by a higher ratio of surface to volume of the nanomaterials. Namely, it is known that nanoparticles have a relatively larger surface area when compared to the same volume of material made up of bigger particles. As particle size decreases, the surface area per unit volume increases. Therefore, materials made of nanoparticles have a much greater surface area per unit volume ratio compared with materials made up of bigger particles. As the surface area per mass of a material increases, a greater amount of the material can come into contact with surrounding materials, thus affecting reactivity and making the material much more efficient for photodegradation of pollutant dyes.

Photocatalytic degradation of crystal violet dye

The photocatalytic activities of the as-prepared Ag_3PO_4 samples were evaluated by the degradation of the cationic crystal violet dye. First, blank experiment was performed by irradiating an aqueous solution of the dye derivates in the absence of photocatalysts and a spectrophotometic analysis of the irradiated samples did not show any measurable loss of the dye (black squares in Fig. 6) indicating that irradiation alone is not capable of degrading CV dye. The effect of Ag_3PO_4 on the removal of CV dyes was investigated and the results are presented in Fig. 6. First, the photodegradation of CV dye on the synthesized Ag_3PO_4 photocatalyst with UV + Vis irradiation was evaluated (red dots in Fig. 6) The Ag_3PO_4 photocatalyst exhibited very good photocatalytic activity for CV dye photodegradation under Vis irradiation. After Vis irradiation for 30 min, 87 % of CV had been photodegraded. The degradation kinetics suppresed slightly

when only Vis light was used (blue triangles in Fig. 6). These results show that the synthesized Ag_3PO_4 nanomaterial works as an excellent photo-catalyst.

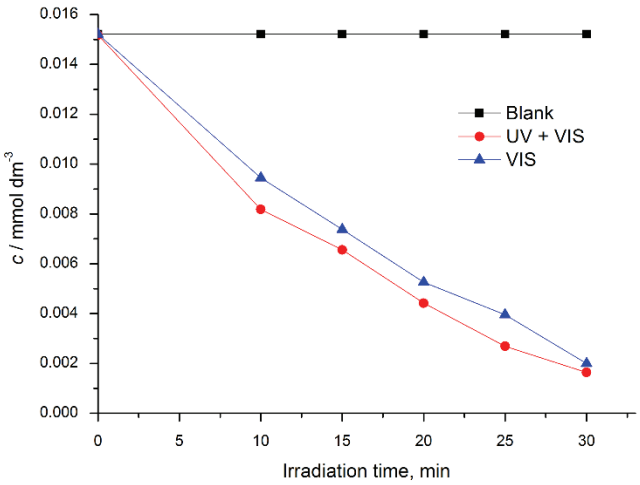

Fig. 6. Photocatalytic degradation of CV dye by Ag_3PO_4 nano-spheres sample, blank experiment (black squares), illuminated with UV + Vis (red dot) and only Vis light (blue triangle).

In the literature data, just a few research papers that deal with photodegradation of crystal violet dye using Ag_3PO_4 photocatalyst were found. Luo and co-authors[37] obtained similar results but with two-times higher concentrations of used photocatalyst. Namely, after Vis irradiation for 30 min, 93.0 % of CV dye was photodegraded, but the initial concentration of Ag_3PO_4 photocatalyst powder was 100 mg of the synthesized Ag_3PO_4 photocatalyst powder.[33] This means that a more than two-times more efficient material was obtained in the present work, which could be explained by the morphology of synthesized powders. Compared to the sample used in the present work, the Ag_3PO_4 used previously had a much larger particle size (about 4000 nm) and consequently a much smaller specific surface area (0.24 m^2 g^{-1}).[34] These are the reasons for the superior efficiency of the sample that was obtained in this using nano emulsification technique, also called the "Ouzo effect".[21]

It seems that material synthesis using the nanoemulsion method could be related to the excellent physical and chemical properties of Ag_3PO_4, *e.g.*: a higher value of the specific surface area, the presence of individual crystal phases, the small size of the crystallite/particles, *etc*.

CONCLUSIONS

A simple and low-cost nanoemulsion synthesis technique based on the Ouzo effect has been successfully used for the preparation of a Ag_3PO_4 photocatalyst. Single-phase Ag_3PO_4 was obtained at room temperature, with crystallite size

≈100 nm. The synthesized sample was micro- and meso-porous, with a specific surface area of 42 m^2 g^{-1}. The applied synthesis route gives a material with a much higher value of the specific surface area in comparison to the other synthesis methods that are described in the literature. This is very important when it comes to the application of photocatalyst. The particles were spherical in shape, with the size of about 100–200 nm. This research showed that synthesized Ag_3PO_4 photocatalyst is efficient for the photodegradation of aqueous CV dye solutions under Vis light. The present study indicates that this simple, effortless, and very efficient synthetic process provides a simple pathway to obtain a highly efficient single-phase Ag_3PO_4 photocatalyst. For these reasons, it is believed that this synthesis method could be applied for large-scale production. Plans for the future are to perform immobilization of photocatalytic material on an extremely porous filter (*e.g.*, made of Al_2O_3 ceramic) in order to allow easy extraction of photocatalytic material from wastewater.

Acknowledgements. This work was supported by the Ministry of Education, Science and Technological Development of the Republic of Serbia (Theme Number: 1702021). The authors Branko Matović and Jelena Maletaskić gratefully acknowledge the financial support from the Laboratory for Advanced Nuclear Energy, Institute of Innovative Research, Tokyo Institute of Technology, 2-12-1, Okayama, Meguro-ku, Tokyo 152-8550, as visiting professors.

ИЗВОД

СИНТЕЗА ВИСОКО ЕФИКАСНОГ Ag_3PO_4 ФОТОКАТАЛИТИЧКОГ НАНОМАТЕРИЈАЛА ПРОЦЕСОМ НАНОЕМУЛЗИФИКАЦИЈЕ

МАРИЈА ПРЕКАЈСКИ ЂОРЂЕВИЋ[1], АЛЕКСАНДРА ЗАРУБИЦА[2], АНА КАЛИЈАДИС[1], БИЉАНА БАБИЋ[3], СВЕТЛАНА БУТУЛИЈА[1], ЈЕЛЕНА МАЛЕТАШКИЋ[1] и БРАНКО МАТОВИЋ[1]

[1]Лабораторија за материјале, Институт за нуклеарне науке „Винча“ – Институт од националног значаја Републике Србије, Универзитет у Београду, поштански фах 522, 11001 Београд, [2]Департман за хемију, Природно–математички факултет Универзитета у Нишу, Вишеградска 33, 18000 Ниш и [3]Институт за физику Београд, Универзитет у Београду, Прегревица 118, 11000, Београд

Наноемулзиона метода заснована на „Ouzo ефекту“ примењена је за једноставну и брзу синтезу Ag_3PO_4 на собној температури. Анализе дифракције рендгенских дијаграма праха и Раманове спетроскопије показали су да је синтетисани прах монофазан. Методом скенирајуће електронске микроскопије утврђено је да су синтетисане честице Ag_3PO_4 сферног облика, просечног пречника 100 nm. Висока вредност специфичне површине добијеног праха мерена је Brunauer–Emmet–Teller методом. Добијени нанопрах Ag_3PO_4 коришћен је као фотокатализатор за фотодеградацију кристално љубичасте боје у воденим растворима. Резултати су показали потпуну деградацију при кратком времену зрачења. Закључује се да је метода наноемулзификације једноставан начин за добијање високо-ефикасног монофазног Ag_3PO_4 фотокатализатора.

(Примљено 3. новембра 2021, ревидирано 27. јуна, прихваћено 28. јуна 2022)

REFERENCES

1. N. Atar, A. Olgun, S. Wang, *Chem. Eng. J.* **192** (2012) 1 (https://doi.org/10.1016/j.cej.2012.03.067)

2. N. Atar, A. Olgun, S. Wang, S. Liu, *J. Chem. Eng. Data* **56** (2011) 508 (https://doi.org/10.1021/je100993m)
3. N. Atar, T. Eren, M. L. Yola, H. Karimi-Maleh, B. Demirdögena, *RSC Adv.* **5** (2015) 26402 (https://doi.org/10.1039/C5RA03735B)
4. A. Kubacka, M. Fernandez-Garcia, G. Colon, *Chem. Rev.* **112** (2012) 1555 (https://doi.org/10.1021/cr100454n)
5. Z. G. Yi, J. H. Ye, N. Kikugawa, T. Kako, S. Ouyang, H. Stuart-Williams, H. Yang, J. Cao, W. Luo, Z. Li, Y. Liu, R. L. Withers, *Nat. Mater.* **9** (2010) 559 (https://doi.org/10.1038/nmat2780)
6. G. H. Huang, Z. L. Ma, W. Q. Huang, Y. Tian,1 C. Jiao, Z. M. Yang, Z. Wan, A. Pan, *J. Nanomater.* **2013** (2013) 1 (https://doi.org/10.1155/2013/371356)
7. H. Wang, Y. S. Bai, J. T. Yang, X. Lang, J. Li, L. Guo, *Chem. Eur. J.* **18** (2012) 5524 (https://doi.org/10.1002/chem.201103189)
8. Z. M. Yang, Y. Y. Liu, L. Xu, G. F. Huang, W. Q. Huang, *Mater. Lett.* **133** (2014) 139 (https://doi.org/10.1016/j.matlet.2014.07.004)
9. X. Guan, J. Shi, L. Guo, *Int. J. Hydrogen Energy* **38** (2013) 11870 (https://doi.org/10.1016/j.ijhydene.2013.07.017)
10. Z. M. Yang, Y. Tian, G. F. Huang, W. Q. Huang, Y. Y. Liu, C. Jiao, Z. Wan, X. G. Yan, A. Pan, *Mater. Lett.* **116** (2014) 209 (https://doi.org/10.1016/j.matlet.2013.11.041)
11. P. Dong, Y. Yin, N. Xu, R. Guana, G. Hou, Y. Wang, *Mater. Res. Bull.* **60** (2014) 682 (https://doi.org/10.1016/j.materresbull.2014.09.047)
12. L. Dong, P. Wang, S. Wang, P. Lei, Y. Wang, *Mater. Lett.* **134** (2014) 158 (https://doi.org/10.1016/j.matlet.2014.07.094)
13. X. Guo, C. Chen, S. Yin, L. Huang, W. Qin, *J. Alloy. Compd.* **619** (2015) 293 (https://doi.org/10.1016/j.jallcom.2014.09.065)
14. Y. Bi, H. Hu, S. Ouyang, G. Lu, J. Cao, Jinhua Ye, *Chem. Commun.* **48** (2012) 3748 (https://doi.org/10.1039/C2CC30363A)
15. Z. Jiao, Y. Zhang, H. Yu, G. Lu, J. Yeb, Y. Bi, *Chem. Commun.* **49** (2013) 636 (https://doi.org/10.1039/C2CC37324F)
16. J. D. Wang, J. K. Liu, C. X. Luo, Y. Lu, X. H. Yang, *Cryst. Growth Des.* **13** (2013) 4837 (https://doi.org/10.1021/cg4009812)
17. S. Kumar, T. Surendar, V. Shanker, *Mater. Lett.* **123** (2014) 172 (https://doi.org/10.1016/j.matlet.2014.02.106)
18. M. Yu Koroleva, E.V. Yurtov, *Russ. Chem. Rev.* **81** (2012) 21 (https://doi.org/10.1070/RC2012v081n01ABEH004219)
19. F. Ganachaud, J. L. Katz. *Chem. Phys. Chem.* **6** (2005) 209 (https://doi.org/10.1002/cphc.200400527)
20. W. Y. Zhou, M. Wang, W. L. Cheung, B. C. Guo, D. M. Jia. *J. Mater. Sci. Mater. Med.* **19** (2008) 103 (https://doi.org/10.1007/s10856-007-3156-9)
21. M. Prekajski, M. Mirković, B. Todorović B, A. Matković, M. Marinović-Cincović, J. Luković. B. Matović, *J. Eur. Ceram. Soc.* **36** (2016) 1293 (https://doi.org/10.1016/j.jeurceramsoc.2015.11.045)
22. *PDXL Version 2.0.3.0 Integrated X-ray Powder Diffraction Software*, Rigaku Corporation, Tokyo, 2011(https://www.rigaku.com/support/software/pdxl)
23. *American Mineralogist Crystal Structure Database (AMCSD)*, (http://rruff.geo.arizona.edu/AMS/amcsd.php, accessed in August, 2021)

24. P. Scherrer, *Gött. Nachr.* **2** (1918) 98 (http://www.digizeitschriften.de/download/PPN252457811_1918/PPN252457811_1918__log15.pdf)
25. E. P. Barret, L. G. Joyner, P. P. Halenda, *J. Am. Chem. Soc.* **73** (1951) 373 (https://doi.org/10.1021/ja01145a126)
26. B. C. Lippens, B. G. Linsen, J. H. De Boer, *J. Catal.* **3** (1964) 32 (https://doi.org/10.1016/0021-9517(64)90089-2)
27. L. Helmholz, *J. Chem. Phys.* **4** (1936) 316 (https://doi.org/10.1063/1.1749847)
28. J. F. Cruz-Filho, T. M. S. Costa, M. S. Lima, L. J. Silva, R. S. Santos, L. S. Cavalcante, E. Longo, G. E. Luz Jr., *J. Photochem. Photobiol. A* **377** (2019) 14 (https://doi.org/10.1016/j.jphotochem.2019.03.031)
29. K. Momma, F. Izumi, *J. Appl. Crystallogr.* **41** (2008) 653 (https://doi.org/10.1107/S0021889808012016)
30. G. Botelho, J. C. Sczancoski, J. Andres, L. Gracia, E. Longo, *J. Phys. Chem., C* **119** (2015) 6293 (https://doi.org/10.1021/jp512111v)
31. B. Chai, J. Li, Q. Xu, *Ind. Eng. Chem. Res.* **53** (2014) 8744 (https://doi.org/10.1021/ie4041065)
32. Z. Wang, L. Yin, M. Zhang, G. Zhou, H. Fei, H. Shi, H. Dai, *J. Mater. Sci.* **49** (2014) 1585 (https://doi.org/10.1007/s10853-013-7841-4)
33. F. Ganachaud, J. L. Katz, *Chem. Phys. Chem.* **6** (2005) 209 (https://doi.org/10.1002/cphc.200400527)
34. K. S. W. Sing, D. H. Everett, R. A. W. Haul, L. Moscou, R. A. Pierotti, J. Rouquerol, T. Siemieniewska, *Pure. Appl. Chem.* **57** (1985) 603
35. S. Lowell, J. E. Shields, M. A. Thomas, M. Thommes, *Charactrization of Porous Solids and Powders: Surface Area, Pore Size and Density*, Kluwer Academic Publishers, Dordrecht, 2004, p. 44 (ISBN 978-1-4020-2303-3)
36. K. Hatakeyama, M. Okuda, T. Kuki, T. Esaka, *Mater. Res. Bull.* **47** (2012) 4478 (https://doi.org/10.1016/j.materresbull.2012.09.057)
37. L. Luo, Y. Li, J. Hou, Y. Yang, *Appl. Surf. Sci.* **319** (2014) 332 (https://doi.org/10.1016/j.apsusc.2014.04.154).

Journal of the Serbian Chemical Society
JSCS-info@shd.org.rs • www.shd.org.rs/JSCS
J. Serb. Chem. Soc. *87* (11) 1297–1311 (2022)
JSCS–5595
Original scientific paper
Published 9 November 2022

Corrosion protection properties of polypyrrole coatings formed onto 316 L SS from a solution containing molybdate and salicylate

CAMILA A. RAMOS[1], MARIA B. GONZÁLEZ[1]*, LORENA I. BRUGNONI[2] and SILVANA B. SAIDMAN[1]

[1]*Chemical Engineering Department, Institute of Electrochemical and Corrosion Engineering, National University of the South, CONICET, Bahía Blanca, Argentina and* [2]*Department of Biology, Biochemistry and Pharmacy, Institute of Biological and Biomedical Sciences, National University of the South, CONICET, Bahía Blanca, Argentina*

(Received 20 April, revised 11 July, accepted 23 September 2022)

Abstract: The electrosynthesis of PPy films onto 316L stainless steel from nearly neutral and alkaline solutions containing molybdate and salicylate is reported. The corrosion behaviour of the coatings constituted by hollow rectangular microtubes was monitored in Ringer solution using open circuit potential measurements, polarization techniques and electrochemical impedance spectroscopy. The polymer formed in a solution of pH 8 was the most efficient in terms of corrosion protection. The coating significantly reduced the pitting corrosion of the substrate. The results were interpreted taking into consideration the polymer electroactivity, the galvanic interaction polypyrrole/substrate and the nature of dopants. Silver species were effectively immobilized onto the hollow rectangular-sectioned microtubes of PPy. The modified coatings demonstrated that they have a good bactericidal activity against *Escherichia coli* and they were also able to protect the substrate against corrosion in Ringer solution.

Keywords: stainless steel; conducting polymer; microtubes.

INTRODUCTION

Stainless Steel 316L (316 L SS) is the most commonly used alloy in medical implants due to its many features, such as accepted biocompatibility, good mechanical and anticorrosive properties and availability at low cost.[1] It is well known that the presence of a thin "passive film" upon the 316L SS surface is responsible of the corrosion resistance of the substrate. Nevertheless, this passive film can be susceptible to breakdown in the presence of Cl^- and as a consequence, pitting corrosion is promoted.[2] In the surroundings of an implant this localized attack

* Corresponding author. E-mail: belen.gonzalez@uns.edu.ar
https://doi.org/10.2298/JSC220420077R

releases metal ions producing a decrease in biocompatibility, and consequently, the implant could be rejected.[3] To overcome this problem, surface treatment techniques are used to improve the corrosion properties of the material.[4] Conducting polymers constitute a physical barrier against corrosive environments, also helps to stabilize the formation of the passive film and, under certain circumstances, they can release corrosion inhibitor anions.[5] Among all the conducting polymers, polypyrrole (PPy) is the most attractive option to modify the surface of implants because of its eco-friendly synthesis, good stability and satisfactory biocompatibility.[6] Corrosion protection of the substrate can be improved if the PPy dopant is a corrosion inhibitor.[7,8] Previously, the electrosynthesis of PPy onto Al from alkaline solution containing MoO_4^{2-} and NO_3^- as dopant anions was repoted.[9] The results obtained showed that MoO_4^{2-} remains entrapped into the polymer matrix, giving greater resistance to pitting corrosion in chloride media. In an earlier study, it was also demonstrated that the electrosynthesis of PPy onto 316L SS from an alkaline solutions containing molybdate and nitrate reduces the pitting corrosion of the substrate. The results are interpreted in terms of the passivating properties of the oxide layer formed in alkaline solution.[10]

On the other hand, salicylate (Sa) is considered to be a non-steroidal and anti-inflammatory drug[11] and it has also been demonstrated that PPy coatings doped with Sa anions provides corrosion protection for different metallic substrates.[12–14] Another interesting feature of the Sa anion is that it not only can act as a dopant of PPy, but also is the responsible of the electrosynthesis of rectangular cross-section microtubes of the polymer.[15,16] The effectiveness of microstructured PPy films doped with Sa anions in protecting 316 L SS from corrosion was studied in a chloride environment. The obtained coating was not enough for the protection of the substrate probably as a consequence of the porous opened structure of the microtubes, allowing the entry of aggressive ions. In order to improve the corrosion protection, a system of two layers was electrodeposited from salicylate solutions of different concentrations. The first layer consisted of granular PPy and the second one, on the top, was constituted by the PPy with microtubes. This bilayered coating exhibited an excellent protective behaviour of 316L SS in chloride solution during considerably long immersion time.[17] A bilayer system onto 316L SS was also studied by our group. A PPy under-layer was electropolymerized in the presence of MoO_4^{2-} and NO_3^- and a microtubular PPy film, from salicylate solution, was formed as a top layer.[18]

Implant-related infection is recognized as a tragic problem, and patients with severe infection often require revision surgery.[19] Current strategies to prevent or control implant-related infection include surface coating, modification of surface chemistry, and modification of surface morphology.[20]

With the objective to provide antibacterial properties, the immobilization of metallic species in polymers has been widely studied in our laboratory. Micro-

structured PPy films were modified with copper species and then were implemented in a laboratory-scale continuous flow system using for disinfection of well water contaminated with *Escherichia coli*. The results indicated that the PPy/Cu-modified electrodes were effective for water disinfection process.[21] In addition, it was also demonstrated that a PPy film doped with Sa is an effective matrix for the immobilization of Ag species. The PPy-Ag modified electrodes exhivery good performance toward inhibition of bacteria activity, concluding that the composite is a promising material for biomedical application.[22]

According to the revised literature, the protection of 316L SS with PPy microtubular was only attained through the formation of a bilayer system. Hence, the purpose of the present work was to investigate the electroformation of simple and protective PPy films with microtubular morphology on 316L SS. Accordingly, nearly neutral and alkaline solutions containing MoO_4^{2-} and Sa ions were employed during the electrosynthesis PPy film. For the development of an antimicrobial surface, the immobilization of silver species on the microstructured PPy matrix was also studied. The anticorrosive properties of different PPy films in Ringer solutions were determined.

EXPERIMENTAL

Materials and methods

Type 316 L SS rods (wt. % are: 17.47 Cr, 10.32 Ni, 1.88 Mn, 1.90 Mo, 0.39 Si, 0.025C and Fe balance) embedded in a Teflon holder with an exposed area of 0.070 cm^2 were used as working electrodes. Before each experiment, the surface was abraded with a 1200 grit finish using SiC, then degreased with acetone and finally washed with triply distilled water. Following this pre-treatment, the electrode was immediately transferred to the electrochemical cell. Potentials were measured and referred against an Ag/AgCl (3 M) electrode and a platinum sheet was used as the counter electrode. A conventional three electrode system and a 20 cm^3 Metrohm cell were used for the electrochemical experiments. The PPy films were obtained potentiostatically from a solution containing 0.50 M Py + 0.50 M NaSa + 0.05 M Na_2MoO_4 at different pH values. The pH of the solution was adjusted by addition of NaOH. The solutions were de-aerated by bubbling N_2 before and during the polymerization. Pyrrole (Sigma–Aldrich) was freshly distilled under reduced pressure before use. Morphological studies of the films metallised with gold were performed by scanning electron microscopy (SEM) LEO 1450 VP coupled using a probe for energy-dispersive scanning (EDS). Electrochemical studies were performed with a potentiostat/galvanostat Autolab/PGSTAT 128N with an electrochemical impedance spectroscopy (EIS) module. The anticorrosion properties of the coatings were investigated in 50 mL of Ringer solution (composition per litre was 8.60 g NaCl, 0.30 g KCl and 0.32 g $CaCl_2{\cdot}2H_2O$) by open circuit potential as a function of time (OCP-time), potentiostatic measurments, potentiodynamic method and electrochemical impedance spectroscopy. Tafel tests were performed by polarizing from cathodic to anodic potentials with respect to the open circuit potential at 0.001 V s^{-1}. Estimation of corrosion parameters was realized by the Tafel extrapolation method. The extrapolation of anodic and cathodic lines for charge transfer controlled reactions gives the corrosion current density (j_{corr}) at the corrosion potential (E_{corr}). Electrochemical impedance spectra were obtained at the open circuit potential (*OCP*) in the frequency range from 10 kHz to 100 mHz, and the signal

amplitude was 10 mV. To detect the presence of released ions, an inductively coupled plasma atomic emission spectrometer (ICP-AES) Shimadzu 9000 was used. Electrical conductivity was measured by the two-probe method using a homemade device. Adherence of the electrosynthesized coatings to the substrate was evaluated by using Scotch® Magic™ Tape 810 (3 M). The antibacterial activity against a reference strain of *E. coli* ATCC 25922 was evaluated by a modified Kirby–Bauer technique.[23] The method was previously standardized by adjusting the microbial inoculation rate and the volume of the agar medium layer. A freezing culture of *E. coli* ATCC 25922 (stored at –70 °C in Tripticase Soy Broth (TSB, BK 046HA, Biokar Diagnostics, Beauvais, France) supplemented with 20 vol. % glycerol (Biopack, Argentina) was used. A loop of frozen cells was cultured in TSB during 24 h at 37 °C. Upon appropriate dilution with sterilized phosphate buffer saline solution, a suspension of about 107 cells mL^{-1} was prepared. One millilitre of this suspension was mixed with 25 mL of Tripticase Soy Agar (BK, Biokar Diagnostics, Beauvais, France) melted and cooled at 43 °C, and then, placed on a Petri dish. The coated electrodes were pressed onto bacteria-overlaid agar and were incubated at 37 °C for 24 h. Then they were removed from the agar and placed in a fresh one. The data were expressed as growth inhibitory zone diameter (mm) for three replicates.[24] Control tests employing unmodified PPy-coated electrodes were also performed.

RESULTS AND DISCUSSION

Polypyrrole coatings

The polymerization solution was prepared from 0.50 M Py + 0.50 M NaSa + 0.05 M Na_2MoO_4, at two different pH values: 8 and 12. It was previously demonstrated that the solution pH has an influence on the electrosynthesis process.[15] When the solution pH is 8, the oxidation potential of Py was 0.90 V.[10] However, in alkaline solution, there was a competition between the salicylate oxidation and PPy deposition, and as a consequence the electroformation of PPy at pH 12 occurs at potentials equal to or higher than 1.3 V. This value was already determined experimentally in previous work.[15] The *j vs. t* transients obtained during the formation of coatings are presented in Fig. 1. As can be seen in the chronoamperometric curves, during the electropolymerization process, after charging the double layer, the current density increases with time until reaching a maximum value. Then *j* decreases and finally rises again at a slower rate. As described in a previous work,[16] the behaviour observed in the curves is associated with the formation of microtubular structures. Under these conditions, the electropolymerization charge was for 4.3 C cm^{-2} for both coatings. A thickness of approximately 11 μm was predicted for the coatings by assuming a film thickness of 1 μm for 0.4 C cm^{-2} charge.[25] Under these circumstances, very adherent films were obtained. The morphology of the generated coatings was observed by the SEM technique. For a better understanding, the coatings were named PPy_8 and PPy_{12}. As might be expected, PPy_8 and PPy_{12} films presented microstructured morphology due to the high salicylate concentrations.[16] As can be seen in Fig. 1, the images reveal that most of the structures have rectangular cross-section with side length changing between 0.5 and 2 μm. The external sur-

face of the microtubes was constituted of the typical globular structure of PPy and the inner side was hollow. The same porous morphology had already been obtained for a PPy film electrosinthetized on 316L SS from a solution containing only Sa.[17]

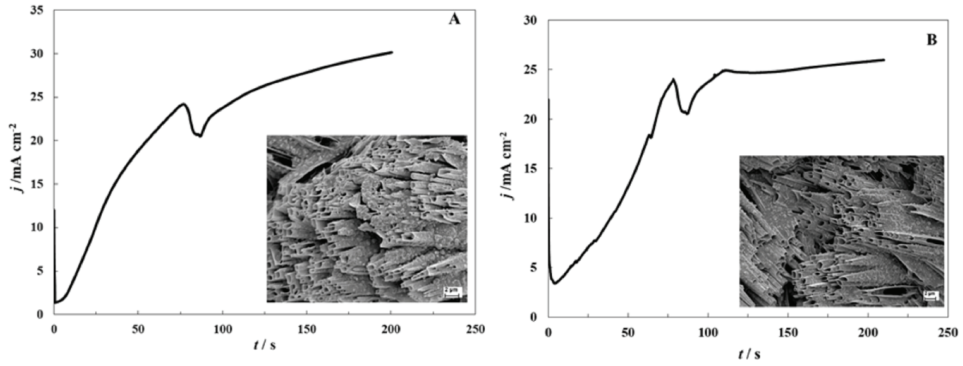

Fig. 1. Chronoamperometric curves obtained during the electrosynthesis of PPy_8 (A) and PPy_{12} (B) films. SEM images of the films are also presented.

Corrosion test

The variation of *OCP* as a function of time was used to estimate the corrosion protection offered by the polymer coatings. The *OCP vs*. time responses for the different samples after exposure to Ringer solution during 10 days are presented in Fig. 2. For comparison, the curve of the uncoated steel is also showed. For the bare 316L SS sample, the *OCP* value stabilizes after the second day of immersion at a value around –0.15 V (curve c).

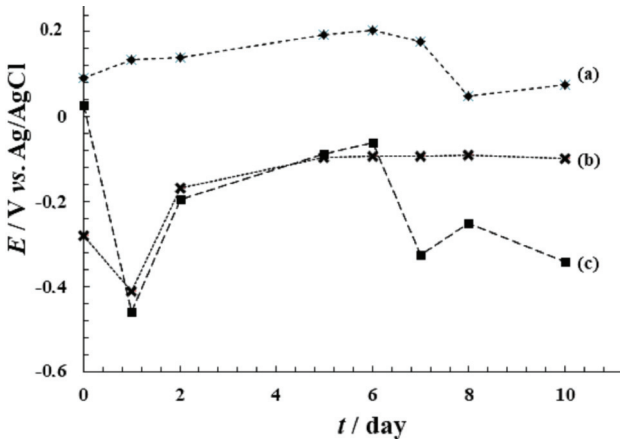

Fig. 2. Time dependence of *OCP* in Ringer solution of 316L SS electrode covered by: PPy_8 (a) and PPy_{12} (b). The variation for a bare steel electrode is also included (c).

As can be seen in curve a, the presence of the PPy_8 film generates an anodic shift of the corrosion potential even after 10 days of immersion, which is associated with an anodic protection mechanism.[26,27] However, the *OCP vs*. time curve corresponding to the electrode coated with PPy_{12} films (curve b), presents values close to the bare steel electrode during the first seven days, and then decreases to –0.40 V. These preliminary results demonstrate that the presence of PPy_{12} did not improve the corrosion protection of the substrate. The quantity of Fe released after *OCP* experience was <0.005 mg L^{-1} and 0.084 mg L^{-1} for the 316L SS electrode covered with PPy_8 and PPy_{12}, respectively. The bare electrode produced a Fe concentration of 1.200 mg L^{-1}. Moreover, the obtained results confirm that the PPy_8 films provided an effective corrosion protection of the substrate.

To acquire more information about the protection level of the PPy films, EIS measurements were performed. The Nyquist plots were recorded during immersion in Ringer solution under *OCP* conditions for a period of 10 days (Fig. 3).

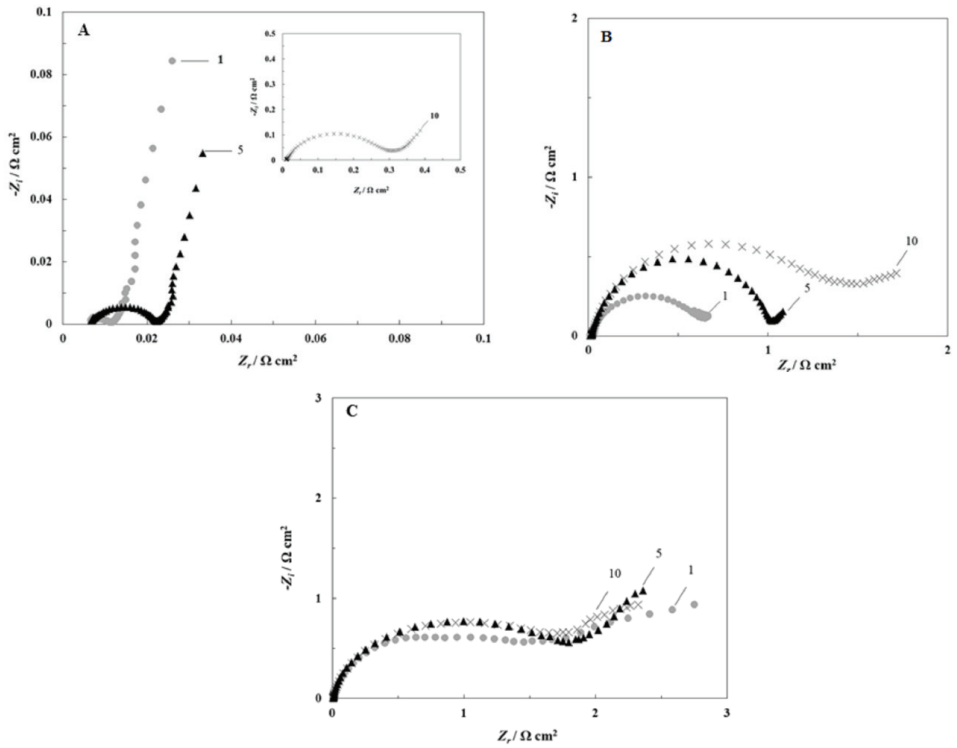

Fig. 3. Nyquist plots registered under *OCP* conditions in Ringer solution during 10 days for a steel electrode covered with: PPy_8 (A) and PPy_{12} (B). The variation for a bare steel electrode is also included (C). The immersion day is indicated on the curve.

In the high-frequency region, the impedance spectrum all samples showed a depressed semicircle associated with a process at the electrode/electrolyte interface. The semicircle diameter represents R_{CT}, interpreted as the charge transfer resistance of the redox reaction of the polymer.[28] In the low-frequency region, a linear response was observed that is associated with the diffusion of ions into the polymer. As can be seen in Fig. 3A, the impedance results show that in the case of the PPy_8 film, the R_{CT} value increases slowly with immersion days. On the contrary, the response of the electrode covered with PPy_{12} shows that the R_{CT} rises noticeably with the exposure time (see Fig. 3B). The Nyquist response of the uncoated electrode of 316L SS were constituted of a semicircle of 2 Ω cm^{-2} in diameter and practically negligible linear part (Fig. 3C). In the case of the PPy_{12} film, the increment in R_{CT} values suggests that the reaction rate of the redox process of polymer declines over time, probably due to the low conductivity of the film. As was mentioned above, the electrosynthesis of PPy film from a solution of pH 12 begins to occur from 1.3 V. At this potential value, it is expected that the polymer obtained is overoxidized.[29] An important characteristic of overoxidized PPy is its poor conductivity and, in terms of corrosion protection, this represents a drawback.

On the other hand, for the electrode coated with PPy_8, the data obtained showed a vertical line in the low frequencies range associated with a semi-infinite Warburg impedance. This behaviour indicates a diffusion-controlled region that involves diffusion of mobile charges in the polymer backbone and mobile ions throughout the PPy coating.[30] In contrast, the data for the electrode covered with PPy_{12} indicates that a contribution of the diffusional process to the total impedance was not observed. Thus, the PPy_8 film presents the best corrosion performance in terms of *OCP*-time and EIS results.

In previous work, the OCP response for a 316L SS electrode coated with a PPy film doped with Sa anions (without MoO_4^{2-}) presented a potential value of around 0.15 V during 20 days of immersion in 0.15 M NaCl. The concentration in solution of Fe determined by ICP was <0.10 mg L^{-1}.[17] Nevertheless, the EIS results demonstrated a marked increase of R_{CT} with time, dominating the impedance behaviour of the covered electrode. The contribution of the diffusional process to the total impedance goes away with exposure time. This EIS response, contrary to the one obtained for PPy_8, indicates that the corrosive species can penetrate the polymer doped only with Sa and reach the substrate. Then, according to these preceding results, it could be concluded that the incorporation of MoO_4^{2-} together with Sa as dopants of PPy film would improve the corrosion protection of the substrate.

Tafel plots were obtained after *OCP* stabilization (3600 s) starting from 0.20 to 0.20 V *vs. OCP* with a potential scan rate of 0.001 V s^{-1}. For uncoated 316L SS, the j_{corr} value was estimated by extrapolation of anodic and cathodic Tafel

lines to the E_{corr} (Fig. 4, curve c). The j_{corr} values of the PPy coated 316L SS were estimated by extrapolation of the cathodic Tafel lines back to the corresponding values of E_{corr} (Fig. 4, curves a and b). According to Fig. 4, the conducting polymer produces a positive shift in the corrosion potential, although the corrosion current densities measured were almost three orders of magnitude higher than those for the uncoated sample (Table I). This result could be interpreted considering that the galvanic interaction between the polymer and the substrate gives rise to oxidation of the substrate and reduction of the polymer, and this mechanism significantly contributes to the total current measured.[31,32]

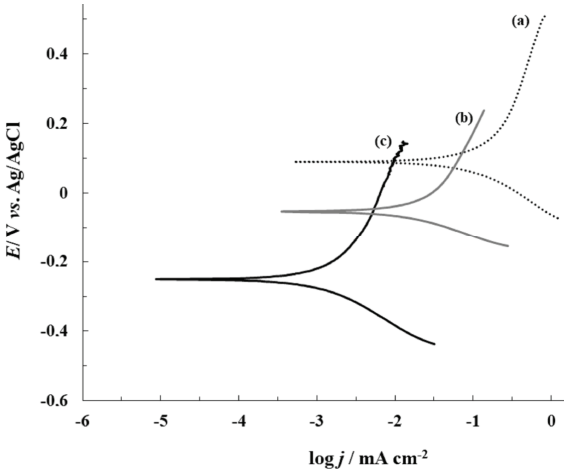

Fig. 4. Tafel curves registered in Ringer solution after OCP measurements for a steel electrode covered with: PPy_8 (curve a) and PPy_{12} (curve b). Tafel polarization plot for the uncoated steel is also included (curve c). Sweep rate: 0.001 V s^{-1}.

TABLE I. Corrosion parameters calculated from the Tafel polarization plots for the bare 316L SS and the substrate covered with PPy_8 and PPy_{12}

Sample	E_{corr} / V	j_{corr} / mA cm^{-2}	b_a / V dec^{-1}	b_c / V dec^{-1}
PPy_8	0.086	0.933	0.28	–0.14
PPy_{12}	–0.075	0.017	0.28	–0.07
Bare 316L SS	–0.26	0.001	0.25	–0.13

More information concerning electrochemical behaviour of the covered electrodes could be obtained through linear polarization in Ringer solution (Fig. 5). For comparison purposes, the response of bare steel is also presented. As can be seen in curve c, the current density increases at 0.35 V, denoting the onset of pitting corrosion. In the case of the covered samples, peaks associated with reversible and irreversible oxidation of the PPy were observed at approximately 1.0 V. At more positive potentials, for the electrode covered with PPy_{12} (curve b), the current density rises abruptly with oscillations denoting the onset of a pitting

corrosion process. On the contrary, the electrode covered with PPy_8 could be polarized to very high positive potentials without any sign of substrate dissolution.

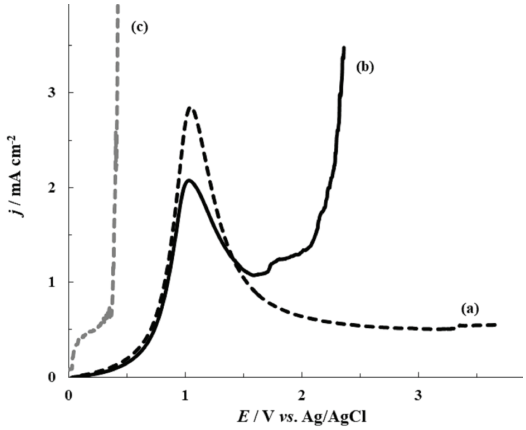

Fig. 5. Polarization curves registered in Ringer solution at 0.001 V s^{-1} for a bare steel electrode covered with: PPy_8 (curve a) and PPy_{12} (curve b). The data for a bare steel electrode is also included (curve c).

In order to evaluate the protection level under more drastic conditions, the current density-time response was recorded at a potential more positive than the one corresponding to the pitting potential of the bare sample (1.0 V *vs.* Ag/AgCl). In Fig. 6, curve c, current density oscillations around a value of 100 mA cm^{-2} were observed. This response could be attributed to pitting corrosion of the substrate. In contrast to this, the measured currents for the electrodes modified with PPy_8 and PPy_{12} are much lower than that corresponding to the uncoated electrode.

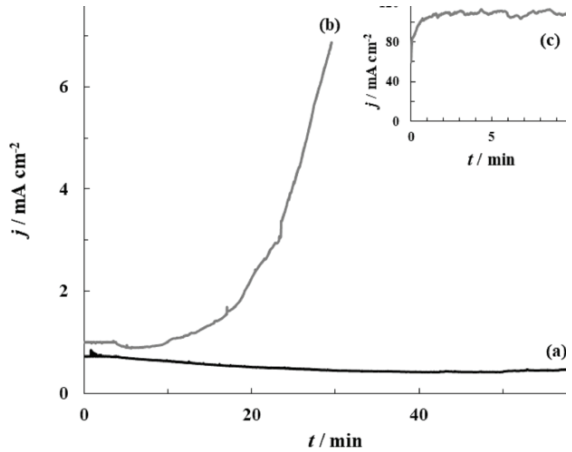

Fig. 6. Chronoamperometric curve obtained at 1 V *vs*. Ag/AgCl in Ringer solution for a bare steel electrode covered with: PPy_8 (curve a) and PPy_{12} (curve b). The figure inset is the result for a bare steel electrode (curve c).

As could be seen in curve b), the response for the electrode covered with PPy_{12} shows that the current density remained at 0.7 mA cm^{-2} for 17 min, but an abrupt increase is observed later, probably due to the attack of Cl^- ions on the 316L SS. However, in the data presented in Fig. 6, curve a, the current density measured for the electrode covered with PPy_8 remained low even after 60 min of applying a constant potential value of 1.0 V (*vs.* Ag/AgCl), which indicates that the polymer electrosythesized at pH 8 onto 316L SS is a protective film. The ICP-AES analysis indicated that the amount of Fe released during the chronoamperometric experience in Ringer solution was <0.005 and 0.039 mg L^{-1} for 316L SS electrode covered with PPy_8 and PPy_{12}, respectively. The uncoated 316L SS electrode released an amount of Fe of 2.760 mg L^{-1}. The data confirmed that the dissolution of the substrate was significantly reduced in the presence of the PPy_8 film.

When the anticorrosion performance of the polypyrrole films were compared, it could be concluded that the coating electrosynthesised in a solution containing MoO_4^{2-} and Sa ions at pH 8 exhibits the best protection performance. These results could be explained in terms of the conductivity of coatings. The conductivity values obtained were 27.2 and 6.6 S m^{-1} for PPy_8 and PPy_{12} films, respectively; and they are within the interval already reported for PPy doped films.[33] These values were estimated considering a film thickness of 11 μm.[25] The difference between the obtained values could be associated with the potential of electrosyhntesis. An increase in the electropolymerization potential results in a decrease in the conductivity of the studied PPy films. As was mentioned previously, the PPy_{12} film was electroformed at 1.3 V and at this potential value, it is expected that the polymer obtained is overoxidized, probably due to the formation of a carboxyl group on the pyrrole ring that disrupts the conjugation of the PPy chain.[29] In addition, galvanic coupling is the most usual corrosion protection mechanism of conductive polymers. The cathodic reaction implicates the reduction of the coating accompanied with the release of the doping anions, whereas the anodic reaction includes the oxidation of the substrate. Then, the O_2 reduction occurs on both the conductive polymer and metal surfaces, promoting the re-oxidation of the polymer film. At least this interaction led to the formation of a protective layer at the metal–film interface.[34,35] This proposed protection mechanism requires an electroactive polymer. Hence, it can be stated that the PPy film obtained at pH 8 gives the best corrosion protection of 316L SS in comparison with PPy_{12} due to the higher conductivity in the film. In addition, the effective corrosion inhibition provided by the PPy_8 could be explained by considering, in the first instance, the galvanic interaction between the electroactive polymer and the substrate. Under these circumstances, the preservation of a passive protective oxide film is promoted. Additionally, due to its large size and negative charge, MoO_4^{2-} remains trapped in the polymer matrix, avoiding the entrance of chloride

ions. Nevertheless, the inhibitors might be released eventually and contribute to the corrosion protection of the alloy.

Silver immobilization

With the aim of providing bactericidal properties to the obtained films, the capacity of the polymer matrix to immobilize metallic species was studied. As commented previously, the electrode covered with PPy_8 presented the best corrosion behaviour in Ringer solution and those, it was selected for metallic immobilization experiments. The immobilization procedure was already described in a previous work[22] and consisted in dipping the electrode covered with PPy_8 film in 0.05 M $AgNO_3$ during 5 h in the dark under *OCP* conditions. The modified polymer was named PPy_8Ag. The analysis by SEM shows the existence of rectangular structures coexisting with rosette-like deposits of 1 μm of diameter. As could be seen in Fig. 7A, the deposits present a highly rough surface and this type of morphology was previously observed in silver microstructures.[36] An EDS analysis (Fig. 7B) demonstrates that the deposits were constituted of silver and the signal of Mo confirms that molybdate is entrapped into the PPy_8 matrix. It was proposed that the salicylate anion fulfils an important function in the immobilization of silver species onto the coating. Metallic cations present in the solution were concentrated in the film as a result of the interaction between Sa^- and Ag^+. Metallic silver was then deposited as a result of a redox reaction between non oxidized segments of the polymer and Ag^+.

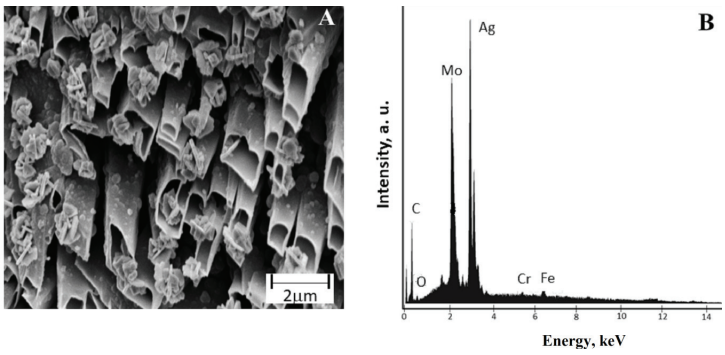

Fig. 7. SEM image (A) and EDS examination (B) of the 316 L SS electrode covered with PPy_8Ag.

The antibacterial activity of PPy_8Ag films against the Gram-negative bacterium *E. coli* was investigated by determining the width of the inhibition zone around the modified electrode. Antibacterial activity of unmodified PPy_8 film against *E. coli* ATCC 25922 consisted of an inhibition zone of approximately 4 mm surrounding the sample. Previously, it was shown that salicylate has notable antibacterial activity and it was also shown that this inhibitory effect is

concentration dependent.[22] Nevertheless, the inhibition area is notoriously increased (12 mm) when PPy_8Ag was analysed. The antibacterial properties of PPy_8Ag film could be described by the insertion of the released Ag^+ and colloid silver particles through the bacteria cell wall.[37]

In order to determine the corrosion properties of the 316L SS electrode covered with PPy_8Ag film, the *OCP*–time dependence and the polarization curve at 1.0 V *vs.* Ag/AgCl were registered in Ringer solution. The obtained curves are shown in Fig. 8. In the first sight, the measured potentials were nobler than the potential of bare steel electrode (–0.15V) even after 10 days of immersion, suggesting that the film was an effective protective coating (Fig. 8A). The result is supported by the determination of the amount of iron released in Ringer solution. A concentration less than 0.005 mg L^{-1} was obtained after 10 days of immersion; this value is identical to the one previously reported for the unmodified PPy_8. The amount of Fe released from PPy_8Ag and PPy_8 during the immersion is much lower than that found for the bare electrode (1.200 mg L^{-1}). The data would confirm that the corrosion protection properties of PPy_8 are not altered by the presence of silver species. In addition, the *j vs. t* transient shown in Fig. 8B is denotes that the density current values remained well below the values obtained for the bare electrode (see Fig. 6, curve c), even after 60 min of experience. The ICP-AES analysis of the amount of Fe released into the Ringer solution gave a value of 0.132 mg L^{-1}. Although this concentration is greater than that obtained previously for the unmodified PPy_8, the data confirms that the dissolution of the alloy was reduced by the presence of PPy_8Ag film, taking into account the measured Fe concentration for the bare electrode (2.76 mg L^{-1}).

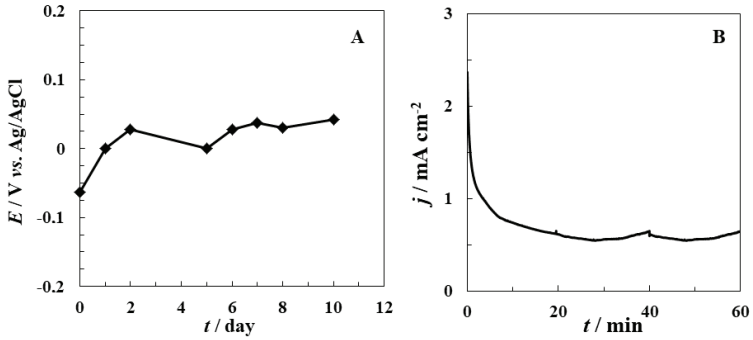

Fig. 8. A)Time dependence of *OCP* in Ringer solution of a 316L SS electrode covered by PPy_8Ag. B) Chronoamperometric curve obtained at 1.0 V *vs*. Ag/AgCl in Ringer solution of a 316L SS electrode covered by PPy_8Ag.

CONCLUSIONS

Single-layer polypyrrole coatings with microtubular morphology were obtained from solutions containing molybdate and salicylate at two different pH

values by a potentiostatic technique on 316L SS. All the corrosion procedures performed were to evaluate the degree of protection of AI 316L SS coated with polypyrrole films electrosynthesized from salicylate and molybdate solutions at different pH values demonstrated that a PPy_8 coating could completely protect the substrate against pitting corrosion in Ringer solution, even when the coated sample is polarized to a potential higher than the breakdown potential of the bare substrate (1 V (Ag/AgCl 3M)). One possible reason for the best corrosion protection properties of PPy_8 is the electroactive polymer ability and the galvanic interaction with the substrate. In addition, the fixed negative charge of MoO_4^{2-} avoids the entrance of chloride into the polymer matrix and also the release of corrosion inhibitor anions from the polypyrrole matrix helps with the protection of the substrate. Silver species were effectively immobilized onto the hollow rectangular-sectioned microtubes of PPy. The antibacterial test against *E. coli* for PPy_8Ag samples demonstrated that they have good bactericidal activity and were was also able to protect 316L SS against corrosion in Ringer solution. Thus, this film has potential applications as a biomaterial with antibacterial properties.

Acknowledgements. The financial support of the Secretaría de Ciencia y Técnica – UNS (PGI 24/M159), the Consejo Nacional de Investigaciones Científicas y Técnicas (CONICET – PIP 112-20150-100147) and the Agencia Nacional de Promoción Científica y Tecnológica (ANPCYT PICT-2019-02758) is gratefully acknowledged.

ИЗВОД

АНТИКОРОЗИВНЕ ОСОБИНЕ ПРЕВЛАКА ПОЛИПИРОЛА ФОРМИРАНИХ НА НЕРЂАЈУЋЕМ ЧЕЛИКУ 316 L ИЗ РАСТВОРА КОЈИ ЈЕ САДРЖАО МОЛИБДАТЕ И САЛИЦИЛАТЕ

CAMILA A. RAMOS[1], MARIA B. GONZÁLEZ[1], LORENA I. BRUGNONI[2] и SILVANA B. SAIDMAN[1]

[1]*Chemical Engineering Department, Institute of Electrochemical and Corrosion Engineering, National University of the South, CONICET, Bahía Blanca, Argentina u* [2]*Department of Biology, Biochemistry and Pharmacy, Institute of Biological and Biomedical Sciences, National University of the South, CONICET, Bahía Blanca, Argentina*

У раду је описана електрохемијска синтеза филмова полипирола на нерђајућем челику 316L из раствора блиских неутралним и алкалних који су садржали молибдате и салицилате. Корозионо понашање превлака које су биле сачињене од шупљих правоугаоних микроцеви је праћено у Рингеровом раствору мерењем потенцијала отвореног кола, поларизационим мерењима и спектроскопијом електрохемијске импеданције. Полимер који је формиран у раствору pH 8 је био најефикаснији у заштити од корозије. Превлака је значајно смањила питинг корозију подлоге. Резултати су дискутовани узимајући у обзир електрохемијску активност полимера, галванску интеракцију између полипирола и подлоге и природу допанта. Хемијске врсте сребра су ефикасно имобилисане у шупљим правоугаоним цевима полипирола. Модификоване превлаке су показале добра бактерицидна својства према Escherichia coli и такође заштиту подлоге од корозије у Рингеровом раствору.

(Примљено 20. априла, ревидирано 11. јула, прихваћено 23. септембра 2022)

REFERENCES

1. M. Z. Ibrahim, A. A. D. Sarhan, F. Y. M. Hamdi, *J. Alloys Compd.* **714** (2017) 636 (https://doi.org/10.1016/j.jallcom.2017.04.231)
2. M. J. K. Lodhi, K. M. Deen, M. C. Greenlee-Wacker, Waseem Haider, *Addit. Manuf.* **27** (2019) 8 (https://doi.org/10.1016/j.addma.2019.02.005)
3. N. S. Manam, W. S. W. Harun, D. N. A. Shri, S. A. C. Ghani, T. Kurniawan, M. H. Ismail, M. H. I. Ibrahim, *J. Alloys Compd.* **701** (2017) 698 (https://doi:10.1016/j.jallcom.2017.01.196)
4. R. K. Gupta, N. Birbilis, *Corros. Sci.* **92** (2015) 1 (https://doi.org/10.1016/j.corsci.2014.11.041)
5. C. Garcia-Cabezon, C. Garcia-Hernandez, M. L. Rodriguez-Mendez, F.Martin-Pedrosa, *J. Mat. Sci. Tech.* **37** (2020) 85 (https://doi.org/10.1016/j.jmst.2019.05.071)
6. W. A. El-Said, M. Abdelshakour, Jin-Ha Choi, Jeong-Woo Choi, *Molecules* **25** (2020) 307 (https://doi:10.3390/molecules25020307)
7. Z. Chen, W. Yang, B. Xu, Y. Guo, Y. Chen, X. Yin, Y. Liu, *Prog. Org. Coat.* **122** (2018) 159 (https://doi.org/10.1016/j.porgcoat.2018.05.022)
8. H. M. Hung, D. K. Linh, N. T. Chinh, L. M. Duc, V. Q. Trung, *Prog. Org. Coat.* **131** (2019) 407 (https://doi.org/10.1016/j.porgcoat.2019.03.006)
9. I. L. Lehr, S.B. Saidman, *Electrochim. Acta* **51** (2006) 3249 (https://doi.org/10.1016/j.electacta.2005.09.017)
10. M. B. González, S. B. Saidman, *Corr. Sci.* **53** (2011) 276 (https://doi.org/10.1016/j.corsci.2010.09.021)
11. R. Amann, B. A. Peskar, *Eur. J. Pharmacol.* **447** (2002) 1 (https://doi.org/10.1016/S0014-2999(02)01828-9)
12. K. Cysewska, M. Gazda, P. Jasiński, *Surf. Coat. Techol.* **328** (2017) 248 (https://doi.org/10.1016/j.surfcoat.2017.08.055)
13. D. O. Flamini, M. I. Valle, M. J. Sandoval, V. L. Massheimer, S. B. Saidman, *Mater. Chem. Phys.* **209** (2018) 76 (https://doi.org/10.1016/j.matchemphys.2018.01.065)
14. A. D. Forero López, I. L. Lehr, L. I. Brugnoni, S. B. Saidman, *J. Magnes. Alloys* **6** (2018) 15 (https://doi.org/10.1016/j.jma.2017.12.005)
15. M. B. González, S. B. Saidman, *Electrochem. Comm.* **13** (2011) 513 (https://doi.org/10.1016/j.elecom.2011.02.037)
16. M. B. González, O. V. Quinzani, M. E. Vela, A. A. Rubert, G. Benítez, S. B. Saidman, *Synth. Met.* **162** (2012) 1133 (https://doi.org/10.1016/j.synthmet.2012.05.013)
17. M. B. González, S. B. Saidman, *Prog. Org. Coat.* **75** (2012) 178 (https://doi.org/10.1016/j.porgcoat.2012.04.015)
18. M. B. González, S. B. Saidman, *Prog. Org. Coat.* **78** (2015) 21 (http://dx.doi.org/10.1016/j.porgcoat.2014.10.012)
19. J. M. Brown, J. B. Mistry, J. J. Cherian, R. K. Elmallah, M. Chughtai, S. F. Harwin, *Orthopedics* **39** (2016) 1129 (https://doi.org/10.3928/01477447-20160819-06)
20. M. Wang, T. Tang, *J. Orthop. Transl.* **17** (2019) 42 (https://doi.org/10.1016/j.jot.2018.09.001)
21. M. B. González, D. O. Flamini, L. I. Brugnoni, L. M. Quinzani S. B. Saidman, *J. Water Health* **16** (2018) 921 (https://doi.org/10.2166/wh.2018.072)
22. M. B. González, L. I. Brugnoni, M. E. Vela, S. B. Saidman, *Electrochim. Acta* **102** (2013) 66 (https://doi.org/10.1016/j.electacta.2013.03.116)

23. V. Maquet, D. Martin, B. Malgrange, R. Franzen, J. Schoenen, G. Moonen, R. Jérôme, *J. Biomed. Mater. Res.* **52** (2000) 639 (https://doi.org/10.1002/10974636(20001215)52:4<639::AID-JBM8>3.0.CO;2-G)
24. P. T. Sudheesh Kumar, S. Abhilash, K. Manzoor, S.V. Nair, H. Tamura, R. Jayakumar, *Carbohydr. Polym.* **80** (2010) 761 (https://doi.org/10.1016/j.carbpol.2009.12.024)
25. Q. Pei, R. Qian, *Electrochim. Acta* **37** (1992) 1075 (https://doi.org/10.1016/0013-4686(92)85225-A)
26. S. Biallozor, A. Kupniewska, *Synth. Met*. **155** (2005) 443 (https://doi.org/10.1016/j.synthmet.2005.09.002)
27. A. A. Hermas, *Corros. Sci.* **50** (2008) 2498 (https://doi.org/10.1016/j.corsci.2008.06.019)
28. C. M. Chang, C. S. Song, H. J. Huang, *J. Chin. Chem. Soc*. **41** (1994) 693 (https://doi.org/10.1002/jccs.199400098)
29. T. Patois, B. Lakard, N. Martin, P. Fievet, *Synth. Met.* **160** (2010) 2180 (https://doi.org/10.1016/j.synthmet.2010.08.005)
30. A. El Jaouhari, A. Chennah, S. Ben Jaddi, H. Ait Ahsaine, Z. Anfar, Y. Tahiri Alaoui, Y. Naciri, A. Benlhachemi, M. Bazzaoui, *Surf. Interfaces* **15** (2019) 224 (https://doi.org/10.1016/j.surfin.2019.02.011)
31. E. Machnikova, M. Pazderova, M. Bazzaoui, N. Hackerman, *Surf. Coat. Technol.* **202** (2008) 1543 (https://doi.org/10.1016/j.surfcoat.2007.07.006)
32. D. O. Flamini, M. I. Valle, M. J. Sandoval, V. L. Massheimer, S. B. Saidman, *Mater. Chem. Phys.* **209** (2018) 76e85 (https://doi.org/10.1016/j.matchemphys.2018.01.065)
33. A. Kaynak, L. Rintoul, G. A. George, *Mater. Res. Bull.* **35** (2000) 813 (https://doi.org/10.1016/S0025-5408(00)00280-4)
34. M. K. Zadeh, M. Yeganeh, M. T. Shoushtari , A. Esmaeilkhanian, *Synth. Met*. **274** (2021) 116723 (https://doi.org/10.1016/j.synthmet.2021.116723)
35. P. P. Deshpande, N. G. Jadhav, V. J. Gelling, D. Sazou, *J. Coat. Technol. Res.* **11** (2014) 473 (https://doi.org/10.1016/j.surfcoat.2007.07.006)
36. K. A. M. Eid, H. M. E. Azzazy, *Int. J. Nanomed.* **7** (2012) 1543 (https://doi.org/10.2147/IJN.S26524)
37. S.A. Ahmad, S. S. Das, A. Khatoon, M. T. Ansari, M. Afzal, M. S. Hasnain, A. K. Nayak, *Mater. Sci. Energy Technol.* **3** (2020) 756 (https://doi.org/10.1016/j.mset.2020.09.002).

Journal of the Serbian Chemical Society
JSCS@tmf.bg.ac.rs • www.shd.org.rs/JSCS
J. Serb. Chem. Soc. *87* (11) 1313–1325 (2022)
JSCS–5596
Original scientific paper
Published 1 August 2022

Elemental composition of selected lichen species growing on the Balkan Peninsula

SNEŽANA TOŠIĆ, ALEKSANDRA PAVLOVIĆ[#], IVANA DIMITRIJEVIĆ*, IVANA ZLATANOVIĆ[#], VIOLETA MITIĆ and GORDANA STOJANOVIĆ[#]

University of Niš, Faculty of Sciences and Mathematics, Department of Chemistry, Višegradska 33, 18000 Niš, Serbia

(Received 23 February, revised 6 May, accepted 11 June 2022)

Abstract: The amount of nineteen elements in eleven different lichen species, six fruticose (*Bryoria capillaris*, *Bryoria fuscescens*, *Cladonia rangiformis*, *Ramalina capitata*, *Usnea chaetophora* and *Evernia prunastri*) and five foliose (*Hypogymnia tubulosa*, *Lobaria pulmonaria*, *Peltigera horizontalis*, *Umbilicaria cylindrica* and *Umbilicaria crustulosa*) from five natural areas of the Balkan Peninsula (Serbia and Bulgaria) were determined by using inductively coupled plasma optical emission spectrometry (ICP-OES). Among macronutrients, the highest content was observed for Ca and K, while Mg and Na were represented in the smallest amount. Fe, Mn, Zn and Ba were the most abundant trace elements in contrast to Cd and Co, whose concentrationc were the lowest.

Keywords: heavy metals; ICP-OES determination.

INTRODUCTION

Lichens occur in all terrestrial ecosystems, including extreme ones. They represent the symbiotic association of fungi and algae with a simple anatomy, without a waxy cuticle layer, stomata and root system. An alga as a photobiont performs photosynthesis and provides the lichen with nutrients while a fungus as a mycobiont absorbs water with nutrients from the substrate. As a result, lichens are autotrophic and can grow on rocks, roofs, tree trunks, leaves of plants in the tropics and even on porcelain, glass, paper, cloth, resin, bones, charcoal, *etc*. They are long-lived perennial organisms and because of weak photosynthesis they grow very slowly.[1,2]

Lichens are used as medicines, food, fodder, dyes perfume, spice and for miscellaneous purposes. More than one thousand primary and secondary metabolites

* Corresponding author. E-mail: ivana.zrnzevic@pmf.edu.rs
[#] Serbian Chemical Society member.
https://doi.org/10.2298/JSC220223049T

with some biological activities such as antioxidant, antibiotic, antimycotic, antiviral, anti-inflammatory, analgesic, antipyretic, *etc*., are known in lichens.[3]

The accumulation of metals in lichens depends on many factors, such as the availability of metals, lichen characteristics, climate conditions, *etc*. The changes in elemental bioavailability (essential and toxic to metabolic processes) depend on factors such as a rapid increase of population, urbanization, industrialization; the use of chemicals in the industry, nuclear energy, and thermic power stations; decreasing green areas, the destruction of forests and erosion; changes in climate *etc*. Air, water and soil pollution are related to these factors. Being non-biodegradable, heavy metals tend to accumulate in living systems and have a long half-life in soil. Fungi, mosses, lichens and plants have been used to detect the deposition, accumulation and distribution of metal pollution either as the bioindicators/biomonitors of air quality or as the bioaccumulators of atmospheric pollutants.

Lichens depend on mineral nutrients from a wet atmospheric deposition (precipitation, fog, dew) and a dry atmospheric deposition (sedimentation, gaseous absorption). Intracellular spaces of the lichen thallus can accumulate and retain metals by trapping insoluble particles, extracellular ion exchange processes, adsorption and active uptake. Lichens tolerate high concentrations of heavy metals by sequestering them as oxalate crystals or lichen acid complexes. As slow-growing and long-living organisms, lichens offer long-term knowledge about levels of heavy metals and other pollutants in the atmosphere.[2]

Lichens have cation exchange properties and take up rapidly soluble elements over the entire thallus surface. Slower and more selective uptake mechanisms also exist. Soil particles and aerosols adsorbed to the surface also contribute to the total element concentrations in the thalli. The exchangeable fraction of metals decreases when the thalli become air-dried. In humid regions, a high correlation exists between the levels of air pollutants and lichen physiology. They can easily lose water but can just as easily compensate it. Because of their high surface/volume ratio they are under the strong influence of atmospheric deposition which is the reason of their use for the biomonitoring purposes. Lichens and mosses have a higher capacity for metal accumulation and are probably most frequently used for biomonitoring. Lichens were found to be more sensitive than mosses to emissions of S and atmophile elements (Hg, Cd, Pb, Cu, V, Zn), while mosses showed a higher concentration of lithophile elements and dust (Al, Cr, Fe, Mn, Ni, Ti). Also, epiphytic and corticolous lichens were preferred to prevent particles coming from the ground.[4]

Lichens as species with wide geographical ranges are widely used for the determination of sulfur dioxide, trace metals, organochlorines, radionuclides. When the amount of harmful substances becomes toxic, lichens die, which is the reason of their absence in heavily polluted areas, but they are nevertheless used for biomonitoring in these areas as well by using so-called transplant techniques.

One of these techniques consists in exposing bags containing lichens to the atmospheric deposition in the studied area to measure the concentrations of the contaminants affecting the samples.[5]

Transportation, industrial activities, fossil fuels, agriculture and other human activities may cause environmental pollution. Biological material is often used for pollutants' monitoring. A high sensitivity of lichens to pollutants, particularly airborne pollutants, is well-known. Metal content of lichens vary mostly with the changes in metal amounts in the atmosphere. The metal content of lichens is usually inversely proportional to the distance from pollution sources. Particulate emissions from local farming (pesticides and fertilizers), traffic, landfills and industries can be transported by the wind. The direction of the dominant wind is important for the removal of atmospheric pollutants and the metal composition of lichen species.[6]

The wind is a driving force that resuspends natural soil material into a fine mixture of light particulates (dust) transportable over a long distance and precipitable on lichens.[2] Dongara *et al.*[7] defined roadway dust as a mixture of different particulates from the Earth's crust (quartz, calcite, feldspars, gypsum, Al, Fe, Ti, Sc, V, Cu, Mn, K, Mg, Na, P, S) and particulates of anthropogenic origin. Paoli *et al.*[8] confirmed that the high concentration of lithogenic elements in lichens is associated with high levels of depositions from airborne soil dust (Fe, Cd, Cr, Ni).

The aim of the present work was to determine the elemental composition of different lichen species from different locations and substrates and to perform the relevant conclusions and/or assumptions about the main factors which may affect this composition, such as lichen taxonomy and live forms and the substrate on which they grow (soil, rocks, tree bark).

EXPERIMENTAL

Reagents

Multi-element standard solutions for ICP, III and IV and single standard solutions of Si and P (TraceCERT, Fluka Analytical, Switzerland) were used as a stock solution for calibration. A nitric acid (Merck, Darmstadt, Germany) was used for complete mineralization of analyzed samples. Certified Reference Material Strawberry Leaves (LGC7162) was used for accuracy testing.

Instrumentation

iCAP 6000 inductively coupled plasma optical emission spectrometer (Thermo Scientific, Cambridge, UK) which combines an Echelle optical design and a charge injection device (CID) solid state detector was used, under the optimal operating conditions, for elements determination. iTEVA operating software was used to control all functions of the instrument. The Mettler Toledo analytical balance (Switzerland) was used to measure the mass. High purity water (conductivity, 0.05 μS cm^{-1}) was obtained using the MicroMed high purity water system, Thermo Electron LED GmbH (Germany).

Operating conditions of ICP-OES. All of measurements were done under the next operating conditions of instrument: flush pump rate 100 rpm, analysis pump rate 50 rpm, RF

power 1150 W, nebulizer gas flow rate 0.7 L min^{-1}, coolant gas flow rate 12 L min^{-1}, auxiliary gas flow rate 0.5 L min^{-1}, dual (axial/radial) viewed plasma mode and sample uptake delay 30 s.

Method validation. The calibration lines were constructed at four wavelengths for each element (Table I).

TABLE I. Analytical lines, correlation coefficients (r), limits of detection (LOD), ratio of the slopes of the external calibration lines and slopes of the lines where the prepared sample solutions have been added to the calibration standards ($Slope_{cal}/Slope_{sam}$) for determined elements in analyzed lichen species and results of methods accuracy; ND – not determined, Recovery = 100(Found amount/Certified amount)

Element	Wavelength nm	r	LOD ppm	$Slope_{cal}/Slope_{sam}$	Amount, mg kg^{-1}		Recovery %
					Certified	Found	
Al	396.152	0.999873	0.001762	0.98	1000[a]	890±8	89.0
B	249.773	0.999971	0.000747	0.97	ND	32±2	–
Ba	455.403	1.000000	0.000052	1.12	107±10	97±4	90.6
Ca	393.366	0.999929	0.000101	1.03	15300±700	13800±800	90.2
Cd	214.438	0.999759	0.000100	0.97	0.17±0.04	0.18±0.03	105.9
Co	228.616	0.999986	0.000348	0.96	0.47±0.11	0.42±0.04	89.4
Cr	357.969	0.999888	0.001692	0.97	2.15±0.34	2.25±0.02	104.6
Cu	324.754	0.999948	0.000584	1.08	10[a]	11.2±0.2	112.0
Fe	259.940	0.999999	0.000514	1.06	818±48	750±20	91.7
K	766.490	0.980135	0.034503	0.99	19600±1000	18000±1000	91.8
Mg	279.553	0.999843	0.000132	0.98	3770±170	3900±200	103.4
Mn	257.610	0.999924	0.000094	1.04	171±10	180±5	105.3
Na	589.592	0.999992	0.000537	1.02	210[a]	188±8	89.5
Ni	231.604	0.999924	0.000475	0.97	2.6±0.7	2.9±0.6	111.5
P	213.618	0.998743	0.004315	1.06	2600±230	2400±200	92.3
Pb	220.353	0.999952	0.002293	0.96	1.8±0.4	2.0±0.2	111.1
Si	288.158	0.999803	0.002780	1.06	ND	770±2	–
V	292.402	0.999945	0.000522	1.05	1.8[a]	1.68±0.02	93.3
Zn	213.856	0.999909	0.000115	0.98	24±5	22.4±0.2	93.3

[a]Non-certified concentration

The selection of the analytical emission line was made based on the sensitivity of the analytical lines, the correlation coefficients, as well as based upon the tables of known interferences, baseline shifts and the background correction (the highest signal-to-background ratio) which was manually selected for the quantitative measurements. The possible matrix interferences were examined by comparing the calibration slopes of the so-called external calibration lines ($Slope_{cal}$) to slope of the standard addition method lines where the prepared sample solutions have been added to the standards for calibration ($Slope_{sam}$). Values of ratio $Slope_{cal}/Slope_{sam}$ closer to 1 indicate a negligible matrix effect at selected wavelengths. In order to test the accuracy of the methods, certified reference material strawberry leaves (LGC716) was used.[9]

Samples

Eleven lichen species were collected from five different locations on the Balkan Peninsula (Serbia and Bulgaria) and were identified and stored in the herbarium at the Department of Biology, Faculty of Sciences and Mathematics, University of Niš. The lichen species,

family, genus, sampling sites, substrate and sampling year are given in Table II. A composite sample of several thalli of each investigated lichen were collected using plastic gloves and a stainless-steel knife. The soil and rock particles and the old parts of lichens were removed. The samples were dried at 40 °C to a constant weight and then ground in a mill. One gram of the obtained powder was weighed and treated with 30 ml of conc. HNO_3, left overnight, and heated on a hot plate until the nitrogen vapor stopped forming or until a clear solution was obtained. After complete mineralization, the obtained solutions were filtered and made up to 50 ml with deionized water.[10]

TABLE II. Descriptions of analyzed lichens and collecting sites

Species	Family	Genus	Thallus type	Sampling sites	Habitat type	Voucher number
Usnea chaetophora Stirt.	Parmeliaceae	*Usnea*	Fruticose	Bulgaria, Pirin, Bansko	Bark of the *Pinus spp.*	9377
Bryoria fuscescens (Gyel) Brodo et Hawksw.	Parmeliaceae	*Bryoria*	Fruticose			9378
Bryoria capillaris (Ach.) Brodo et Hawkisw.	Parmeliaceae	*Bryoria*	Fruticose			9376
Ramalina capitata (Ach.) Nyl.	Ramalinaceae	*Ramalina*	Fruticose	Serbia, Stara Planina, Babin zub	Siliceous rocks	9374
Umbilicaria crustulosa (Ach.) Frey	Umbilicariacea	*Umbilicaria*	Foliose			9373
Umbilicaria cylindrica (L.) Duby	Umbilicariacea	*Umbilicaria*	Foliose			9375
Hypogymnia tubulosa (Schaer.) Hav.	Parmeliaceae	*Hypogymnia*	Foliose	Serbia, Seličevica, Donje Vlase, Grčke pojate	Bark of the *Pinus spp.*	10355
Cladonia rangiformis Hoffm.	Cladoniaceae	*Cladonia*	Fruticose-squamulose	Serbia, Suva planina,	On the ground	10889
Peltigera horizontalis (Huds.) Baumg.	Peltigeraceae	*Peltigera*	Foliose	Duga Poljana	below *Quercus cerris*	10890
Evernia prunastri (L.) Ach.	Parmeliaceae	*Evernia*	Fruticose	Serbia, Vlasinska visoravan, Vlasina Rid	Bark of the *Pinus spp.*	10892
Lobaria pulmonaria L. (Hoffm.)	Lobariaceae	*Lobaria*	Foliose	Serbia, Stara Planina, Babin zub	Beech trunks, basal parts	10891

Statistical analysis

All measurements were carried out in triplicate and presented as the mean ± standard deviation (*SD*). Shapiro-Wilk test of normality, ANOVA with Tukey's post hoc test, the Pear-

son's correlation study and hierarchical cluster analysis were done using a statistical package IBM SPSS 20, US.

RESULTS AND DISCUSSION

The contents of determined elements in eleven samples of lichens shown as mean values of triplicate determination with standard deviations are presented in Tables III and IV. A one-way analysis of variance (ANOVA) with Tukey's post--hoc test was used to establish which metals significantly differed in the mean content between the all analysed samples and the results of this statistical method are also given in these tables.

Table III. Content of determined elements±*SD*, mg kg^{-1}, in analyzed samples of fruticose lichens (standard deviation for triplicate determination; mean values in the same row with the same letters indicate no significant differences ($p < 0.05$); a is always lower than b and b is always lower than c, *etc.*

Element	Lichen					
	Usnea chaetophora	*Bryoria fuscescens*	*Bryoria capillaris*	*Ramalina capitata*	*Cladonia rangiformis*	*Evernia prunastri*
Al	366±4^{a,c}	261±3	180±2	1665±8	2103±11	356±5^{b,c}
B	5.35±0.08^{b}	6.42±0.04^{c}	17.49±0.09	4.16±0.09^{a}	5.8±0.1^{b,c}	8.6±0.2
Ba	11.24±0.06^{a}	6.73±0.05^{b}	34.8±0.1	10.87±0.02^{a}	32.5±0.2	6.33±0.08^{b,c}
Ca	3570±36^{e}	2234±7^{a}	3345±17^{c}	3152±23^{d}	2223±26^{a}	3643±18^{e}
Cd	0.174±0.014^{a,e,f}	0.148±0.005^{e}	0.078±0.001	0.444±0.001	0.405±0.008	0.179±0.015^{a,d}
Co	0.189±0.028^{a,c,d}	0.781±0.01	0.011.0±0.0001	0.663±0.026	1.167±0.016	0.238±0.006^{d,e,f}
Cr	1.16±0.02^{c}	0.63±0.07^{a}	0.50±0.02^{a}	4.27±0.07^{b}	4.18±0.08^{b}	2.78±0.08^{d}
Cu	6.18±0.09^{a}	5.68±0.03	7.6±0.1	10.04±0.02	8.29±0.06^{b}	6.2±0.1^{a}
Fe	319±4	254±2	166.9±0.8	2089±8	2358±11	471±4^{a,b}
K	2239±6^{a,b}	2376±42	2250±22^{a,c}	1199±13	1489±18	1639±9
Mg	580±6^{c}	475±9^{a}	524±5^{b}	612±7	746±2	480±2^{a}
Mn	77.5±0.8	45.0±0.5	48.1±0.2	37.74±0.05	252±2	32.1±0.2^{a}
Na	9.75±0.07^{b}	9.7±0.2^{b}	15.4±0.2	7.7±0.2^{c}	3.66±0.03^{a}	3.68±0.04^{a}
Ni	1.12±0.04^{a}	1.17±0.03^{a}	0.78±0.02	2.66±0.05	3.71±0.08	5.01±0.06
P	991±34^{a,e}	1167±15	1074±7^{c}	616±3^{d}	1020±21^{b,e,f}	589±5^{d}
Pb	3.4±0.2^{a,c,f}	6.53±0.05^{h}	3.5±0.4^{a,e,g}	18.10±0.07	3.12±0.07^{b,c,e}	4.4±0.2
Si	63±7	45.7±0.6	150.3±0.9	94.3±0.3	24.7±0.2^{a}	27.1±0.6^{a}
V	0.778±0.005	0.49±0.03	0.38±0.04	4.70±0.02	5.34±0.05	0.93±0.06
Zn	28±1	33.4±0.4	42.6±0.3^{b}	37.2±0.2^{a}	24.8±0.2	19.1±0.2

It is evident from the obtained results that the contents of the investigated macroelements follow this decreasing order: Ca > K > P > Mg > Na in six samples and K > Ca > P > Mg > Na in three samples. The order is quite similar in the rest of the samples – the most abundant are Ca and K and the least abundant were Mg and Na. The regularity observed in the case of macroelements is considerably less pronounced in other tested elements. Fe, Mn, Zn and Ba are the most abundant trace elements while Cd and Co are present in the lowest content. *P. horizontalis* has the highest content of most elements (Al, Ba, Co, Cu, Fe, K, Mn, Ni, P). *U. cylindrica* is the next in the sequence with the highest

content of Cd, Cr, Mg, Pb, V. Unlike them, *B. capillaries* contains the smallest quantities of most elements (Al, Cd, Co, Cr, Fe, Ni, V). The slightest variations are in the content of macro elements and among them the lowest are in Ca while they are the highest in the case of Co, Mn, Cr, Fe, Si even up to two orders of magnitude. It is evident, from the results of the One-way Anova, that the investigated species show the smallest differences in the content of Pb, P, Cd, Co and Ca and the biggest in the content of V, Si, Ni, Mn and Zn.

TABLE IV. Content of determined elements±*SD*, mg kg^{-1}, in analyzed samples of foliose lichens; *SD* – standard deviation for triplicate determination; mean values in the same row with the same letters indicate no significant differences ($p < 0.05$); a is always lower than b and b is always lower than c, *etc*.

Element	Lichen				
	Umbilicaria crustulosa	*Umbilicaria cylindrica*	*Hypogymnia tubulosa*	*Peltigera horizontalis*	*Lobaria pulmonaria*
Al	421±4	1914±8	578±4	2627±13	$365±4^{a,b}$
B	22.6±0.7	$4.4±0.3^{a}$	13.3±0.2	9.5±0.6	12.4±0.2
Ba	$5.72±0.04^{c}$	23.8±0.2	19.15±0.07	83.8±0.8	30.7±0.2
Ca	$1293±29^{b}$	$1309±10^{b}$	13843±82	$3220±34^{d}$	$3314±43^{c}$
Cd	$0.202±0.001^{b,d,f}$	$0.567±0.01^{c}$	$0.214±0.005^{b}$	$0.560±0.013^{c}$	0.369±0.022
Co	$0.144±0.022^{b,c}$	2.290±0.01	$0.285±0.01^{e}$	2.492±0.022	$0.179±0.014^{a,b,f}$
Cr	$0.99±0.08^{c}$	11.90±0.08	1.88±0.09	5.77±0.09	$3.02±0.02^{d}$
Cu	$8.15±0.04^{b}$	$9.30±0.09^{c}$	8.61±0.06	17.1±0.8	$9.03±0.04^{c}$
Fe	$477±4^{a,c}$	2293±9	766±6	3413±35	$466±5^{b,c}$
K	3138±11	1763±13	$2238±9^{b,c}$	6458±88	2631±6
Mg	715±5	1793±11	$570±8^{c}$	1419±10	$531±2^{b}$
Mn	18.23±0.09	58.4±0.3	23.64±0.07	729±12	$30.1±0.2^{a}$
Na	11.62±0.09	10.60±0.06	$7.56±0.04^{c}$	4.71±0.03	6.61±0.02
Ni	0.967±0.007	4.74±0.04	5.52±0.05	7.87±0.08	2.31±0.02
P	1572±4	1224±10	$1004±7^{a,b}$	2063±32	$1055±10^{c,f}$
Pb	$14.55±0.05^{d}$	22.4±0.4	$14.3±0.2^{d}$	$7.02±0.09^{h}$	$3.03±0.2^{b,f,g}$
Si	245±2	86.1±0.4	123±3	17.3±0.1	73.0±0.5
V	1.47±0.02	8.28±0.04	1.94±0.01	7.76±0.08	1.28±0.04
Zn	128.9±0.3	56.2±0.1	$43.39±0.06^{b}$	$37.2±0.8^{a}$	26.34±0.07

Bargagli *et al.*[10] determined the total concentration of macro- and trace elements in thalli of epilithic *U. decussate* from thirty-seven sites of ice-free areas from continental Antarctica in a period of ten years. No impact of human activities was detected, and the investigated time period did not show significant variations in this terrestrial ecosystem. They concluded that the ad/absorption of soil and rock dust particles (atmospheric deposition) is the main source of macro- and trace elements. The higher average contents of lithophilic elements (Al, Fe, and Mn) are probably due to a greater amount of dust particles in lichens' thalli than to changes in the environmental bioavailability of metals. The average concentration of Pb, Cu, Zn, Cr, Mn, and Fe were among the lowest ever reported for

lichens of genus *Umbilicaria.* The higher content of the most elements was found in two types of lichens from genus *Umbilicaria* (*U. crustulosa* and *U. cylindrica*) analyzed in our work compared to the average contents of the examined species in the work of Bargagli *et al.*[10] Icel and Cobanoglu[4] analysed ten air pollutants in eight naturally growing lichens sampled at ten urban and suburban sites in the city of Istanbul using atomic absorption spectrometry and the concentrations are as follows: Mn > Zn > Pb > Cu > Al > Ni > Cr > Fe > Co > Cd. Some obtained average values are much smaller than in our study (Al and Fe); some are higher (Cu, Mn, Zn, Ni, Pb and Cr) and some are the same (Cd and Co). The behavior is the same if the same species tested in both studies are compared (*Cladonia sp.*, *H. tubulosa*, *E. prunastri*). Pb in one sample reaches a value of 119 μg g^{-1}, which is 5 times more than the maximum determined in our study. Icel and Cobanoglu[4] also used reference material IAEA 336 lichen (*E. prunastri*) as a control material and based on the obtained contents concluded that quite high levels of the elemental pollution in the area, especially for Pb, Cr and Cu, exist. Compared to the values in this reference material, the results in our study show some significantly increased levels in: *R. capitata* (Al, Fe, Pb); *U. cylindrica* (Al, Fe, Cr, Pb, Co); *C. rangiformis* (Al, Fe, Co, Mn); *P. horizontalis* (Al, Fe, Co, Cu, Mn); *U. crustulosa* (Pb, Zn); *H. tubulosa* (Fe, Pb). Dogrul *et al.*[11] found the following amounts of some heavy metals as pollutants in seven types of lichens: Cu (137.94 μg g^{-1}); Mn (466.67 μg g^{-1}); Cd (3.22 μg g^{-1}); Zn (1037.56 μg g^{-1}); Pb (225.85 μg g^{-1}); Cr (28.90 μg g^{-1}); Co (1.60 μg g^{-1}) and Ni (11.40 μg g^{-1}) in the industrial regions which are greater than in the investigated samples from the Balkan Peninsula even up to 10 times for Pb, 8 times for Zn and Cu and 6 times for Cd which indicates the importance of the air pollution impact.

Aslan *et al.*[12] determined the contents of six elements (Fe, Ba, Sr, K, Ca and Ti) in eight lichen species from rural and subrural sites of different regions in Turkey as well as in their substrates-soil, rocks, and bark of *Pinus Silvestre* and noticed that lichens may reach high levels of some metals even when these plants are growing in rural and isolated sites. The most abundant elements are Ca, K and Fe which is in accordance with the results of this work but the determined contents are higher (1.595–13.984 % for Ca; 2.615–9.190 % for K and 0.920––6.705 % for Fe). The same examined species, *R. capitata*, contains 36 times more potassium, 10 times more calcium and 5 times more iron compared to our research which is probably the consequence of different atmospheric depositions caused by different substrate compositions and weather conditions. The concentrations are as follows: 2.615–9.190 % K; 1.595–13.984 % Ca; 0.041–0.205 % Ti; 0.920–6.705 % Fe; n.d.–0.021 % Sr and n.d.–0.023 % Ba. They noticed that two crustose species (*R. melanophthalma* and *R. chrysoleuca*) which were collected from the same region and the same substrata accumulated a slightly different amount of Ca and Fe which is a probably consequence of different metal-

-accumulating capability while some other crustose species (*L. muralis*) which are from a different habitat had a different amount. Because of this, they concluded that lichens do not get any metals from their substrata, they accumulate only atmospheric depositions and distinct metal/accumulating capabilities of lichen species exist. They explained some greater metal contents by the foliose structure of this species as an additional factor which was noticed also in our work. All the largest certain contents, except sodium, are in foliose species.

Aslan *et al.*[6] determined the following concentrations in six lichen species: 3.707–5.210 % K; 1.410–6.563 % Ca; n.d.–0.069 % Ti; n.d.–2.022 % Fe and n.d.–0.021 % Ba. They noticed that some samples have similar levels of metal concentration while some have higher or lower levels which supports the hypothesis that lichens get very little or no metals from their substrates. The different element concentrations in these species are a consequence of a different thallus structure as well as different conditions of collection stations. The higher values of some elements may be the result of a large surface area, larger intercellular space in medulla and cortex of some species, while the higher value of potassium is explained by using some potassium containing fertilizers in these areas. The higher values in some fruticose as compared to some others indicate the importance of station selection in determining metal content in lichens. One of the species, *E. prunastri, was* examined in both studies. The contents of the investigated elements determined in the research of Aslan *et al.*[6] are higher: 20 times for K, 6 times for Fe and 4 times for Ca compared to our research. The situation is the same when comparing contents in species that belong to the same genus: *U. florida* and *U. longissimi* with *U. chaetophora* and *H. physodes* with *H. tubulosa.* These facts also support the above mentioned: the great influence of the different conditions at sampling sites.

Stamenković *et al.*[2] determined the content of 19 heavy metals in two epiphytic lichen species *Evernia prunastri* (L.) Ach. as fructose and *Parmelia sulcata* Taylor as foliose from two southeast places in Serbia and found that *P. sulcata* contains higher amounts of most of the elements which is in accordance with the higher affinity for metal uptake by folio species in our study. Comparing the content of the tested metals, a higher content of Fe, Mn, Ni, Cr, Ba and especially Pb in *E. prunastri* is observed in our study which confirms the significant influence of various factors on the amount of metals in the lichen in addition to the dominant influence of the type of lichen.[2] The concentration of the terrigenous element Fe was the highest determined at both locations, from 273.11 to 810.36 μg g^{-1} of dry lichens followed by Zn, Mn, Cu, Ba, Ti. The elevated values of Co and Cr were present, 1.17–2.74 and 1.40–1.70 μg g^{-1}, respectively. They also detected some amounts of Ag, Pb and Hg in some samples (1.63, 1.38, 1.38 μg g^{-1}, respectively). The results of this indicated that *P. sulcata* showed a tendency to accumulate Fe, Ni, and Ti despite the *E. prunastri* which prefer-

entially concentrated Cu in both areas unlike the results in our research which show a slightly increased affinity *E. prunastri* towards the accumulation of Ni in the group with other fruticose species. These facts indicate that the interspecific differences in heavy metal accumulation are related to their morphological, anatomical, and physiological features, such as metal-absorbing abilities, surface area, size of intercellular space, permeability of cell membrane and *pH* values. The concentration of potential toxic heavy metals (Cr, Ag, Pb and Hg) were approximately the same in both species in both areas. Fe, Ni and Ti displayed a significant and Cu, Ag, Pb and Ag slight positive correlation with each other which indicates their association in lichens, while Ba with Co, Cr and Zn; Cu with Fe; Ni with Mn and Ti with Cu showed a slight negative.[13]

The element concentration data were submitted to the Pearson's correlation coefficient analysis, and the coefficients matrix is shown in Table S-I (available as Supplementary material) with a significant correlation at $p < 0.01$ and $p < 0.05$. It is evident that a good correlation exists between the elements which are naturally present in the soil and rocks, *i.e.*, alkali and alkaline earth metals, iron, silicon, aluminium, vanadium, copper, cobalt, chromium, nickel, *etc*. Pb does not correlate with any element, Zn correlates only with Si, and Cd only with Al, and they are assumed to be of dominantly anthropogenic origin, especially Pb. Stamenković *et al.*[2] noticed that some of the elements showed a negative correlation with each other, meaning they are probably competing for the same cell wall exchange sites. Bargagli *et al.*[10] found that the relationships between lithophilic elements from soil and rock dust particles were the most significant.

The hierarchical cluster analysis of the samples (Fig. 1) based on the content of all of the investigated elements shows the existence of several clusters and sub clusters which include different lichen species, family and genus; different sampling sites, thallus types and habitat types. A cluster analysis was performed on the data sets using Ward's method with squared Euclidean distances as a measure of similarity between the element concentrations.

Regardless of the obvious involvement of all these factors on the content of minerals, the following observations are evident. The greatest similarity exists between the samples belonging to the same family. All five members of the *Parmeliaceae* family are in the same cluster, in two close sub clusters. Also, all the species in this cluster which belong to the epiphytic lichens grow on the barks as same substrate. The remaining species are classified in the other two clusters and their common features are also substrate, soil, or rocks. It can be concluded that the species of lichens and at the same time type of habitant are the main factors which influence the mineral content. The hierarchical cluster analysis of the samples (Fig. 2) based on the content of heavy metals only shows a greater similarity between different types of samples, from different locations and substrates, which may indicate the absence of some pronounced pollution.

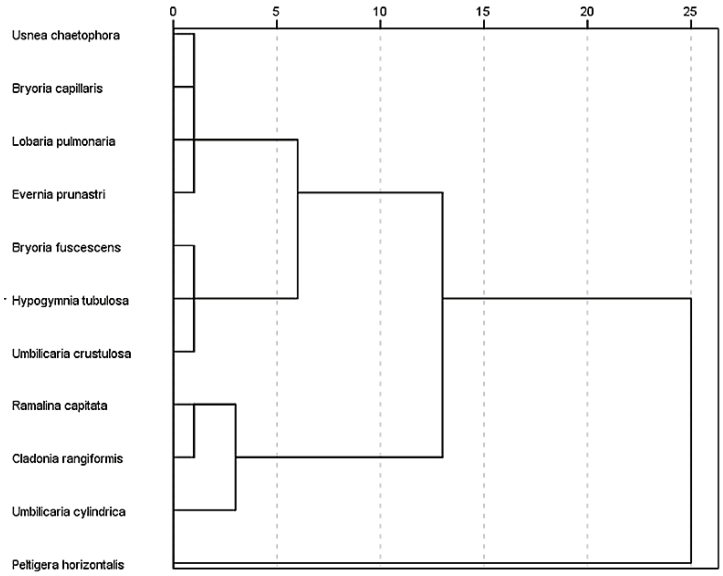

Fig. 1. Hierarchical dendrogram for investigated lichens based on all metals' contents.

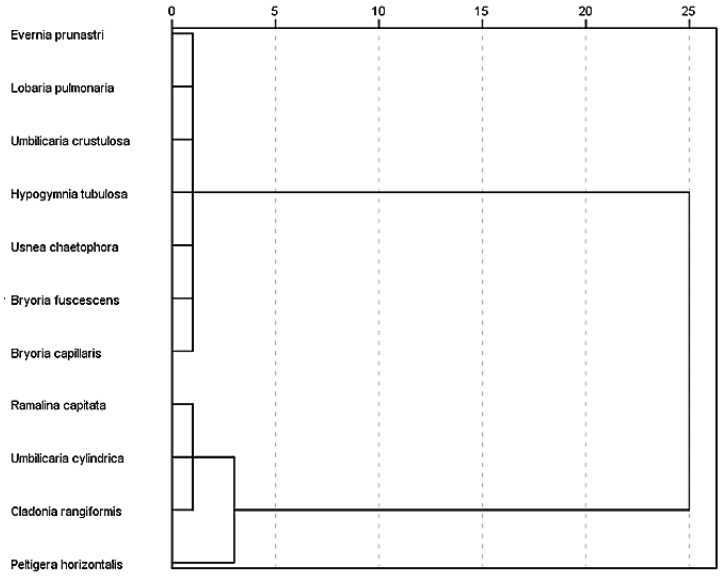

Fig. 2. Hierarchical dendrogram for investigated lichens based on heavy metals' contents.

Stamenković *et al.*[2] found the distinction between the soil origin, *i.e.*, lithogenic (Mn, Cu and Ti) and the atmospheric elements (Ni, Co, Cr, Ag, Pg and Hg) under the anthropogenic influence and the long-distance atmospheric transport of

particulates from vehicle exhaust emissions using cluster analysis. Mn and Cu can partly come from fertilizers and manures.

CONCLUSION

The obtained results show that the most common macroelements are calcium and potassium while iron, manganese, zinc, and barium are the most abundant trace elements. Also, *P. horizontalis* has the highest content of most elements while *B. capillaries* contains the smallest quantities of most elements. The results of this research as well as the results of other authors' research point to the fact that many factors influence the content of elements in lichen samples such as: species, family, genus, thallus type, metal bio-absorbing capabilities of lichens, sampling site, habitat type, weather conditions, state of environmental especially pollutants present in atmosphere. Based on the results of the hierarchical cluster analysis, it can be concluded that the species of lichens, and at the same time, the type of habitant, *i.e.*, substrate (soil, rocks, barks) are the main factors which influence the mineral content of the investigated lichens.

SUPPLEMENTARY MATERIAL

Additional data and information are available electronically at the pages of journal website: https://www.shd-pub.org.rs/index.php/JSCS/article/view/11647, or from the corresponding author on request.

Acknowledgement. The research was supported by Ministry of Education, Science and Technological Development of the Republic of Serbia (Projects No. 451-03-68/2022-14/ /200124).

ИЗВОД

ЕЛЕМЕНТАЛНИ САСТАВ ОДАБРАНИХ ВРСТА ЛИШАЈЕВА КОЈИ РАСТУ НА БАЛКАНСКОМ ПОЛУОСТРВУ

СНЕЖАНА ТОШИЋ, АЛЕКСАНДРА ПАВЛОВИЋ, ИВАНА ДИМИТРИЈЕВИЋ, ИВАНА ЗЛАТАНОВИЋ, ВИОЛЕТА МИТИЋ и ГОРДАНА СТОЈАНОВИЋ

Универзитет у Нишу, Природно–математички факултет, Департман за хемију, Вишеградска 33, 18000 Ниш

Коришћењем оптичке емисионе спектрометрије са индуктивно спрегнутом плазмом (ICP-OES) одређен је садржај 19 елемената у 11 различитих врста лишајева, шест фрутикозних (*Bryoria capillaris*, *Bryoria fuscescens*, *Cladonia rangiformis*, *Ramalina capitata*, *Usnea chaetophora* и *Evernia prunastri*) и пет фолиозних (*Hypogymnia tubulosa*, *Lobaria pulmonaria*, *Peltigera horizontalis*, *Umbilicaria cylindrica* и *Umbilicaria crustulosa*), сакупљених са пет природних станишта на Балканском полуострву (Србија и Бугарска). Међу макронутријентима, највећи садржај је забележен за Ca и K, док су Mg и Na заступљени у најмањој количини. Fe, Mn, Zn и Ba су били најзаступљенији елементи у траговима за разлику од Cd и Co чија је концентрација била најнижа.

(Примљено 23. фебруара, ревидирано 6. маја, прихваћено 11. јуна 2022)

REFERENCES

1. E. S. Bernasconi, I. E. De Vito, L. D. Martinez, J. Raba, *Ars. Pharm*. **41** (2000) 249 (https://revistaseug.ugr.es/index.php/ars/article/view/5721/13228)
2. S. S. Stamenković, T. Lj. Mitrović, V. J. Cvetković, N. S. Krstić, R. M. Baošić, M. S. Marković, N. D. Nikolić, V. Lj. Marković, M. V. Cvijan, *Arch. Biol. Sci.* **65** (2013) 151 (https://doi.org/10.2298/ABS1301151S)
3. N. T. Manojlovic, P. J. Vasiljevic, P. Z. Maskovic, M. Juskovic, G. Bogdanovic--Dusanovic, *Evid. Based Complement. Alternat. Med.* **2012** (2012) 452431 (https://doi.org/10.1155/2012/452431)
4. Y. Icel, G. Cobanoglu, *Fresenius Environ. Bull.* **18** (2009) 2066 (https://www.researchgate.net/publication/287706544_Biomonitoring_of_atmospheric_heavy_metal_pollution_using_lichens_and_mosses_in_the_city_of_Istanbul_Turkey)
5. A. Basile, S. Sorbo, G. Aprile, B. Conte, R. Castaldo Cobianchi, *Environ. Pollut*. **151** (2008) 401 (https://doi.org/10.1016/j.envpol.2007.07.004)
6. A. Aslan, G. Budak, E. Tirasoglu, A. Karabulut, *J. Quant. Spectrosc. Radiat. Transf*. **97** (2006) 10 (https://doi.org/10.1016/j.jqsrt.2004.12.032)
7. G. Dongarra, G. Sabatino, M. Triscari, D. Varrica, *J. Environ. Monit*. **5** (2003) 766 (https://doi.org/10.1039/B304461K)
8. L. Paoli, A. Corsini, V. Bigagli, J. Vannini, C. Bruscoli, S. Loppi, *Environ. Pollut.* **161** (2012) 70 (https://doi.org/10.1016/j.envpol.2011.09.028)
9. M. E. Ghanjaoui, M. L. Cervera, M. EI. Rhazi, M. de la Guardia, *Food Chem*. **125** (2011) 1309 (https://doi.org/10.1016/j.foodchem.2010.09.091)
10. R. Bargagli, F. Borghini, C. Celesti, *Ital. J. Zool*. **67** (2000) 157 (https://doi.org/10.1080/11250000009356371)
11. A. Dogrul, N. H. Akyol, I. Yolcubal, G. Cobanoglu, in *Proceedings of the International Fourth Symposium on Atmospheric Sciences*, 2008, Istanbul Technical University, Istanbul, Turkey, 2008, pp. 99–104 (https://www.jmo.org.tr/resimler/ekler/f2b49181d2539e7_ek.pdf)
12. A. Aslan, G. Budak, A. Karabulut, *J. Quant. Spectrosc. Radiat. Transf*. **88** (2004) 423 (https://doi.org/10.1016/j.jqsrt.2004.04.015)
13. S. Loppi, S. A. Pirintsos, *Environ. Pollut.* **121** (2003) 327 (https://doi.org/10.1016/S0269-7491(02)00269-5).

Journal of the Serbian Chemical Society
JSCS@tmf.bg.ac.rs • www.shd.org.rs/JSCS
J. Serb. Chem. Soc. 87 (11) S445 (2022) *Supplementary material*

SUPPLEMENTARY MATERIAL TO

Elemental composition of selected lichen species growing on the Balkan Peninsula

SNEŽANA TOŠIĆ, ALEKSANDRA PAVLOVIĆ#, IVANA DIMITRIJEVIĆ*, IVANA ZLATANOVIĆ#, VIOLETA MITIĆ and GORDANA STOJANOVIĆ#

University of Niš, Faculty of Sciences and Mathematics, Department of Chemistry, Višegradska 33, 18000 Niš, Serbia

J. Serb. Chem. Soc. 87 (11) (2022) 1313–1325

Table S-1. Pearson's correlation coefficients between element concentrations in lichens

	Al	B	Ba	Ca	Cd	Co	Cr	Cu	Fe	K	Mg	Mn	Na	Ni	P	Pb	Si	V	Zn
Al	1																		
B	-.456	1																	
Ba	**.637***	.007	1																
Ca	-.115	-.225	.222	1															
Cd	**.893****	-.454	.544	-.130	1														
Co	**.869****	-.456	.637	-.215	.831	1													
Cr	**.727***	-.480	.322	-.276	.856	**.815****	1												
Cu	**.758****	-.013	.870	.065	.732	**.697***	.449	1											
Fe	**.996****	-.431	.666	-.095	.901	**.874****	**.723***	**.805****	1										
K	.348	.266	.788	.108	.294	.473	.047	**.784****	.399	1									
Mg	**.735****	-.253	.521	-.345	.784	**.904****	**.894****	**.612***	**.739****	.395	1								
Mn	**.726***	-.144	.899	.202	.549	**.707***	.279	**.851****	**.750****	**.827****	.506	1							
Na	-.450	.445	-.244	-.196	-.433	-.284	-.203	-.305	-.460	-.130	-.032	-.429	1						
Ni	**.661***	-.265	.607	-.069	.616	**.669***	.557	**.689***	**.703***	.462	.563	**.655***	**-.650***	1					
P	.390	.341	.686	-.251	.332	.558	.172	**.678***	.412	**.891****	.559	**.713***	.089	.304	1				
Pb	.316	-.071	-.205	-.650	.435	.346	.573	.183	.330	-.153	.522	-.196	.219	.188	.039	1			
Si	-.403	.792	-.342	-.466	-.354	-.440	-.281	-.182	-.398	-.089	-.138	-.455	**.696***	-.481	.127	.401	1		
V	**.956****	-.433	.571	-.249	.934	**.921****	**.882****	**.719***	**.954****	.303	**.883****	**.608***	-.318	**.663***	.401	.494	-.307	1	
Zn	-.104	.680	-.196	-.623	-.077	-.072	-.046	.035	-.101	.166	.176	-.158	.481	-.259	.441	.495	**.861****	-.006	1

*Correlation is significant at the 0.05 level (2-tailed); **Correlation is significant at the 0.01 level (2-tailed).

* Corresponding author. E-mail: ivana.zrnzevic@pmf.edu.rs

Journal of the Serbian Chemical Society
JSCS@tmf.bg.ac.rs • www.shd.org.rs/JSCS
J. Serb. Chem. Soc. 87 (11) 1327–1340 (2022)
JSCS–5597
Original scientific paper
Published 5 May 2022

Optimization of the slaughterhouse water treatment rate by a new *Marinobacter carbonoclasticus* SF and its biosurfactant

NADIA MIHOUBI[1], SAMIRA FERHAT[1]*, REDHA ALOUAOUI[1], ABDELLAH IBRIR[1], MOHAMED NEDJHIOUI[2] and ABDELMALEK BADIS[3]

[1]*Biomaterial and Transport Phenomena Laboratory (LBMPT), Yahia FARES University, Faculty of Technology, Department of Process Engineering, 26000-Medea, Algeria,* [2]*Materials and Environment Laboratory (LME), Yahia FARES University, Faculty of Technology, Department of Process Engineering, 26000-Medea, Algeria and* [3]*Natural Products Chemistry and Biomolecules Laboratory (LNPC-BioM), Saad Dahleb University, Faculty of Technology, Department of Industrial Chemistry,19000-Blida, Algeria*

(Received 29 October 2021, revised 5 March, accepted 7 March 2022)

Abstract: The aim of this study consists of the production of a bio-surfactant from a new bacterial strain, *Marinobacter hydrocarbono clasticus* SF (96.76 % similarity) isolated from soil contaminated by hydrocarbons in Hassi-Messaoud (Southern Algeria) to treat liquid effluent from slaughterhouse water. The characteristics of organic matter biodegradation tests were discussed. Despite the high pollutant load and the unfavorable physicochemical composition of the effluent, the specific growth rate of the isolated strain after 10 days of incubation in the range of 0–30 g L^{-1} of NaCl was at neutral pH 7.4 and temperature of 45 °C. The best bio-surfactant production yield was obtained after 72 h of incubation and under the optimal production conditions such as diesel as carbon source, ammonium chloride as nitrogen source, and a C/N ratio of 5. The bio-surfactant produced is of glycolipid type with a low critical micellar concentration (*CMC*), good emulsifying power, and chemical and functional stability. Significant pollutant removal efficiency was obtained using the bacterial strain (up to 82 %) and the bio-surfactant (up to 96 %). Several anions, such as nitrates, phosphates, ammonium, and suspended solids, were measured.

Keywords: effluent; isolate; characterization; glycolipid; depollution.

INTRODUCTION

Water is a staple of most major feed processing companies. This water loaded with organic matter is discharged into the environment. It therefore becomes a major source of pollution for the receiving environment.

* Corresponding author. E-mail: ferhatsamira@yahoo.fr
https://doi.org/10.2298/JSC211029023M

To reduce the risk of contamination, wastewater must be treated by physical, chemical and biological methods. Slaughterhouses produce wastewater from slaughterhouse washing operations containing blood, triperia-tubular washing water and digestive contents, barn washing water, yard and truck washing water, as well as water from various devices and installations.

These effluents have a reddish appearance and are heavily loaded with fragments of meat, fat, excrement, stomach contents, trimming debris, blood clots, pieces of horns and hooves, scum, faeces, and straw. The volume of wastewater is linked to the number of slaughtered animals and varies according to the size of the slaughterhouse, the mode of operation and especially the type of slaughtered animals. The main problem of slaughterhouse effluent is the treatment of fats and organic matter that are present in large quantities.[1] Several authors were interested in aerobic[2] and anaerobic[3] processes for the characterization and the treatment of this type of wastewater.

Unlike other developed countries, Algeria provides little information on the quality of slaughterhouse wastewater, its characterization, and its treatment.[4,5] The treatment of this effluent is strongly recommended because it can be responsible for an irreversible ecological imbalance as well as the eutrophication of the waters of the receiving environment.

Microorganisms can remove hydrophobic organic compounds (HOCs) considered as contaminants because they harm the environment and human health.[5] Thus, the biodegradation of HOCs by hydrocarbonoclaste bacteria requires specific cellular functions to allow their assimilation and transport into the cytoplasm where they are metabolized.[6]

This type of bacteria, such as the genus *Marinobacter*, has been studied with the aim to characterize the biosurfactants and their properties that they excrete.[5] Biosurfactants are one of the main products of the bioeconomy because of their diverse economic activities,[7] low toxicity and useful physicochemical properties, they are promising for the environment bioremediation activities, including oil spill clean-up, removal of heavy metal contaminants and wastewater treatment.[8]

Among biosurfactants, rhamnolipids and other natural biosurfactants that can replace conventional surfactants could play a crucial role in the decontamination of contaminated water and soil.[9] It should be noted that there is a strong worldwide demand for surfactants in the various fields mentioned above.

Slaughterhouse treatment using the original bacterial strain *Marinobacter carbonoclasticus* and the biosurfactant produced from this strain were considered as alternatives to physicochemical methods used in wastewater treatment because synthetic surfactants are threatened with extinction due to the depletion of fossil sources. In this study, a bacterial strain *M. carbonoclasticus* SF was isolated from oil-contaminated soil in southern Algeria and identified by 16S rRNA sequencing.

The parameters influencing the growth of the isolate were determined. This review aims to discuss the most significant factors that influence and enhance microbial growth and the activity of this strain to treat slaughterhouse water as well as its power to produce biosurfactants. The impact of different parameters, such as pH, temperature and salinity, on the stability and emulsifying activity of the produced biosurfactant were investigated. Quantitative methods allowed the use of the isolated bacterial strain and the biosurfactant to be confirmed for the treatment of slaughterhouse water by measuring the chemical oxygen demand (*COD*), the biological oxygen demand over 5 days (BOD_5), as well as the rate of phosphates, nitrates, ammonium and suspended solids.

EXPERIMENTAL

Sampling of slaughterhouse water

The sample was taken at the exit of the slaughterhouse in Medea (Algeria), placed in inert polyethylene bottles, and stored at 4 °C. The analyzes were performed on the same day.

Isolation, growth conditions and identification of bacteria

Soil samples contaminated with hydrocarbons were taken in the region of Hassi-Messaoud (southern Algeria), transferred directly into sterile bottles, and stored in the dark at 4 °C until their use. The samples were pre-treated to determine pH, salinity, and electrical conductivity. Approximately 10 g of sediment, diluted 10 times with sterile water, was subjected to mechanical agitation for 24 h, then centrifuged at 4500 rpm for 20 min and filtered through a millipore filter (0.45 μm).[10] The pH was measured using a Metler Toledo pH meter comprising a selective electrode in contact with the solution. The conductivity was measured using a Consort C831 type conductivity meter (multi-parameter analyzer). The salinity (*S*) of the solid sample was obtained by comparing the result of the conductivity (σ) to the conductivity (κ) of a 32.43 g L^{-1} KCl solution according to:[11]

$$S = \frac{35\sigma}{\kappa} \tag{1}$$

where *S* is the salinity of the sample; σ is the conductivity of the sample in mS cm^{-1}; κ is the conductivity of a 32.43 g L^{-1} KCl solution.

The successive dilution method was used for the isolation. Thus, two grams of preserved sample were placed in 50 mL of basic enrichment culture medium containing 1 vol. % crude oil, then incubated at 37 °C at 180 rpm (shaker rotary, GFL3005, Germany). Transplanting was performed several times under the same conditions.

The SF bacterial strain used to produce the biosurfactant was maintained on nutrient agar. Crude oil was used as the sole carbon source in a minimum culture medium to enrich the strain for 14 h at 37 °C.[12] The optimal conditions for growth of the isolated bacterial strain (pH, temperature and salinity) were determined by measuring the specific growth rate (V_{max}) according to:

$$V_{max} = \frac{\log DO - \log(DO\ \tau_0)}{\tau_i} \tag{2}$$

where τ_0 is the initial incubation and τ_i the incubation time (h).

Analysis of the 16S rRNA gene sequence as well as physiological and biochemical characteristics allowed the SF strain to be identified. The isolated strain underwent phylogenetic analyses by DNA sequencing corresponding to the 16S subunit of 16S ribosomal RNA (16S rRNA). For this, several steps were necessary.[13] The extraction of the genomic DNA (centrifugation, incubation and finally the resulting pellet containing the DNA was suspended in 20 µl of sterile water then stored at –20 °C) allowed genotypic identification of the isolated strain. Electrophoresis, quantification of genomic DNA extracted on agarose gel, and polymerase chain reaction (PCR) amplification of the 16S rRNA gene were performed using two universal primers, one forward (Fal125: AGAGTTTGATCCTGGCTCAG) extended from base position 8 to 27, and the other reverse (Ral126:

AAGGAGGTGATCCAAGCC, extended from base position 1.541 to 1.525, designed from the conserved zones within the rRNA operon of *Escherichia coli*.[14] An automatic sequencer automated 3100 genetic analyzer (Applied Biosystems) from the Biotechnology Centre of Sfax (CBS, Tunisia) for the analysis of electrophoresis and the quantification of the PCR product, Restriction analysis of the amplified ribosomal DNA, their purification and the 16S ribosomal DNA sequence. The sequence results were imported into BioEdit v5.0.9 and the complete or partial sequence of the fragment was reconstructed. Searching BLAST (blast, non-redundant) with the complete sequence, *via* GenBank,[13] identified the strain studied by comparison with the closest strains.

Production of biosurfactant

The bacterial strain isolated from the soil, identified previously, was kept in Petri dishes containing nutrient agar, recultivated monthly and stored at 4 °C. The culture medium used for production of the biosurfactant was incubated in Luria-Bertani broth consisting of 10 g of peptone: 5 g of yeast extract and 5 g of NaCl at pH 7. After 6 h incubation, a volume of gas oil at 1 vol. % was added followed by incubation for 72 h, shaking at 200 rpm and at a temperature of 45 °C. After centrifugation at 6000 rpm for 20 min, the biomass was separated from the supernatant containing the biosurfactant.

Optimization of operating parameters for biosurfactant production

Selection of carbon source and concentration. The type of carbon source used in bioprocesses is of paramount importance, it greatly influences the production yield, the quality, and the quantity of the biosurfactants produced.[15] In the present study, four carbon sources (1 vol. % were used to select the optimal source and to ensure maximum biosurfactant production: vegetable oil, olive oil, crude oil and hexadecane (Merck, Darmstadt). All substrates were sterilized using a 0.22 µm filter. The concentration of the optimized carbon source was determined by varying the concentration within a range of 0.5, 1, 2 and 3 %. The reduction in surface tension was measured with a tensiometer (TSD132389, Gibertini, Italy), which was also used with the emulsification index as a tool for selecting the carbon source and its concentration for optimal biosurfactant production.[15]

Selection of nitrogen source and concentration. Besides the carbon source, bacteria need nitrogenous substances to synthesize their proteins. Different sources of nitrogen (2 % g L^{-1}) were added to the culture medium: NH_4Cl, $NaNO_3$, NH_4NO_3 and urea. After optimization, its concentration was determined in the range 1, 2, 3 and 4 %.

Optimization of the C/N ratio. Several C/N ratios of 5, 10, 30, 40 and 50 were studied by varying the concentration of the carbon source while keeping the concentration of the nitrogen source constant.

Kinetic study of the production in a free cell. A culture was prepared with the optimal synthesis conditions determined with the aim to study the kinetics of biosurfactant production by following the variations of the surface tension and of the emulsification index for a period ranging from 0 to 120 h.

Biosurfactant separation and purification. After optimal incubation of the production culture medium, the separation of the biosurfactant was performed by three-volume acetone in an ice water bath, kept for 24 h at 4 °C and followed by centrifugation at 200 rpm. The product was then dissolved in distilled water and recovered several times in acetone. The obtained crude biosurfactant was considered to be a partially purified.

Characterization of the biosurfactant. The characterization of the obtained biosurfactant was performed by first determining the surface tension of the biosurfactant and the emulsification number E_{24}. The emulsification index is defined as the ratio between the length of the total phase of the mixture (supernatant-hydrocarbon/oil) and the emulsified phase in which equal volumes of supernatant and hydrocarbon or oil (4 ml) were placed in a test tube and mixed with a vortex (VTX 400, France) at the maximum speed for 2min.

Analysis by FTIR was performed to determine the functional groups present in the biosurfactant product and to allow a preliminary structural characterization. A quantity of the precipitate obtained after drying the biosurfactant was dissolved in potassium bromide (KBr) (1/100 ratio), then the cell containing this mixture was placed in the light path that had a wavenumber between 500 and 4000 cm^{-1}.[16]

The critical micellar concentration (*CMC*) is an important parameter. The *CMC* corresponds to the lowest value of the surface tension of the biosurfactant. Above this concentration, no effect was observed on the surface activity. The *CMC* value was determined by plotting the surface tension against the concentration of biosurfactant in the solution.[17] In a test tube, a quantity of the separated precipitate was dissolved in distilled water. The mixture was manually stirred for 30 s and left to stand for 5 min. The emulsifying power of the biosurfactant was determined by mixing equal volumes of the supernatant and the hydrocarbon/oil (kerosene, heptane and olive oil), then stirred for 2 min at maximum speed and left to stand for 24 h. The interfacial tensions were again measured.

The surface tension values were calculated at different temperatures (20, 50, 70 and 120 °C), pH (2 to 11) and salinity (5 to 100 %) by incubation of the supernatant in the culture medium for 20 min.

Slaughterhouse water treatment

Characterization of the sample. The pH hydrogen potential was determined using WTWProfiLine pH 3310 pH meter. The measurement was performed with moderate stirring. The conductivity expressed in millisiemens per centimeter was measured using a Hanna Instruments HI8633 portable conductivity meter. Suspended solids (SS), refers to particles with a size between 10 nm and 1 µm, determined by vacuum filtration. They were determined by filtration through glass fibres using a vacuum filtration apparatus.[17]

The *COD* was determined according to the method described by Rodier,[17] under very precise operating conditions, Organic materials contained in the water were oxidized by an excess of potassium dichromate in an acidic medium and in the presence of silver sulphate and mercury sulphate. The BOD_5 reflects the amount of biodegradable effluent.

The amount of oxygen consumed was determined by incubating a volume of effluent for 5 days at 20 °C in the dark. The trace elements contained in the dosed effluent, such as nitrates, phosphates and ammonium, were determined using a typical spectrophotometer (DR/ /4000 V spectrophotometer, 230 Vac, Hach, USA) and glass cells with a capacity of 25 mL;

detection in the visible range 300–1000 nm. Analysis of the compounds was realized after complexation with an added reagent that develops a colour. The nitrate assay was performed at 415 nm, ammonium at 655 nm, and phosphates at 880 nm.[18]

Treatment with biosurfactant and isolated strain. The slaughterhouse water was treated with 0.1 g of the obtained biosurfactant dissolved in 5 ml of distilled water, introduce into 500 mL of waste (slaughterhouse), incubated at 45 °C and at a speed of 150 rpm. Sampling and analysis were performed every 24 h for 7 days. In addition, water treatment was by the isolated strain. The microorganism used was the isolated aerobic bacterial strain *Marinobacter hydrocarbonoclasticus*. An amount of bacterial species was placed in LB medium and incubated on an orbital shaker at 45 °C and 150 rpm for 48 h. 3 % of the medium were put into 500 mL of polluted waste water, incubated at 45 °C and 150 rpm. A sample was taken every 24 h for measurement and analysis.

RESULTS AND DISCUSSION

Phylogenetic analysis

Molecular identification of the biosurfactant producing isolate was performed by sequencing the 16S rRNA gene and comparing to sequences from the NCBI 16S rRNA database with the 16S rRNA sequences of the isolate and the closely related strain. A rooted phylogenetic tree was constructed that is illustrated in Fig. S-1 of the Supplementary material to this paper. Analysis of the 16S rRNA gene sequence as well as physiological and biochemical characteristics allowed the strain SF to be identified as an *Marinobacter hydrocarbonoclasticus* species. Strain SF exhibits 99.76 % similarity using BLASTn with the type of strain of *M. hydrocarbonoclasticus*, ATCC 27132T (GenBank accession No. AB021372). The data were made available to ENA in Europe and to the ADN database in Japan.[19]

The accession number of the isolated strain SF is KX959991. A wide variety of *Marinobacter* species were described. *Marinobacter* sp. strains were collected from various locations around the world, exclusively from marine or halophilic habitats, with diverse physiochemical characteristics including seawater, sediments, marine hot-water springs, sea ice, deep seafloor, saline soil and offshore oil-producing well. Consistent with their habitat, most *Marinobacter* strains are moderate halophiles. Similarly, two new strains, SL014B61AT and SL014B11A, were isolated from an oil-polluted saline soil from Gudao in the coastal Shengli oil field, located in eastern of China. These two strains belonged to *Marinobacter* species.[20] Yi-Jing Luo *et al.*[21] were able to isolate *Marinobacter shengliensis* sp. from saline soil contaminated with oil, the isolates were found to grow at 10–40 °C (optimum 35 °C), pH 6.0–9.0 (optimal pH 8.0), and NaCl concentrations of 0.5–18.0 % (optimum 3.0–6.0 % NaCl). The specific growth rate was calculated according to Eq. (2). According to Fig. S-2a of the Supplementary material, it was observed that after 10 days of incubation, the SF strain grew over a pH range between 6 and 10.5, with a growth optimum at pH 7.4. Additionally, it is able to

grow over a temperature range of 15 to 50 °C, with an optimum at 45 °C, as shown in Fig. S-2b.

The NaCl concentration for the growth of the SF strain was between 0 and 100 g L^{-1} with optimal growth between 0–30 g L^{-1}. No growth was observed at an NaCl concentration of 110 g L^{-1}, as shown in Fig. S-2c. Bacteria usually grow and live in an environment with a temperature range between 10 and 45 °C and in the pH range of 6–9.5.[22] The NaCl content is important for *M. hydrocarbonoclasticus*, because it can affect both the shape and flagellation of these cells.[23]

Production of biosurfactant

The production and characterization of a biosurfactant by the isolated strain SF by free cells was studied in batch cultures using the medium (LB) under conditions of temperature of 45 °C, pH 7.4, salinity of 30 % and a stirring speed of 200 rpm.

To date, the bacterial strain *M. carbonoclasticus* isolated from Algerian soil contaminated by hydrocarbons capable to produce biosurfactants has not been exploited. The strategy adopted was stepwise optimization and hence, by varying only one factor at a time, the kinetics of biosurfactant production were established. The optimum carbon source was gasoil at a concentration of 1 vol. %, a surface tension of 27.94 mN m^{-1} and an E_{24} of 75 % and a yield of 3.3 g L^{-1}.

There was also high induction of biosurfactant on all the hydrocarbons tested on diesel fuel (4.11 g L^{-1}).[24] In the present study, ammonium chloride was used as source of inorganic nitrogen (ST = 28.59 mN m^{-1} with an E_{24} of 68 %). SF species can grow on all four nitrogen sources, but ammonium chloride is the most efficient nitrogen source (2 %) compared to ammonium nitrate, sodium nitrate and urea.

The choice of inorganic source over organic nitrogen depends on the composition of the medium or the microbial strain.[25]

The synthesis kinetics were followed by a culture of the species *M. carbonoclasticus* SF in a medium containing diesel as the carbon source and NH_4Cl as the nitrogen source with different C:N mass ratios. The optimized C:N ratio 5:1 was achieved. This is the optimal condition for enhanced biosurfactant by *M. carbonoclasticus* SF. In a similar study conducted by Jimoh and Lin,[13] they found that a diesel fuel: $(NH_4)_2SO_4$ ratio of 3:1 resulted in the greatest production of biosurfactant.

The production of the biosurfactant started from the first hours of incubation, proven by the decrease in surface tension. This led to the use of a preculture that gives an appropriate and significant initial inoculum under optimal fermentation conditions favouring the production and a short lag phase.

After 72 h of fermentation, the production of the biosurfactant reached its maximum (ST = 27.94 mN m^{-1}) with a stable emulsion (E_{24} = 75 %). For 120

hours, monitoring the pH showed the stability of the biosurfactant and its production that is associated with the increase in biomass, as shown in Fig. 1. It is a production associated with growth (secondary metabolism).

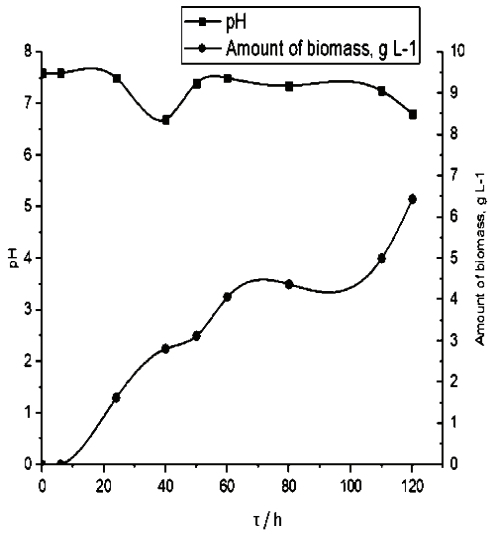

Fig. 1. Variation of pH and biomass with time.

Preliminary characterization of the biosurfactant

The results of a structural analysis of biosurfactant are shown in Fig. S-3 of the Supplementary material. A band greater than 3200 cm^{-1} was visible, indicating the presence of free hydroxyl groups of the rhamnose ring (-OH). Absorptions bands at around 2960 cm^{-1} are attributed to the symmetric C–H stretch of CH_2 and CH_3 groups of the aliphatic chains. Carbonyl ester groups are predicted by vibrations at 1100 cm^{-1}. The valence carbonyl band was found at 1685 cm^{-1}, corresponding to CO strain vibrations. The deformation vibration at 1450 cm^{-1} confirms the presence of alkyl groups. A similar study conducted by Ron and Rosenberg.[26] showed that almost all biosurfactants have an ester or carboxylic acid group in their structures and confirm the presence of bonds formed between carbon atoms and hydroxyl groups in the chemical structures of the glycosidic part. The biosurfactant obtained from the bacterial strain isolated from soil contaminated by hydrocarbons is initially a glycolipid. The determination of the biosurfactants *CMC* is crucial since there is no further modification in the surfactant activity above this concentration.[2] It is obvious from Fig. 2 that the surface tension decreased with increasing biosurfactants concentration until reaching 28.5 mN m^{-1} for a biosurfactant concentration greater than or equal to 850 mg L^{-1}.

Therefore, the critical micellar concentration (*CMC*) of the obtained product was 850 mg L^{-1}. Raddadi *et al.*[27] isolated 16 *Marinobacter* sp. such as strains

from harbour sediments. They found *CMC* values greater than 900 mg L^{-1}. Comparable results were found by Zenati *et al.*[28] for *M. carbonoclasticus* SDK644 isolated from a marine environment. The *CMC* was 788 mg L^{-1}.

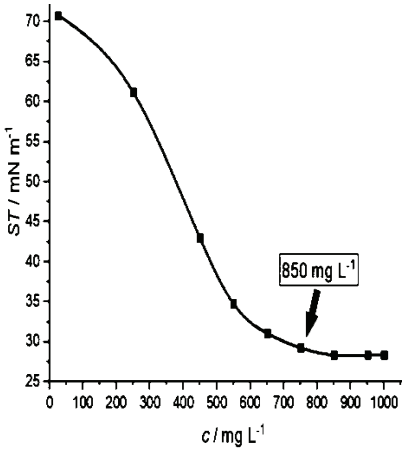

Fig. 2. Surface tension against the biosurfactant concentration.

The *CMC* is an index used to evaluate the surfactant activity and is the minimum concentration of biosurfactants necessary to reach the lowest values of surface tension, from which begins the formation of micellar aggregates. The interfacial tension of the mixture (supernatant/hydrocarbon or oil) showed a lowering capacity of the surface tension from 28 to 12 mN m^{-1}, The decrease in interfacial tension and the uniformity of the bubbles confirm the good emulsifying power of the biosurfactant on oils and hydrocarbons with good stability. The biosurfactant has a foaming power and foam stability was observed within 10 min. The biosurfactant produced was thermostable. Several studies showed that the glycollipids were unaffected by the rise in temperature (121 °C).[29] Moreover, the surfactant properties of the biosurfactant isolated from the SF strain remained stable in the pH range 2–11 and at a salinity of 5 to 100 mg L^{-1}. Hentati *et al.*[30] confirmed the stability of biosurfactants produced by a bacterial strain *Bacillus stratosphericus*, at different temperatures (4 to 121 °C) and pH (2.1–12) and salinity (0 to 150 %). A thermophilic and halotolerant strain of *Pseudominas aeruginosa*, isolated from petroleum contaminated soil, produced a biosurfactant when grown in media containing salinity in the range of 0–6 %.[31]

Slaughterhouse water treatment

Characterization of the sample. Some parameters which characterize the slaughterhouse waters were determined at pH 7.5 and a temperature of 11.5 °C. These parameters and their effluent water limit values are given in Table I.

Indeed, the blood present in this type of effluent mainly contains protein complexes (fibrogen, coagulation protein, antibodies, *etc*.) that are active at neutral pH. The slaughterhouse waste is characterized by high alkalinity, high chemical oxygen demand, high volatile content, high ammonium, and phosphorus content.[33] The high BOD_5 value can be explained by the abundance of organic matter (rumen debris), by the concentration of this effluent and by the blood of slaughterhouse waste as well as the *COD* value. The COD/BOD_5 ratio of 1.13 is less than 3 in line with that of predominantly domestic urban wastewater.[32] Therefore, the wastewater from this urban discharge has a high organic load, and is easily biodegradable and hence biological treatment of slaughterhouse water is suitable. To characterize industrial pollution, the BOD_5/COD ratio must be considered, the latter being equal to 0.88, the polluted water is loaded with OM, unstable water with the risk of odour release.

TABLE I. Physicochemical parameters of slaughterhouse water and their limit values

Values	*COD* / mg L^{-1}	BOD_5 / mg L^{-1}	c_{SS} / mg L^{-1}
Limit[32]	800	250	200
In slaughterhouse waters	1920	1700	12.5

Treatment with biosurfactant and isolated strain

With isolated strain. *M. hydrocarbonoclasticus* exhibits significant enzymatic activities, which allow the bacteria to degrade hydrophobic substances in an aerobic environment.[34] Therefore, *M. hydrocarbonoclasticus* can be considered as a potential bioremediation agent. Good results were obtained using this strain for the treatment of polluted water. Pollution by organic matter contained in an effluent can be evaluated by the chemical oxygen demand (*COD*). According to Fig. S-4a of the Supplementary material, in the light of the results found, it was noticed a considerably remarkable decrease in *COD* from the first day with a purification efficiency of 80 % (*COD*) and 85 % (BOD_5), which explains the purifying power of the *Marinobacter* sp. used. At the end of the treatment, the obtained *COD* value is within the standards required for discharges. Likewise, for BOD_5, given the high biodegradability of the effluent to be treated. Rates of up to 81 % reduction in organic matter (OM) contained in the slaughterhouse water were obtained, which allow to conclude the effectiveness of the biological treatment method. The disadvantages of this method, it presents problems related to the reduction of the concentrations of activated sludge, the need for supervision by experts in the design of biological systems and the high cost of the elimination of large quantities of effluents from sludge during treatment. Gnowe *et al*.[35] in their study, used the biological treatment method for the treatment of slaughterhouse water. Organic matter reduction rates of up to 81 % were obtained. This percentage is demonstrated in Fig. S-4b. Moreover, as shown in

Figs. S-4c and d, the presence of ammonium and MO in the medium facilitated the bioelimination of phosphates (dephosphatation), the suspended solids increased considerably with increasing quantity of nitrates and decreasing quantity of ammonium. This is due to the nitrification of the wastewater which consists in an oxidation of ammoniacal nitrogen into nitrites, which in turn oxidize and transform into nitrates.[36] After the second day (homogeneous sample), suspended solids increased markedly. This could be explained by the formation of aggregates during the treatment (concentration of pollution in the form of sludge) The reduction in phosphates and ammonium, with the formation of nitrates (nitrification) created a favourable environment for the biodegradation and reflect the good purifying capacity of the strain used. Wastewater temperature values of less than 30 °C were recorded, they are considered as the limit values for direct discharge into the receiving environment, The pH values varied slightly and remained around 7.5. When the pH was lower than 5 or higher than 8.5, the growth of microorganisms was directly affected. The electrical conductivity reflects the degree of overall mineralization, the measured values varied between 0.88 and 3.5 mS cm^{-1}. This increase can be explained by the formation of new ions during the oxidation of organic matter and by substantial variation of the mineralization.

With biosurfactant. The slaughterhouse water treatment was performed using a biosurfactant produced from the bacterial strain *M. carbonoclasticus* SF. The good results shown in Fig. S-5a of the Supplementary material confirmed the effectiveness of the use of the biosurfactant in the field of polluted water treatment.

As illustrated in Fig. S-5b, the obtained purification efficiency was 82 and 96 % for *COD* and BOD_5, respectively. A decrease in the concentration of phosphates and ammonium, an increase in nitrates and a large amount of suspended solids were observed. The study conducted by Al-Wahaib *et al.*[37] on different media to produce biosurfactants using strains of *Marinobacter* sp. found that biodegradation efficiencies were of 90, 84, 76 and 72 % for crude oil, diesel, C32 and C40, respectively. An excellent treatment of contaminants was found. This is due to the low CMC value and the good emulsifying power of the biosurfactant obtained.[37]

CONCLUSION

The strain isolated from Algerian soil polluted by hydrocarbons was a *Marinobacter carbonoclasticus* SF. The latter was able to grow on a minimum culture medium consisting of diesel as a carbon source (1 %), ammonium chloride as a nitrogen source (2 %), and a C/N ratio of 5 under optimal conditions of pH 7.4, a temperature of 45 °C, and salinity of 0–30 %. The isolated strain showed its ability to produce a glycolipid-type biosurfactant after 72 h of incubation, a surface tension of 27.94 mN m^{-1} was obtained and an emulsification number of

75 %. The *CMC* of the biosurfactant was 850 mg L^{-1} and a yield of 3.3 g L^{-1}. The obtained biosurfactant was both thermally and chemically stable. Physico-chemical pollution parameters of the wastewater from the municipal slaughter-house of the city of Medea (Algeria) have values that relatively exceed the limit values for discharges into the receiving environment (Oued Lahrech) which represents a real risk that requires a thorough treatment. The water treatment trials resulted in significant depollution rates, whether by the isolated bacterial strain *M. hydrocarbonoclasticus* SF (more than 81 %) or by the biosurfactant produced by this strain (more than 96 %).

SUPPLEMENTARY MATERIAL

Additional data and information are available electronically at the pages of journal website: https://www.shd-pub.org.rs/index.php/JSCS/article/view/11335, or from the corresponding author on request.

Acknowledgment. The first part of this work was funded by the AUF (University Agency of the Francophonie, project contract no.6313PS652).

ИЗВОД

ОПТИМИЗАЦИЈА ТРЕТМАНА ВОДЕ ИЗ КЛАНИЦЕ ПОМОЋУ НОВОГ *Marinobacter carbonoclasticus* SF И ЊЕГОВОГ БИО-СУРФАКТАНТА

NADIA MIHOUBI[1], SAMIRA FERHAT[1], REDHA ALOUAOUI[1], ABDELLAH IBRIR[1], MOHAMED NEDJHIOUI[2] и ABDELMALEK BADIS[3]

[1]Biomaterial and Transport Phenomena Laboratory (LBMPT), Yahia FARES University, Faculty of Technology, Department of Process Engineering, 26000-Medea, Algeria, [2]Materials and Environment Laboratory (LME), Yahia FARES University, Faculty of Technology, Department of Process Engineering, 26000-Medea, Algeria и [3]Natural Products Chemistry and Biomolecules Laboratory (LNPC-BioM), Saad Dahleb University, Faculty of Technology, Department of Industrial Chemistry,19000-Blida, Algeria

Циљ ове студије је производња био-сурфактанта из новог соја бактерија, *Marinobacter hydrocarbonoclasticus* SF (96,76 % сличности), изолованог из земљишта контаминираног угљоводоницима у Hassi-Messaoud (Јужни Алжир), за пречишћавање течних ефлуента из воде која долази из кланице. Размотрене су карактеристике тестова биоразградње органске материје. Упркос великом оптерећењу загађујућим материјама и неповољном физичко–хемијском саставу ефлуента, специфична брзина раста изолованог соја после 10 дана инкубације била је на неутралном pH 7,4 и температури од 45 °C, у опсегу од 0–30 g L^{-1} NaCl. Најбољи производни принос био-сурфактанта је постигнут након 72 h инкубације и под оптималним условима као што су дизел као извор угљеника, амонијум-хлорид као извор азота и однос C/N од 5. Произведени био-сурфактант гликолипидног типа са ниском критичном мицеларном концентрацијом (*CMC*), добрим емулгационим својствима и хемијском и функционалном стабилношћу. Значајна ефикасност уклањања загађивача постигнута је коришћењем бактеријског соја (до 82 %) и био-сурфактанта (до 96 %). Измерена је концентрација неколико јона, као што су нитрати, фосфати, амонијум, као и суспендоване чврсте супстанце.

(Примљено 29. октобра 2021, ревидирано 5. марта, прихваћено 7. марта 2022)

REFERENCES

1. V. Johan, M. O. Mizier, *Water, Industry*, *Nuisances* **269** (2004) 33 (http://bdsp-ehesp.inist.fr/vibad/index.php?action=getRecordDetail&idt=294996)
2. D. A. Lovett, S. M. Travers, K. R. Davey, *Water Research* **18** (1984) 429 (https://doi.org/10.1016/0043-1354(84)90150-7)
3. R. Borja, C. J. Banks, Z. Wang, A. Mancha, *Bioresour. Technol.* **65** (1998) 57 (https://doi.org/10.1016/S0960-8524(98)00004-2)
4. M. A. Bull, R. M. Sterritt, J. N. Lester, *Environ. Technol. Lett*. **3** (1982) 117 (https://doi.org/10.1080/09593338209384107)
5. K. Q. Camin, in *Proceedings of 25*th *Industrial Waste Conference*, Purdue University, Lafayete, IN, 1970, p. 193
6. J. K. Volkman, E. J. Tanoue, *J. Ocean*. **58** (2002) 265 (https://doi.org/10.1023/A:1015809708632)
7. P. Grażyna. A. Varenyam, *Inter. J. Mol. Sci*. **21** (2020) 2152 (https://doi.org/10.3390/ijms21062152)
8. K. Guemiza, L. Coudert, S. Metahni, G. Mercier, S. Besner, J. F. Blais, *J. Hazar. Mater*. **333** (2017) 194 (https://doi.org/10.1016/j.jhazmat.2017.03.021)
9. S. T. Malkapuram, V. Sharma, S. P. Gumfekar, S. Sonawane, S. Sonawane, G. Boczkaj, S. M. M. Seepana, *Sustain. Energy Tech. Asses*. **48** (2021) 101576 (https://doi.org/10.1016/j.seta.2021.101576)
10. S. Ferhat, S. Mnif, A. Badis, K. Eddouaouda, R. Alouaoui, A. Boucherit, N. Mhiri, N. Moulai-Mostefa, S. Sayadi, *Int. Biodet. Biodeg*. **65** (2011) 1182 (https://doi.org/10.1016/j.ibiod.2011.07.013)
11. D. L. Corwin, K. Yemoto, *Met. Soil Anal*. **2** (2017) 1 (https://doi.org/10.2136/msa2015.0039)
12. S. Mnif, M. Chamkha, S. Sayadi, *J. App. Microb.* **107** (2009) 785 (https://doi.org/10.1111/j.1365-2672.2009.04251.x)
13. A. A. Jimoh, J. Lin, *Ecotox. Envir. Saf.* **184** (2019) 109607 (https://doi.org/10.1016/j.ecoenv.2019.109607)
14. B. Tuleva, N. Christova, B. Jordanov, B. Nikolova-Damyanova, P. Petrov, *Naturforschung, C* **60** (2005) 577 (https://doi.org/10.1515/znc-2005-7-811)
15. S. Ferhat, R. Alouaoui, A. Badis, N. Moulai-Mostefa, *Biotechnol. Biotechnol.Equip.* **31** (2017) 733 (https://doi.org/10.1080/13102818.2017.1309992)
16. J. E. Zajic, W. Seffens, *Crit. Rev. Biotech*. **1** (1984) 87 (https://doi.org/10.3109/07388558309082580)
17. J. Rodier, *Dunod*, 8th ed., Paris, 2005, p. 1384 (ISBN 2-10-049636-0)
18. S. F. Altschul, W. Gish, W. Miller, E. W. Myers, D. J. Lipman, *J. Mol. Biol.* **215** (1990) 403 (http://dx.doi.org/10.1016/S0022-2836(05)80360-2)
19. G. Jun, C. Hua, Y. Su-Lin. Yu, Q. Ri, Y. Bin, G. Yu-Feng, Z. Jin-Yi, W. Xiao-Lei, *Int. J. Syst. Evolut. Microb.* **57** (2007) 250 (https://doi.org/10.1099/ijs.0.64522-0)
20. L. Yi-Jing, X. Bai-Sheng, L. Xiang-Lin, C. Man, W. Ya-Nan, C. Heng-Lin , C. Hua, W. Xiao-Lei, *Anton. Van Leeuw.* **107** (2015) 1085 (https://doi.org/10.1007/s10482-015-0401-y)
21. P. Elumalai, P. Parthipan, M. Huang, B. Muthukumar, L. Cheng, M. Govarthanan, A. Rajasekar, *Environ. Pol.* **289** (2021) 117956 (https://doi.org/10.1016/j.envpol.2021.117956)
22. M. J. Gauthier, B. R. Christen, L. Fernandez, M. Acquaviva, P. Bonin, J. C. Bertrand, *Int. J. Syst. Bact*. **42** (1992) 568 (https://doi.org/10.1099/00207713-42-4-568)

23. A. M. Elazzazy, T. S. Abdelmoneim, O. A. Almaghrabi, *Saud. J. Biol. Sci.* **22** (2015) 466 (https://doi.org/10.1016/j.sjbs.2014.11.018)
24. D. Ghribi, S. Ellouz-Chaabouni, *Biotech. Res. Int.* **2011** (2011) 653654 (https://doi.org/10.4061/2011/653654)
25. E. Z. Ron, E. Rosenberg, *Environ. Microbiol.* **3** (2001) 229 (https://doi.org/10.1046/j.1462-2920.2001.00190.x)
26. N. Raddadi, L. Giacomucci, G. Totaro, F. Fava, *Micr. Cel. Fact.* **16** (2017) 186 (https://doi.org/10.1186/s12934-017-0797-3)
27. B. Zenati, A. Chebbi, A. Badis. K. Eddouaouda, H. Boutoumi. M. El Hattab, D. Hentati, M. Chelbi, S. Sayadi, M. Chamkha, A. Franzetti, *Ecotox. Environ. Saf.* **154** (2018) 100 (https://doi.org/10.1016/j.ecoenv.2018.02.032)
28. R. S. Makkar, S. S. Cameotra, I. M. Banat, *AMB Exp*. **1** (2011) 5 (https://doi.org/10.1186/2191-0855-1-5)
29. D. Hentati, A. Chebbi, F. Hadrich, I. Frikha, F. Rabanal, S. Sayadi, A. Manresa, M. Chamkha, *Ecotox. Environ. Saf*. **167** (2018) 441 (https://doi.org/10.1016/j.ecoenv.2018.10.036)
30. M. Kumar, V. León, A. De Sisto Materano, O. A. Ilzins, L. Luis, *World J. Microb. Biotech*. **24** (2008) 1047 (https://doi.org/10.1007/s11274-007-9574-5)
31. C. C. Azubuike, C. B. Chikere, G. C. Okpokwasili, *World J. Microb. Biotech.* **32** (2016) 180 (https:// doi.org/10.1007/s11274-016-2137-x)
32. D. Belghyti, Y. El Guamri, G. Ztit, M. Ouahidi, M. Joti, A. Harchrass, H. Amghar, O. Bouchouata, K. El kharrim, H. Bounouira, *Afr. Sci*. **5** (2009) 153 (https://doi.org/10.4314/afsci.v5i2.61730)
33. X. Xingjian, L. Wenming, T. Shuhua, Tian, W.Wei, Q. Qige, J. Pan, G. Xinmei, L. Fengjiao, L. Haiyan, Y. Hongwen, *Front. Microb*. **9** (2018) 2885 (https://doi.org/10.3389/fmicb.2018.02885)
34. W. D. Gnowe, E. Noubisié, G. B. Noumi, *Chem. Environ. Eng*. **2** (2020) 100048 (https://doi.org/10.1016/j.cscee.2020.100048)
35. B. N. Uba, *Biores. Technol.* **51** (1995) 143 (https://doi.org/10.1016/0960-8524(94)00105-A)
36. D. Al-Wahaib, D. Al-Bader, D. K. Al-Shaikh Abdou, M. Eliyas, S. S. Radwan, *J. Mol. Microb. Physiol*. **26** (2016) 261 (https://doi.org/10.1159/000445686)
37. M. Maikudi Usman, A. Dadrasnia, K. T. Lim, A. F. Mahmud, S. Ismail, *AIMS Bioeng.* **3** (2016) 289 (https://doi.org/10.3934/bioeng.2016.3.289).

Journal of the Serbian Chemical Society
JSCS@tmf.bg.ac.rs • www.shd.org.rs/JSCS
J. Serb. Chem. Soc. 87 (11) S446–S449 (2022) *Supplementary material*

SUPPLEMENTARY MATERIAL TO

Optimization of the slaughterhouse water treatment rate by a new *Marinobacter carbonoclasticus* SF and its biosurfactant

NADIA MIHOUBI[1], SAMIRA FERHAT[1]*, REDHA ALOUAOUI[1], ABDELLAH IBRIR[1], MOHAMED NEDJHIOUI[2] and ABDELMALEK BADIS[3]

[1]*Biomaterial and Transport Phenomena Laboratory (LBMPT), Yahia FARES University, Faculty of Technology, Department of Process Engineering, 26000-Medea, Algeria,* [2]*Materials and Environment Laboratory (LME), Yahia FARES University, Faculty of Technology, Department of Process Engineering, 26000-Medea, Algeria and* [3]*Natural Products Chemistry and Biomolecules Laboratory (LNPC-BioM), Saad Dahleb University, Faculty of Technology, Department of Industrial Chemistry,19000-Blida, Algeria*

J. Serb. Chem. Soc. 87 (11) (2022) 1327–1340

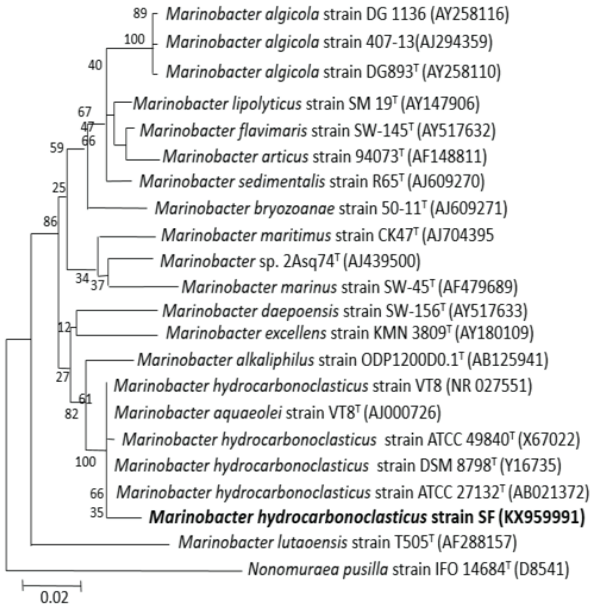

Fig. S-1. Phylogenetic tree based on 1500 nucleotides of the 16S rRNA gene sequence of the SF strain, showing its phylogenetic position among related species of the genus *Marinobacter*. Bootstrap percentages are given at node level. Access numbers (Genbank) are given in brackets. Scale bar equals approximately 2 % nucleotide divergence.

* Corresponding author. E-mail: ferhatsamira@yahoo.fr

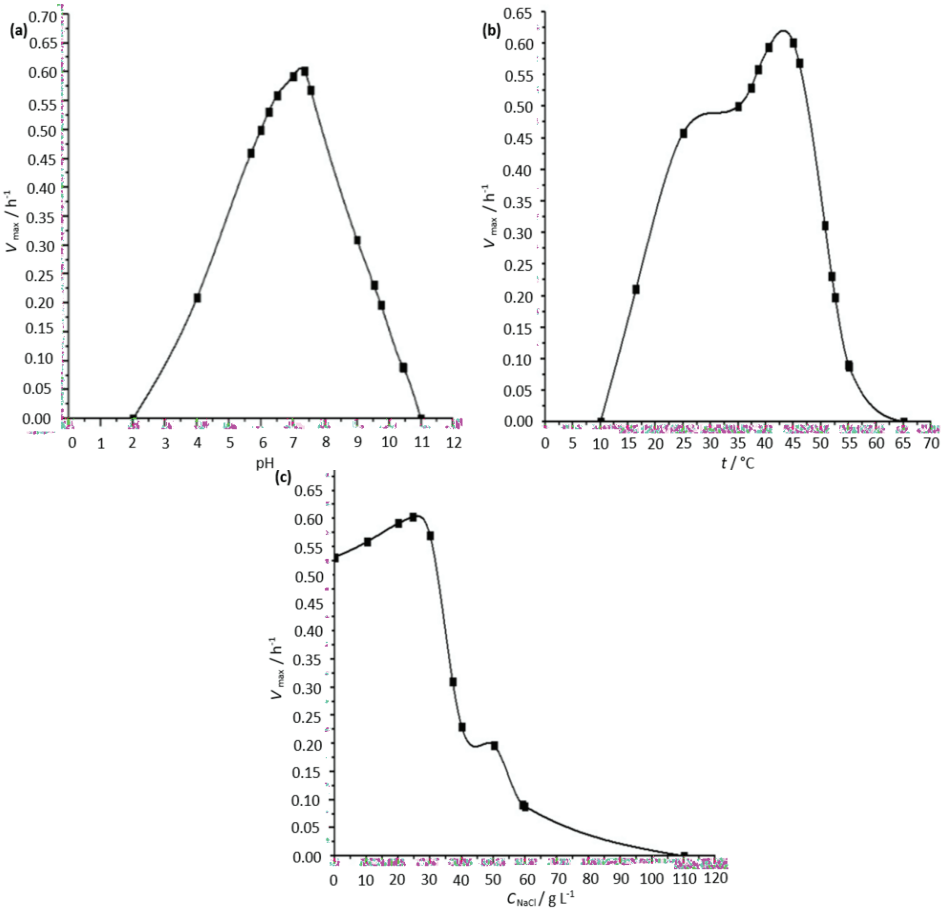

Fig. S-2. Influence of: a) pH, b) temperature and c) concentration of NaCl on bacterial growth.

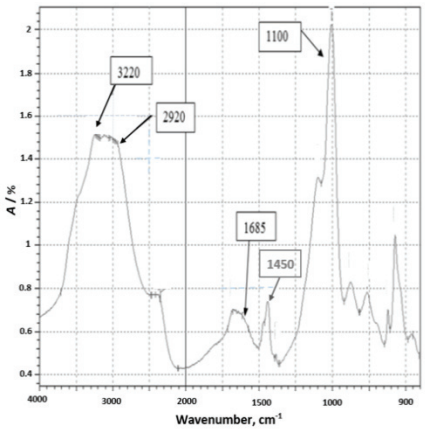

Fig. S-3 FTIR spectra (500-4000 cm^{-1}) of biosurfactant product.

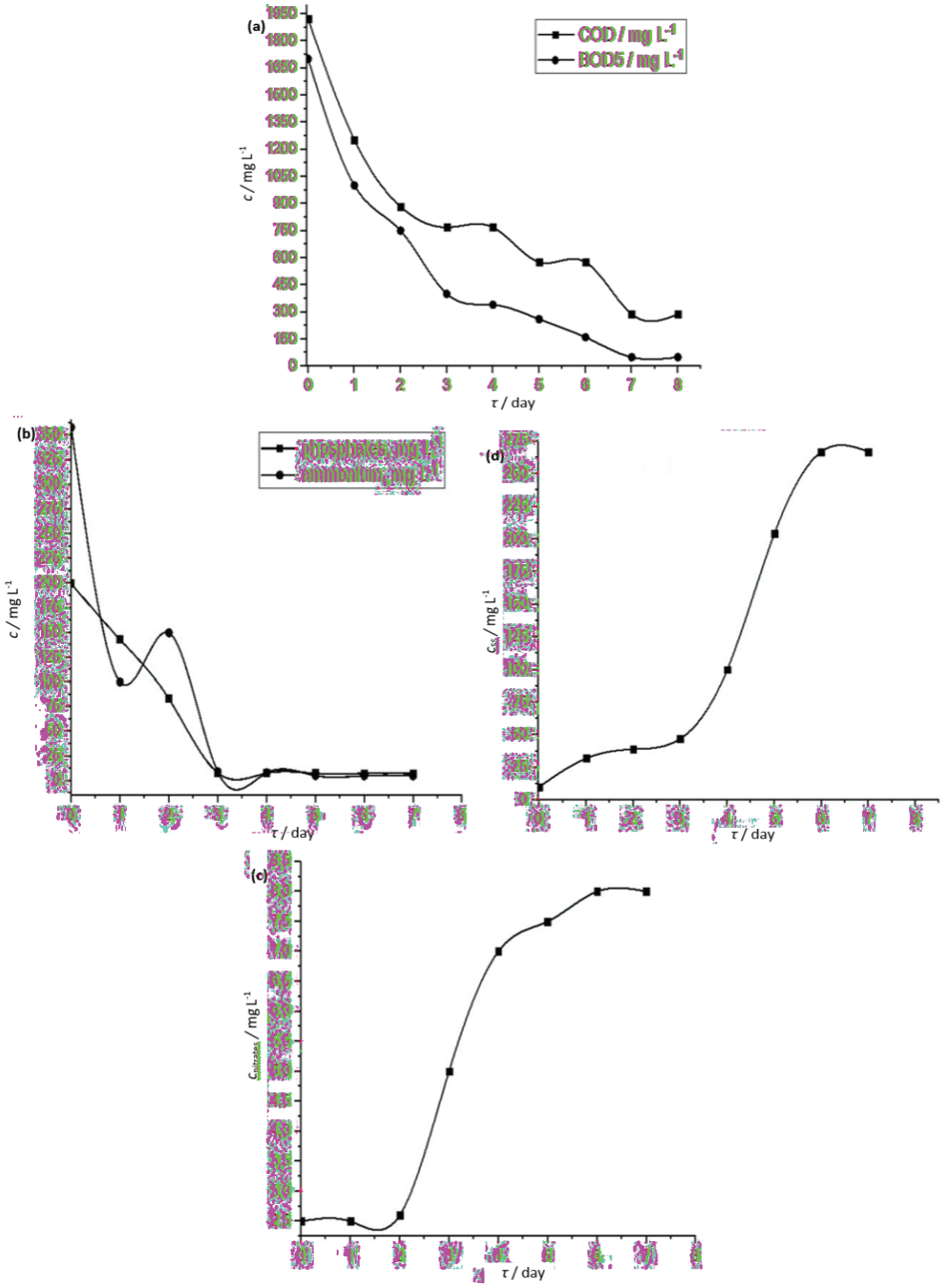

Fig. S-4. Variation in the level of a) *COD*, BOD_5, b) phosphates, ammonium, c) nitrates and d) suspended matter; after 120 h of treatment with isolated *marinobacter* SF.

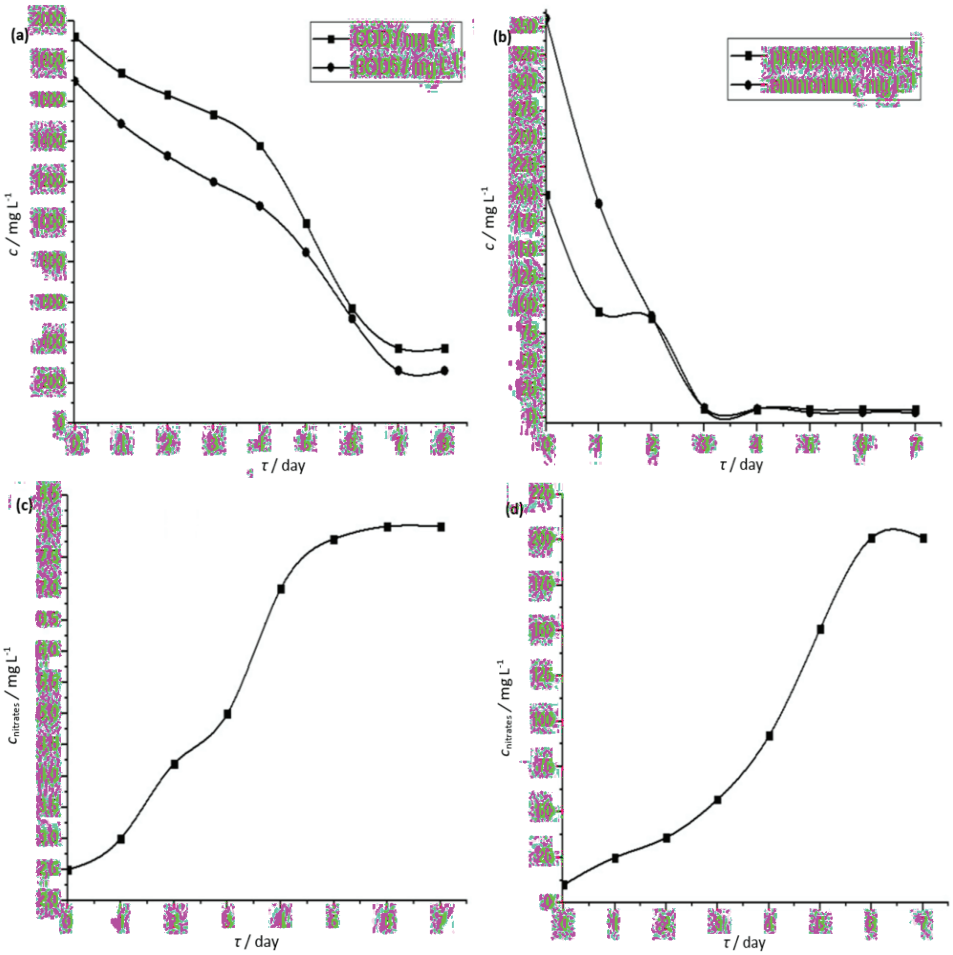

Fig. S-5. Variation in the level of: a) *COD*, BOD_5, b) phosphates, ammonium, c) nitrates and d) suspended matter; after 120 h of treatment with the biosurfactant.

Journal of the Serbian Chemical Society
JSCS@tmf.bg.ac.rs • www.shd.org.rs/JSCS
J. Serb. Chem. Soc. *87* (11) 1341–1345 (2022)
EuCheMS news

DIVISION OF ANALYTICAL CHEMISTRY
EUROPEAN CHEMICAL SOCIETY

EUCHEMS NEWS

European Analytical Column No. 50•

SLAVICA RAŽIĆ[1]*#, MARCELA A. SEGUNDO[2]**, DIANE TURNER[3]***, MANUEL MIRÓ[4]× and ANTJE J. BAEUMNER[5]^

[1]Department of Analytical Chemistry, Faculty of Pharmacy, University of Belgrade, Vojvode Stepe 450, 11222 Belgrade, Serbia,[2]Department of Chemical Sciences, Faculty of Pharmacy, University of Porto, R Jorge Viterbo Ferreira, 228, 4050-313 Porto, Portugal, [3]Anthias Consulting Ltd., 1 Hamden Way, Papworth Everard, Cambridgeshire, CB23 3UG, UK, [4]FI-TRACE group, Department of Chemistry, University of the Balearic Islands, Carretera de Valldemossa km 7.5, E-07122 Palma de Mallorca, Spain and [5]Institute of Analytical Chemistry, Chemo- and Biosensors, University of Regensburg, Universitätsstr. 31, 93053 Regensburg, Germany

The European Analytical Column is the voice of the Division of Analytical Chemistry (DAC) as a Professional Network of chemical societies and their members working in all fields of analytical sciences within the European Chemical Society (EuChemS). The strategy for 2021–2023 comprehends the promotion of Analytical Chemistry to a wider community, co-operation with other Professional Networks and to support members' activities, particularly through Study Groups and Task Forces. This year we have invited active scientists to share their thoughts about the near future of Analytical Chemistry. Please help us to expand this discussion among the community and feel free to share your opinion and thoughts through our social media and networks!

1. DAC-EUCHEMS ACTIVITIES

One of the main activities of DAC-EuChemS is the promotion of organization of Euroanalysis conference. Every two-years, one of the participating scientific chemical societies will host Euroanalysis, with active involvement of local scientists in the organization. Euroanalysis XXI is scheduled to 2023 and it will

* Correspondence E-mails: (*)slavica.razic@pharmacy.bg.ac.rs; (**)msegundo@ff.up.pt; (***)dct@anthias.co.uk; (×)manuel.miro@uib.es; (^)antje.baeumner@ur.de
# Serbian Chemical Society member.
• Reprint from *Analytical and Bioanalytical Chemistry*, https://doi.org/10.1007/s00216-022--04373-0, with permission from Springer.

take place in Geneva, Switzerland, under the auspices of the Swiss Chemical Society (https://www.euroanalysis2023.ch/), organized by Prof. Eric Bakker (University of Geneva), Dr. Marc Suter (EAWAG), Dr. Franka Kalman (HES Sion) and Dr. Bodo Hattendorf (ETH Zurich).

Other ongoing activities of DAC-EuChemS are performed within Study Groups. These include "Bioanalytics", "Chemometrics", "Education", "Electroanalytical Chemistry", "History", "Nanoanalytics", "Quality Assurance", and "Sample Preparation". Please visit the DAC-EuChemS website for updated reports (https://www.euchems.eu/divisions/analytical-chemistry/) and contact the Heads of the Study Groups in order to have more information or to participate in their activities.

Collaboration with other Professional networks within EuChemS is also sought. In particular, exchange of invited lectures and organization of special thematic sessions in is planned to take place in the 18th International Conference on Chemistry and the Environment (https://icce2023.com/) and Euro Food Chem XXII conferences, organized by the Division of Chemistry and the Environment (DCE-EuChemS) and by the Division of Food Chemistry (DFC-EuChemS), respectively.

Lastly, one of DAC-EuChemS objectives is to support its delegates on the organization of local events open to the international community through dissemination of the event within the Professional Network, including online events. The Steering Committee of DAC-EuChemS will be happy to receive input for additional activities. Feel free to contact one of the following persons: Slavica Ražić, University of Belgrade, Serbia (Chair), Marcela Segundo, University of Porto, Portugal (Secretary), Martin Vogel, University of Münster, Germany (Treasurer), Jiří Barek, Charles University, Czech Republic, Charlotta Turner, Lund University, Sweden, Sibel A. Özkan, Ankara University, Turkey, and Franka Kalman, University of Applied Sciences and Arts of Western Switzerland, Switzerland.

2. ANALYTICAL CHEMISTRY IN 2030: A GLIMPSE OF OPPORTUNITIES AND CHALLENGES

In the second part of this column, we would like to share our thoughts of the present state and future perspectives of Analytical Chemistry, as views of our guest authors, Diane Turner, Manuel Miró and Antje Baeumner. In that sense and order, and without ambition to cover all fields, let us tackle some of general and particular points and impacts in a few research areas. And, maybe, just maybe, to open the discussion with the next edition of EAC.

Analytical chemistry is used in most industries from petrochemical to clinical and consumer products to food and environment. In academia, not only is it extensively researched and used in chemistry departments, but also in engineer-

ing, earth sciences, planetary sciences, archaeology, biology and beyond. The uses of analytical chemistry are many, from quality control to the identification of components in a sample mixture, and the most important questions when thinking and preparing for sample analyses is why you are performing their analysis and what questions you are seeking to answer. The results from sample analysis can be used to determine the next steps in a manufacturing environment, to decide if a product is safe for use or to consume, to present in a PhD thesis or as evidence in a court of law.

There has, for many years, unfortunately been a large gap between using analytical chemistry in an academic setting compared to using it in regulated industry. Even though method validation and quality control are taught at universities, it has been a long-time coming in reaching research projects, with many publications not showing or even mentioning any basic quality control. There are many aspects to consider when developing a method and validating it, from sample collection, storage and transportation, to sample preparation, sample analysis, data analysis and reporting, the use of blanks, standards, internal standards, the consideration of different sample matrices and method performance parameters. Then there is on-going quality control and quality assurance (QC/QA) with system suitability checks, analytical quality control (AQC) standards, replicates, checks for carryover and extraction efficiency and the monitoring of a wide range of other method performance parameters, dependent on the analytical technique employed and the variables that can affect the results of that technique. When performing quantitative sample analysis there are a lot of standard QC procedures that can be followed, but many of these can be extended into qualitative analysis too. If two samples appear to give different results, are they truly different or is the method not robust and there is poor accuracy and/or precision due to the analytical instrument or any of the steps from sample collection through to reporting? Is a compound genuinely not in a sample or is it below the method detection limit? If so, what is the method detection limit, not just the instrument limit of detection? What is the uncertainty of your result?

For many projects a full method validation to ISO 17025 standards is not required however, a method should always be checked that it is suitable for the sample(s) and compound(s) to be analysed. Generally, the more samples to be analysed, especially if the matrix varies, the more validation and on-going quality control is needed to ensure that not only is the method suitable but remains suitable and gives the correct results for all samples. At the start, a well-thought-out plan for method development, validation and quality control is needed and that needs to be referred to and evidenced in any reporting, whether that is a publication, poster or a document for court. The current drive towards proof of the quality of results is welcomed and in the not-too-far distance future could be

mandatory for all analytical methods in research as well as industry, especially if presenting into the public domain.

Considering another perspective and its multidisciplinary nature, analytical chemistry is proven superb to tackle the current societal challenges as recently demonstrated by the fast development of sensing platforms in response to the demands occasioned by the SARS-CoV-2 pandemic. The intimate relationship between analytical chemistry and material science ranging from paper-based (fluidic) systems to nanotechnology including silica, polymeric and metal nanoparticles trigger the development of simple point-of-need/care sensing devices for customized screening applications. Nanotechnology actually is acting as a bridge to expand analytical chemistry to a plethora of companion disciplines to help answering scientific challenges. Theranostic applications are clear examples on how the interplay between analytical chemistry, nanoscience and biosciences offer unrivalled opportunities against relevant biomarker identification. Inspired by the industry 4.0 technological pillars (*e.g.*, internet of things), wearable sensors and remote sensing approaches enable real-time identification of changing physiological/environmental conditions, yet further developments are still called for to improve detectability and selectivity issues. Instrumental developments for confirmatory results are linked to efforts toward designing advanced mass spectrometry analysers to leverage imaging, ambient detection and collision cross-sections for reliable high-throughput analysis.

Material science has impacted the entire analytical process right from the first step of sampling to offer new devices for in-situ sample preparation and microextraction for targeted or suspect analysis to the detection step by exploiting the unique plasmonic and electrochemical features of nanoparticles and nanoclusters. A technological breakthrough in this field, mostly linked to polymers but also to noble metal chemistry, which nurtured analytical chemistry is the so-called "Additive Manufacturing" (*i.e.*, 3D-printing). Advanced technologies such as laser sintering, photopolymer inkjet, low-force stereolithography and fused deposition modelling are revolutionizing several subdisciplines, such as microfluidics, electrochemical and optical sensing, and sample preparation in terms of fast prototyping of devices and straightforward printing of electrodes and optical detection components, aided by the plethora of functional materials available with distinct optical, conducting and thermal properties and chemical resistance that can be simultaneously processed. We foresee that higher resolution printers at affordable prices with improved minimum printing size features in X, Y and Z axes will be available in most of the analytical chemistry labs and also technological companies in the near future, because mass production and commercialization of 3D printed analytical devices are becoming a reality.

Going *via* next road of highly potential science, the field of biosensors is currently seeing a dramatic increase in societal interest and demands for imp-

rovement much beyond the current state of the art. Wearables and point-of-care tests (POCT) receive the greatest public attention due to the increasingly ubiquitous availability of simple, portable, read-out devices (cell phones, watches) and the critical need for POCT during the recent pandemic. In the future, such sensors must achieve lower limits of detection than they provide today, they must allow for multiplexing and especially enable quantitative detection with high reliability and not only provide qualitative or semi-quantitative results. Since the absolute requirement for simplicity of use puts strict limits on technologies used within such sensors, one can predict innovation and advancements to not be derived necessarily from new detection principles, but rather from improved signaling agents, advanced (nano)materials, and artificial-intelligence-assisted read-out apps.

Furthermore, the improvement of sample preparation strategies for bio- and chemosensors in general will be of great demand. It is obvious that good results cannot be obtained from a badly acquired sample, and some sample clean-up through centrifugation, multiple pipetting steps and the like is difficult to implement in most applications and cannot be employed at all in wearable sensors. Thus, in the next 2–5 years, analytical and engineering research should focus on overcoming these ubiquitous challenges that are limiting most of the current bio- and chemosensors targeting on-site applications.

As mentioned earlier, another area of great development in the coming years will be the move toward digitalization, particularly as far as bio- and chemosensors are concerned regarding their integration into the internet-of-things, digital diagnostics, telemedicine, and remote environmental and food monitoring. As much as physical sensors are seamlessly integrated into large systems, also bio- and chemosensors will continue moving in this direction. Alongside this will come a need to develop sensor technologies that allow for easy mass production, use of sustainable materials and production technologies, and result in products that do not increase the environmental burden caused by their waste. Considering that a dramatic increase in the use of bio- and chemosensors is predictable, these last points need to become design criteria in the development of innovative new bio- and chemosensors in the coming decade.

We can continue our walk from one to another area of Analytical Chemistry and ask ourselves is the sky the limit? It's allowed in our minds but advancements in other scientific fields, such as material science, physics and biology will certainly have their impacts and pave the road in advancements of analytical chemistry in close future. Far future? We do not dare to think about it yet. We can follow the best science, that is sure…

Journal of the Serbian Chemical Society
JSCS-info@shd.org.rs • www.shd.org.rs/JSCS
J. Serb. Chem. Soc. *87* (11) 1347–1348 (2022)

IN MEMORY TO

Professor Nikos Katsaros (1938–2022)

On January 19, 2022, our dear colleague, and friend, Professor Nikos Katsaros passed away. He worked at the "Demokritos" Natural Sciences Research Center and was the former President of the Association of Greek Chemists (AGC, EEX).

Nikos Katsaros was born in Gimari, Corfu, in 1938, lived and grew up in Athens. He studied at the University of Athens, where he was admitted 2nd in the Department of Chemistry out of 750 candidates and received his B.S. degree in chemistry in 1961. He completed his studies at the University of Massachusetts, USA, wherefrom he received an M.S. in 1967 and a Ph.D. in 1968. He then served as a Visiting Research Fellow at Brookhaven National Laboratory, Upton, NY, USA. In 1969, he joined the University of Georgia, USA, as an Assistant Professor of Chemistry. In 1970, Nikos was appointed Researcher at the "Demokritos" Nuclear Research Center. In 1972, he served as Visiting Research Fellow at Imperial College London, United Kingdom. From 1976 to 2004, he worked as a Principal Researcher at the National Center for Natural Sciences Research (EKEFE) "Demokritos". Also, in 1983–1998, he served as Visiting Professor of Chemistry at the University of Maryland, USA.

From 1989 to 1993 he served in the Hellenic Ministry of Industry, Energy and Technology, as Secretary General for Research and Technology and in 2004–2005 as President of the Hellenic Food Organization (EFET). Professor Katsaros served for four terms as President of the Association of Greek Chemists (AGC) and twice as its Vice-President. He was also a member of the Chemistry Europe Fellow and was honored in 2020 for his services. He was the Honorary Member of the Serbian Chemical Society.

His research interests included inorganic biochemistry, food chemistry, food safety, radiochemistry, environmental chemistry, and toxic waste management. He published over 200 scientific articles and texts on these subjects. Prof. Katsaros was the member of Editorial Board of the Journal of the Serbian Chemical Society.

The field of education has always been at his heart and therefore he had unceasing activity either in organizing and participating in Postgraduate Programs of Greek Universities (Ioannina, Patras and National and Kapodistrian University of Athens), or in teaching at private colleges such as Deree College and New York College, where he worked until recently as Head of the Department of Human Nutrition and Life Sciences.

Nikos Katsaros was distinguished for his intelligence. He was an emblematic president of the EEC, AGC. He had distinct qualifications, which he used in his studies, in research, in his scientific activities and in his social struggles. In the context of the activities of the Association of Greek Chemists, he had the initiative of organizing many Panhellenic Chemistry Conferences, Greece–Cyprus Chemistry Conferences and the establishment of the institution of the Panhellenic Student Chemistry Competitions.

As part of European and Western Balkan community, he, as president of the Association of Greek Chemists, was founder and main driving force of series of International Conferences of the Chemical Societies of the South-Eastern European Countries (SEEC). As a consequence of this visionary approach the conferences brought together and interconnected SEEC chemists into close partnership where from the scientific collaboration on many bilateral and multilateral projects emerged.

While being president of AGC in spring 1999 he, and complete AGC leadership, made a self-organized visit to Serbian Chemical Society bringing dioxin standards and HPLC/MS spare parts to our institutions analyzing the toxic chemical effects after NATO bombing of Serbia. Also, the AGC management insisted, and visited freshly bombed HCl, ammonia and chlorine production sites at Petrohemija, Pančevo, and bombed oil refinery in Novi Sad. This friendly gesture of Nikos, and AGC, will be kept in Serbian chemists' hearts forever.

We, your colleagues, your friends and associates say goodbye today to Nikos Katsaros, a worthy scientist, family man, visionary and useful social worker.

Have a nice trip, kiss Nikos, dear colleague, and late partner.

May your memory be eternal.

Prof. Panayotis P. Siskos
Prof. Bogdan A. Šolaja
Prof. Branislav Nikolić